Durham University

Durham E-Theses

Plasma polymerisation of organosilanes

Jose Luis Cardozo Fonseca

How to cite:

Fonseca, Jose Luis Cardozo (1994) Plasma polymerisation of organosilanes. Doctoral thesis, Durham University.

Use policy

The full-text may be used and/or reproduced, and given to third parties in any format or medium, without prior permission or charge, for personal research or study, educational, or not-for-profit purposes provided that:

- a full bibliographic reference is made to the original source
- a https://etheses.durham.ac.uk/id/eprint/10490/ is made to the metadata record in Durham E-Theses
- the full-text is not changed in any way

The full-text must not be sold in any format or medium without the formal permission of the copyright holders.

Please consult the full Durham E-Theses policy for further details.

Academic Support Office, The Palatine Centre, Durham University, Stockton Road, Durham, DH1 3LE
e-mail: e-theses.admin@durham.ac.uk Tel: +44 0191 334 6107
https://etheses.durham.ac.uk

University of Durham

A thesis entitled

PLASMA POLYMERISATION OF ORGANOSILANES

Submitted by

José Luís Cardozo Fonseca

Diploma in Chemical Engineering - Universidade Federal do Rio de Janeiro

M.Sc. in Polymer Science and Technology - Universidade Federal do Rio de Janeiro

A candidate for the Degree of Doctor of Philosophy

7 April 1994

The copyright of this thesis rests with the author. No quotation from it should be published without his prior written consent and information derived from it should be acknowledged.

12 SEP 1994

To Marianinha

Acknowledgements

The work described in this thesis was carried out under the supervision of Dr. J.P.S. Badyal and I wish to record my sincere appreciation of his help and encouragement throughout.

I would like to thank Mr. K. Appleby for building the emission spectrometer used in this work., Ms. Janet Hopkins for carrying out the permeability measurements and Mr. Campbell P. Barker for performing depth profile experiments, as well as all the people from lab CG 98 for the good time - in particular to Peter Ratcliffe, Campbell Barker and Alan Hynes for proof-reading parts of this thesis. Thanks also to Dr. David C. Apperley, for carrying out solid state NMR experiments.

Many thanks to Márcia for her patience with me and to my parents, back home, for their constant support (even at a distance).

Finally I would like to thank Brazil's Conselho Nacional de Desenvolvimento Científico e Tecnológico (CNPq) for financial support during the course of this work.

The work described in this thesis was carried out at the University of Durham between March 1991 and March 1994. Except where acknowledged by reference, it is the original work of the author and has not been submitted in whole or part for any other degree.

The author would like to officially register that part of the experimental work carried out in this thesis was carried out by the following individuals:

1. Dr. D.C. Apperley acquired the NMR spectra analised in this thesis;

2. Mr. C.P. Barker performed the experiments of depth profiling;

3. Ms. J. Hopkins carried out the permeability measurements.

The results arising from this work have been published , have been submitted, or will be submitted to the following papers (listed below with a reference number):

1. ***Title:*** *Plasma Polymerization of Hexamethyldisilane onto Polyethylene Film*

   Authors: Fonseca, J.L.C.; Badyal, J.P.S.

   Journal: *Macromolecules* **1992**, *25*, 4730.

2. ***Title:*** Plasma Enhanced Chemical Vapor Deposition of Bulk Organosilicon Solids Using Hexamethyldisilane Precursor

   Authors: Fonseca, J.L.C.; Apperley, D.C.; Badyal, J.P.S.

   Journal: *Chemistry of Materials* **1992**, *4*, 1271.

3. ***Title:*** Plasma Polymerisation of Tetramethylsilane

   Authors: Fonseca, J.L.C.; Apperley, D.C.; Badyal, J.P.S.

   Journal: *Chemistry of Materials* **1993**, *5*, 1676.

4. ***Title:*** Application of Plasma Polymerized Hexamethyldisilane as Barrier Coating for Reactive ion Etching

   Authors: Fonseca, J.L.C.; Badyal, J.P.S.

   Journal: Proceedings of the 11th International Symposium on Plasma Chemistry, Loughborough, August 1993, page 927.

5. ***Title:*** Plasma Polymerization of Hexamethyldisilane and Tetramethylsilane Precursors

   Authors: Fonseca, J.L.C.; Apperley, D.C.; Badyal, J.P.S.

   Journal: Proceedings of the 11th International Symposium on Plasma Chemistry, Loughborough, August 1993, page 1098.

6. ***Title:*** The Growth and Reactive Ion Etching of Organosilicon Plasma Polymers
   Authors: Fonseca, J.L.C.; Tasker, S.; Barker, C.P.; Badyal, J.P.S.
   Journal: Proceedings of the International Symposium on Plasma Polymerization / Deposition: Fundamental and Applied Aspects, Las Vegas, November 1993, page 20 (abstract).

7. ***Title:*** Glow Discharge Oxidation of Plasma Polymerised Organosilicon Layers
   ***Authors*:** Fonseca, J.L.C., Barker, C.P.; Hopkins, J.; Badyal, J.P.S.
   Journal: *Chemistry of Materials*, submitted.

8. ***Title:*** Glow Discharge Oxidation of Polycyclohexylmethylsilane and Polyphenylmethylsilane Thin Films.
   Authors: Fonseca, J.L.C., Barker, C.P.; Badyal, J.P.S.

The author officially recognises that this thesis contains reproduced text from the mentioned papers. The reproduced parts are listed below:

- Sections 2.2.2, 2.3.2, 2.4.2, 2.5.2, and 2.6.2 are reproduced from the experimental sections of papers [1] to [8];
- Chapter 3 is reproduced from the experimental, discussion and conclusion sections of paper [3];
- Chapter 4 is reproduced from the experimental, discussion and conclusion sections of papers [1] and [2];
- Chapter 5 is reproduced from the introduction, experimental, discussion, and conclusion sections of paper [7],
- Chapter 6 is reproduced from the experimental, discussion, and conclusion sections of paper [8].
- The first paragraph of Chapter 7 is reproduced from paper [3]; the second paragraph at page 153 is reproduced from paper [2].

- All figures from Chapter 3 to Chapter 7 are reproduced from papers [1] to [8]

Summary

Non-equilibrium glow discharge polymerisation is an attractive rout for the dry deposition of organosilicon layers. Such coatings have potential uses as biocompatible interfaces and photolithographic masks. In this thesis, the plasma polymerisation of the structurally related tetramethylsilane (TMS) and hexamethyldisilane (HMDS) monomers is described under identical experimental conditions. This approach offers the scope for mechanistic conclusions to be drawn.

Emission Spectroscopy, X-ray Photoelectron Spectroscopy (XPS), Solid State Nuclear Magnetic Resonance (Solid State NMR), Attenuated Total Reflection Fourier Transform Infrared Spectroscopy (ATR-FTIR), and Atomic Force Microscopy (AFM) have been used to study the plasma polymerisation of both carbosilicon monomers. The resultant plasma polymers consist of a network of -Si(CHx)y- groups. Hexamethyldisilane is found to be more reactive monomer and this has been attributed to the presence of the Si-Si bond in the HMDS molecule. Emission spectroscopy showed that hydrogen was the predominant by-product. In the case of the tetramethylsilane precursor, a higher concentration of conjugated species was detected in the plasma phase and also within the deposited layer.

Longer periods of plasma polymerisation result in the formation of a fine powder. These bulk materials were analysed by XPS, FTIR, and Solid State NMR. Prolonged exposure to air results in the incorporation of alcohol, ether, Si-O-C, Si-O-Si, and Si-OH functionalities into the plasma polymer network.

Finally, both types of organosilicon plasma polymer were evaluated as reactive oxygen etch barriers, and compared with conventional polysilane photoresists (polycyclohexylmethylsilane and polyphenylmethylsilane). Emission spectroscopy and XPS showed that the organosilicon plasma polymers behave as efficient reactive oxygen ion etch barriers, and offer the advantage of being capable of being deposited in a dry process step.

Contents

Chapter One: Introduction 1

1.1. General considerations about discharge plasmas 2

1.2. Glow discharge plasmas 3

1.3. Examples of plasma processes 7

1.4. Plasma polymerisation 10

1.5. Organosilanes as gases for plasma assisted processes 14

1.6. Objective of this work 16

Chapter Two: Experimental techniques 22

2.1. Introduction 23

2.2. Emission Spectroscopy 25

2.2.1. Main principles 25

2.2.2. Experimental set up 30

2.3. X-ray Photoelectron Spectroscopy 31

2.3.1. Main principles 31

2.3.2. Experimental set up 37

2.4. ATR-FTIR Spectroscopy 37

2.4.1. Main principles 37

2.4.2. Experimental set up 40

2.5. Solid State Nuclear Magnetic Resonance 41

2.5.1. Main principles 41

2.5.2. Experimental set up 47

2.6. Atomic Force Microscopy 47

2.6.1. Main principles 47

2.6.2. Experimental set up 47

2.7. Other techniques used in this work 50

2.7.1. Permeation measurements 50

2.7.2. Elemental analysis (CHN) 51

2.7.3. X-ray diffraction 51

Chapter Three: Plasma Polymerisation of Tetramethylsilane 56

3.1. Introduction 57

3.2. Experimental: Reactor set up 60

3.3. Results 60

3.3.1. X-ray Photoelectron Spectroscopy 60

3.3.2. Fourier Transform Infrared Spectroscopy 65

3.3.3. Solid State NMR 71

3.3.4. Emission Spectroscopy 74

3.4. Discussion 77

3.5. Conclusions 79

Chapter Four: Plasma polymerisation Hexamethyldisilane 83

4.1. Introduction 84

4.2. Experimental 84

4.3. Results 84

4.3.1. X-ray Photoelectron Spectroscopy 85

4.3.2. Fourier Transform Infrared Spectroscopy 92

4.3.3. Solid State NMR 99

4.3.4. Emission Spectroscopy 103

4.4. Discussion 105

4.5. Conclusions 107

Chapter Five: Glow discharge oxidation of plasma polymerised organosilicon layers 109

5.1. Introduction 110

5.2. Experimental 111

5.3. Results 111

5.3.1. X-ray Photoelectron Spectroscopy 111

5.3.2. ATR-FTIR Spectroscopy 119

5.3.3. Atomic Force Microscopy 122

5.3.4. Emission Spectroscopy 122

5.3.5. Gas Permeation 130

5.4. Discussion 130

5.5. Conclusions 131

Chapter Six: Glow discharge oxidation of polycyclohexylmethylsilane and polyphenylmethylsilane thin films 134

6.1. Introduction 135

6.2. Experimental 135

6.3. Results 136

6.3.1. X-ray Photoelectron Spectroscopy 136

6.3.2. Fourier Transform Infrared Spectroscopy 142

6.3.3. Emission Spectroscopy 142

6.4. Discussion 146

6.5. Conclusions 147

Chapter Seven: Final Discussion and Conclusions 149

Appendix: Research Colloquia given at Durham University from March 1991 to March 1994. 155

Chapter One

INTRODUCTION

Contents

1.1. General considerations about discharge plasmas 2

1.2. Glow discharge plasmas 3

1.3. Examples of plasma processes 7

1.4. Plasma polymerisation 10

1.5. Organosilanes as gases for plasma assisted processes 14

1.6. Objective of this work 16

1.1. General considerations about discharge plasmas

During the 1920's Irving Langmuir was studying various types of mercury-vapour discharges, and he noticed similarities in their structure - near the boundaries as well as in the main body of the discharge. While the region immediately adjacent to a wall or electrode was already called a "sheath", there was no name for the quasi-neutral matter filling most of the discharge space. He decided to call it "plasma".

Colleagues working with him at the General Electric Research Laboratory[1] acknowledged that he related the term to blood plasma. One version of the story has been that the similarity was in carrying particles, while another account speculated that it originated from the Greek term, meaning "to mould", since the glowing discharge usually moulded itself to the shape of the container.

Plasmas are conductive and, as a result, can respond to local changes in potential. The distance over which a small potential can perturb a plasma is known as the self shielding or Debye length. The Debye length is found to be[2]

$$\lambda_D = \sqrt{\frac{\varepsilon_0 k T_e}{4\pi n_e^2}} \quad (1.1)$$

where ε_0 is the permittivity of free space, kT is a term describing the electron energy, and n and e are the electron density and charge, respectively.

The field of plasma chemistry deals with the occurrence of chemical reactions in a partially ionised gas composed of ions, electrons, photons and neutral species. This state of matter can be produced through the action of either very high temperatures or strong electric or magnetic fields. In a discharge, free electrons gain energy from an imposed electric field and lose this energy through collisions with neutral gas molecules. The transfer of energy to the molecules leads to the formation of a variety of new species including metastables, atoms, free radicals, and ions. These products are all chemically active and thus can serve as precursors to the formation of new stable compounds.

There are many types of electric discharge and the properties of the plasma produced can differ widely. The plasma produced by arcs or plasma jets lead to an equilibrium situation in which the electron and gas temperature are nearly identical[3]. The very high gas temperatures (> 5000 K) measured in these plasmas make them very suitable for processing inorganic materials and organic compounds with very simple structures. More complex materials and polymers cannot be treated under these conditions since they would degrade rapidly.

Glow discharge plasmas are characterised by average electron energies of 1-10 eV and electron densities of 10^9-10^{12} cm^{-3}. An additional characteristic of such plasmas is the lack of equilibrium between the electron temperature T_e and the gas temperature T_g. Typical ratios for $\frac{T_e}{T_g}$ lie in the range of 10-100 [4]. The absence of thermal equilibrium makes it possible to obtain a plasma in which the gas temperature may be near ambient values at the same time that electrons are sufficiently energetic to cause rupture of molecular bonds. It is this characteristic which makes glow-discharge plasmas well suited for the promotion of chemical reactions involving thermally sensitive materials.

1.2. Glow Discharge Plasmas

The diagram of a typical non equilibrium plasma appears is Figure 1.1[5]. The wall (assumed to be a glass wall) provides electrical insulation and is sealed to isolate the plasma from the ambient. Power is supplied to the plasma from an external circuit, which consists of a voltage source in series with a "ballast" impedance. The ballast impedance is needed to limit the flow of current through the plasma, which generally has a "negative" impedance. This means that the voltage between the anode and cathode decreases when the current flowing through the plasma increases. The plasma itself is far from homogeneous Figure 1.1 identifies five distinct plasma regions, labelled *a* through *e*. These five regions are readily visible to the eye in many d.c. plasma systems.

The cathode dark space, region *a*, and the negative glow, region *b*, are the least well understood parts of the plasma. These regions are a consequence of the cathode's reluctance to provide electrons to the plasma. The cathode dark space is a region adjacent to the cathode through which current flows by virtue of a very large electric field. Part of the current is carried by electrons which are swept away from the cathode by the field. The remainder of the current is carried by positive ions which bombard the cathode surface to produce more electrons. The region is visibly dark, because there are few energetic electrons adjacent to the cathode surface capable of exciting atoms. The voltage drop through the region of high electric field is termed the cathode fall. The electrons which have left the cathode and been energised by the cathode fall accumulate and deposit their energy in the negative glow. This is a region of high electron density and intense excitation and ionisation. Since the negative glow contains ample electrons, very little electric field is needed to maintain the current through it. The value of the cathode fall voltage can vary from 10 V to 1 kV, depending on the current density at the cathode surface, the temperature of the cathode surface, and the gases and materials involved.

Following the Faraday dark space *c*, the positive column, region *d*, is a region some distance from the cathode characterised by axial uniformity and quasi-charge neutrality. The positive column may be made arbitrarily long, or eliminated entirely, by adjusting the distance from the anode to the cathode. Electrons, far more mobile than the equally numerous ions, are the dominant carriers of current. The pressure is sufficiently low that the dominant loss of electrons and ions is by diffusion to and recombination on the walls, rather than recombination in the plasma. The plasma establishes an electric field sufficiently high that new electrons created by ionisation are able to replace those lost to recombination. The electron density adjusts to the value needed to carry the electric current.

The anode fall, *e*, is a region in which the plasma properties are likely to be different from those in the positive column due to the influence of the anode. In many practical devices the anode has a smaller cross-sectional area than the positive column,

which leads to a plasma constriction and a rise in the electric field. Depending on the system, other regions can be visible: the cathode glow, the negative glow, the anode glow, etc.

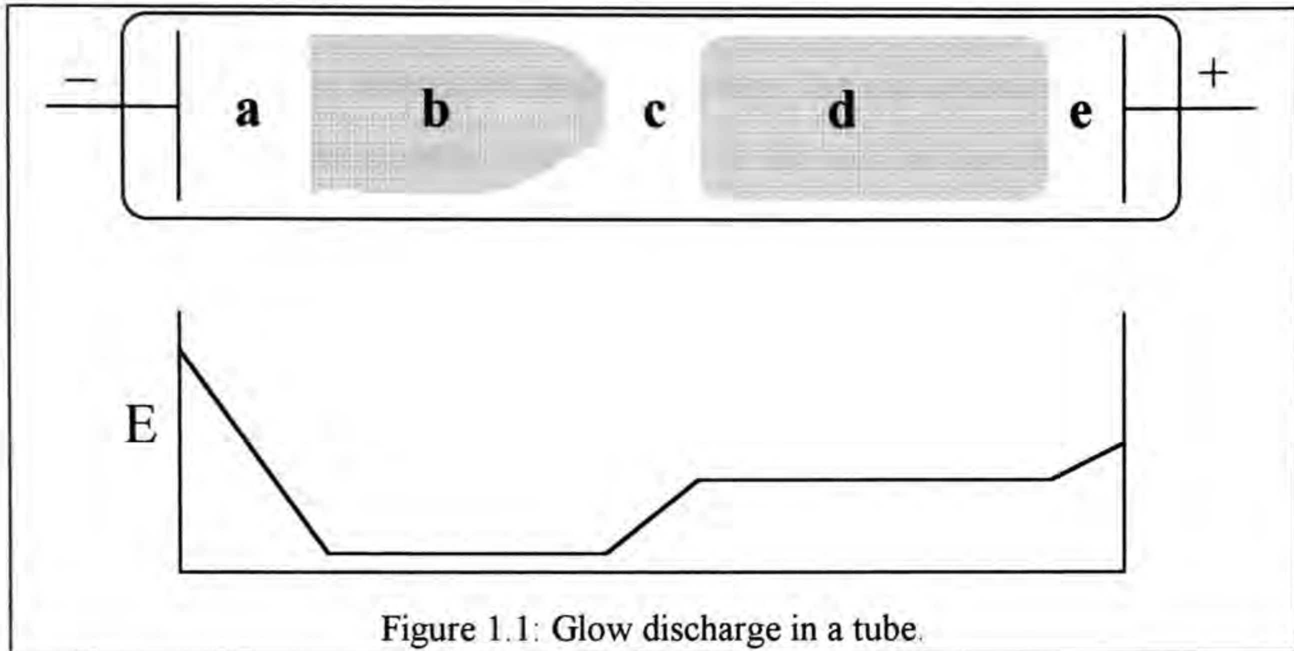

Figure 1.1: Glow discharge in a tube.

Electrons are the workhorses of non equilibrium plasmas. They gain kinetic energy from the electric field, and ideally lose most of that kinetic energy to inelastic collisions, resulting in new chemical species or exciting atomic/molecular levels which radiate photons. The electron temperature T_e defined in terms of the mean electron kinetic energy is generally within a factor of two of 1 eV = 11600 K. The electron density n_e is generally within an order of magnitude of 10^{12} cm^{-3} in the negative glow and positive column regions of these devices. For this density and T_e = 11600 K, the Debye length is

$$\lambda_D = \sqrt{\frac{kT_e}{4\pi n_e^2}} = 7\text{x}10^{-4} \text{ cm} \qquad (1.2)$$

Since the typical container diameter (laboratory conditions) is of the order of D = 1 cm, the plasma condition

$$\frac{\lambda_D}{D} << 1 \qquad (1.3)$$

is readily met, ensuring quasi-charge neutrality.

Regarding a.c. discharges, at frequencies above 1 MHz, direct contact between the electrodes and the plasma is no longer necessary. The energy can be fed indirectly by capacitive or inductive coupling (Figure 1.2). In the case of capacitive coupling, the electrodes enclose the plasma tube. For inductive coupling, the tube lies on the axis of the coil.

For work in normal unshielded laboratories, care must be taken not to interfere with radio or other equipment. Only certain frequency bands, e.g., the industrial frequencies, or radio-control frequencies, are permitted for scientific experiments. For plasma experiments, generators with fixed frequency (13.56 MHz is largely used) and adjustable power are preferred. In addition to the generator, it is necessary to have a matching network which transforms the impedance of the generator to that of the load. The proper matching of impedances is necessary to obtain an efficient coupling of power to the discharge. For laboratory purposes, transmitters with power output up to 300 W are usually sufficient.

The particular application often determines the pressure which is used[5a]. For example, in the sputter deposition of thin films, low pressures are required (no more than a few tens of millitorr, and often only a few millitorr) in order that the ions can traverse the sheath region between the glow discharge and target without losing significant kinetic energy (collisionless sheath). The low pressure is also needed to ensure that most of the material which is sputtered from the target can reach the substrates without being collisionally scattered to the walls of the vacuum chamber, or back to the target from which it came. When high-energy ion bombardment is not required, higher pressures can be used and, in fact, are necessary when large outputs of gas are needed.

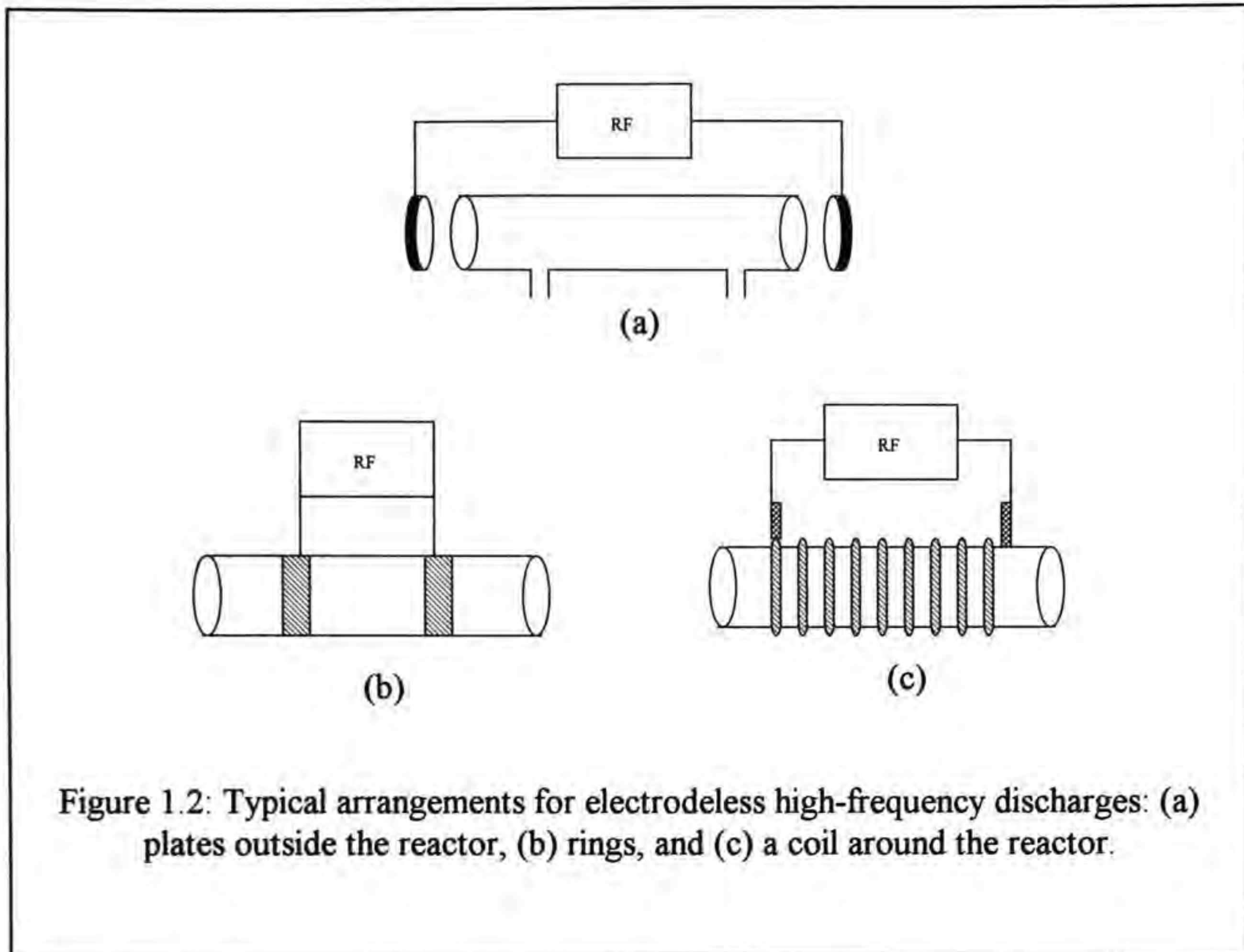

Figure 1.2: Typical arrangements for electrodeless high-frequency discharges: (a) plates outside the reactor, (b) rings, and (c) a coil around the reactor.

1.3. Examples of Plasma Processes

Nowadays plasma technology plays a very significant rule in industry processing of surfaces[6-17]. A few apparatus configurations that are used for some of the principal plasma-assisted deposition processes are schematically illustrated in Figure 1.3.

i. Glow Discharge Sputtering *a*, in which coating atoms are ejected from a target electrode as a consequence of the momentum exchange associated with the bombardment of ions from a plasma and condensed on suitably placed substrates, constitutes one of the oldest applications of plasmas in material processing[18,19]. Low pressure (0.1-10 Pa) inert gas plasmas (usually argon) are generally used. However, reactive sputtering, in which at least one species of a multicomponent coating is introduced in the gas phase has become increasingly more important[23].

ii. Ion Plating[20,21], *b*, is a process in which ion bombardment of the substrates, prior to deposition for substrate cleaning and during deposition for modifying coating properties, is accomplished by making the substrate(s) the cathode electrode of a low pressure (usually d.c.) plasma discharge in a mixture of the coating flux and an inert working gas (usually argon at about 4 Pa). The coating flux is usually provided by evaporation, as shown, but sputtering may be used. The working gas may contain active species (reactive plating)[22]. Ion plating is generally applied to metal coatings on metal substrates.

iii. In Activated Reactive Evaporation (ARE)[24,25], *c*, a plasma discharge is sustained in a flux of the evaporated material and a reactive gas. The dissociation and ionisation which are induced in the low pressure (1 - 5 Pa) reactive gas increase its reactivity on the surface of the growing coating and promote the formation of stoichiometric compounds. The plasma may be driven by a d.c. or an r.f. potential. ARE is commonly used for depositing metal oxides, carbides and nitrides.

iv. In Plasma Assisted (or Enhanced) Chemical Vapour Deposition[26,27] reactant gases are passed through a low pressure (1-1000 Pa) plasma discharge where dissociation, ionisation and gas phase reactions are induced which permit coatings to be deposited at much lower substrate temperatures than would be the case if the reactions were simply driven thermally by the hot substrates. Apparatuses with the configuration shown in Figure 1.3d, or the parallel plate arrangement shown in Figure 1.3e, are often used. The discharges are generally driven at frequencies in the range from 300 Hz to the microwave range, with 13.56 MHz being the most common. Plasma-assisted etching[28,29], essentially the inverse of PECVD is used in the fabrication of integrated circuits with small critical dimensions.

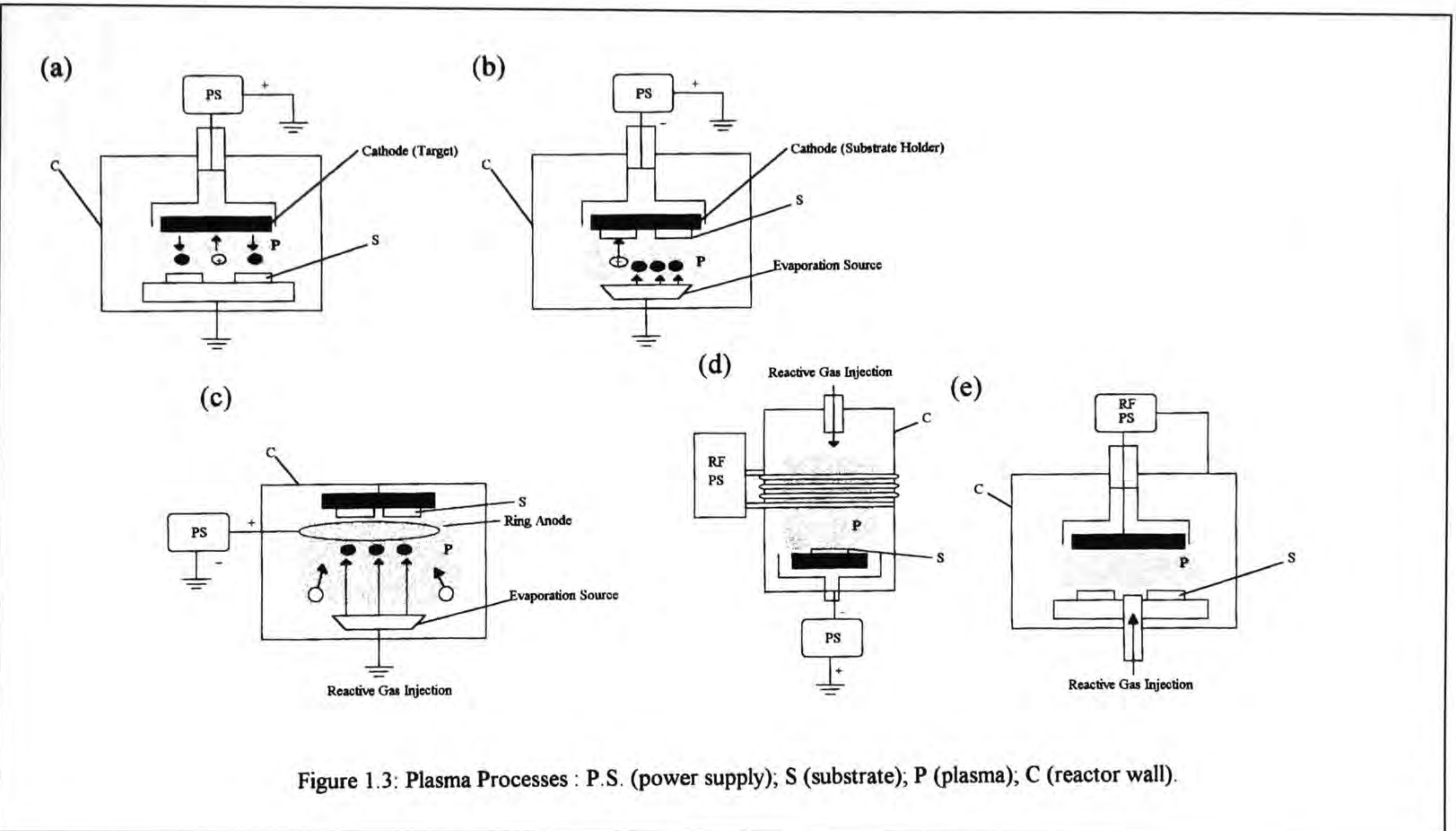

Figure 1.3: Plasma Processes : P.S. (power supply); S (substrate); P (plasma); C (reactor wall).

1.4. Plasma Polymerisation

The term plasma polymerisation is generally used as a way to distinguish between deposition on substrates maintained at ambient or near-ambient temperature (plasma polymerisation), or at elevated substrate temperatures (plasma enhanced chemical vapour deposition), being the result of a plasma polymerisation of eminently organic character, and the product of a PECVD process being usually inorganic.

Plasma polymerisation refers to the formation of polymeric materials by using either the plasma state of monomers or reactive species created in the plasma state[31-39]. Although the plasma state is generally identified by the ionisation of the gases, and ionisation is the essential step in creating plasmas, the population of ions in a low pressure plasma is small compared with that of neutral species[30].

Deposition of polymers from monomers in vacuum does not occur as in conventional polymerisation reactions. Due to a low ceiling temperature for polymerisation in vacuum, most polymerisations, such as addition polymerisation of vinyl monomers, do not yield materials with high enough molecular weight to be recognised as polymers. Plasma-state polymerisation seems to be an exception in which polymeric materials deposit from vacuum.

The species formation in vacuum can be explained by means of the scheme depicted in Figure 1.4[40]. In the scheme representation, M_x refers to an unexcited neutral species that can be the original monomer molecule or any dissociation product. Activated species capable of participating in chemical reactions to create a covalent bond are designed by $M\bullet$. Difunctional activated species are shown as $\bullet M\bullet$. Subscripts i, j and k merely indicate differences in the sizes of the species involved.

An important aspect of the polymer-forming mechanism is that the major reactions which lead to an increase in molecular size are the reactions between a reactive species and a molecule which constitute the propagation reaction in chain-growth polymerisation. As shown in Figure 1.4, the overall reaction contains two major routes to rapid step growth. Cycle I is via repeated activation of reaction products from

monofunctional activated species and the repeated reaction of these species. Cycle II is via difunctional or multifunctional activated species. Chain-growth polymerisation carried out by activated species, particularly free radicals, of certain monomers is possible under certain conditions; since such reactions as shown in (1) and (4) do not propagate in vacuum (low ceiling temperature), fraction (3) is a cross cycle reaction which converts a difunctional activated species into a monofunctional activated species.

Therefore, as soon as a plasma is created, the gas phase is no longer the vapour of the original monomer but becomes a complex mixture of the original monomer, ionised species, excited species of the original monomer, excited species of fragments from the monomer, and gas products that do not participate in polymer formation. Because the vacuum must be maintained by solid surfaces, the plasma also interacts with

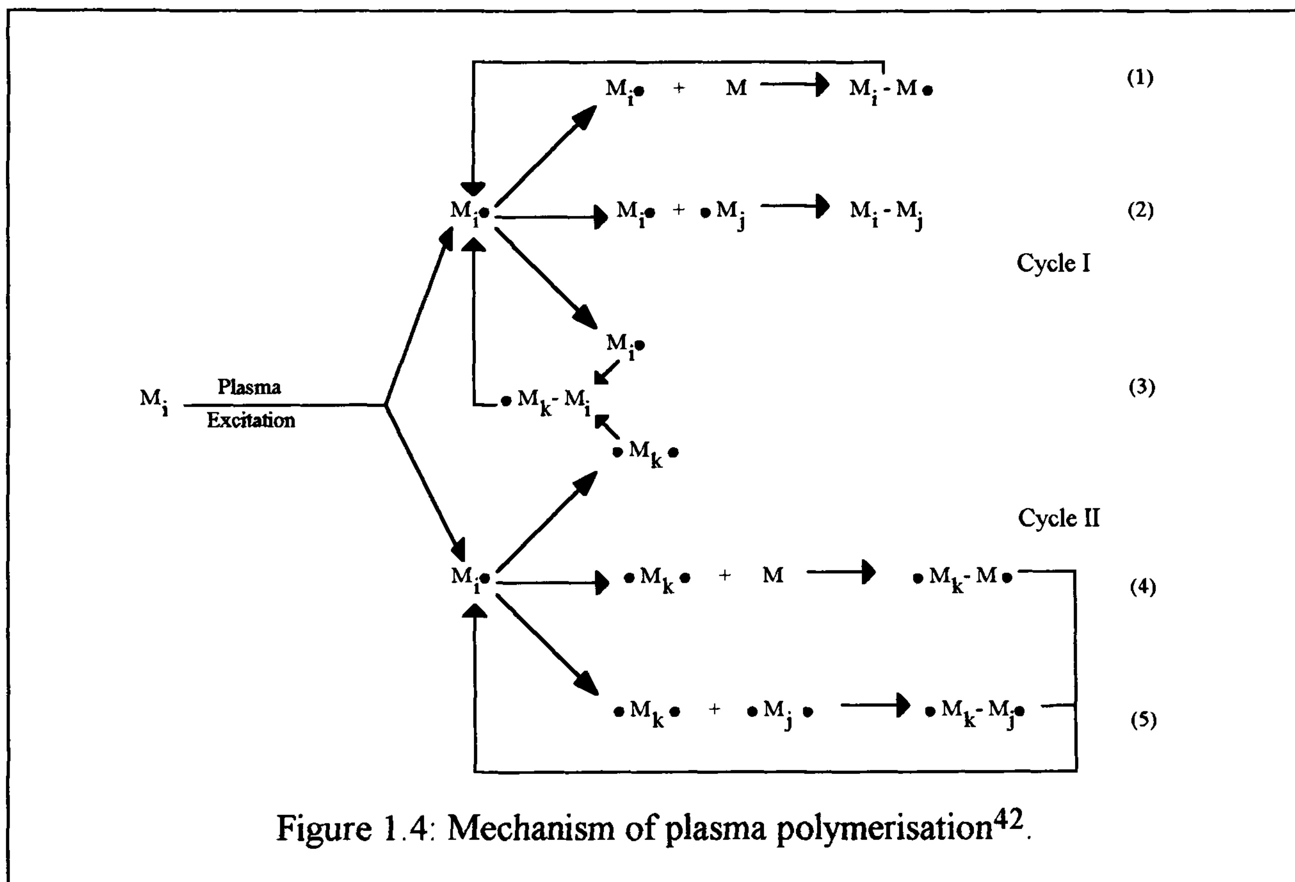

Figure 1.4: Mechanism of plasma polymerisation[42].

wall materials as well as any other materials that exist in the plasma, such as substrates and supports. So, polymer-forming intermediates and gas by-products may also originate from solid materials with which plasma interacts. In this sense, any material that reacts with plasma becomes a source of monomer for plasma polymerisation. In other words, the net polymerisation (or ablation, etching of the surface) will be a result of the balance between these processes, the so called CAP model (Competitive Ablation

Polymerisation)[41-45], which is depicted in Figure 1.5. One can easily visualise that plasma polymers formed following this route will possess high and randomically crosslinked structure, with trapped active centres (usually free radicals) and, as a consequence, completely different from conventional polymers.

It is important to recognise that the discharge power level described for plasma polymerisation is a system-dependent parameter. Once the molecules present in the plasma are broken and recombined at random (the equilibrium species being dependant on the stability - strength - of the formed molecular bonds), it is said that plasma assisted polymerisation obeys an atomic rule, not a molecular one[46-49]. So, when analysing a steady-state flow system, it is more convenient to work with mass flow rates than molecular ones. For a fixed geometry and pressure, if one wants to characterise the behaviour of a plasma in relation to power, one must be aware of the plasma power

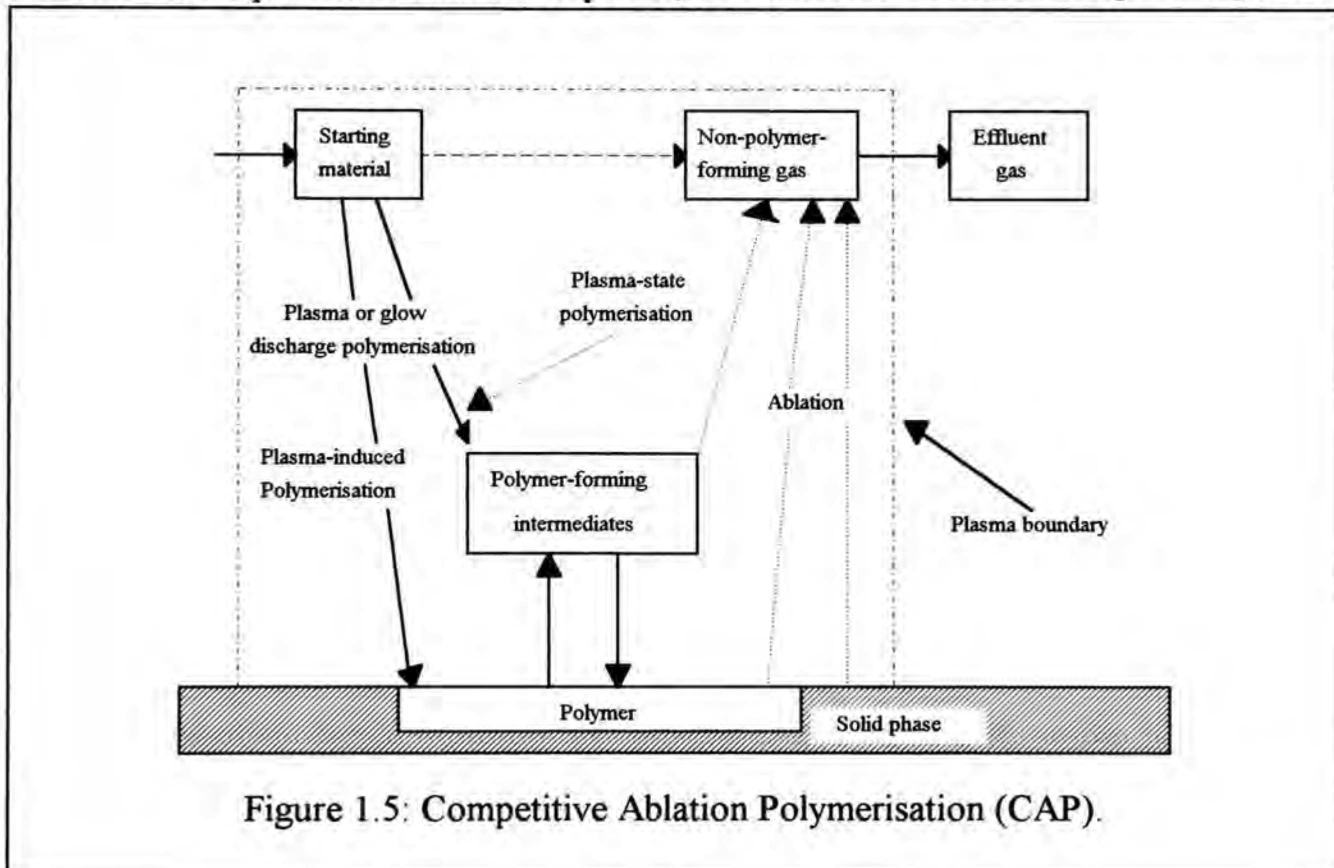

Figure 1.5: Competitive Ablation Polymerisation (CAP).

density, defined as $\frac{W}{F_M}$[46-49], where F_M is the mass flow rate and W the discharge power. In other words, the composite parameter $\frac{W}{F_M}$ represents the energy input per unit of mass of monomer.

The value of F_M can be estimated assuming the gas inside the reactor behaves as an ideal one[50]. For an ideal gas we have:

$$m = \left(\frac{MV}{RT}\right)P \tag{1.4}$$

where m is the mass of gas inside the reactor, M is the molecular weight of the gas, V is the volume of the reactor, R is the universal gas constant, T the gas temperature, and P the gas pressure.

In a reactor which is continually fed by monomer at a mass flow rate F_M, if one closes the outlet of the reactor to the pump at a time $t = 0$ (leaving the monomer inlet open), F_M is related to the increase of the pressure as it follows:

$$F_M = \frac{dm}{dt} = \left(\frac{MV}{RT}\right)\left.\frac{dP}{dt}\right|_{t=0} \tag{1.5}$$

If one estimates the value of $\left.\frac{dP}{dt}\right|_{t=0}$ as $\frac{\Delta P}{\Delta t}$ (the ratio between the change in pressure in the reactor and the time spent during this change), one has:

$$F_M \approx \left(\frac{MV}{RT}\right)\frac{\Delta P}{\Delta t} \tag{1.6}$$

The description of the reactor used in this thesis, as well as the experimental procedure used to obtain the data for equation (1.6) can be found in section 3.2 of Chapter 3.

1.5. Organosilanes as gases for plasma assisted processes

Since the earliest days of plasma chemistry, there has been keen interest in using organosilicon compounds for several reasons[51]:

1. Silicon is not only among the most abundant elements in the earth's crust (and therefore relatively cheap), but it can be ultra-purified to the sub-ppm or even ppb levels.
2. This chemical family, comprising many hundreds of compounds, includes several dozen which are sufficiently volatile near ambient temperature to be used with relative ease in normal plasma-chemical procedures;
3. Organosilicon compounds tend to be relatively non toxic, and they are generally of low flammability or non-flammable, relatively cheap, and available from commercial sources.
4. Conventional organosilicon polymers and elastomers play an important role in macromolecular science, both from the fundamental and applied points of view. It is therefore logical that researchers should be interested in exploring plasma-generated counterparts to these materials.
5. The natural chemical affinity between pure, single-crystalline silicon (c-Si) and organosilicon plasma polymers, since modern semiconductor technology is largely based on the use of silicon.

Si can also be doped, and it possesses a chemically stable oxide (SiO_2) which is among the best electrical insulating materials known. The ability to grow perfect thin SiO_2 by thermal oxidation of c-Si is largely responsible for the evolution of VLSI and ULSI (very- and ultra-large-scale integrated circuit) technologies, respectively. Plasma chemistry plays a major role in the fabrication of c-Si based VLSI technology[52,53]:

a. Plasma etching (or rather, "reactive ion etching", RIE) is the most practical way of directionally etching Si, its compounds, semiconductors, and various metals and polymers used in VLSI fabrication.

b. Plasma deposition (or rather, "plasma-enhanced chemical vapour deposition", PECVD) of inorganic silicon compounds silicon nitride, -oxide, and -oxynitride) from mixtures of silane (SiH_4), ammonia (NH_3), nitrogen, nitrous oxide (N_2O) or other gases and combinations thereof, is also indispensable to VLSI, for these materials are used in devices both as insulation and as passivating layers. PECVD has allowed processing temperatures to be lowered to the 250°C to 350°C range (compared with > 700°C for conventional CVD); an advantage of low temperature processing is that diffusive broadening of existing interfaces or junctions in devices is reduced to insignificance.

Needless to say, these inorganic compounds are chemically quite distinct from organosilicon plasma polymers. This distinction becomes somewhat less clear, however, in the case of amorphous "silicon carbide" films, prepared by PECVD from a suitable mixture of silane and a hydrocarbon: these thin film materials, symbolised by a-SiC:H, may have rather similar elemental composition to a plasma polymer grown from organosilanes[54-60], which are important in optical, biomedical applications, permeselective membranes and vapour barriers. Some of these monomers are listed in Table 1.1.

Table 1.1: some organosilicon compounds and their structural formulae.

Monomer	Structural formula
Tetramethylsilane	Me_4Si
Ethyltrimethylsilane	$EtSiMe_3$
Vinyltrimethylsilane	$H2C{=}CHSiMe_3$
Ethynyltrimethylsilane	$HC{\equiv}CSiMe_3$
Allyltrimethylsilane	$H_2C{=}CHCH_2SiMe_3$
Trimethylchlorosilane	Me_3SiCl
Phenylsilane	$PhSiH_3$
p-Chlorophenylsilane	$Cl\text{-}PhSiH_3$
Diphenylsilane	Ph_2SiH_2
Bis(trimethylsilyl)methane	$(Me_3Si)_2CH_2$
Disilylbenzene	$(H_3Si)_2C_6H_4$

1.6. Objective of this work

The emphasis in the study of the plasma polymerisation of hexamethyldisilane (HMDS) has been the determination of physical and chemical properties of HMDS derived films for different applications[61]. The objective of this work is to chemically characterise the plasma polymerisation of HMDS by means of the surface analysis of deposited films and plasma diagnostics. Since obtained results are system dependent, the deposition of hexamethyldisilane (HMDS) derived films will be compared to the deposition from TMS (tetramethylsilane) plasmas (monomer which has already been extensively studied[62-68]) under identical experimental conditions. Finally, a comparison between the performance of both plasma polymers and standard polysilanes as reactive ion etch barriers has been carried out.

References

1. Tonks, L., *Amer. J. Phys.* **1967**, *35*, 857.
2. Franklin, R., *Plasma Phenomena in Gas Discharges*, Chapter 1, Claredon Press: Oxford, 1976.
3. Dresvin, S.V.; Donskoi, A.V.; Goldfarb, V.M.; Klubnikin, V.S.; Dresvin, S.V., *Physics and Technology of Low-Temperature Plasmas*, Iowa University Press: Ames, 1977, page 284.
4. Dresvin, S.V.; Donskoi, A.V.; Goldfarb, V.M.; Klubnikin, V.S.; Dresvin, S.V., *Physics and Technology of Low-Temperature Plasmas*, Iowa University Press: Ames, 1977, page 369.
5. Franklin, R., *Plasma Phenomena in Gas Discharges*, Chapter 2, Claredon Press: Oxford, 1976.

5a. Coburn, J.W., *IEEE Trans. Plasma Sci.* **1991**, *19*, 1048.

6. Lukovsky, G.; Parsons, G.N., *Optoelectronics* **1990**, *24*, 119.
7. Parsons, G.N.; Tsu, D.V.; Wang, C.; Lucovsky, G., *J. Vac. Sci. Technol.* **1989**, *A7*, 1124.
8. Johnson, N.M.; Walker, J.; Doland, C.M.; Winer, K.; Street, R.A., *Appl. Phys. Lett.* **1989**, *54*, 1872.
9. Rudder, R.A.; Fountain, G.G.; Markunas, R.J., *J. Appl. Phys.* **1986**, *60*, 3519.
10. Postill, J.B; Rudder, R.A.; Hattangady, S.V.; Fountain, G.G.; Markunas, R.J., *Appl. Phys. Lett.* **1990**, *56*, 734.
11. Huelsman, A.D.; Zien, L.; Relf, R., *Appl. Phys. Lett.* **1988**, *52*, 726.
12. Tsu, D.V.; Parsons, G.N.; Lukovsky, G., *J. Vac. Sci. Technol.* **1988**, *A6*, 1849.
13. Tsu, D.V.; Lucovsky, G.; Mantini, M., *Phys. Rev.* **1985**, *B33*, 7069.
14. Rostaing, J.C.; Coeuret, F.; Drevillon, B.; Etemadi, R.; Godet, C.; Hul, J.; Parey, J.Y.; Yakolev, V.A., *Thin Solid Films* **1993**, *236*, 58.
15. Chen, L.J.; Hsia, S.T.; Chen, K.C., *Jpn. J. Appl. Phys.* **1993**, *1-32*, 6119.
16. Kim, Y.T.; Lee, C.W.; Min, S.K., *Jpn. J. Appl. Phys.* **1993**, *1-32*, 6126.

17. Huelsman, A.D.; Reif, R.; Fonstad, C.G., *Appl. Phys. Lett.* **1987**, *50*, 206.
18. Vessen, J.L.; Cuomo, J.J. , *Thin Film Processes*, Vossen, J.L.; Kern, W. (eds.), page 11, Academic Press: New York, 1978.
19. Thornton, J.A., *Deposition Technologies for Film Coatings*, Bunshah, R.F. et al. (eds.), page 244, Noyes: Park Ridges, NJ, 1982.
20. Matttox, D.M., *J. Vac. Sci. Technol.* **1973**, *10*, 47.
21. Mattox, D.M. in Bunshah, R.F. et al., *Deposition Technologies for Films and Coatings*, page 244, Noyes: Park Redge, NJ, 1982, 244.
22. Avaritsiotis, J.N.; Howson, R.P., *Thin Solid Films* **1981**, *80*, 63.
23. Moruzzi, J.L.; Kiermasz, A.; Eccleston, W., *Plasma Phys.* **1982**, *24*, 605.
24. Bunshah, R.F.; Raghuram, A.C. *J. Vac. Sci. Technol.* **1972**, *9*, 1385.
25. Bunshah, R.F., *Deposition Technologies for Films and Coatings*, Bunshah, R.F. *et al.* (eds.), Noyes: Park Ridge, NJ, 1982, 335.
26. Hollahan, J.R.; Rosler, R.S., *Thin Film Processes*, Vossen,L.; Kern, W. (eds), page 335, Academic Press: New York, 1978.
27. Bonifeld, T.D. in Bunshah, R.F. *et al.*, *Deposition Technologies for Films and Coatings*, page 365, Noyes: Park Ridge, NJ, 1982.
28. Colburn, J.W., *J. Vac. Sci. Technol.* **1982**, *21*, 557.
29. Flamm, D.L.; Donnely, V.M, *Plasma Chem. Plasma Proc.* **1981**, *1*, 317.
30. Nguyen, V.S.; Uderhill, J.; Fridman, s.; Pan, P., *J. Electrochem. Soc.* **1985**, *132*, 1925.
31. Clark, D.T., *J. Vac. Sci. Technol.* **1986**, *A4*, 1049.
32. Clark, D.T., *Pure & Appl. Chem.* **1985**, *57*, 941.
33. Favia, P. Caporiccio, G.; d'Agostino, R., *J. Polym. Sci., Polym. Chem. Ed.* **1994**, *32*, 121.
34. Matsuyama, H.; Kariya, A.; Teramoto, M., *J. Appl. Polym. Sci.* **1994**, *51*, 689.
35. Yamada, Y.; Kurobe, T., *Jpn. J. Appl. Phys.* **1993**, *1-32*, 5090.
36. Mattson, B.; Stenberg, B., *J. Appl. Polym. Sci.* **1993**, *50*, 1247.

37. Supiot, P.; Callebert, F.; Dessaux, O.; Goudnard, P., *Plasma Chem. Plasma Process.* **1993**, *13*, 539.

38. Csernica, J.; Prince, M., *Polymer* **1993**, *34*, 2670.

39. Munro, H.S.; Ward, R.J.; Davies, M.C.; Short, R.D., *Polymer* **1993**, *34*, 2250.

40. Yasuda, H. *J. Polym. Sci., Macromol. Rev.* **1981**, *16*, 199.

41. Yasuda, H.; Hsu, T., *J. Polym. Sci., Polym. Chem. Ed.* **1978**, *16*, 415.

42. Yasuda, H.; Hsu, T., *Surf. Sci.* **1978**, *76*, 232.

43. Masuoka, T.; Yasuda, H., *J. Polym. Sci., Polym. Chem. Ed.* **1981**, *19*, 2937.

44. Masuoka, T.; Yasuda, H., *J. Poly. Sci., Polym. Chem. Ed.* **1982**, *20*, 2633.

45. Yasuda, T.; Gaziki, M.; Yasuda, H., *J. Appl. Polym. Sci., Appl. Polym. Symp.* **1984**, *38*, 201.

46. Yasuda, H.; Hirotsu, T., *J. Appl. Polym. Sci.* **1978**, *22*, 1195.

47. Westwood, A.R., *Eur. Polym. J.* **1971**, *7*, 363.

48. Yasuda, H.; Hirotsu, T., *J. Polym. Sci., Polym. Chem. Ed.* **1978**, *16*, 743.

49. Yasuda, *Macromol. Rev.* **1981**, *16*, 199.

50. Roth, A., *Vacuum Technology*, Elsevier: Amsterdam, 1982, page 17.

51. Crossman, L.D.; Baker, J.A., *Polysilicon technology*, in *Semiconductor Silicon*, The Electrochemical Society: Pennington, N.J., 1977.

52. Sugano, T., *Applications of Plasma Processes to VLSI Technology*, Wiley: New York, 1985.

53. Einspruch, N.G.; Brown, D.M. (eds.), *VLSI Electronics Microstructure Science. Vol 8 Plasma Processing for VLSI*, Academic Press: New York, 1984.

54. Inagaki, N.; Yamazaki, H., *J. Appl. Polym. Sci.* **1984**, *29*, 1369.

55. Haller, I., *J. Electrochem. Soc.* **1982**, *129*, 180.

56. Olhafen, P.; Cutro, J.A.; Haller, I., *J. Electron. Spectrosc.* **1984**, *34*, 105.

57. Inagaki, N.; Kondo, S.; Hirata, M.; Urushibata, H., *J. Appl. Polym. Sci.* **1985**, *30*, 3385.

58. Vasile, M.J.; Smolinsky, G., *J. Electrochem. Soc.* **1972**, *119*, 451.

59. Sachdev, K.G.; Sachdev, H.S., *Thin Solid Films* **1983**, *107*, 245.

60. Inagaki, N., *Proc. ACS Div. of Polymeric Materials: Science and Engineering* **1987**, *56*, 797.

61. Wróbel, A.M.; Kowaski, J.; Grebowicz, J.; Kryszewski, M., *J. Macromol. Sci.-Chem.* **1982**, *A17*, 433.

62. Inagaki, N.; Koyama, M., *J. Polym. Sci., Polym. Chem. Ed.* **1983**, *21*, 183.

63. Hirotsu, T., *J. Appl. Polym. Sci.* **1979**, *24*, 1957.

64. Inagaki, N.; Nishio, Nishio, T.; Katsuura, K., *J. Polym. Sci., Polym. Lett. Ed.* **1980**, *18*, 765.

65. Inagaki, N.; Ohnishi, Y.; Chen, K.S., *J. Appl. Polym. Sci.* **1983**, *28*, 3629.

66. Inagaki, N.; Nejigaki, K.; Suzuki, K., *J. Polym. Sci. Polym. Chem. Ed.* **1983**, *21*, 3181.

67. Catherine, Y.; Zamouche,A., *Plasma Chem. Plasma Process.* **1985**, *5*, 353.

68. Inagaki, N.; Kishi, A., *J. Polym. Sci., Polym. Chem. Ed.* **1983**, *21*, 1847.

Chapter Two

EXPERIMENTAL TECHNIQUES

Contents

2.1. Introduction 23

2.2. Emission Spectroscopy 25

2.2.1. Main principles 25

2.2.2. Experimental set up 30

2.3. X-ray Photoelectron Spectroscopy 31

2.3.1. Main principles 31

2.3.2. Experimental set up 37

2.4. ATR-FTIR Spectroscopy 37

2.4.1. Main principles 37

2.4.2. Experimental set up 40

2.5. Solid State Nuclear Magnetic Resonance 41

2.5.1. Main principles 41

2.5.2. Experimental set up 47

2.6. Atomic Force Microscopy 47

2.6.1. Main principles 47

2.6.2. Experimental set up 50

2.7. Other techniques used in this work 50

2.7.1. Permeation measurements 50

2.7.2. Elemental analysis (CHN) 51

2.7.3. X-ray diffraction 51

2.1. Introduction

One can divide the methods of analysis used in plasma polymerisation into two groups: plasma diagnostics (which is for monitoring the gaseous phase) and surface or bulk methods (related to the characterisation of the solid products of plasma polymerisation).

Gas phase diagnostic in a glow discharge is a useful tool for studying plasma polymerisation mechanisms, particularly the initiation step, because it provides information on monomer fragmentation processes: for example, the identity of polymerisation precursors. The gas phase can be best analysed using mass spectroscopy and emission spectroscopy[1-11].

An indirect diagnostic method, the combined use of gas chromatography and mass spectroscopy techniques has been used to examine the gaseous reaction products from audio frequency glow discharges in a number of methylsiloxane and methylsilazane monomers[12-14]. In this technique, the species sampled from the reactor effluent were first separated by gas chromatography, following which they were identified by mass spectroscopy; it turned out that the method is sensitive to the detection of the light hydrocarbons rather than of heavier products.

There are only a few reports dealing with diagnostics of organosilicon plasmas with emission spectroscopy[15,16]. This technique has been used to examine rf plasmas of tetramethylsilane (TMS)[15] and of TMS/H_2 mixture[16].

In most plasma polymerisation experiments, one produces only very small quantities of solid product (plasma polymer), typically milligrams. Further, this material is generally insoluble in organic solvents due to its high degree of crosslinking. These factors greatly complicate the characterisation of plasma polymers by several analytical methods generally used for conventional polymers; instead, more sophisticated tools must be used. The structures of plasma polymers have been examined by numerous modern and "classical" techniques. These include infrared[17-20] and ultraviolet[21,22] absorption spectroscopies, Auger electron spectroscopy[23-26], X-ray photoelectron

spectroscopy[27-31], secondary ion mass spectroscopy[32,33], solid-state nuclear magnetic resonance spectroscopy[34], combined pyrolisis/gas chromatography/mass spectroscopy[35], electron spin resonance spectroscopy[36], X-ray diffraction[37,38], thermogravimetric analysis[39], transmission electron microscopy[40] and scanning electron microscopy[41].

Because when working with plasma polymers, one mainly works with surfaces, the most important methods, regarding the solid phase, are the photoelectric spectroscopies, IR spectroscopy (using the reflection mode of operation), as well as microscopy. However, depending on the amount of produced material, bulk sensitive methods can also be used.

The considerations above, as well as the availability of equipment, restricted the main methods used in the analysis of both plasma and solid phases to the following techniques:

1. Emission Spectroscopy (ES)
2. X-ray Photoelectron Spectroscopy (XPS)
3. Attenuated Total Reflection Fourier Transform Infrared (ATR-FTIR) Spectroscopy
4. Solid State Nuclear Magnetic Resonance (NMR) Spectroscopy
5. Atomic Force Microscopy (AFM)

The main principles of these methods (as well as the experimental set up used in this work - apart from the deposition equipment, which is described in section 3.2 of Chapter 3) are, therefore, explored in the next sections. Additionally, brief information about experimental methods used in a lower scale (X-ray diffraction, permeation experiments, and elemental analysis) are described in this chapter.

2.2. Emission Spectroscopy

2.2.1. Main principles

Atomic emission spectroscopy is closely related to the early developments of quantum mechanics[42-44]: the occurrence of discrete lines in the emission spectrum of atomic hydrogen, first observed by Balmer in 1885, indicated one of the first flaws in classical physics.

Following the developments of Planck and Einstein, in 1913 Bohr created the first atomic quantum theory for atoms (or ions) with 1 electron. This theory originated a variation from Sommerfeld: while Bohr's hydrogen atom had an electron performing circular orbits around the nucleus, the later theory presented the possibility of elliptical ones.

After de Broglie proposed that with any moving body there is associated a wave (1924), Born related this wave to a probability density and Shrödinger postulated the fundamental law of quantum mechanics:

$$H\psi = E\psi \tag{2.1}$$

where H is the Hamiltonian operator (related to the sum of kinetic and potential energy of the particle):

$$H = -\frac{\hbar}{2m}\left(\frac{\partial^2}{\partial x^2}+\frac{\partial^2}{\partial y^2}+\frac{\partial^2}{\partial z^2}\right)+V \tag{2.2}$$

E is total energy of the particle, m is the mass of the particle, V is its potential energy and ψ is the wave function associated to the particle, being the product $\psi\psi^*$ (where ψ^* is the complex conjugate of ψ) associated to the probability density (dP) in the following way:

$$dP = \psi\psi^* \, d\tau \tag{2.3}$$

where $d\tau$ is an infinitesimal element of volume.

With the formulation of the uncertainty principle by Heisenberg (1927) and the contribution of Dirac (1928) - accounting for relativistic effects in the Shrödinger equation - the basic tools for the developing of spectroscopic theories, as we know today, were firmly established. Calculations of orbitals, terms, and states of polyelectronic atoms were then carried out mainly through the approximate method of solution of the Shrödinger equation devised by Hartree, the self-consistent (SFC) method.

When analysing molecules, usually use is made of the Born-Oppeinheimer approximation:

$$\psi = \psi_e \psi_v \psi_r \qquad (2.4a)$$

and

$$E = E_e + E_v + E_r \qquad (2.4b)$$

where the indices e, v and r denote electronic, vibrational and rotational, (total energy - E - or wave function - ψ) respectively. This approximation makes possible the treatment of emission spectroscopy (and all other kinds of electronic spectroscopy) easier, since electronic, vibrational, and rotational analysis can be carried out separately.

Figure 2.1 shows a typical potential energy diagram for an electronic transition in a diatomic molecule (absorption). Here the vibrational energy levels are shown, but not the rotational levels. If the experiment is carried out at room temperature, then only the $\upsilon = 0$ level of the lower state will be appreciably populated. In electronic spectra, there is no simple selection rule governing the change in vibrational quantum number, so transitions to all the vibrational levels of the upper state may be observed in principle. Thus at low resolution the absorption spectrum will consist of a series of peaks, corresponding to the vibrational transitions $0 \rightarrow 0$, $0 \rightarrow 1$, $0 \rightarrow 2$, etc.

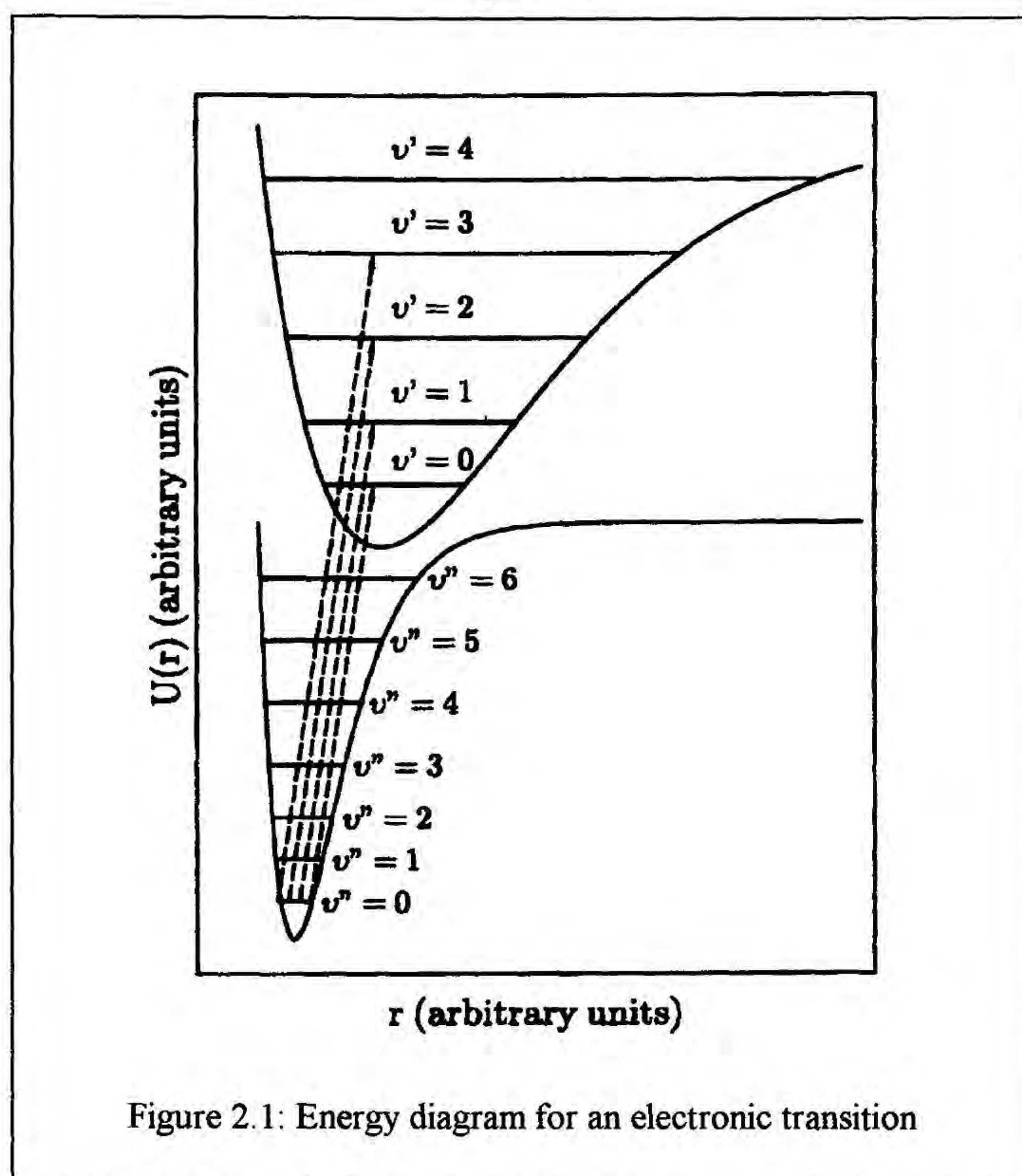

Figure 2.1: Energy diagram for an electronic transition

The differences in vibrational energy in the upper state between the levels with quantum numbers υ and 0 is

$$\Delta E_{vib} = h\nu_{vib}\upsilon - xh\nu_{vib}\upsilon(\upsilon+1) \tag{2.5}$$

Therefore the frequencies of the peaks in the electronic spectrum are given by

$$\nu = \nu_{00} + \nu_{vib} - \nu_{vib}x\upsilon(\upsilon+1) \tag{2.6}$$

where ν_{00} is the frequency of the $0 \rightarrow 0$ transition and x is the anharmonicity constant.

If each of the peaks in the electronic spectrum is studied at higher resolution, it is found to consist of a series of lines, which is due to changes in the rotational quantum

number. The structure is very similar to that seen in infrared spectroscopy. P and R branches ($\Delta J = -1$ and $+1$) are observed for all diatomic molecules; Q branches ($\Delta J = 0$) are observed only if there is a change in electronic orbital angular momentum between the two states.

The equation giving the frequencies of lines in the R branch is

$$h\nu = \Delta E = \Delta E_{el} + \Delta E_{vib} + 2B' + (B' - B'')J^2 + (3B - B'')J \tag{2.7}$$

where $B = \dfrac{h^2}{8\pi^2 \mu r^2}$, μ is the reduced mass, and r the distance between the two atoms centres.

Thus for low values of J the lines are roughly equally spaced, but as J increases the J^2 term causes the lines to converge, as in vibrational spectra $B'' > B'$. However, this convergence is slow, and not observed in many cases. In electronic spectra, the difference between B' and B'' may be very much larger, as the internuclear separations in different electronic states can be widely different. If the internuclear separation is greater in the upper state, then $B' < B''$ ($B \propto 1/r^2$), and the R branch will show a band-head. This is shown in Figure 2.2b. Thus the observation of band-heads immediately tells us whether the internuclear separation is larger in the ground state or in the upper state, and this in turn suggests whether a bonding electron (producing an increase in bond length) or an antibonding electron (producing a decrease in the bond length) is being excited. A band such as that shown in Figure 2.2b shows a definite cut-off at high frequencies and a tail at low frequencies, and is said to be red-degraded. One such as in Figure 2.2a, where the tail is now towards high frequencies (the blue end of the spectrum), is said to be blue-degraded or violet-degraded.

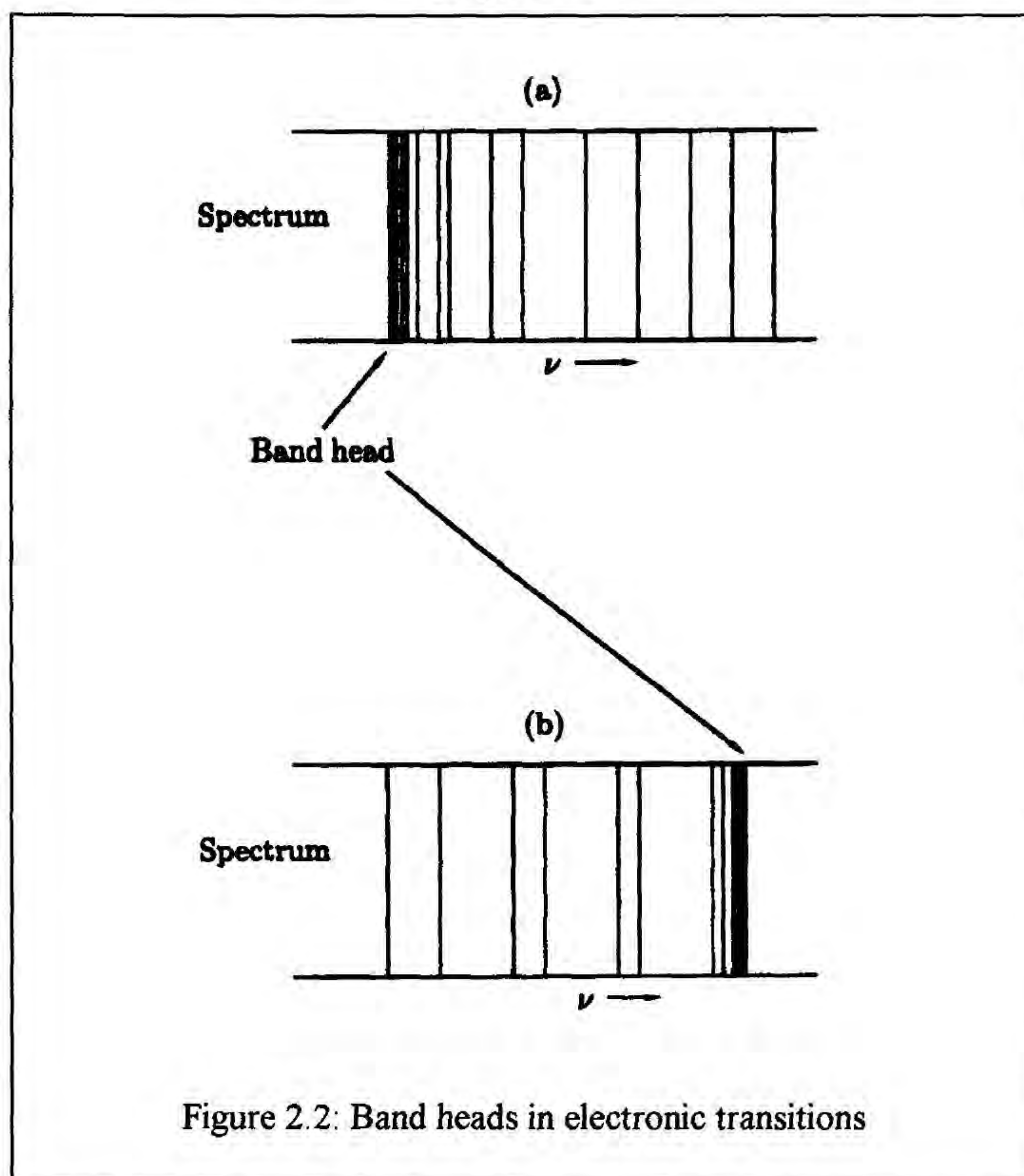

Figure 2.2: Band heads in electronic transitions

Electronic spectra are frequently observed in emission rather than absorption; as electronic excitation energies are typically much larger than thermal energies, at room temperature, it is necessary to provide energy to raise molecules to their excited states. This is commonly achieved by electric discharges or by simple heating.

The general appearance of an emission spectrum is more complex than that of the corresponding absorption spectrum, even if only one electronic transition is considered. In the absorption experiment, normally only the lowest vibrational energy level is occupied, whereas in emission experiments it is common for many vibrational levels to be occupied. This difference is illustrated in Figure 2.3. On the other hand, it can be an advantage, since it is possible to observe transitions between several electronic states.

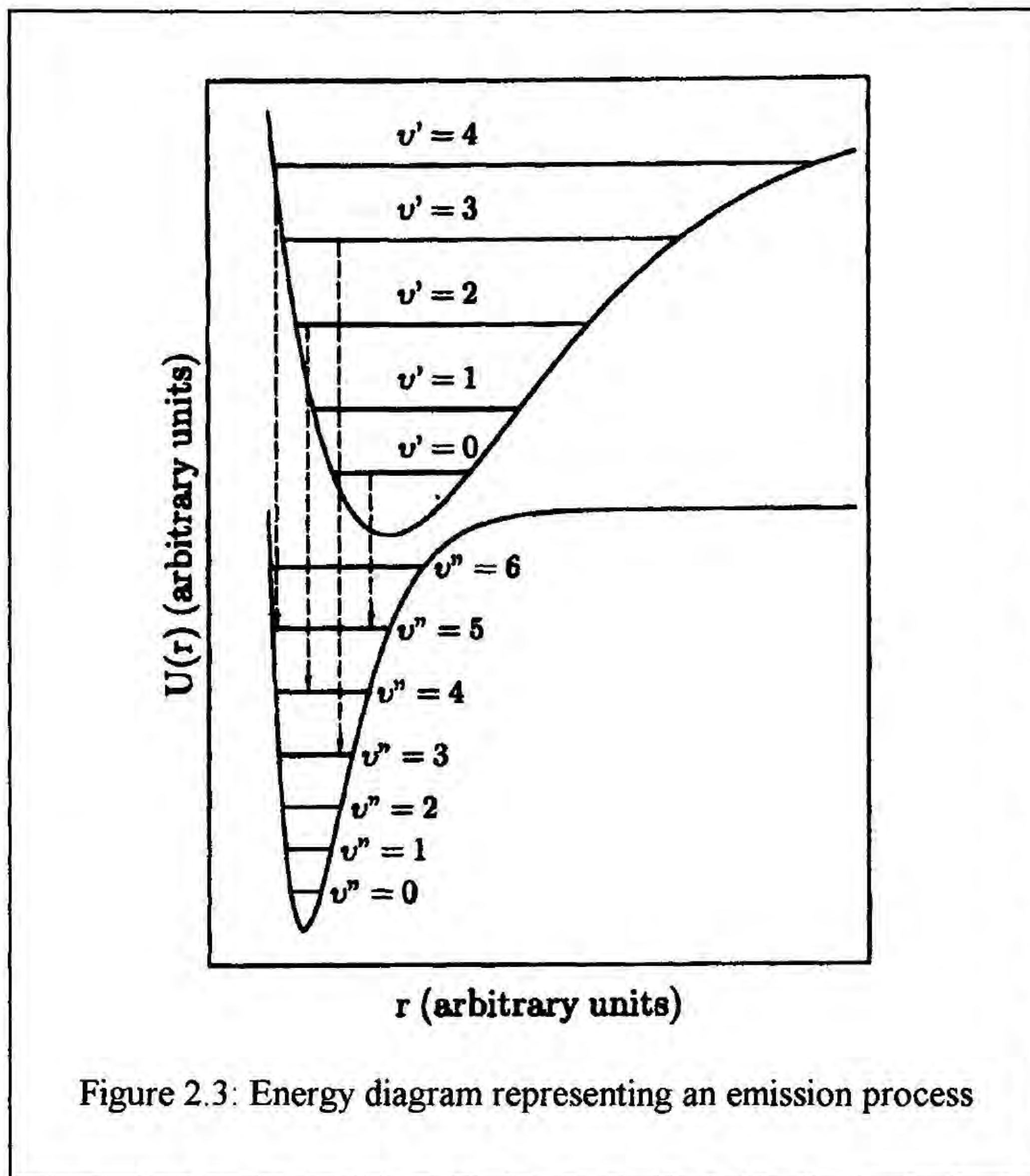

Figure 2.3: Energy diagram representing an emission process

2.2.2. Experimental set up

In this work, a computer controlled UV emission spectrometer based upon a Czerny-Turner type monochromator was used for plasma glow analysis. The reactor was coupled to it via a quartz window. This instrument could scan the spectrum continuously from 180 to 500 nm at 0.5 nm resolution.

2.3. X-ray Photoelectron Spectroscopy

2.3.1. Main principles

X-ray Photoelectron Spectroscopy (XPS) is based on the following principle[45,46]:

- Monochromatic short wavelength radiation is used in order to detach electrons from the sample, the kinetic energy of the electrons being measured by means of an electron analyser. The difference in energy between the exciting photons of frequency ν and the electrons detached (E_{kin}) is equal to the binding energy of the electron.

$$E_B = h\nu - E_{kin} \quad (2.8)$$

The XPS spectrum therefore gives information about the binding energies or ionisation energies of electrons in the sample investigated. According to the Koopman's Theorem[47], the ionisation energies describe the sequence of atomic or molecular orbitals quantitatively. This is shown schematically in Figure 2.4 for two orbitals 1 and 2 of different energy, separated by I_1 and I_2 from the zero level of energy, attributed arbitrarily to the detached electron without surplus kinetic energy and outside the attractive potential of the positive ion left during ionisation. The ionisation energies measured by XPS are one-electron ionisation energies.

Depending on the magnitude of hv, two experimental variants of electron spectroscopy can be distinguished[48]:

1. excitation in the far-UV ($h\nu \approx 20$ eV): this method is often called Ultra Violet Photo Electron Spectroscopy (UPS);
2. X-ray excitation ($h\nu \approx 1500$ eV): XPS. Using this high energy excitation, even firmly bound core electrons can be detached.

In solids, the detached electrons are rapidly thermalised, at least in the bulk (Figure 2.5) of the sample. Within a very thin surface layer, however, of the order of $\delta \approx 2$ nm, the electrons are allowed to leave the surface without loss in kinetic energy, so that Equation (2.8) can be applied. Hence XPS is uniquely suited for studying surfaces.

The block diagram in Figure 2.6 shows the most important parts of an XPS spectrometer. The X-ray sources most commonly used are MgK_{α} (1253.7 eV, 0.99 nm) and AlK_{α} (1486.6 eV, 0.83 nm). The sample (film or powder) is kept under vacuum of about 10^{-5} Pa on a sample holder. The kinetic energy of the electrons detached is determined in most commercial instruments using a double-focusing electrostatic analyser. The number of electrons of a given energy is counted and recorded as a function of their kinetic energy.

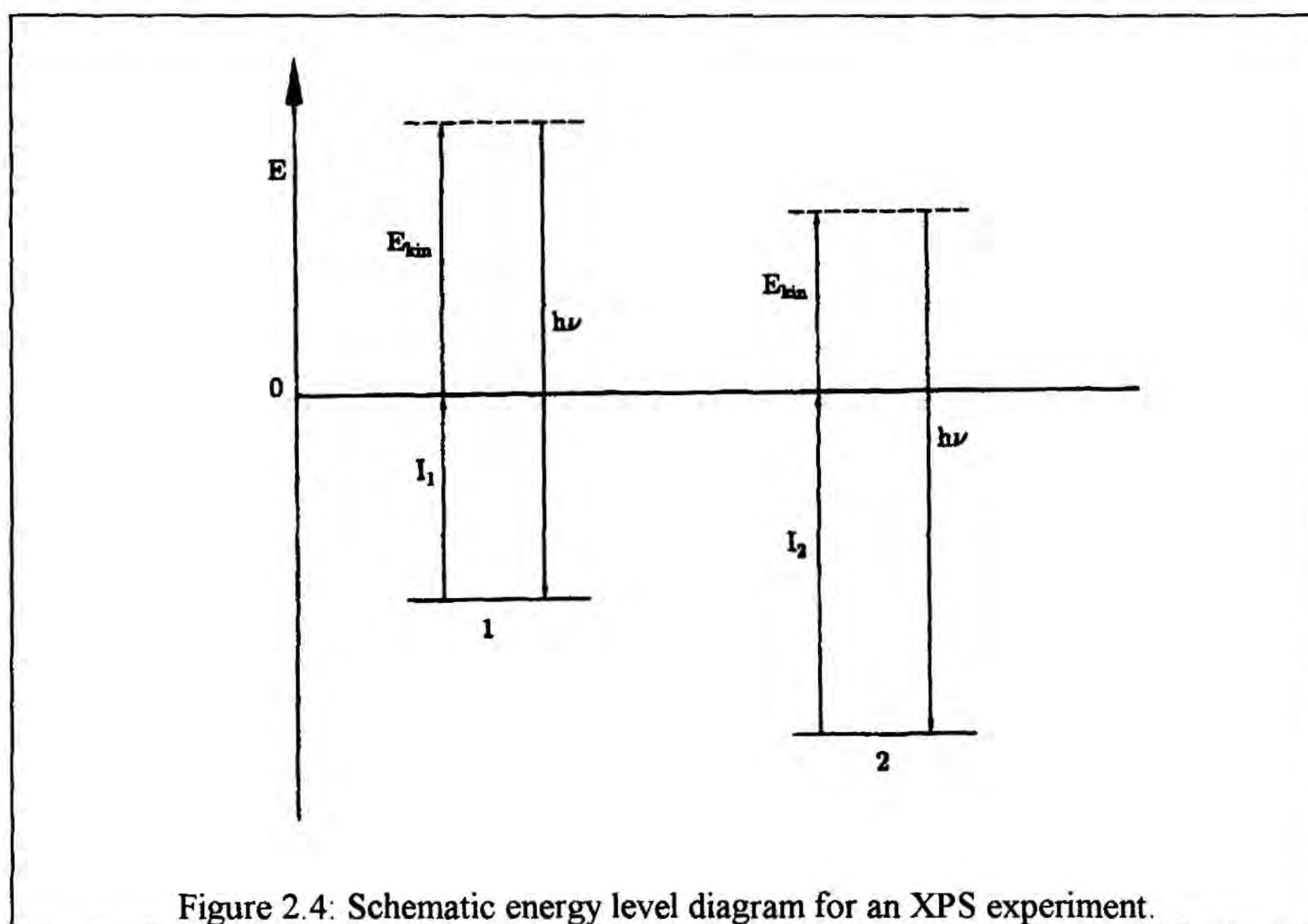

Figure 2.4: Schematic energy level diagram for an XPS experiment.

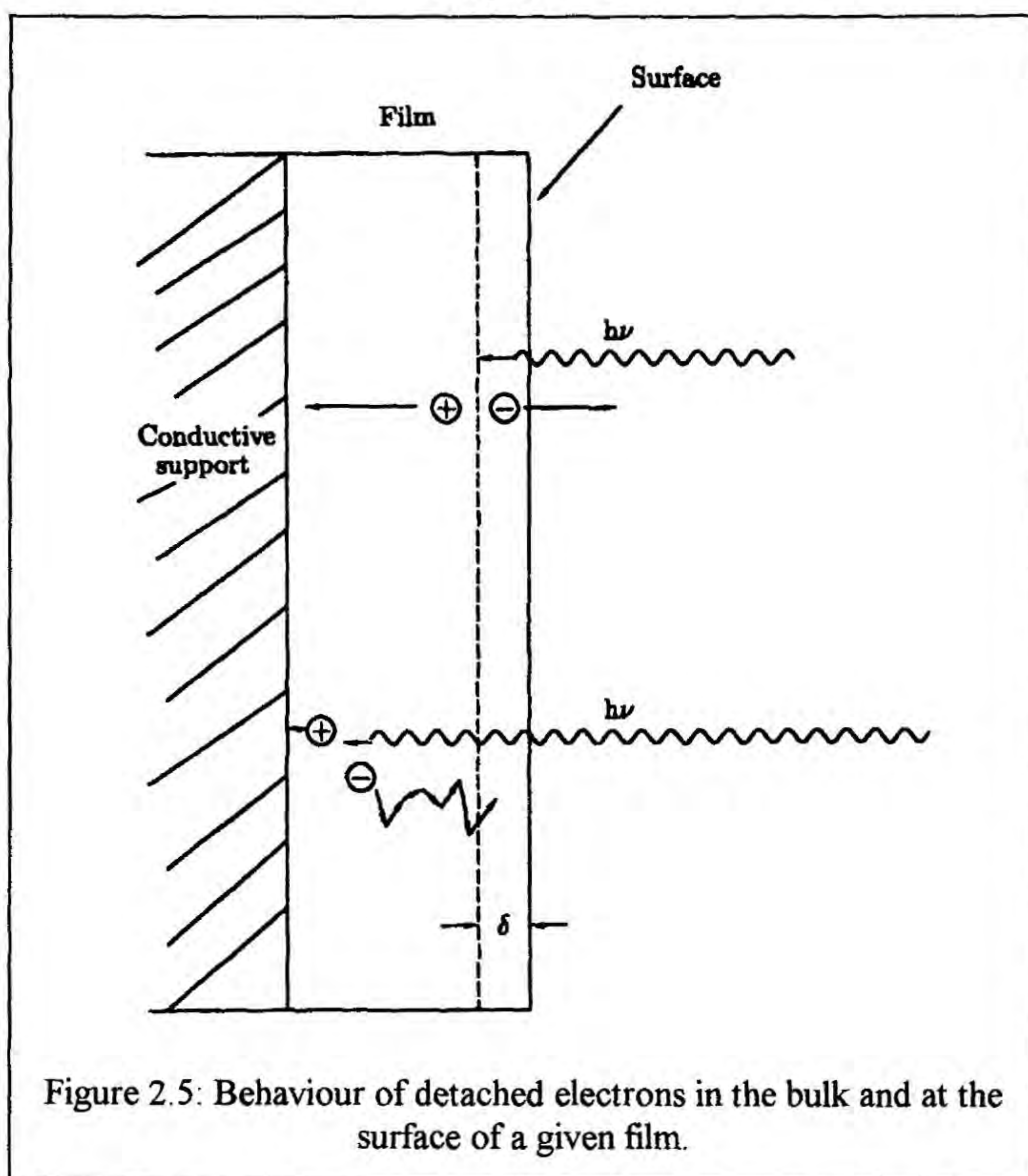

Figure 2.5: Behaviour of detached electrons in the bulk and at the surface of a given film.

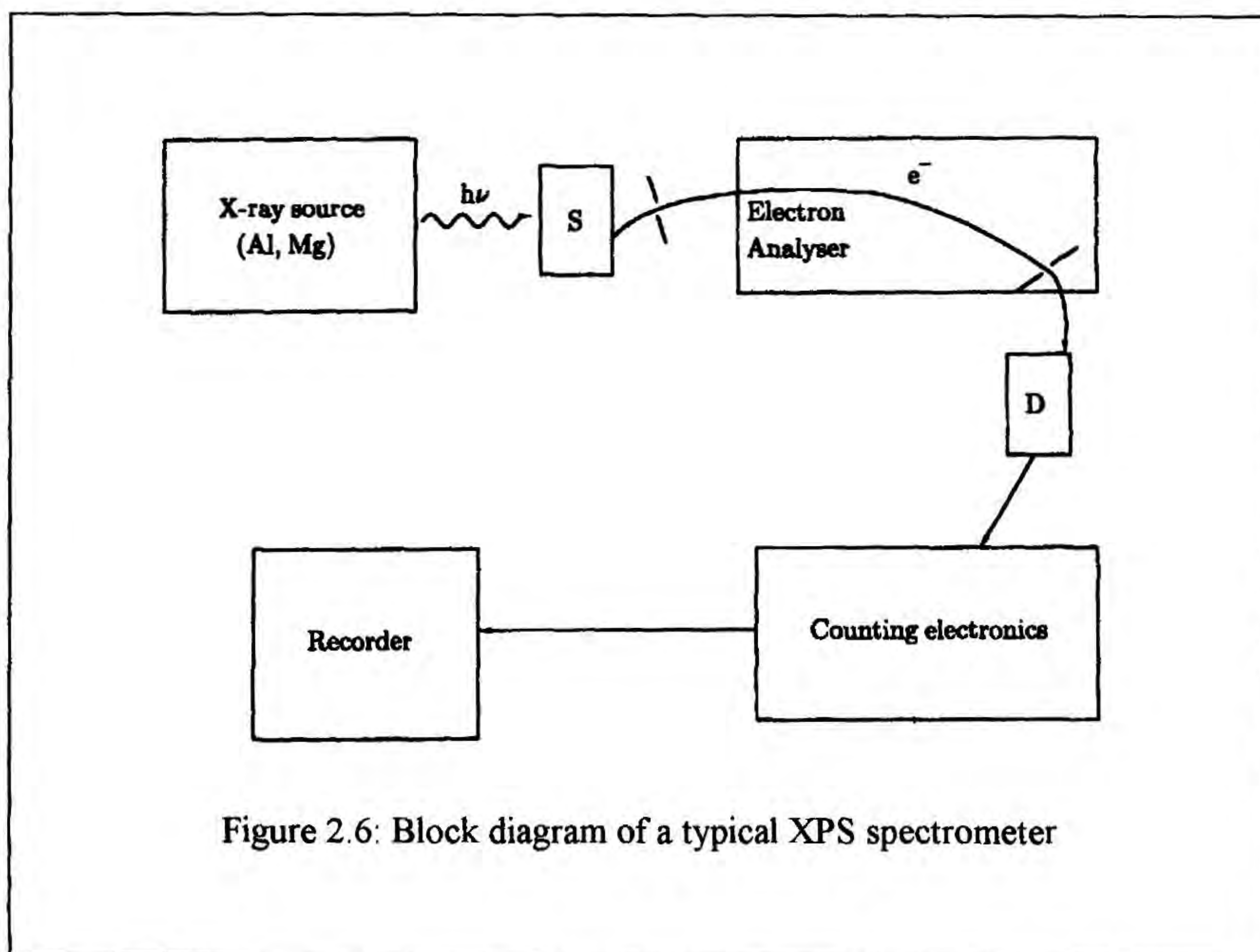

Figure 2.6: Block diagram of a typical XPS spectrometer

The electrons detached and analysed either originate from loosely bound outer (valence) electrons or from tightly inner (core) electrons. If a X-ray photon removes an electron from the n-th (core) orbital, the energy I_n is consumed and the corresponding peak in the spectrum is in general strong. With a certain probability, simultaneous energy-consuming processes may occur, as indicated in Figure 2.7, which decrease the kinetic energy of the detached core electron and cause satellite peaks at lower E_{kin}. The energy differences to the corresponding main peak are similar to those observed in ionisation (shake-off) or optical excitation (shake-up) of valence electrons, although the selection rules are different in the latter case.

Shake-up and shake-off occur simultaneously with the ejection of a core electron. Other processes follow after these processes, since the electron system is left in a highly excited and short-lived state which is deactivated by[49]

- X-ray fluorescence (emission of photons);
- Electron emission (Auger effect).

The Auger electrons are also recorded and can be distinguished from true "XPS electrons" using different excitation wavelengths, the kinetic energy of Auger electrons being independent of the exciting photon energy.

The information gained from the spectral position of XPS peaks relates to the binding energy differences between the different orbitals. The line-width gives further information, provided the influence of instrumental broadening can be minimised. The total line-width (Δ) of core-electron peaks is composed of three additive terms[50], Equation (2.9), related to the half-width of X-ray excitation Δ_x, the half-width due to the spectrometer (electron analyser), Δ_S, and the natural line-width Δ_r:

$$\Delta^2 = \Delta_x^2 + \Delta_s^2 + \Delta_r^2 \qquad (2.9)$$

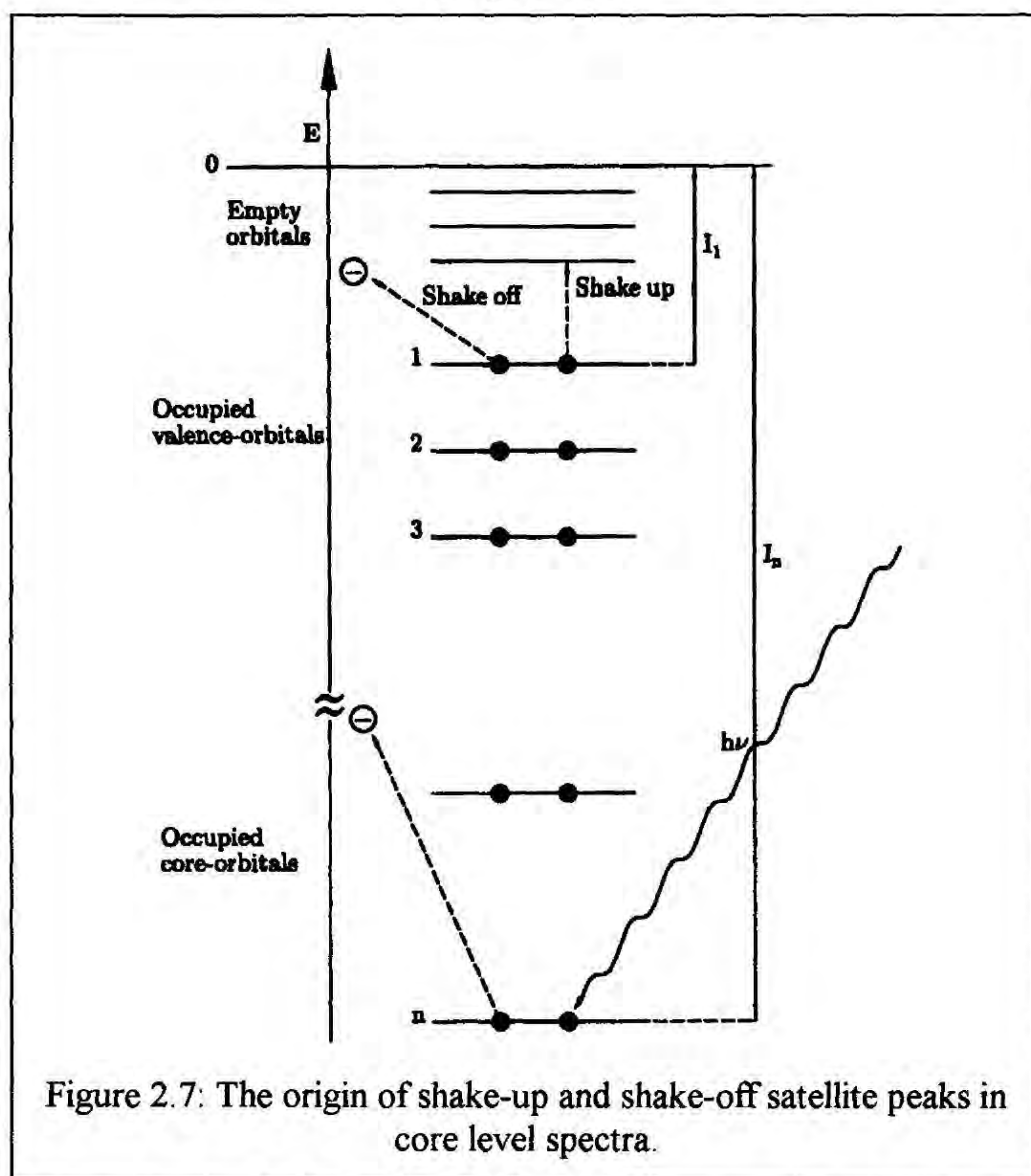

Figure 2.7: The origin of shake-up and shake-off satellite peaks in core level spectra.

For non-monochromatised Mg or Al(K_α) radiation, Δ_x amounts to 0.7 and 0.9 eV, respectively, for monochromatic Al radiation $\Delta_x = 0.55$ eV. In modern spectrometers Δ_S can be neglected. The natural line-width is related to the uncertainty principle[51], Equation (2.10):

$$\Delta E \cdot \Delta t \geq \frac{h}{2\pi} \qquad (2.10)$$

As a consequence, Δ_r is determined by the lifetime of the excited positive hole left by the electron detachment, which can have the magnitude of $\tau = 10^{-16}$s[52,53]. According to Equation (2.10), with $\tau = \Delta t$ for Δ_r (= ΔE) one obtains a value of the order of 1 eV.

Core electron peaks are prominent in XPS spectra since their binding energy is nearer to the photon energy of exciting X-rays than that of weakly bound valence

electrons thus facilitating the energy uptake. Core electrons are less directly involved in binding the atoms to monomers and polymers, compared to the valence electrons which belong to molecular rather than atomic orbitals or to energy bands. Core electrons are, however, influenced by the mode of binding, as evidenced by shifts in ionisation energies relative to the free atom values. The free atom values are characteristic of the element and the orbital considered.

The shifts are called, by analogy to NMR, "Chemical Shifts", and depend on the electron densities near the nuclei on account to the shielding of the positive charge of the nuclei.

The core electron peaks in the XPS spectrum therefore can be used in order to identify the atoms present in the polymer - and more specifically near the surface -, their mode of binding and their relative abundance. As an example, Figure 2.8 depicts the XPS spectrum of the C(1s) region of a fluorinated plasma polymer[69]. One can clearly see the different chemical environments present in the plasma polymer.

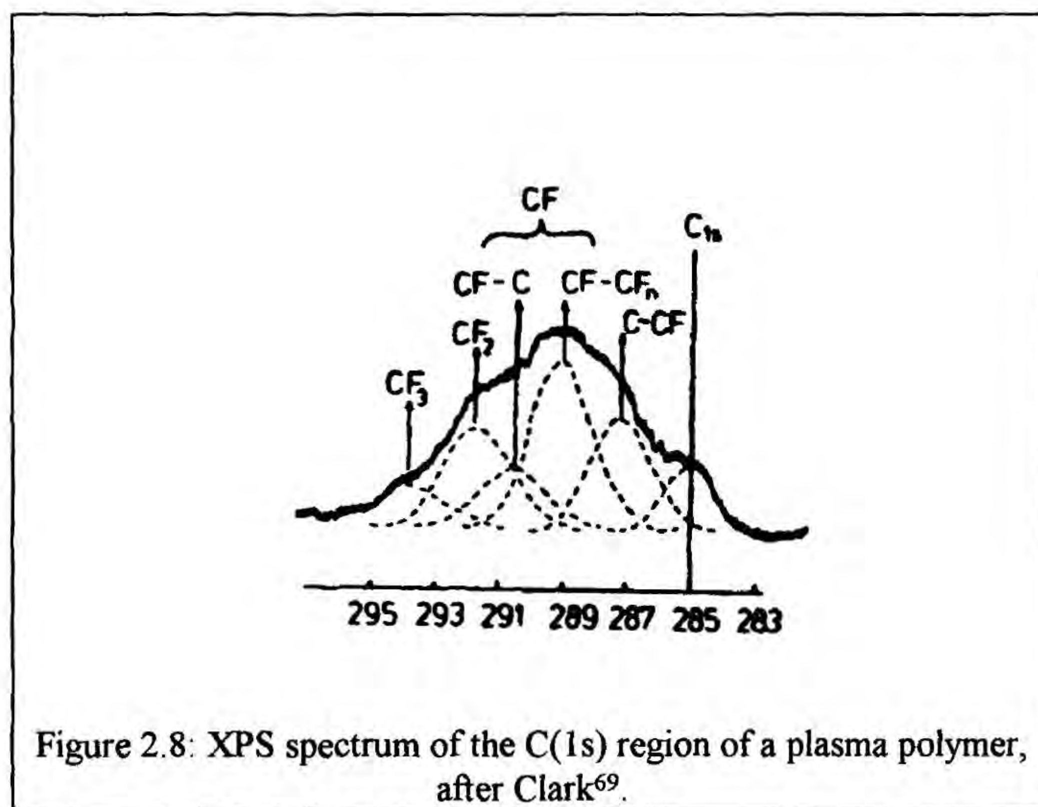

Figure 2.8: XPS spectrum of the C(1s) region of a plasma polymer, after Clark[69].

2.3.2. Experimental set up

X-ray photoelectron spectra were acquired on a Kratos ES200 surface analysis instrument operating in the fixed retarding ratio (22:1) analyser mode. Magnesium K_{α} X-rays were used as the photoexcitation source with an electron take-off angle of 30° from the surface normal. Instrument performance was calibrated with respect to the gold $4f_{7/2}$ level at 83.8 eV with a full width at half maximum (FWHM) of 1.2 eV. No radiation damage was observed during the typical time scale involved in these experiments. An IBM PC computer was used for data accumulation and component peak analysis (assuming linear background subtraction and Gaussian fits with fixed FWHM). All binding energies are referenced to the hydrocarbon component at 285.0 eV[53a]. Instrumentally determined sensitivity factors for unit stoichiometry were taken as C(1s) : O(1s) : Si(2p) equals 1.00 : 0.55 : 1.05 (this consists in the ratio between the intensities peaks related to the same number of atoms of carbon, oxygen, and silicon).

Argon depth profiling studies were performed on a Vacuum Generators ESCALAB instrument, using constant analyser energy mode photoelectron detection (CAE, 50 eV pass energy), and a cold cathode ion gun (Vacuum Generators AG21, 1-2% energy spread) for substrate etching. Aconstant flux of 3 keV Ar^{+} ions was mainteined during depth profiling experiments by keeping the ion current fixed at 1.0 μA.

2.4. ATR-FTIR Spectroscopy

2.4.1. Main principles

The infrared (IR) spectroscopy is based on excitation of molecular vibrations by absorption of photons in the spectral region of 0.75 to 2.5 μm (near IR), 2.5 to 50 μm (medium IR), and 50-1000 μm (far IR)[54]. The most important selection rule is the change in the dipole moment during excitation. This selection rule is to be attributed to interaction of the sample with the electric field of the electromagnetic radiation. Totally

symmetric vibrations are forbiden in IR absorption, since by definition the dipole moment cannot change during a transition. Strong IR-absorptions are displayed by polar groups which already in the ground state have a strong dipole moment (μ_0), perhaps the best known example being the carbonyl group:

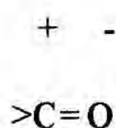

$$\mu_0 = 2 \text{ to } 3 \text{ Debye.}$$

As a rule, IR transitions of transparent or soluble polymers are measured using transmission (absorption) techniques, the samples being thin films or solutions in CCl_4, CS_2 or other solvents for limited spectral ranges. In these experiments, reflection is eliminated by conducting the reference beam through a twin cuvette that is filled with the solvent used to dissolve the compound in question.

Recording film spectra, reflection cannot be excluded completely, since the reference (if there is any) often has not exactly the same reflection behaviour as the sample. Ideally, a very thin film of the sample (a polymer, for example) should serve as a reference, the effective sample thickness being the difference between sample and reference film. Two kinds of polymer samples require special reflection techniques in order to yield useful vibrational spectra:

- Polymers layers on opaque substrates, highly IR scattering samples, certain resins and rubbers not measurable in transmission.
- Oxidised or otherwise surface-modified films, if the surface of the polymer is to be studied in order to elucidate the nature and extent of modification.

Reflection of electromagnetic radiation at smooth surfaces shows maxima in the region of strong absorption bands due to the increase in the refractive index. Diffuse

reflection and scattering at surfaces, at the other hand, yields maxima in regions of minimal absorption of the sample, since in these spectral regions the losses due to absorption of radiation are very low. The same is true for *attenuated total reflection* (ATR)[55] of IR radiation, a technique combining total reflection in a crystal, covered by the sample (e.g. a polymer film) and absorption in the thin surface layer which is penetrated by the I.R. beam (Fig. 2.9). The penetration depth into the medium with lower refractive index (polymer) depends in a complex manner on the wavelength, the refractive indices n_1 (crystal) and n_2 (sample) and on the angle of reflection; as an order of magnitude, the penetration depth is given by the following expression:

$$d_p = \frac{\lambda}{2\pi\sqrt{\sin^2\theta - n_2/n_1}} \qquad (2.11)$$

where λ is the wavelength and θ is the angle of reflection and can be estimated at $\lambda/10$, i.e. roughly 100 to 1000 times the value estimated for the surface layer involved in XPS.

In practice, multiple reflection is used in order to increase the effective path length, Figure 2.9b. Since the optical constants of polymer and crystal vary as a function of wavelength so that the depth of penetration varies, too, the ATR spectrum is not identical with the absorption spectrum, although the spectral position of the bands are the same.

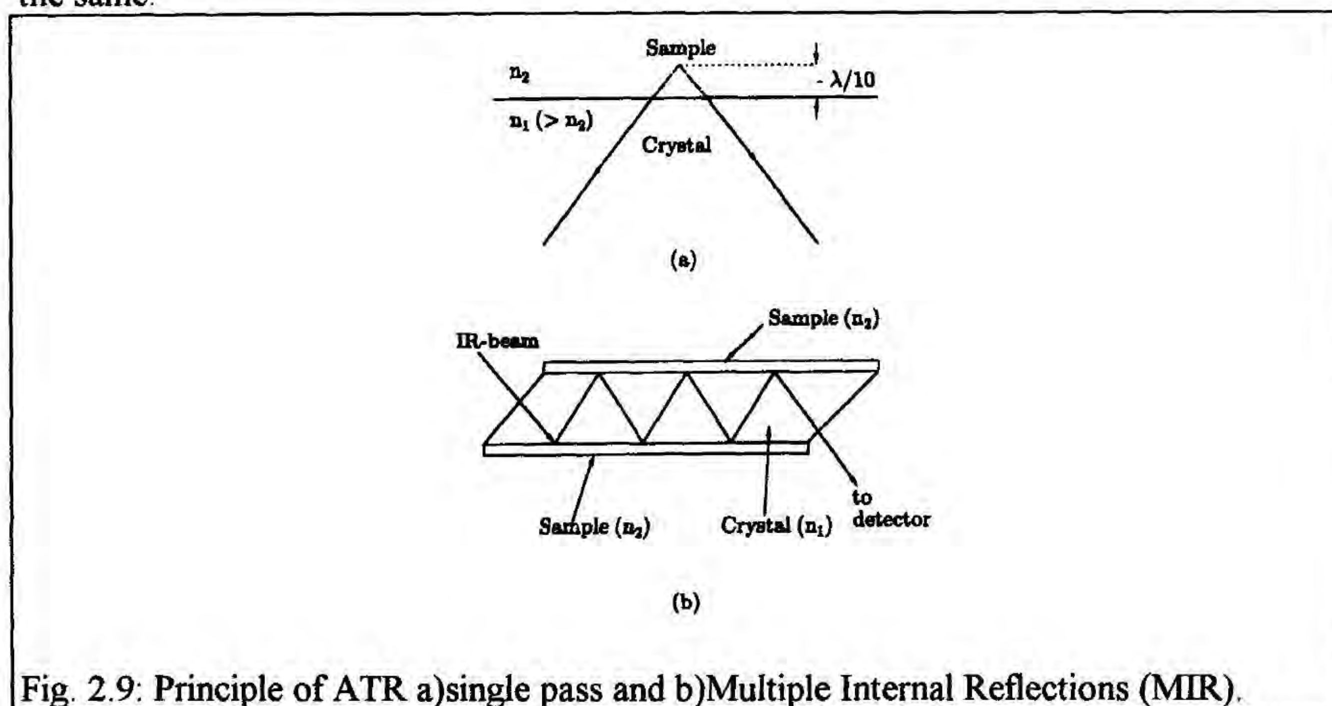

Fig. 2.9: Principle of ATR a)single pass and b)Multiple Internal Reflections (MIR).

Figure 2.10 shows a typical application of ATR-FTIR in the characterisation of plasma polymer coatings[67]. It can be seen that, despite the thickness of 50-200 nm of the films, the method is capable of detecting differences in the chemical composition of two systems which only differs on the substrate.

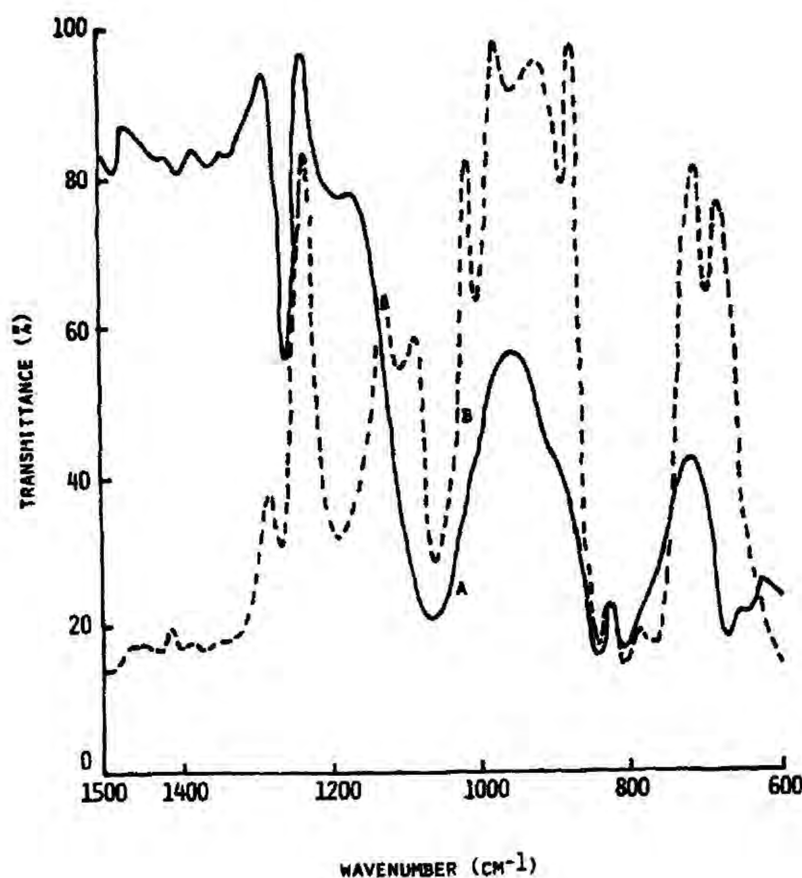

Figure 2.10: ATR-FTIR spectra of organosilane plasma polymers deposited on different substrates, after Coopes[67].

2.4.2. Experimental set up

Infrared absorbance spectra of liquids, powdered materials, and coated films were taken on a FTIR Mattson Polaris instrument. Powdered materials were mixed with dried KBr, then pressed into a disc, and characterised by the transmission method. Liquid samples were diluted in CCl_4 (3% weight/volume solution). Samples prepared with polyethylene substrates were mounted onto a variable angle attenuated total reflection

(ATR) cell fitted with a KRS-5 crystal. An incident beam angle of 45° was used, which resulted in 14 internal reflections[55a]. Typically, 100 scans were acquired at a resolution of 4 cm^{-1}.

2.5. Solid State Nuclear Magnetic Resonance

2.5.1. Main principles

In its simplest form, nuclear magnetic resonance (NMR) is the study of the properties of molecules containing magnetic nuclei by observing the magnetic fields at which they come into resonance with an applied field of definite frequency. In the field of 1 T the resonance condition is fulfilled for protons with 42.578 MHz radiation, and so NMR is a radiofrequency technique. Early NMR spectrometers used fields of about 1.1 T, but much higher fields are available using superconducting magnets, and modern spectrometers operate at up to about 10 T, which corresponds to resonance at over 400 MHz.

Nearly each element has one or more magnetic isotopes (see Table 2.1); only those isotopes which are formally build up by the He nuclei have no magnetic moment: ^{4}He, ^{8}Be, ^{12}C, ^{16}O, ^{20}Ne, ^{24}Mg, ^{28}Si etc. In principle, therefore, it should be possible to use nearly all elements in NMR spectroscopy, although for reasons of sensitivity only ^{19}F can be measured on conventional continuous mode spectrometers[56]. The main causes for low NMR sensitivity of an isotope are low natural abundance and small magnetic moments. Furthermore, the nuclear quadrupole moment of certain nuclei (e.g. ^{14}N, ^{17}O, ^{33}S) broadens the spectra so that the effective sensitivity of measuring these isotopes is decreased. The disadvantage of low sensitivity may well be overcompensated by very weak spin-spin coupling due to low abundance (only very few pairs of the same isotope such as ^{13}C-^{13}C) once a method for recording spectra with a high degree of sensitivity is found. Such a method has become available (PFT-NMR) which combines excitation by

short (μs) rf pulses with Fourier-transformation of the signals obtained. On the other hand, the sensitivity of conventional continuous mode recording cannot be substantially increased due to saturation if the excitation power is increased (in addition to limitations in time and field stability during signal to noise improvement by averaging)[57].

Table 2.1: Comparison between CW-NMR and PFT-NMR spectroscopy.

Item to be compared	CW-NMR	PFT-NMR
rf-Radiation	Continuous	Pulsed
Intensity (power)	Small	High
Spectral purity of radiation	Monochromatic	Polychromatic
Magnetic field	Variable (in field sweep operation)	Constant
Signal	$I(\nu)$ or $I(B)$	$I(t)$ — FT→ $I(\nu)$ or $I(B)$
Signal averaging	Time consuming	Rapid
Nuclei	^{1}H, ^{19}F	All nuclei if natural abundance is sufficient
Solid state	Broad-line NMR	High resolution possible (MAS-CP)

Using the pulse method, one spectrum per pulse is stored, the minimal repetition time being five times the spin-lattice relaxation time ($5T_1$). If non equivalent nuclei are present, the longest T_1 has to be used to calculate the repetition time. If T_1 is small, a large number of spectra can be stored and used for computational signal to noise averaging.

The rf excitation pulses in PFT-NMR cover a frequency range which is at least as broad as the spectrum expected. They, therefore, contain all frequencies needed for a full NMR spectrum to be recorded if the magnetic field is kept constant during the experiment. Owing to the shortness of the pulses, the power level of the exciting radiation can be much higher than in conventional CW-NMR spectroscopy. The magnetic nuclei of the sample which the apparatus has been tuned, e.g., ^{13}C, ^{15}N, etc., absorb their characteristic frequencies from the radiation offered to them whereby the

magnetic moments are aligned with respect to the external magnetic field. The signal $I(t)$ resulting after the pulse from reorientation of the excited spins corresponds to the interferogram in FT-IR spectroscopy, *i.e.* it contains the full spectral information in a coded form. Using the Fourier transformation technique, the signal $I(t)$ is transformed into the NMR spectrum $I(\nu)$ or $I(B)$. The signal $I(t)$ is called FID (free induced decay).

The most important nucleus in polymer spectroscopy is ^{13}C since[58,59]:

- Nearly all polymers show C-atoms in the main chain, or at least in side-groups.
- The range of chemical shifts is very large (200 ppm)
- Spin-spin coupling between neighbouring atoms (^{13}C-^{13}C) - not to be eliminated by spin decoupling - is very weak owing to the low natural abundance (see Table 2.2); the probability of such contacts is about 10^{-4}.

Table 2.2: Nuclear spins of important isotopes

Element	Main isotope nuclear spin = 0	Isotopes nuclear spin > 0 (natural abundance percent)	Approximative sensitivity relative to ^1H
H	-	^1H: 1/2 (99.98) ^2H=D: 1(1.5 x 10^{-2})	1 10^{-2}
C	^{12}C	^{13}C: 1/2 (1.11)	1.6 x 10^{-2}
N	-	^{14}N: 1 (99.64) ^{15}N: 1/2 (0.36)	10^{-3} 10^{-3}
O	^{16}O	^{17}O: 5/2 (3.7x10^{-2})	3x10^{-2}
F	-	^{19}F: 1/2 (100)	0.83
Si	^{28}Si	^{29}Si: 1/2 (4.7)	8x10^{-3}
P	-	^{31}P: 1/2 (100)	0.07
S	^{32}S	^{33}S: 3/2(0.74)	2x10^{-3}
Cl	-	^{35}Cl: 3/2 (75.4) ^{37}Cl: 3/2 (24.6)	5x10^{-3} 3x 10^{-3}

The technique leading to well resolved solid state spectra (MAS)[60,61] was first explored by polymer spectroscopists. The main reasons for low intensity, broad ^{13}C-NMR spectra in solids are[62]:

a) Anisotropic magnetic dipole-dipole interaction, mostly ^{13}C-H;
b) Anisotropy of chemical shift;
c) Long relaxation time T_1 (several minutes for ^{13}C in solids) - limiting the repetition frequency.

Restriction (c) is a problem of sensitivity, whereas (a) and (b) are fundamental restrictions. The experimental solution of high resolution in solid state ^{13}C-NMR requires the following combination of techniques[63]:

1) High power ^1H-decoupling;
2) Rotation of the sample about the magic angle $\Rightarrow$ Magic Angle Spinning (MAS);
3) Cross polarisation (CP).

High power ^1H-decoupling (1) solves the problem of dipolar broadening (a). This could, in principle, be solved by (2) at a very high rotation speed. MAS (2) is based on the fact that both intrinsic broadening mechanisms (a) and (b) contain the term $(3\cos^2\theta - 1)$. This is visualised in Figure 2.11 for the ^{13}C-^1H interaction. The above term is zero at θ = 54°44′ relative to the external magnetic field. If the sample is rapidly rotated at this angle, as indicated in Figure 2.11, the average θ for all vectors (dipoles) in the sample is the magic angle and all dipole interactions as well as chemical shift anisotropies cancel. The rotation has to be faster than the frequency of the broadening mechanism to be eliminated; considering a ^{13}C NMR spectrum, a 10 ppm broadening would be eliminated by a spinning frequency of several kHz.

Cross polarisation (3) overcomes the long T_1 of ^{13}C sequence by a sequence of suitable pulses which transfer the polarisation from slowly decaying ^{13}C to the much

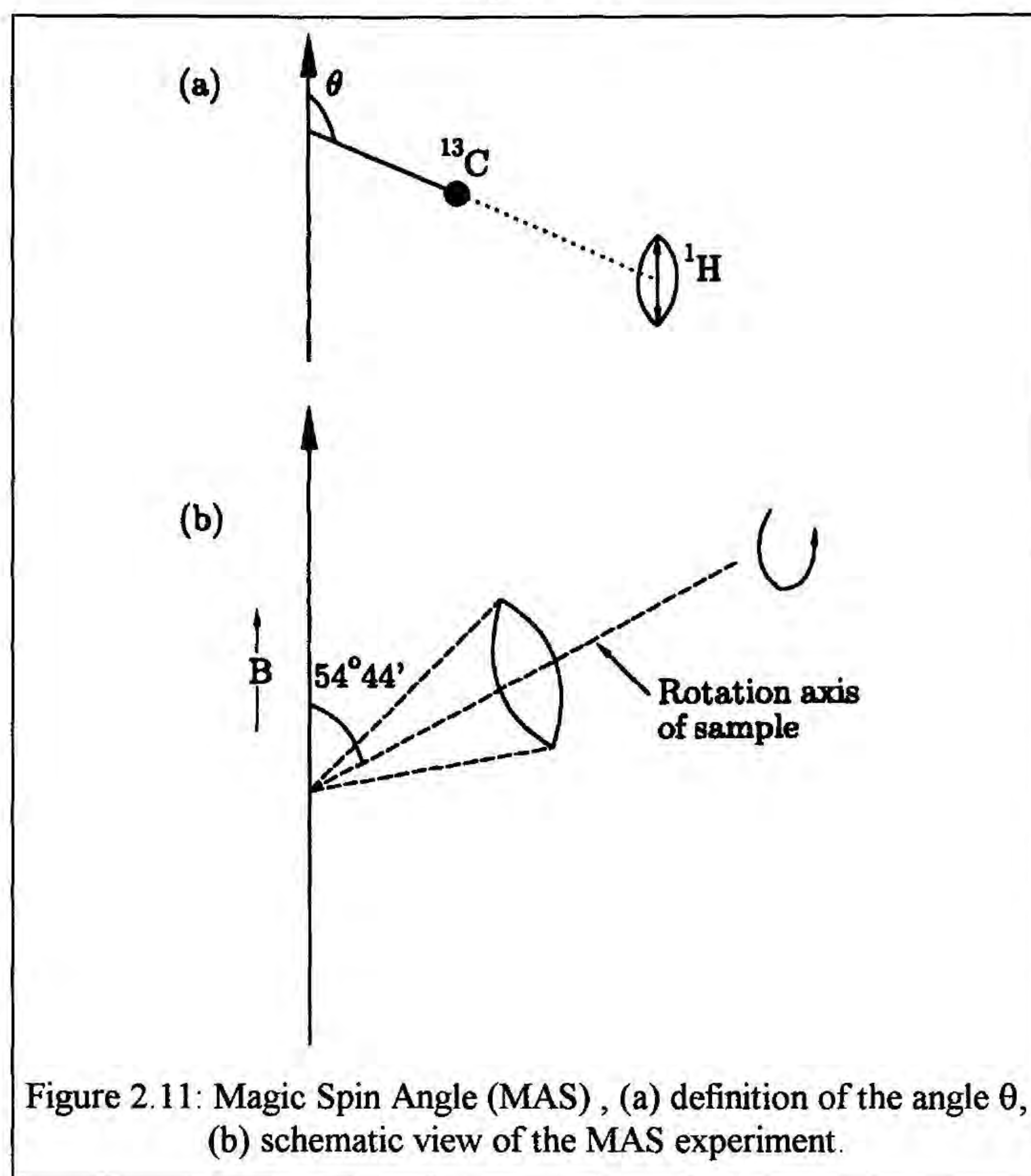

Figure 2.11: Magic Spin Angle (MAS), (a) definition of the angle θ, (b) schematic view of the MAS experiment.

faster relaxing ^{1}H system. This principle of CP is shown in Figure 2.12 by means of a hydrostatic analogue. The transfer of polarisation from the ^{13}C to ^{1}H system is induced essentially by simultaneous irradiation with both ^{13}C and ^{1}H resonance frequencies.

Using the CP-MAS method, even insoluble materials, e.g. crosslinked polymers (like plasma polymers) can be studied with a resolution high enough for chemical analysis. The only prerequisite is the presence of a magnetic nucleus in the sample. Figure 2.13 depicts NMR spectra of a commercial epoxy resin using techniques (1), (2) and (3)[68].

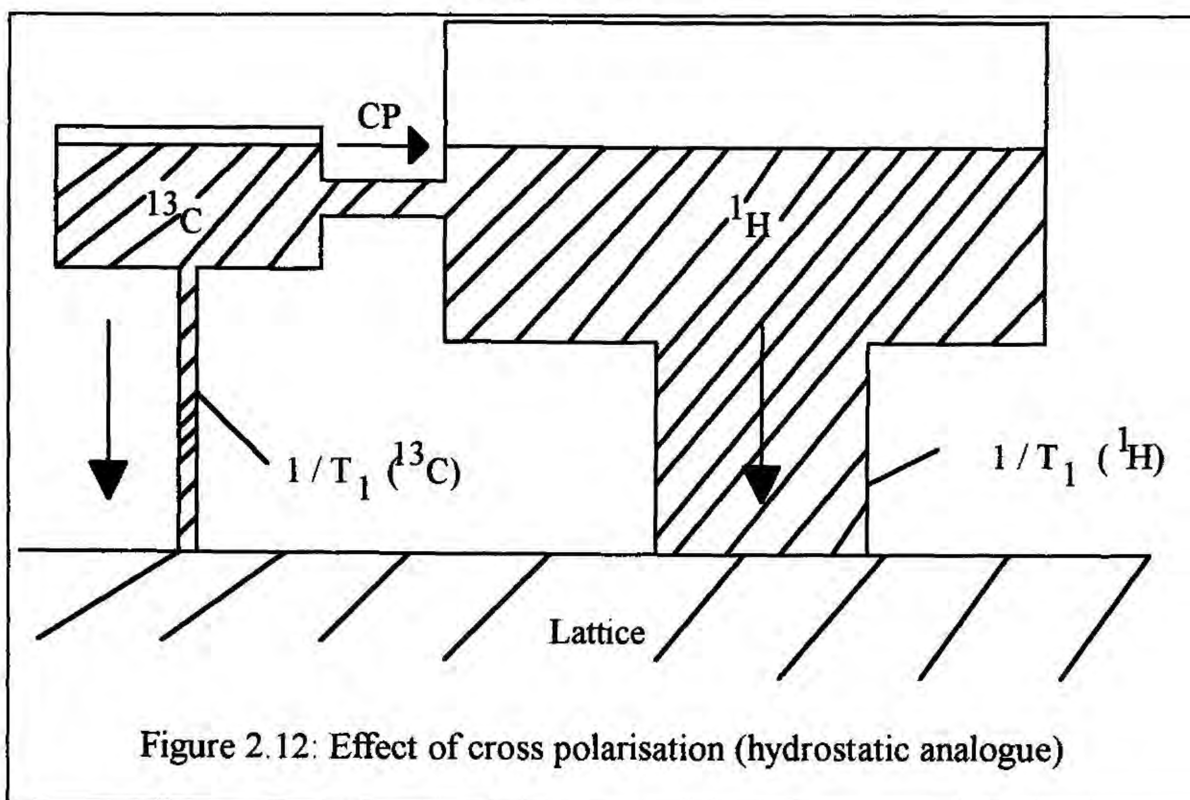

Figure 2.12: Effect of cross polarisation (hydrostatic analogue)

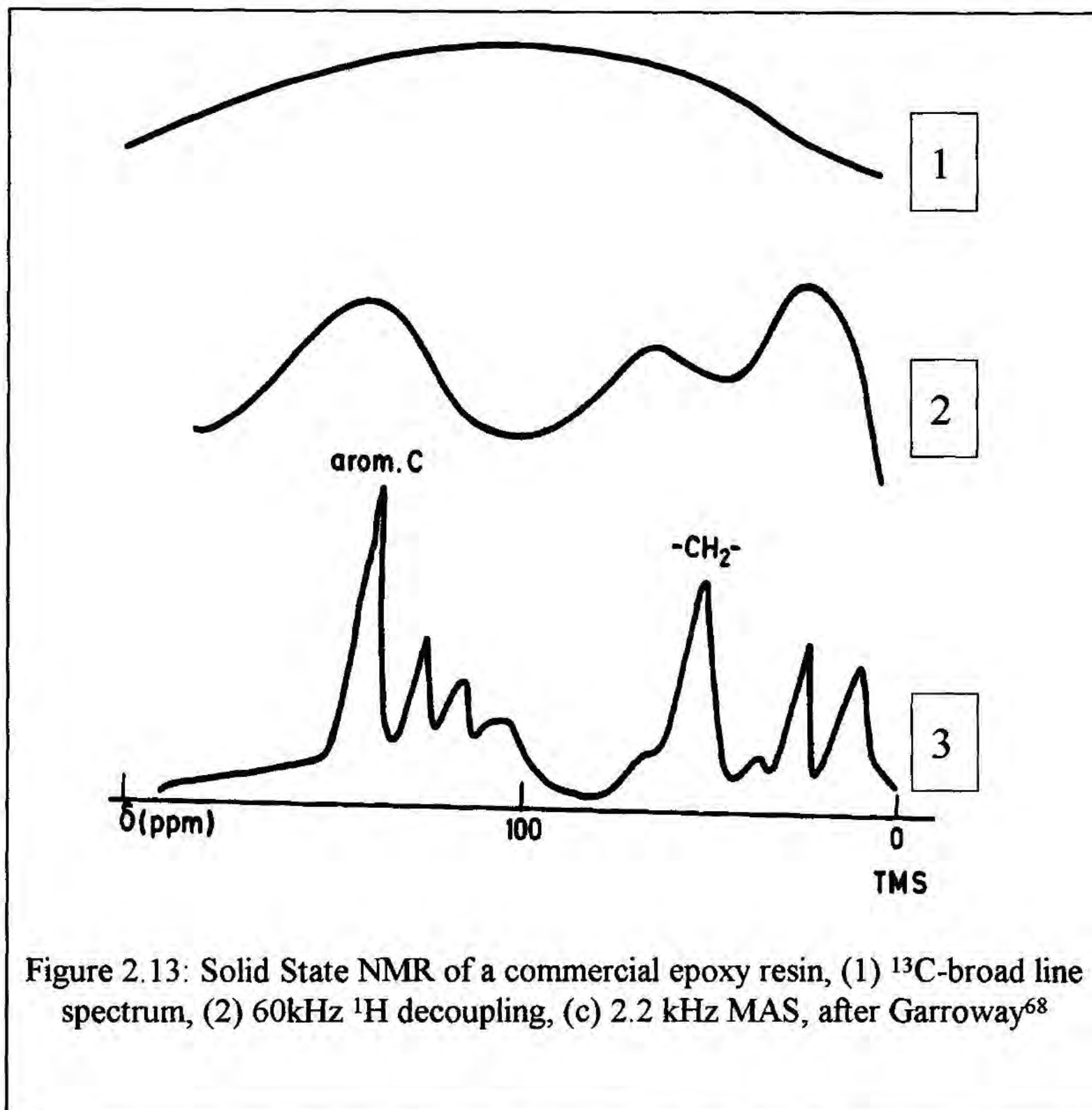

Figure 2.13: Solid State NMR of a commercial epoxy resin, (1) ^{13}C-broad line spectrum, (2) 60kHz ^{1}H decoupling, (c) 2.2 kHz MAS, after Garroway[68]

2.5.2. Experimental set up

Solid-state NMR spectra were taken on a Varian VXR-300 spectrometer equipped with a Doty Scientific magic-angle-spinning (MAS) probe. ^{29}Si NMR signals were recorded at 59.6 MHz, and ^{13}C at 75.4 MHz. Tetramethylsilane was used as the chemical shift reference.

2.6. Atomic Force Microscopy

2.6.1. Main principles

In force microscopy a probing tip is attached to a cantilever-type spring. In response to the force between tip and sample the cantilever, also called lever, is deflected[64,65]. Images are taken by scanning the sample relative to the probing tip and digitising the deflection of the lever or the z-movement of the piezo scanner as a function of the lateral position x, y. Typical spring constants are between 0.001 to 100 N/m and motions from microns to ≈ 0.1Å are measued by the deflection sensor (Figure 2.14). Typical forces between probing tip and sample range from 10^{-11} to 10^{-6} N. For

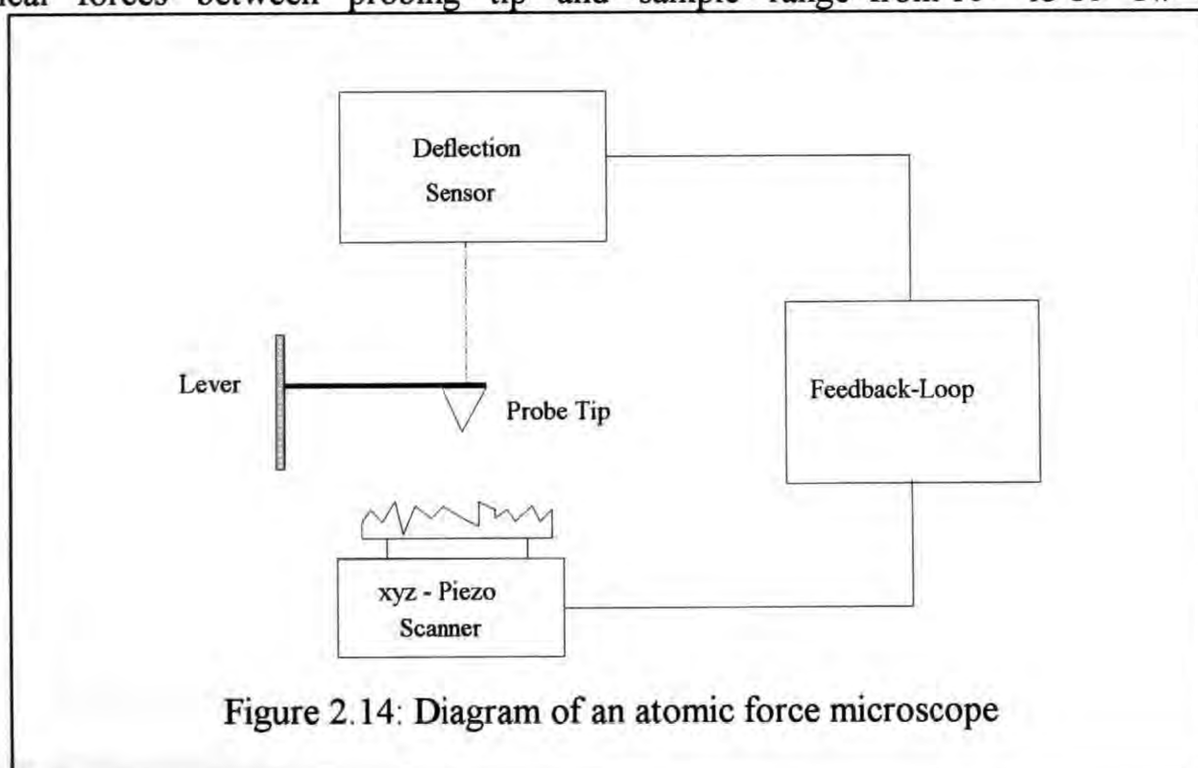

Figure 2.14: Diagram of an atomic force microscope

comparison the interaction between two covalently bonded atoms is of the order of 10^{-9} N at separations of ≈ 1 Å. Therefore, non-destructive imaging is possible with these small forces. Two force regimes are distinguished: Contact and non-contact mode. When the microscope is operated in non-contact mode at tip-sample separations of 10 to 100 nm, forces, such as van der Waals, electrostatic, magnetic or capillary forces can be sensed and give information about surface topography, distribution of charges, magnetic domain or liquid film distribution. At smaller separations at the order of 1 Å the probing tip is in contact with the sample. In this mode, ionic repulsion forces allow the surface topography to be traced with high resolution. Under best conditions atomic resolution is achieved. In addition, frictional forces and elastic or plastic deformations can be detected under appropriate conditions.

When operating in the static mode, the cantilever-type spring bends in response to the force F which acts on the probing tip until the static equilibrium is established. As derived from Hooke's law, the deflection z_t of a cantilever is proportional to the force $F = c_b z_t$ where the proportional constant is the spring constant c_b. A beam with constant cross-section has a spring constant which is given by

$$c_B = \frac{3EI}{l^3} \qquad (2.12)$$

where E is the Young's modulus, l the length and I the fourth moment of area. For a rectangular beam of width b and thickness d the moment of inertia I is given by

$$I = \frac{bd^3}{12} \qquad (2.13)$$

With the dimensions $1 \times 10 \times 100 \mu m^3$ of a Si-cantilever ($E = 1.69 \cdot 10^{11} N/m^2$) a spring constant of c_b = 0.42 N/m is derived. In the static mode, typical forces between 10^{-10} to 10^{-6} N are measured.

While scanning the surface the deflection can be kept constant by regulating the height of the sample relative to the probing tip. This mode, called the equiforce mode is

the most common mode. The height profiles of a homogeneous sample (neglecting variations of elasticity) measured with van der Waals or repulsive ionic forces, are interpreted as topography. As an alternative the height position of the sample is kept constant and the variations of the lever deflection are digitised. This mode, called variable deflection mode, allows high scanning speeds. For atomic scale imaging this mode is quite common, because the height variations are small on this limited area. Thus the interpretation is similar to the equiforce mode.

In the dynamic mode the lever is oscillating close to its resonance frequency. A distance-dependent force $F(z)$ shifts the resonance curve. An effective spring constant is defined by

$$c_{eff} = c_B - F_z' \qquad (2.14)$$

A repulsive force ($F_Z' < 0$) stabilizes the spring and increases the resonance frequency, whereas an attractive force destabilises the spring and lowers the resonance frequency (f):

$$f \propto \sqrt{c_{eff}} = \sqrt{c_B - F_z'} \qquad (2.15)$$

In the ac-mode the feedback loop either asserts constant amplitude (slope detection) or keeps the frequency constant (FM-detection). Both methods have the same physical content: the resonance curve is fixed to a certain position during the whole scan and profiles of constant gradient are measured. As an alternative the feedback loop is disabled and variable gradient images are acquired. Again, the constant gradient images are easier to interpret, whereas the variable gradient mode allows higher scan speeds. In the ac-mode, force gradients between 10^{-5} and 10 N/m are measured. With a simple force law of the form $F_z = const \cdot z^{-n}$ the corresponding forces at a distance of z = 10 nm range between 10^{-13} to 10^{-7} N.

*2.6.2. **Experimental set up***

A Digital Instruments Nanoscope III atomic force microscope was used to examine the topographical nature of the studied surfaces. All of the AFM images were acquired in air using the non-contact tapping mode, and are presented as unfiltered data.

2.7. Other techniques used in this work

*2.7.1. **Permeation measurements***

The permeability measurements were carried out using the sample preparation chamber of a Kratos ES300 X-ray photoelectron spectrometer in a set up as shown in Figure 2.15. Discs of 22 mm were cut from polymer films of known thickness (measured using an α-step 300). The permeants were monitored using a quadropole mass spectrometer. With each gas which was passed through the membrane, the system was calibrated so as to relate the ion gauge's sensitivity factors to the m/e signal intensity via a linear relationship (Pressure = Constant · m/e signal).

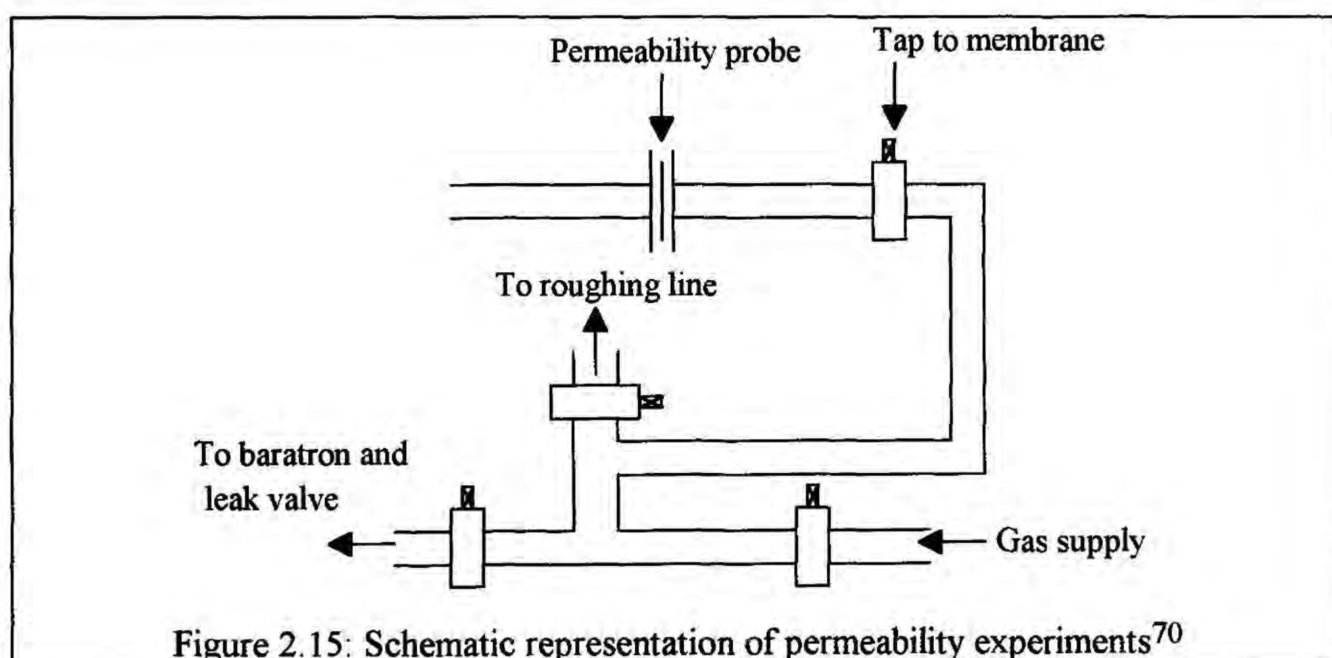

Figure 2.15: Schematic representation of permeability experiments[70]

2.7.2. Elemental Analysis

Elemental microanalysis was done on a Carlo Erba Elemental Analyser (model 1106). This apparatus operates in the following way[71]: The samples are weighed in Ag containers and dropped from a sampler into a reactor, where they are pyrolised immediately. From this point all the analysis is carried out by a microcomputer. A mixture consisting of CO, CO_2, H_2, N_2, $C_xH_yO_z$ and N_xO_y is then submitted to further oxidation (through the reaction with a CuO at 1000 °C), so that, as a result, all the CO, H_2 and $C_xH_yO_z$ is converted to CO_2 and H_2O. The resulting mixture undergoes further reaction with Cu so that excess of oxygen is removed, as well as nitrogen oxides are converted to nitrogen. Now the mixture consists in CO_2, H_2O and N_2. It is separated in its components via gas chromatography and their concentrations determined through thermal conductivity measurements. The calculation of the percentages of carbon, hydrogen and nitrogen are then performed by the computer.

2.7.3. X-Ray Diffraction

When a X-ray beam falls on an atom, two processes may occur: (1) the beam may be absorbed with an ejection of electrons from the atom, or (2) the beam scattered. It has been seen in this chapter that the first case corresponds to the utilisation of X-rays as a beam for electronic spectroscopy, while the second case is useful in the determination (or characterisation of occurrence of) crystalline structure in solids. In this way, a diffuse pattern as a result of X-ray diffraction within a sample indicates absence of crystalline character; on the other hand, the presence of an organised pattern of diffraction indicates its presence[72].

In this work, a Philips X-ray diffractometer (model PW1009/80) fitted with a CuK_α (λ = 1.5443 Å) tube, and a Debye-Scherrer camera was used to evaluate whether powders possessed any crystalline character.

References

1. Davies, P.B.; Martean, P.M., *Adv. Mater.* **1992**, *4*, 729
2. Charles, C.; Boswell, R.W.; Porteous, R.K., *J. Vac. Sci. Technol.* **1992**, *A-10*, 398.
3. Baggerman, J.A.G.; Collart, E.J.H.; Visser, R.J., *J. Appl. Phys.* **1992**, *71*, 5799.
4. McIntosh, R.E.; Kotfila, *M.S., IEEE Trans. Plasma Sci.* **1981**, *PS-9*, 63.
5. Sugai, H.; Toyoda, H., *J. Vac. Sci. Technol.* **1992**, *A-10*, 1193.
6. Tsu, D.V.; Parsons, G.N.; Lucovsky, G.; Watkins, M.W., *J. Vac. Sci. Technol.* **1989**, *A-7*, 1115.
7. Kline, L.E.; Partlow, W.D.; Young, R.M.; Mitchell, R.R.; Congedo, T.V., *IEEE Trans. Plasma Sci.* **1991**, *19*, 278.
8. Clark, D.T.; Dilks, A., *J. Polym. Sci., Polym. Chem. Ed.* **1980,** *18*, 1233.
9. Penry, B.J.; Speller, D.V.; Barefoot, R.R.; Vanloon, J.C., *Can. J. Appl. Spectr.* **1993,** *38*, 131.
10. Iwakuro, H.; Tokonami, M.; Duroda, T.; Tawaki, S.; Kitatsuji, Y., *Jpn. J. Appl. Phys.* **1993**, *1-32*, 5487.
11. Pretty, J.R.; Blubagh, E.A.; Caruso, J.A., *Anal. Chem.* **1993**, *65*, 3396.
12. Vasile, M.J.; Smolinsky, G., *Int. J. Mass Spectrom. Ion Phys.* **1973**, *12*, 133.
13. Vasile, M.J.; Smolinsky, G., *Int. J. Mass Spectrom. Ion Phys.* **1974**, *13*, 381.
14. Smolinsky, G.; Vasile, M.J., *Int. J. Mass Spectrom. Ion. Phys.* **1973**, *12*, 147.
15. Koinuma, H.; Funabashi, M.; Kishio, K.; Kawasaki, M.; Hirano, T.; Fueki, K., *Jpn. J. Appl. Phys.* **1986**, *25*, 1811.
16. Kokai, F.; Kubota, T.; Ichijo, M.; Wakai, K., *Proc. ACS Div. of Polymeric Materials: Science and Engineering* **1988**, *56*, 505.
17. Sachdev, K.G.; Sachdev, H.S., *Thin Solid Films* **1983**, *107*, 245.
18. Secrist, D.R.; Mackenzie, J.D., *J. Electrochem. Soc.* **1966**, *113*, 914.
19. Priestley, E.B.; Call, P.J., *Thin Solid Films* **1972**, *14*, 105.
20. Mackens, U.; Merkt, U., *Thin Solid Films* **1982**, *97*, 53.
21. Osada, Y.; Mizumoto, A.; Tsuruta, H., J. *Macromol. Sci.-Chem.* **1986**, *59*, 1776.

22. Osada, Y.; Mizumoto, A.; Tsuruta, H., *J. Macromol. Sci.-Chem.* **1987**, *A24*, 403.
23. Nguyen, V.S.; Underhill, J.; Fridman, S.; Pan, P., *J. Electrochem. Soc.* **1985**, *132*, 1925.
24. Kny, E.; Levenson, L.L.; James, W.J.; Averbach, R.A., *Thin Solid Films* **1981**, *85*, 23.
25. Kny, E.; Levenson, L.L; James, W.L.; Averbach, R.A., *J. Phys. Chem.* **1980**, *84*, 1635.
26. Oehr, C.; Suhr, H., *Thin Solid Films* **1987**, *155*, 65.
27. Beamson, G; Clark, D,.T.; Kendrick, J.; Briggs, D., *J. Electr. Spectr.Relat. Phenom.* **1991**, *57*, 79.
28. Bottino, F.A.; Pollicino, A.; Recca, A.; Pawson, D.; Short, R.D.; Clark, D.T., *Polym. Degr. Stab.* **1991**, *32*, 71
29. Evans, J.F.; Prohaska, G.W., *Thin Solid Films* **1984**, *118*, 171.
30. Inagaki, N.; Kobayashi, H.; Shimohira, K., *Polym. Bull.* **1984**, *11*, 29.
31. Hirotsu, T., *J. Appl. Polym. Sci.* **1979**, *24*, 1957.
32. Bailey, A.H.; Darbyshire, D.A.; Overbury, A.P.; Pitt, C.W., *Vacuum* **1986**, *36*, 139.
33. Shard, A.G.; Munro, H.S.; Badyal, J.P.S., *Polym. Comm.* **1991**, *32*, 177.
34. Tajima, I; Yamamoto, M., *J. Polym. Sci., Polym. Chem. Ed.* **1985**, *23*, 615.
35. Wróbel, A.M.; Kryszwski, M.; Gaziki, M., *J. Macromol. Sci.-Chem.* **1983**, *A20*, 583.
36. Yasuda, H.; Hsu, T., *J. Polym. Sci., Polym. Chem. Ed.* **1977**, *15*, 81.
37. Mukhersee, S.P.; Evans, P.E., *Thin Solid Films* **1972**, *14*, 105.
38. Ing, S.W.; Davern, W., *J. Electrochem. Soc.* **1965**, *112*, 284.
39. Oberbeck, W.F.; Mayham, K.C.; James, W.J., *J. Appl. Polym. Sci.* **1978**, *22*, 2805.
40. Wróbel, A.M. Kryszwski, M.; Gazicki, M., *Polymer* **1976**, *17*, 673.
41. Tien, P.K.; Smolinsky, G.; Martin, R.J., *Appl. Opt.* **1972**, 11, 637.
42. Hollas, J.M., *Modern Spectroscopy*, Chapter 7, Wiley: New York, 1988.

43. Straughan, B.P., Walker, S. (eds), *Spectroscopy*, vol. 3, Chapman and Hall: London, 1990

44. Herzberg, G., *Atomic Spectra and Atomic Structure*, Dover Publications: New York, 1944.

45. Siegbahn, K., *Electron Spectroscopy. Progress in Reaserch and Applications*, Caudano, R., Verbist, J. (eds.), Elsevier: Amsterdam, 1974.

46. Briggs, D. Seah, M.P, In Briggs, D.; Seah, M.P. (eds.) *Practical Surface Analysis*, Willey: Chichester, 1990, page 1.

47. Atkins, P.W., *Molecular Quantum Mechanics*, Chapter 12, Oxford Student Edition: Oxford, 1983.

48. Carlson, T.A., *Photoelectron and Auger Spectroscopy*, Plenum Press: New York, 1975

49. Turner, N.H.; Schreifels, J.A., *Anal. Chem.* **1992**, *64*, 502R.

50. Clark, D.T., *Structural Studies of Macromolecules by Spectroscopic Methods*, Jvin, K.J. (ed.), Wiley: London, 1976.

51. Eisberg, R. and Resnick, R., *Quantum Physics of Atoms, Molecules, Solids, Nuclei, and Particles*, Wiley: New York, 1985

52. Hayat, U., PhD Thesis, University of Durham, 1983.

53. Wagner, C.D.; Gale, L.H; Raymond, R.H., J. Vac. Sci. Tech. **1978**, *15*, 518.

53a. Johansson, G.; Hedman, J.; Berndtsson, A.; Klasson, M.; Nilsson, R.; *J. Electron Spectr.* **1973**, *2*, 295.

54. Harrick, N.J., *Internal Reflection Spectroscopy*, Harrick Scientific Corp.: New York, 1967.

55. Mirabella, F.M., *J. Polym. Sci. Polym. Phys. Ed.* **1983**, 21, 2403.

55a. Graf, R.T.; Koekig, J.L.; Ishida, H., *Introduction to Optics and Infrared Spectroscopic Techniques*, in *Fourier Transform Infrared Characterization of Polymers*, Ishida, H. (ed.), Plenum Press: New York, 1987.

56. Martin, M.L.; Martin, G.J.; Delpuech, J., *Practical NMR Spectroscopy*, Heyden: London, 1980.

57. Shaw, D., *Fourier Transform NMR Spectroscopy*, Elsevier: Amsterdam, 1984.

58. Pasika, W.M. (ed.), *ACS Symp. Ser.* **1979**, *103*.

59. Randall, J.C., *Polymer Sequence Determination Carbon-13 Method*, Academic Press: New York 1977.

60. Schaefer, J., Stejskal, E.O., *J. Am. Chem. Soc.* **1976**, *98*, 1031.

61. Schaefer, J.; Stejskal, E.O.; Buchdall, R., *Macromolecules* **1977**, *10*, 384.

62. Lyerla, J.R., in Fava, R.A. (ed.), *Method of Experimental Physics*, vol 16, Academic Press: New York.

63. Mehring,M., *Principles of High Resolution NMR in Solids*, Springer: New York, 1983.

64. Meyer, E., *Progress in Surface Science* **1992**, 41, 3.

65. Kuk, Y.; Silverman, P.J., *Rev. Sci. Instrum.* **1989**, *60*, 165

66. Clark, D.T.; Abu-Shbak, M.M., *J. Polym. Sci., Polym Chem. Ed.* **1983**, 2907.

67. Coopes, I.H.; Griesser, H.J., *J. Appl. Polym. Sci.* **1989**, *37*, 3413.

68. Garroway, A.N.; Moritz, W.B.; Resing, *ACS Symp. Ser.* **1979**, *103*, 67.

69. Clark, D.T.; Abu-Shbak, M.M., *J. Polym. Sci., Polym. Chem. Ed.* **1983**, *21*, 2907.

70. Hopkins, J., *First Year Report*, page 58, Durham University, 1993.

71. Elemental Organic Microanalysis Yesterday and Today, Carlo Erba Strumentazione

72. Warren, B.E., *X-Ray Diffraction*, Addison-Wesley, London, 1969.

Chapter Three

PLASMA POLYMERISATION OF TETRAMETHYLSILANE

Contents

3.1. Introduction 57

3.2. Experimental: Reactor set up 57

3.3. Results 60

- 3.3.1. X-ray Photoelectron Spectroscopy 60
- 3.3.2. Fourier Transform Infrared Spectroscopy 65
- 3.3.3. Solid State NMR 71
- 3.3.4. Emission Spectroscopy 74

3.4. Discussion 77

3.5. Conclusions 79

3.1. Introduction

Although plasma polymerisation is a very powerful tool for surface engineering, it has the onus of being completely system dependent[1-6]. That makes a comparison between the behaviour of a particular precursor and a standard precursor widely used in the literature very difficult, so that both monomers should be plasma polymerised in exactly the same conditions (including the geometry of the reactor[7-10]). In the case of organosilanes, tetramethylsilane (TMS) can be considered a standard precursor[11-18].

In this chapter, the plasma polymerisation of tetramethylsilane (TMS) over a range of energies is described. Both thin layers and powders have been synthesised. Freshly deposited and aged materials have been characterised by XPS, FTIR, NMR, and XRD, in conjunction with UV emission analysis of the TMS glow discharge itself. This combination of analyses on the same product offers a much deeper insight into the polymerisation and structural aspects of these carbosilicon materials.

3.2. Experimental: Reactor set up

Tetramethylsilane (TMS, 99.9% Aldrich Chemical Company - vapour pressure = 1 atm at 27 °C) was degassed by multiple freeze-pump-thaw cycles. Two types of substrate were used: low density polyethylene film for thin plasma polymer coatings (LDPE, Metal Box, 0.1 mm thickness), and glass slides for bulk powder product (1 mm thickness). Both were cleaned with isopropyl alcohol, and dried prior to use.

Glow discharge experiments were carried out in an electrodeless cylindrical glass reactor (4.5 cm diameter, 490 cm^3 volume) enclosed in a Faraday cage. It was fitted with a monomer inlet, a Pirani pressure gauge, and a 47 L min^{-1} two-stage rotary pump attached to a liquid nitrogen cold trap. A 13.56 MHz radio frequency (RF) source was inductively coupled to a copper coil (4 mm tube diameter, 9 turns, spanning 11.0 - 18.5 cm from the monomer inlet) via a matching network, Figure 3.1.

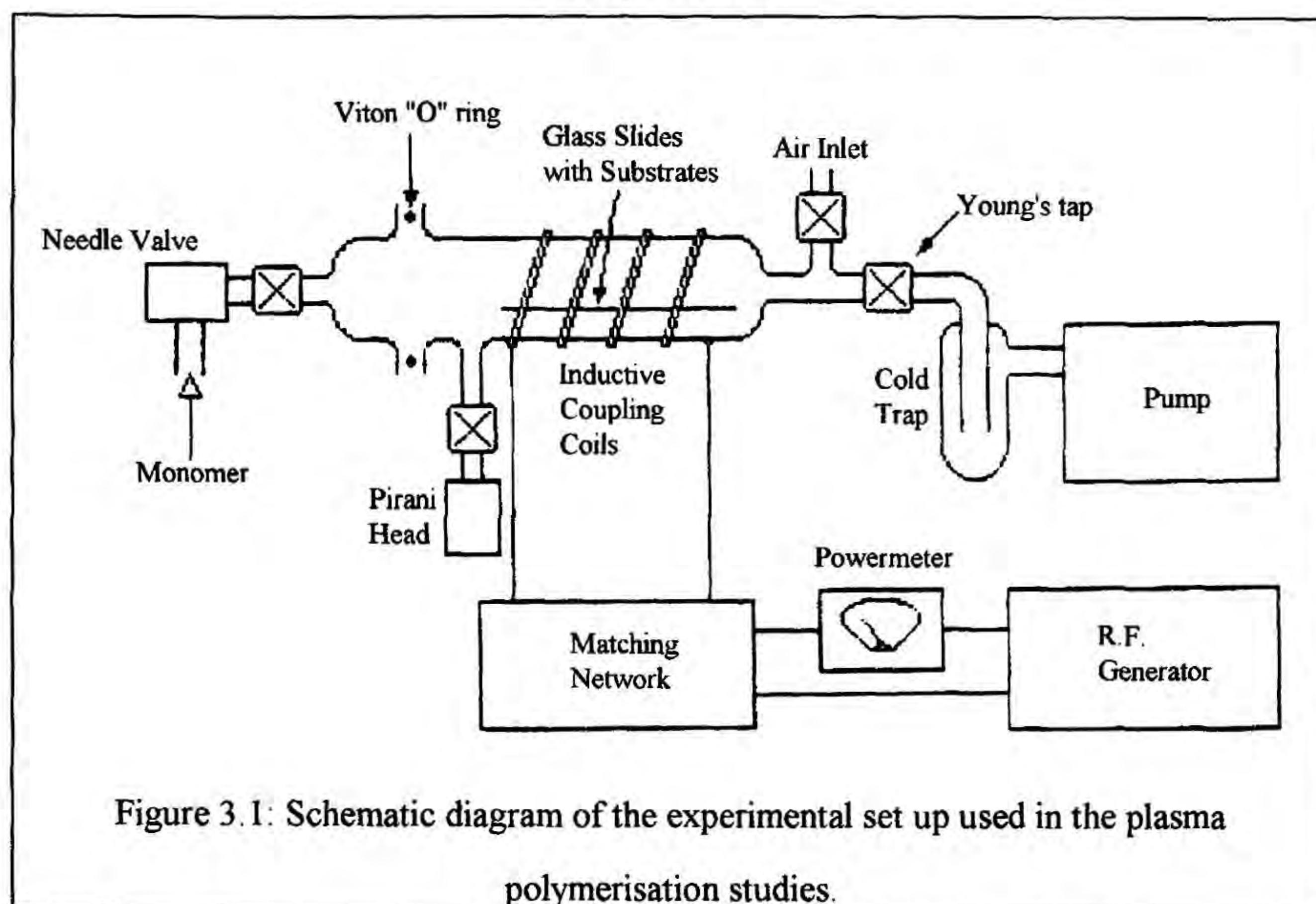

Figure 3.1: Schematic diagram of the experimental set up used in the plasma polymerisation studies.

Monomer flow rate was controlled using a fine needle valve. Glow discharges at less than 5 Watts power were sustained by pulsing the plasma[19]. All joints were grease-free. All the depositions were carried out using a continuous mass flow of monomer (F_M), which was estimated using the equations described in Chapter 1 (page 13). Experimentally that means that after having a given constant pressure in the reactor (due to the continuous and unknown flow of monomer F_M), the outlet to the pump is then abruptly closed. The increase in pressure ΔP, as well as its related time interval Δt are measured and used in the mentioned equations.

Starting from a clean reactor (a reactor scrubbed with detergent, rinsed with isopropyl alcohol, and dried), a complete cycle of deposition consisted of the following steps:

i. The reactor was additionally cleaned with air plasma (1 hour, power = 50 W, pressure = 0.1 Torr). When using glass slides as substrates, the cleaning plasma was carried out with them inside. When using polyethylene films as substrates, that was done without them, since oxygen containing plasmas drastically modify the surface

of these films, by oxidation[20];

ii. The reactor was pumped down to 0.001 Torr and the leak rate was estimated. It was never higher than 2.6 x 10^{-10} kg/s;

iii. Monomer was admitted in the reaction chamber (continuous flow), resulting in an increase of pressure to 0.1 Torr and the monomer flow rate F_M was estimated (F_M = 3.6 x 10^{-8} kg/s - i.e. at least 99.3% of total mass flow is the organosilane precursor);

iv. Monomer flown through the reactor for 5 minutes;

v. The deposition was initiated;

vi. After the deposition was finished, the reactor was pumped down to 0.001 Torr and mantained at this pressure for 5 minutes;

vii. The sample (or substrate) was removed from the reactor and submitted to the desired analysis.

Since plasma polymerisation is very dependent on all the physical parameters (which may vary from one experimental set up to another one), use was made of six experiments, in order to "anchor" this experimental set up (by comparing the results of TMS deposition to the results of other systems in the literature), making it possible a relative comparison with any other different monomer in our system:

a. Using polyethylene films, glow discharge polymerisations were carried out (time = 10 minutes) for several values of W/F_M. These films were analysed by XPS and ATR-FTIR techniques. These substrates were located at 6.5 cm from the monomer inlet;

b. Excitation of the polyethylene surface by argon plasmas (powers varying form 5 to 50 W), followed by pumping down the system to 0.001 Torr and the flow of organosilane monomer in the absence of a glow discharge. These experiments were designed to verify if the monomer would react with an excited surface (rich in free radicals). In other words, to test the susceptibility of the monomer to plasma initiated polymerisation;

c. Deposition of plasma polymer onto a 21 cm length polyethylene film, at a value of W/F_M = 280 MJ/kg (the condition in which the deposition rate is highest, as subsequently shown), and posterior XPS analysis. In this experiment, it was verified the relationship between the composition of the surface and the distance from the reactor inlet;
d. Deposition of plasma polymer for 30 min on glass slides (W/F_M = 280 MJ/kg);
e. Deposition of powders (W/F_M = 280 MJ/kg) - time of deposition: 6 hours. This experiment was designed to obtain material for FTIR, NMR spectroscopy, X-ray diffraction (XRD), and elemental (CHN) analysis, as well as ageing studies;
f. Ignition of organosilane plasmas in a reactor coupled (via a quartz window) to an emission spectrometer.

For the sake of comparison with the bulk plasma polymer, an FTIR spectrum of TMS diluted in CCl_4 (3 % w/v) was carried out. The experimental set up used for each method of analysis can be found in Chapter 2.

3.3. Results

Short deposition times resulted in a uniform coating, whereas longer periods (6 hours) produced a substantial amount of non-crystalline powder. The powder was infusible, insoluble (THF, toluene, alcohols, NaOH 10 % - even using temperatures as high as 90 °C). The deposit was brown in colour, and did not visibly change in appearance with time. Elemental microanalysis of plasma polymer powder produced at the maximum deposition rate (W/F_M = 280 MJ/kg) yielded a H/C ratio of 1.9.

3.3.1. X-ray Photoelectron Spectroscopy

The C(1s) XPS envelope of a thick layer of TMS plasma polymer coated onto a

glass substrate (Figure 3.2) contains a maximum at 285.0 eV related to the presence of C-C, C-H and C-Si environments[21,22]. The Si(2p) region shows a single feature centred at 100.7 eV, which indicates the presence of Si-H and Si-C environments[21-23]. A small peak at 533.0 eV related to O(1s) level was observed in the spectra of fresh plasma polymer films. The oxygen content, calculated as a fraction of total carbon, silicon and oxygen amount, was less than 3%. This probably originates from trapped free radicals in the plasma polymer reacting on air exposure during transport from the deposition chamber to the X-ray photoelectron spectrometer. Corresponding C(1s), Si(2p), and O(1s) spectra taken following prolonged exposure to air (one month) displayed a significant degree of oxidation. Oxygen content was much greater in this case (11%). A pronounced shoulder is evident in the C(1s) envelope which can be attributed to the occurrence of >C-O- (286.6 eV), >C=O / -O-C-O- (287.9 eV), -O-C=O (289.0 eV), and -O-CO-O- (290.4 eV) functionalities[24]. A corresponding shift in the Si(2p) peak towards higher binding energy (101.2 eV) is seen, this is probably due to the presence of Si-O (102.2 eV) and O-Si-O (104.0 eV) silicon environments[25].

Figure 3.3 summarises the influence of W/F_M upon Si/C ratio for freshly deposited TMS plasma polymer layers onto a polyethylene substrate. The oxygen content measured in these experiments was consistent with values reported above for glass substrates (i.e. less than 3%), and therefore heating of the polyethylene substrate by the RF field can be ruled out. No silicon species were detected in the absence of a glow discharge. The Si/C atomic ratio passes through a maximum with increasing W/F_M, and then drops to zero. Related measurements show that the Si/C ratio decreases on moving downstream from the monomer inlet, Figure 3.4. Furthermore the Si/C ratio is found to be independent of deposition time, and therefore the coating must be homogeneous.

Activation of polyethylene film with an argon plasma (5 to 50 W), followed by exposure to TMS monomer (in the absence of a glow discharge) did not result in any silicon uptake by the substrate. Therefore organosilicon deposition must be terminated at the precise moment at which the plasma is extinguished.

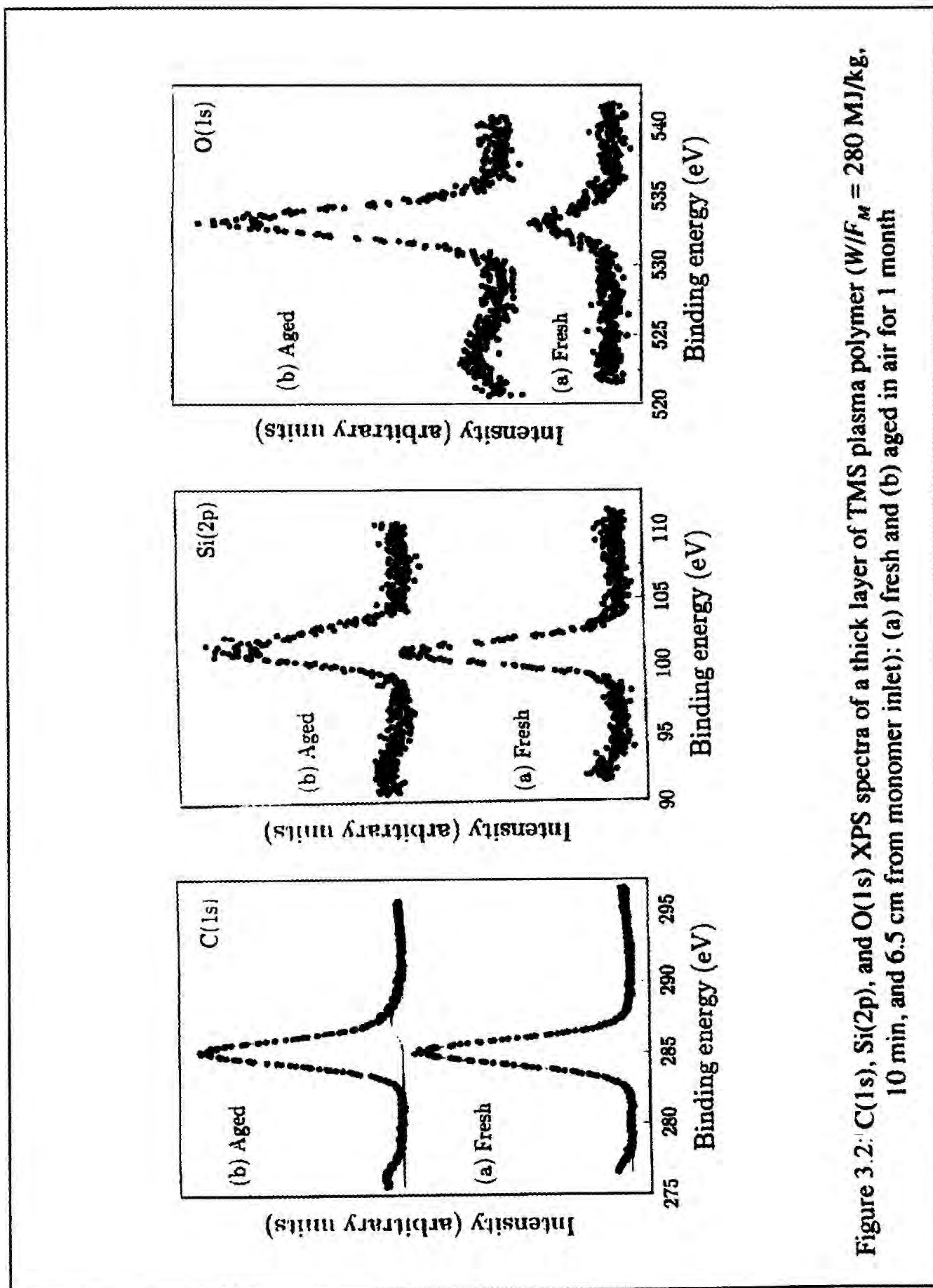

Figure 3.2: C(1s), Si(2p), and O(1s) XPS spectra of a thick layer of TMS plasma polymer (W/F_M = 280 MJ/kg, 10 min, and 6.5 cm from monomer inlet): (a) fresh and (b) aged in air for 1 month

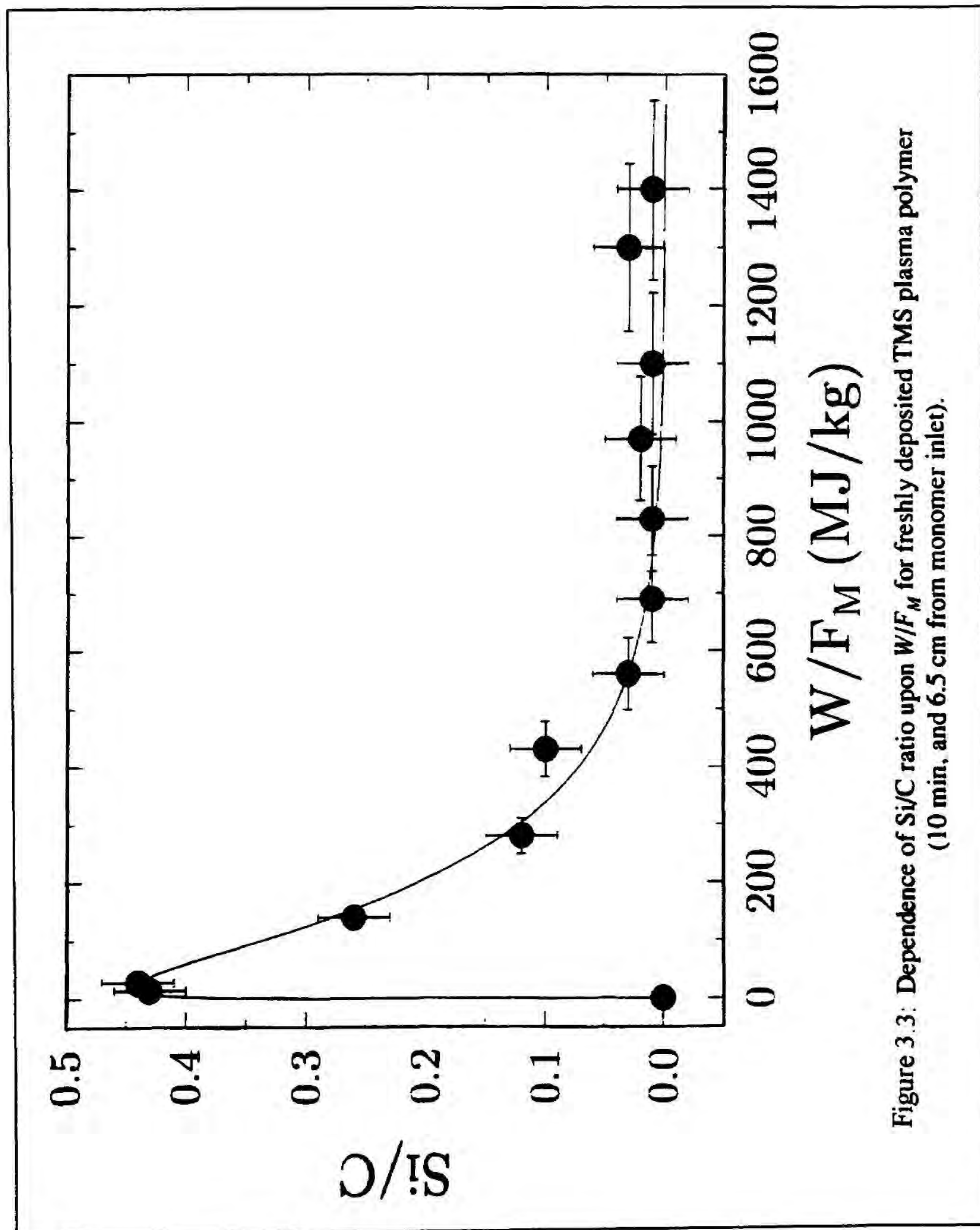

Figure 3.3: Dependence of Si/C ratio upon W/F_M for freshly deposited TMS plasma polymer (10 min, and 6.5 cm from monomer inlet).

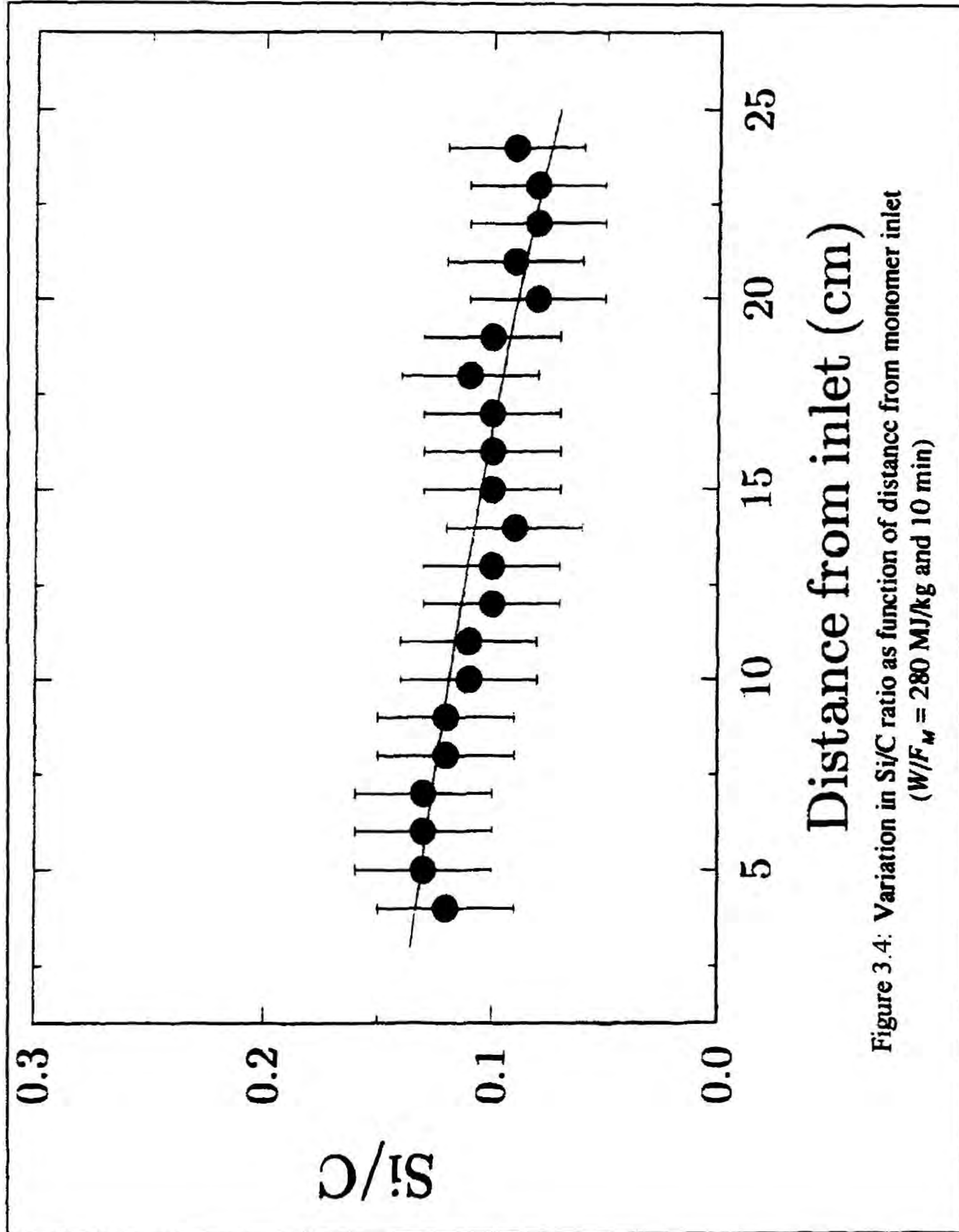

Figure 3.4: Variation in Si/C ratio as function of distance from monomer inlet (W/F_M = 280 MJ/kg and 10 min)

3.3.2. Fourier Transform Infrared Spectroscopy

Figure 3.5 is a compilation of the FTIR transmission spectra of TMS monomer, fresh and aged TMS plasma polymer powder. Characteristic absorption bands for TMS are assigned in Table 5.1. Quantitative analysis was avoided because this kind of analysis is suitable for diluted systems in transmission experiments (exactly the opposite conditions of this work). An absortion at 2300 cm^{-1} (CO stretching due to CO_2 from the atmosphere[27]) was sometimes present in the spectra.

Table 5.1: Infrared absorption bands for tetramethylsilane[26]

Absorbance / cm^{-1}	Assignment
2955	C-H asymmetrical stretching in CH_3
2891	C-H symmetrical stretching in CH_3
1248	CH_3 symmetric bending in $Si[CH_3]_n$
864	CH_3 rocking in $Si[CH_3]_n$
694	Si-C stretching

The strong absorbances for freshly deposited TMS plasma polymer powder are listed in Table 3.2. Exposure of this material to air for one month, resulted in all of the above cited infrared absorption bands for the fresh powder shifting to slightly higher frequencies. This can be explained by the presence of trapped reactive centres in the solid participating in crosslinking, and thereby increasing the amount of strain in the material[27]. Oxidation is also observed[32] with bands appearing at 3426 cm^{-1} (OH stretching[27]), 1707 cm^{-1}(C=O stretching[27]), and 1632 cm^{-1} (asymmetrical stretching mode of C=O in carboxylates, or C=C stretching in unconjugated olefins[27]). The relative intensities of the 1250 cm^{-1} (CH_3 symmetric bending in $Si[CH_3]_n$), and 1026 cm^{-1} (Si-O-Si and/or Si-O-C asymmetric stretching and/or CH_2 wagging in Si-$(CH_2)_n$-Si) bands increase.

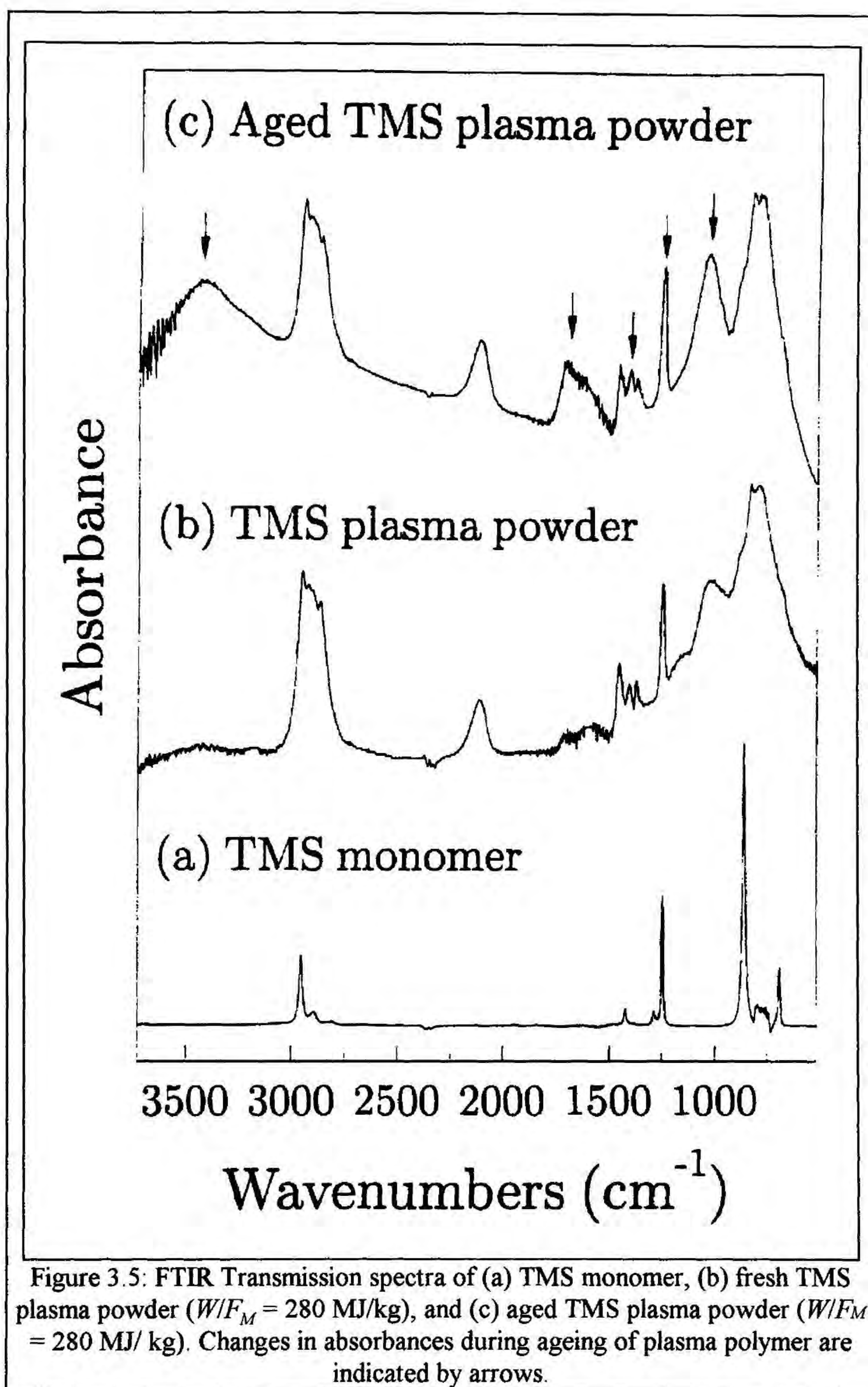

Figure 3.5: FTIR Transmission spectra of (a) TMS monomer, (b) fresh TMS plasma powder (W/F_M = 280 MJ/kg), and (c) aged TMS plasma powder (W/F_M = 280 MJ/ kg). Changes in absorbances during ageing of plasma polymer are indicated by arrows.

Table 3.2: Infrared absorption bands for freshly deposited TMS plasma polymer powder[12,14,21,26-31] (W/F_M = 280 MJ/kg).

Absorbance / cm^{-1}	Assignment
2955	C-H asymmetrical stretching in CH_3
2926	C-H asymmetrical stretching in CH_2
2906	C-H symmetrical stretching in CH_3
2870	C-H symmetrical stretching in CH_2
1460	methyl asymmetric bending in CH_3-C
1375	methyl symmetric bending in CH_3-C
1632	>C=C< stretching
2110	Si-H stretching
1408	CH_2 symmetrical scissoring in Si-CH_2
1250	CH_3 symmetric bending in Si[CH_3]$_n$
1026	Si-O-Si and/or Si-O-C asymmetric stretching and/or CH_2 wagging in Si-[CH_2]$_n$-Si
833	CH_3 rocking in Si[CH_3]$_n$, n = 2, 3
791	CH_3 rocking in Si[CH_3]$_n$, n = 1,2
685	Si-C stretching

Figure 3.6 compares ATR infrared spectra of clean and coated polyethylene film as a function of W/F_M. Characteristic infrared absorbance bands for clean polyethylene film are assigned in Table 3.3. Polyethylene coated with plasma polymer exhibits the following extra features: 2118 cm^{-1} (Si-H stretching), 1250 cm^{-1} (CH_3 symmetrical bending in Si[CH_3]$_n$), 1040 cm^{-1} (Si-O-Si and/or Si-O-C, and/or CH_2 wagging in Si-[CH_2]$_n$-Si), 834 cm^{-1} (CH_3 rocking in Si[CH_3]$_n$, n = 2,3), 790 cm^{-1} (CH_3 rocking in Si[CH_3]$_n$, n = 1, 2), 689 cm^{-1} (Si-C stretching). One obvious difference between these

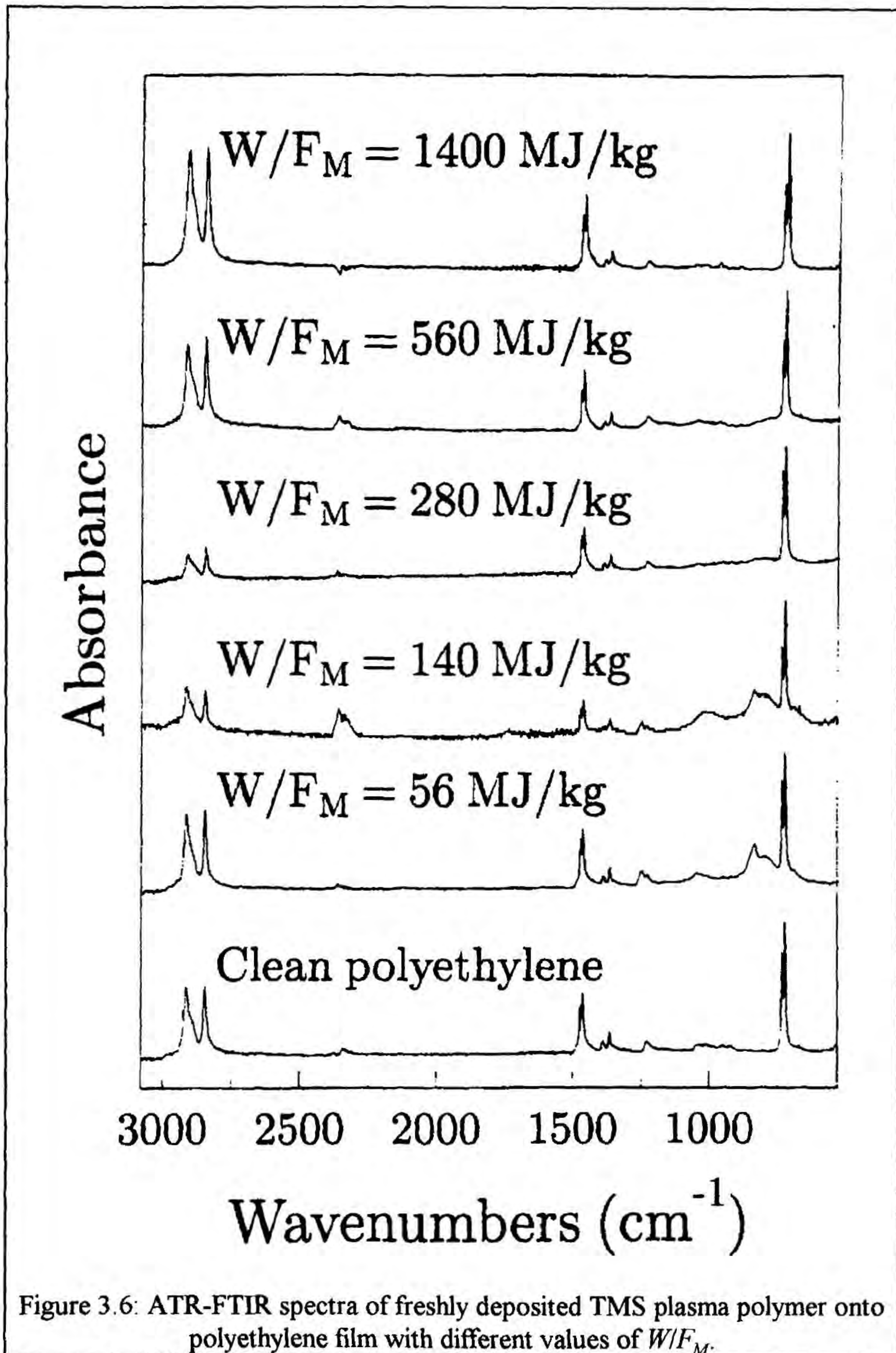

Figure 3.6: ATR-FTIR spectra of freshly deposited TMS plasma polymer onto polyethylene film with different values of W/F_M.

Table 3.3: Infrared absorption bands for clean polyethylene film[27,32-34].

Absorbance / cm^{-1}	Assignment
2915	asymmetrical C-H stretching in CH_2
2847	symmetrical C-H stretching in CH_2
1472	CH_2 bending
1462	CH_2 bending
1366	CH_2 wagging and/or symmetrical CH_3 movements
729	CH_2 rocking
720	CH_2 rocking

spectra and their transmission counterparts is the attenuated plasma polymer C-H stretching bands. This can be explained in terms of there being a smaller depth of penetration at higher wavenumbers for the ATR technique, which in turn gives rise to weaker signal intensities[35]. Also the variable attenuation in the characteristic polyethylene bands can be explained in terms of infrared penetration depth being lower at higher wavenumbers (i.e. this region of the ATR - FTIR spectrum is more sensitive towards any surface modification). Low W/F_M values yield an increase in silicon related absorptions (Si-$[CH_2]_n$-Si, Si$[CH_3]_n$) with a concomitant loss of polyethylene C-H stretching bands. As the glow discharge power increases, all silicon related absorbances diminish, until eventually just polyethylene features remain. In other words, there is no deposition of plasma polymer. Greatest loss in intensity of the characteristic polyethylene peaks (2915 cm^{-1} and 2847 cm^{-1}) occurs at approximately W/F_M = 280 MJ/kg, these experimental conditions correspond to the maximum deposition rate of plasma polymer and were therefore employed for powder formation.

Infrared spectra of coated polyethylene films located in different regions of the glow discharge are collated in Figure 3.7. The observed variations in organosilicon features imply that the rate of plasma polymerisation drops on moving downstream from the precursor inlet.

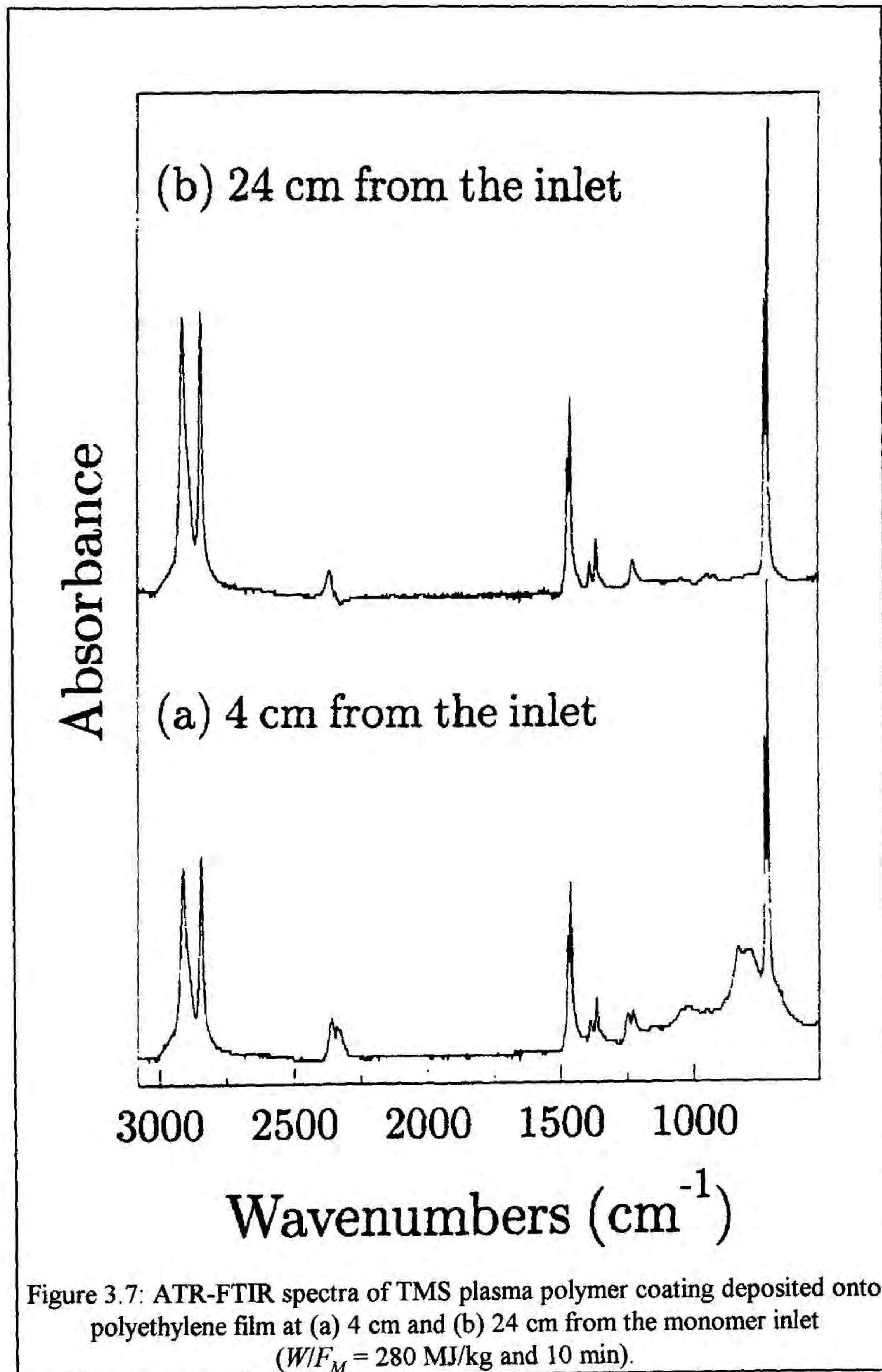

Figure 3.7: ATR-FTIR spectra of TMS plasma polymer coating deposited onto polyethylene film at (a) 4 cm and (b) 24 cm from the monomer inlet (W/F_M = 280 MJ/kg and 10 min).

3.3.3. Solid State NMR

^{13}C and ^{29}Si NMR spectra of fresh and aged TMS plasma polymer powder are shown in Figures 3.8 and 3.9 respectively. All NMR measurements are referenced to tetramethylsilane (TMS). Characteristic features observed in these spectra have been assigned in accordance with data published elsewhere[27,28,36-39]. ^{13}C and ^{29}Si peaks of greatest intensity are located at around 0 ppm. Therefore the major chemical environments present in the plasma deposit can be regarded as being similar to those known for the TMS reference compound.

A shoulder is evident in the ^{13}C NMR spectrum of fresh TMS plasma polymer powder (Figure 3.8) at approximately 20-50 ppm, this may be characteristic of either silicon carbide species[36] or sp^3 carbon atoms located within a hydrocarbon chain. Some degree of unsaturation in the plasma polymer is observed in the 120 - 180 ppm range (the occurrence of carbonyl groups in the fresh TMS plasma polymer is unlikely, since bulk oxidation was ruled out by XPS studies).

On leaving the collected material to age in air, there is an increase in intensity of the 20-50 ppm shoulder, which implies that a significant degree of crosslinking has taken place. A small number of alcohol functionalities in the 60 - 70 ppm region are also present.

The ^{29}Si NMR spectrum of fresh powder (Figure 3.9) consists of a strong signal centred at 1.8 ppm, and a shoulder at -11 ppm range. The former is characteristic of $-Si[CH_3]_3$ fixed to hydrocarbon chain ends, and the latter can be attributed to one or more of the following: double bond silicon environments (δ = -11.8 ppm for cis-$[CH_3]_3SiCH{=}CHSi[CH_3]_3$); or the presence of silicon carbide; or $(CH_3)R_2SiH$ provided R has an alkyl chain containing at least two $[-CH_2-]$ linkages (δ = -10.9 ppm for $[CH_3][n\text{-}C_3H_7]_2SiH$, δ = -9.8 ppm for $[CH_3][n\text{-}C_4H_9)]_2SiH$, δ = -9.8 ppm for $[CH_3][n\text{-}C_5H_{11}]_2SiH$, δ = -9.9 ppm for $[CH_3][n\text{-}C_6H_{13})_2SiH]$). The shoulder at +6.6

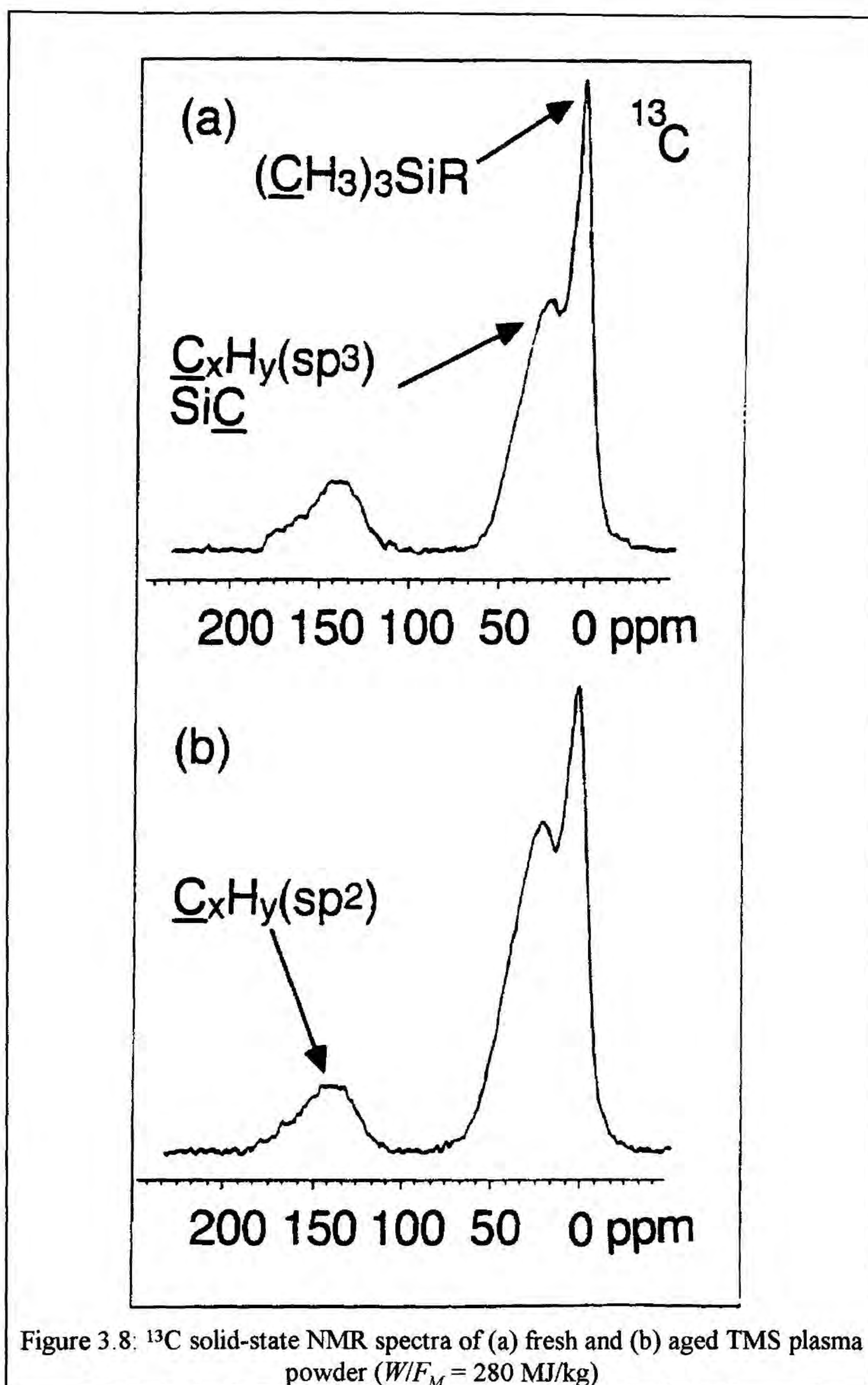

Figure 3.8: ^{13}C solid-state NMR spectra of (a) fresh and (b) aged TMS plasma powder ($W/F_M = 280$ MJ/kg)

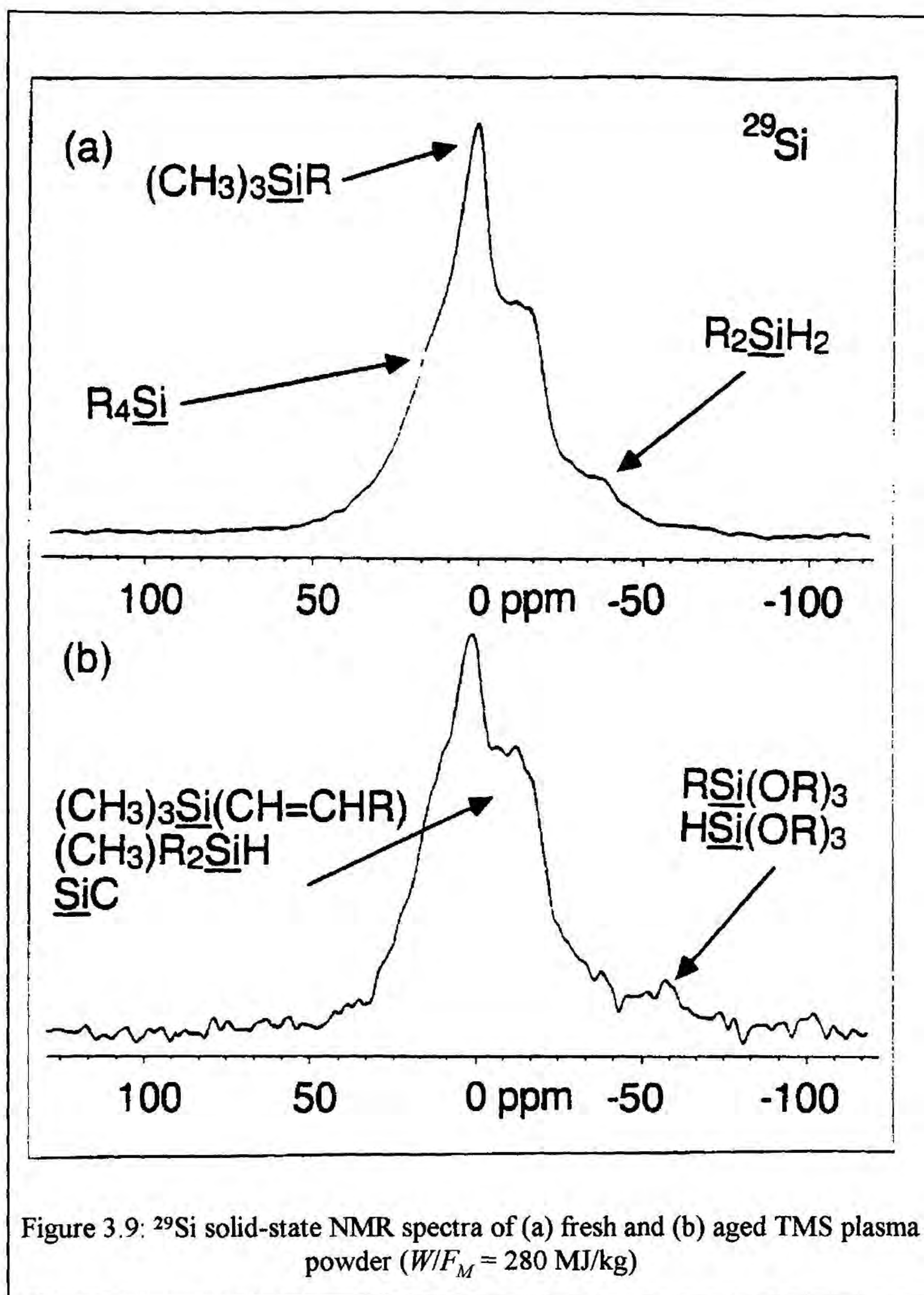

Figure 3.9: ^{29}Si solid-state NMR spectra of (a) fresh and (b) aged TMS plasma powder (W/F_M = 280 MJ/kg)

ppm is most likely to be silicon centres bonded to hydrocarbon chains where not more than one R chain is a methyl group (δ = +6.5 ppm for $[C_2H_5]_3Si[CH_3]$, δ = +7.1 ppm for $[C_2H_5]_3Si[C_2H_5]$, δ = +6.9 ppm for $[C_2H_5]_3Si[n\text{-}C_4H_9]$). The weak feature at -36.0 ppm could be some form of $R^1R^2SiH_2$ linkage (δ = -37.7 ppm for $[CH_3]_2SiH_2$).

The ^{29}Si NMR shoulders at 6.6 ppm, and -10 to -20 ppm increase during ageing, this can be ascribed to either crosslinking processes, or the creation of more silicon carbide type linkages. In addition a weak peak is visible in the -50 to -80 ppm range, this can be assigned to the emergence of $RSi[OR]_3$ and $HSi[OR]_3$ environments.

3.3.4. Emission Spectroscopy

Figure 3.10 depicts the emission spectra of TMS plasmas at 5W (140 MJ/kg) and 10 W (280 MJ/kg). Most of the lines in these spectra originate from electronic transitions within the hydrogen molecule (230-310 nm vibrational-rotational continuum, 363.3 nm, 367.3 nm, 379.9 nm, 385.8 nm, 387.1 nm, 388.6 nm, 406.1 nm, 406.6 nm, 406.9 nm, 417.4 nm, 420.1 nm, 422.0 nm, 433.8 nm, 449.0 nm, 449.6 nm, 455.4 nm, 458.0 nm, 461.5 nm, 463.2 nm, and 461.5 nm)[40,41], and hydrogen atom Balmer lines (486.1 and 434.1 nm)[42]. These assignments were checked by running pure hydrogen plasmas (Figure 3.11). Other strong lines are due to the $C^3\Pi_u \rightarrow B^3\Pi_g$ transition for a nitrogen molecule[43]: 315.9 nm ($\upsilon' = 1$, $\upsilon'' = 0$), 337.1 nm (0, 0) and 357.7 nm (0, 1). It is important to take into consideration that these nitrogen lines are weaker by an approximate factor of 2000 compared to their intensity in a pure nitrogen plasma, and therefore the actual amount of molecular nitrogen in the reactor during TMS plasma polymerisation must be less than 0.05 vol. %. Finally, a band corresponding to the $A^2\Delta \rightarrow X^2\Pi$ transition for a CH radical was observed at 431.4 nm[44,45]. It proved impossible to assign any silicon related features because of the intense hydrogen lines.

As the W/F_M value is increased from 140 MJ/kg (5W) to 280 MJ/kg (10 W), all of the emission lines related to atomic and molecular hydrogen become relatively more intense. Therefore a larger amount of atomic and molecular hydrogen is generated at

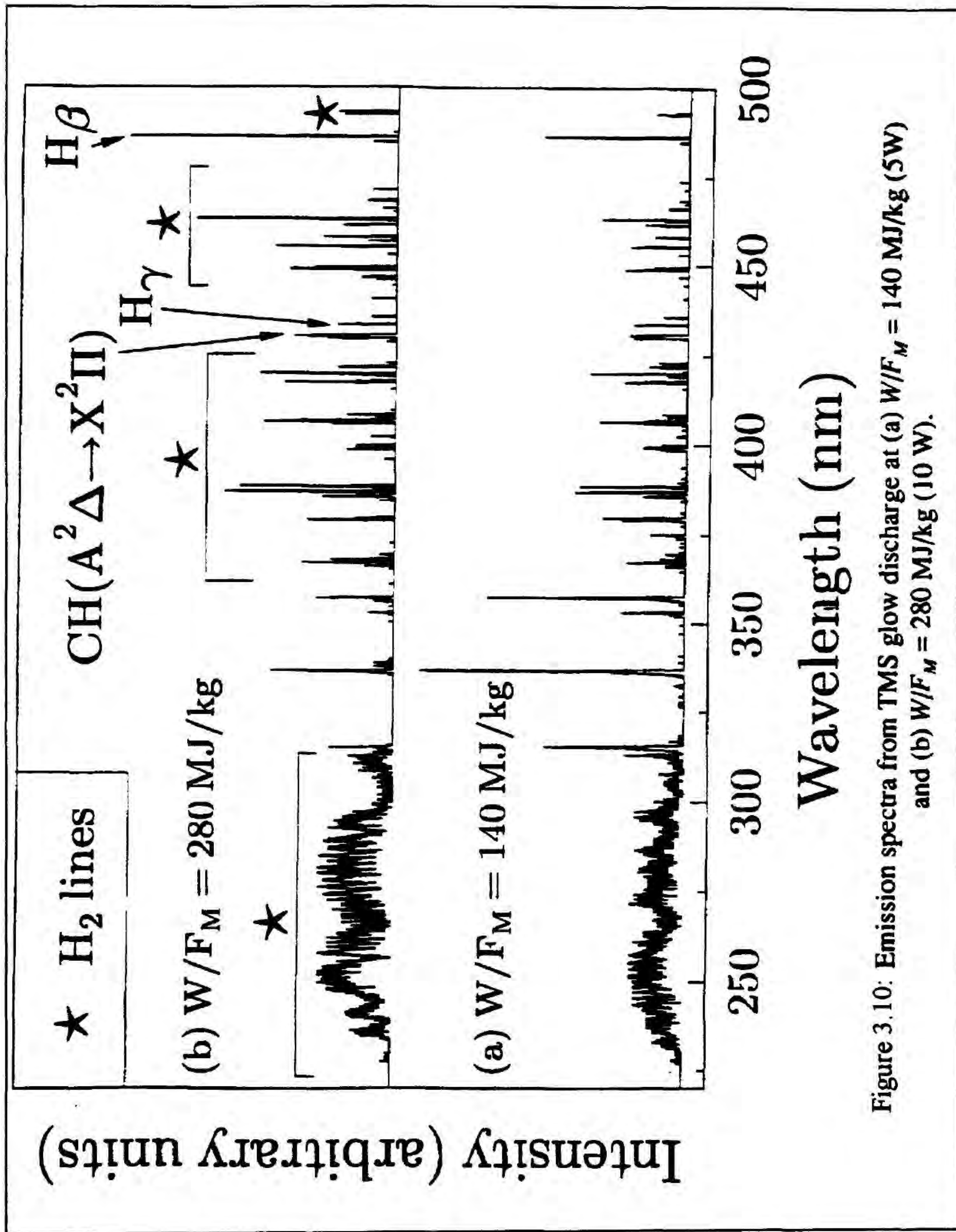

Figure 3.10: Emission spectra from TMS glow discharge at (a) W/F_M = 140 MJ/kg (5W) and (b) W/F_M = 280 MJ/kg (10 W).

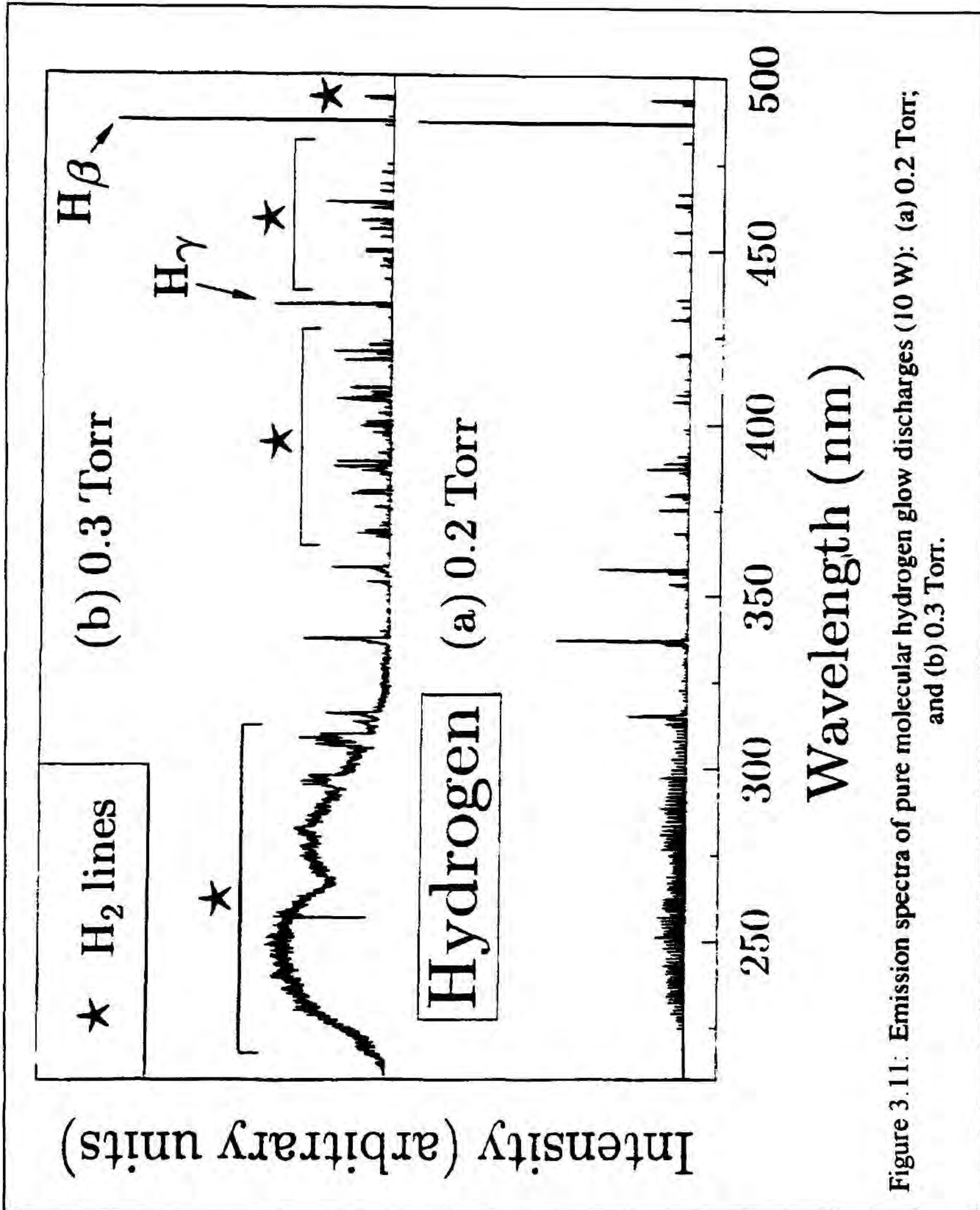

Figure 3.11: Emission spectra of pure molecular hydrogen glow discharges (10 W): (a) 0.2 Torr; and (b) 0.3 Torr.

higher powers due to greater fragmentation of the TMS molecule. Some gaps are evident within the molecular hydrogen 225-350 nm emission continuum at 238-240 nm, 243-247 nm, 255-258 nm, 290-293 nm, and 298-313 nm. The most likely explanation for these absences is that the TMS plasma medium contains unsaturated species which absorb strongly at these wavelengths. For instance, acetylene absorbs in the 220-240 nm range[46,47], another possibility may be the propargyl radical (CH_2-C=CH) which exhibits diffuse bands at 290-345 nm (strongest being at 332 nm, 321.7 nm, and 311.9 nm[48]), or perhaps diacetylene which has 700 narrow bands between 297 to 206.8 nm[49].

3.4. Discussion

Plasma polymerisation processes are widely regarded as being highly complex in nature. Typically they involve dissociation, generation, and recombination of polymerisable species within either the partially ionised gas itself and/or at the substrate surface[1,50]. Such reactions are perpetuated by electron impact and ultraviolet radiation. In simple terms:

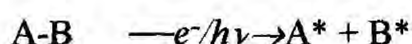

$$\text{A-B} \xrightarrow{e^-/h\nu} \text{A}^* + \text{B}^*$$

Where A and B may be individual atoms or molecular fragments which generate activated species A* and B* (ions and radicals). These intermediates can subsequently recombine to form new chemical species, or impinge onto a growing polymeric layer. This description is appropriate for shorter deposition times, however powdered material is generated over longer periods due to the high internal stresses associated with thicker coatings[51,52]. Such an explanation is supported by the observation that polyethylene films coated with thick TMS plasma polymer layers tend to curl up.

Bond energy values are as follows[53,54]: 292 $kJmol^{-1}$ (Si-C), 322 $kJmol^{-1}$ (Si-H), and 416 $kJmol^{-1}$ (C-H). Therefore Si-C and Si-H bonds are the weakest. Incorporation

of $[CH_3]_nSi$ species into the plasma polymer (as detected by NMR, FTIR, and mass spectrometry[31]) is consistent with the cleavage of $[CH_3]_3Si\text{-}CH_3$ and $[CH_3]_3SiCH_2\text{-}H$ bonds; which leads to predominantly the following primary reactions:

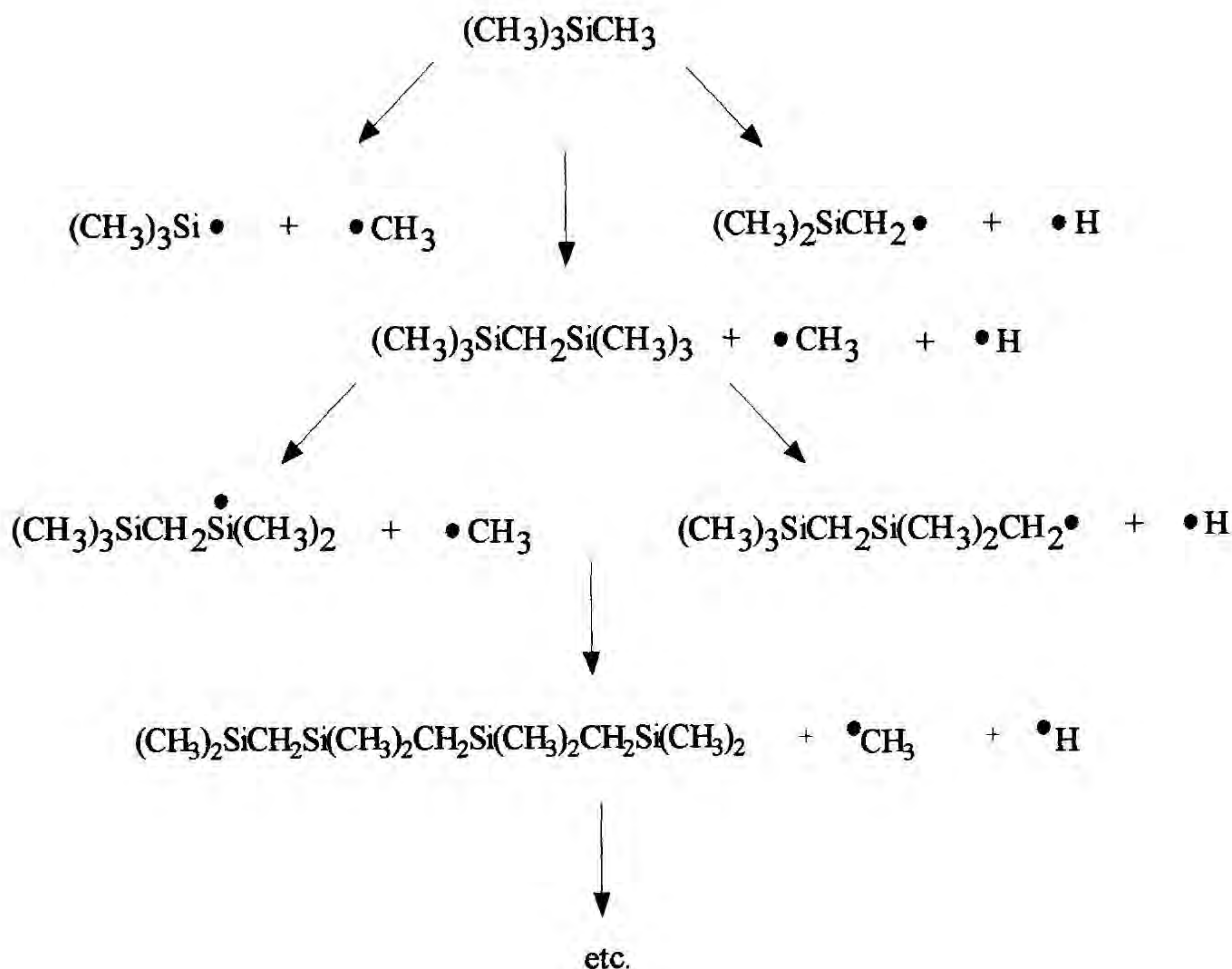

Radical creation along the growing chain will result in branching, thereby creating a random three dimensional network of $-[CH_3]_nSi-$ linkages. Weak Si-Si and strong C-C bonds may also form via homorecombination of carbon and silicon radicals respectively. In TMS plasma polymer, a significant degree of unsaturation, crosslinking, Si-H groups, and possibly some embedded silicon carbide moieties were found. These products could

originate from secondary interactions between electrons, ions, hydrogen atoms, and photons with the growing polymeric matrix. Additional unsaturated species may form via the plasma polymerisation of methyl species generated during the primary fragmentation of the TMS molecule. Ageing is most likely to be a manifestation of trapped free radical centres in the plasma polymer undergoing recombination or reacting with air, with perhaps some hydrolysis of Si-H bonds (the chemical reactions envolved in this process can be found in Chapter 7). There may possibly be silicon carbide species trapped within the organosilicon network, since the use of a heated substrate during plasma polymerisation is reported to result in silicon carbide[55].

3.5. Conclusions

Plasma polymerisation of tetramethylsilane at low powers and short periods result in continuous films, whereas longer times generate a coarse powder. The plasma polymer structure is believed to contain a random three dimensional network of $-[CH_3]_nSiH_m-$ linkages in conjunction with a significant degree of unsaturation, crosslinking and possibly some silicon carbide moieties. These materials undergo oxidation on storage in air. All the results were found in agreement with results already published in the literature.

References

1. H. Yasuda, H., *Plasma Polymerization* Academic Press: Orlando, 1985.
2. Jensen, R.J.; Bell, A.T.; Soomg, D.S., *Plasma Chem. Plasma Process.* **1983**, *3*, 163.
3. Yasuda, H. in Vossen, J.; Kern, W. (eds.), *Thin Film Processes*, p. 361, Academic Press: New York, 1978.

4. Nomura, H.; Kramer, P.W.; Yasuda, H., *Thin Solid Films* **1984**, *118*, 187.

5. Morosoff, N.; Newton, W.; Yasuda, H., *J. Vac. Sci. Technol.* **1978**, *15*, 1815.

6. Poll, H.U.; Arzt, M.; Wickleder, K.H., *Eur. Polym. J.* **1976**, *12*, 505.

7. Morosoff, N.; Yasuda, H.; Brandt, E.S.; Reilley, C.N., *J. Appl. Polym. Sci.* **1979**, *23*, 3449.

8. Morosoff, N.; Yasuda, H., *ACS Symp. Ser.* **1979**, *108*, 163.

9. Rice, D.W.; O'Kane, D.F., *J. Electrochem. Soc.* **1976**, *123*, 1308.

10. O'Kane, D.F.; Rice, D.W., *J. Macromol. Sci. - Chem* **1976**, *A10*, 5677..

11. Inagaki, N.; Kishi, A., *J. Polym. Sci. Polym. Chem. Ed.* **1983**, *21*, 2335.

12. Inagaki, N.; Nishio, Nishio, T.; Katsuura, K., *J. Polym. Sci., Polym. Lett. Ed.* **1980**, *18*, 765.

13. Inagaki, N.; Ohnishi, Y.; Chen, K.S., *J. Appl. Polym. Sci.* **1983**, *28*, 3629.

14. Inagaki, N.; Nejigaki, K.; Suzuki, K., *J. Polym. Sci. Polym. Chem. Ed.* **1983**, *21*, 3181.

15. Catherine, Y.; Zamouche,A., *Plasma Chem. Plasma Process.* **1985**, *5*, 353.

16. Maisonneuve, M.; Segui, Y.; Bui, A., *Thin Solid Films* **1976**, *33*, 35.

17. Inagaki, N.; Koyama, M., *J. Polym. Sci., Polym. Chem. Ed.* **1983**, *21*, 183.

18. Hirotsu, T., *J. Appl. Polym. Sci.* **1979**, *24*, 1957.

19. Clark, D.T.; Shuttleworth, D., *J. Polym. Sci. Polym. Chem. Ed.* **1980**, *18*, 27.

20. Shard, A.G.; Badyal, J.P.S; *Macromolecules* **1992**, **25**, 2053.

21. Inagaki, N; Katsuoka, H., *J. Memb. Sci.* **1987**, *34*, 297.

22. Clark, D.T.; Feast, W.J., *J. Macromol. Sci. Rev. Macromol. Chem.* **1975**, *12*, 191.

23. Kokai, F.; Kubota, T.; Ichjyo, M.; Wakai, K., *J. Appl. Polym. Sci. Appl. Polym. Symp.* **1988**, *42*, 197.

24. Clark, D.T.; Dilks, A. *J. Polym. Sci. Polym. Chem. Ed.* **1979**, *17*, 957.

25. Laoharojanaphand, P.; Lin, T.J.; Stoffer, J.O., *J. Appl. Polym. Sci.* **1990**, *40*, 369.

26. Hamada, K.; Morishita, H., *Spectroscopy Lett.* **1986**, *19*, 815.

27. Painter, P.C.; Coleman, M.M.; Koenig, J.J., *The Theory of Vibrational Spectroscopy and Its Application to Polymeric Materials,* Wiley: New York,

1982.

28. Tajima, I.; Yamamoto, M., *J. Polym. Sci. Polym. Chem. Ed.* **1987**, *25*, 1737.
29. Cai, S.; Fang, J.; Yu, Xuehai, *J. Appl. Polym. Sci.* **1992**, *44*, 135.
30. Coopes, I.H.; Griesser, H.J., *J. Appl. Polym. Sci.* **1989**, *37*, 3413.
31. Wrobel, A.M.; Czeremuskin, G.; Szymanowski, H.; Kowalski, J., *Plasma Chem. Plasma Process.* **1990**, *10*, 277.
32. Szeto, R.; Hess, D.W., *J. Appl. Phys.* **1981**, *52*, 903.
33. Luongo, J.P.; Schonhorn, H., *J. Polym. Sci. Polym. Chem. Ed.* **1968**, *6*, 1649.
34. Luongo, J.P., *J. Polym. Sci. Polym. Letts.* **1964**, 2, 75.
35. Mirabella, F.M., *Appl. Spec. Rev.* **1985**, *21*, 45.
36. Apperley, D.C.; Harris, R.K.; Marshall, G.L.; Thompson, D.P., *J. Am. Ceram. Soc.* **1991**, *74*, 777.
37. Marsmann, H., *NMR: Basic Principles and Progress* **1981**, *17*, 65.
38. Assink, R.A.; Hays, A.K.; Bild, R.W., *J. Vac. Sci. Technol.* **1985**, *A3*, 2629.
39. Gamboji, R.J.; Cho, D.L.; Yasuda, H.; Blum, F.D., *J. Polym. Sci. Polym. Chem. Ed.* **1991**, *29*, 1801.
40. Pearse, R.W.B.; Gayon, A.G., *The Identificatoin of Molecular Spectra*, Chapman and Hall: London, 1976.
41. Dike, G.H., *The Hydrogen Molecule Wavelength Tables of G.H. Dieke*, ed. Crosswhite, H.M., Wiley: New York, 1972.
42. Hollas, J.M., *Molecular Spectroscopy*, Wiley: New York, 1987.
43. *Spectroscopic Data Relative to Diatomic Molecules*, Rosen, B., Pergamon: Oxford, 1970.
44. Kiess, N. H.; Broida, H. P., *Astrophys. J.* **1956**, *123*, 166.
45. Moore, C.E.; Broida, H.P., *J. Res. Nat. Bur. Stand.* **1959**, *A-63*, 19.
46. Woo, S.C.; Liu, T.K.; Chu, T.C.; Chih, W., *J. Chem. Phys.* **1938**, *6*, 240.
47. Innes, K.K, J. *Chem. Phys.* **1954**, *22*, 863.
48. Ramsay, D.A.; Thistlewaite, P., *Canad. J. Phys.* **1966**, *44*, 1381.
49. Woo, S.C. and Chu, T.C., *J. Chem. Phys.* **1937**, 786.

50. Bell, A.T., *Fundamentals of Plasma Chemistry*, in *Techniques and Applications of Plasma Chemistry*, Hollahan, J.R. and Bell, A.T. (eds.), Wiley: New York (1974).

51. Morinaka, A.; Asano, Y,, *J. Appl. Polym. Sci.* **1982**, *27*, 2139.

52. Clark, D.T.; Abrahman, M.Z., *J. Polym. Sci. Polym. Chem. Ed.* **1982**, *20*, 1729.

53. Weast, R.C.; Astle, M.J. (eds.), *CRC Handbook of Chemistry and Physics*, CRC Press:, Boca Raton, Florida, 1982.

54. Pilcher, G.; Leitão, M.L.P.; Yan, Y.M.; Walsh, R., *J. Chem. Soc. Faraday Trans.* **1991**, *87*, 841.

55. Zhang, W.; Lelogeais, M.; Ducarroir, M., *Jpn. J. Appl. Phys.* **1992**, *31*, 4053.

Chapter Four

PLASMA POLYMERISATION OF HEXAMETHYLDISILANE

Contents

4.1. Introduction 84

4.2. Experimental 84

4.3. Results 84

- 4.3.1. X-ray photoelectron spectroscopy 85
- 4.3.2. Fourier transform infrared spectroscopy 92
- 4.3.3. Solid state NMR 99
- 4.3.4. Emission spectroscopy 103

4.4. Discussion 105

4.5. Conclusions 107

4.1. Introduction

In this chapter use is made of hexamethyldisilane ($[CH_3]_3Si-Si[CH_3]_3$) as the precursor. This monomer contains a weak Si-Si linkage, which should make it much more susceptible towards plasma polymerisation than that found for comparable monosilicon containing precursors.

4.2. Experimental

The experimental set up used in this chapter is the same one used in Chapter 3 (pages 57-60), apart from the following points:

- Hexamethyldisilane (HMDS, 98%, vapour pressure = 0.006 atm at 27 °C, Aldrich Chemical Co.) was used as the precursor;
- The mass flow rate was $F_M = 4.3 \times 10^{-8}$ kg/s (the organosilane precursor accounts for at least 99.4 % of the gaseous contents in the reaction chamber, as in the case of the TMS monomer);
- Deposition of powder and material for ageing studies were carried out at $W/F_M = 120$ MJ/ kg (power = 5 Watts).

4.3. Results

Freshly deposited powder was found to change from brown to yellow in appearance after prolonged exposure to air. This material was highly resistant towards chemical attack (eg. alkali solutions, organic solvents at high termperatures), and it was also found to be mechanically tough. Micro analysis gave a H/C ratio of 2.3. Powder X-ray diffraction measurements yielded no evidence for any degree of crystallinity in either the unaged or oxidised powders.

4.3.1. X-ray photoelectron spectroscopy

Figures 4.1 to 4.3 show XPS spectra of fresh powder deposited at 5 Watts (W/FM = 120 MJ/kg) onto a glass slide and its subsequent ageing. In the C(1s) region, the main peak at a binding energy of 285.0 eV can be assigned to C-H, C-C and C-Si environments[1,2]. There is also a very slight shoulder at 287.9 eV which is probably due to a small amount of surface oxidation during transport through air to the electron spectrometer (a corresponding O(1s) signal at 533.2 eV is observed). A strong peak centred at 101.1 eV was found for the Si(2p) core level, this is characteristic of Si-H and Si-C bonds[1,2]. From the XPS data, the relative composition of the fresh material was estimated to be 75% carbon, 21% silicon and 4% oxygen (XPS can not detect the amount of hydrogen).

On ageing, the C(1s) envelope develops a pronounced shoulder towards greater binding energies. This can be attributed to the presence of carbon singly bonded to one oxygen atom (-C-O- ≈286.6 eV), carbon singly bonded to two oxygen atoms or carbon doubly bonded to one oxygen atom (-O-C-O-, -C=O ≈ 287.9 eV) and carboxylate groups (-O-C=O ≈ 289.0 eV)[3]. The Si(2p) peak centre also increases in value to 101.4 eV with an accompanying shoulder at higher binding energy. Again this can be taken as evidence for silicon bonded to oxygen (Si-O at 102.2 eV and SiO_2 at 104.1 eV)[4]. Following oxidation, the relative atomic composition was calculated to be 66% carbon, 18% silicon, and 15% oxygen.

Figure 4.4 summarises the variation of Si/C ratio as a function of plasma power, it can be seen that the relative amount of silicon falls off continually with increasing wattage. It can also be seen that the deposition rate of silicon containing films is very low at plasma powers in excess of 20 W (W/F_M = 470 MJ/kg). Also the dependence of Si/C ratio on the position of the substrate within the reactor is described in Figure 4.5, (5 Watts, 10 min). The amount of silicon incorporated into the deposited layer drops on moving downstream from the monomer inlet. Figure 4.6 illustrates the relationship

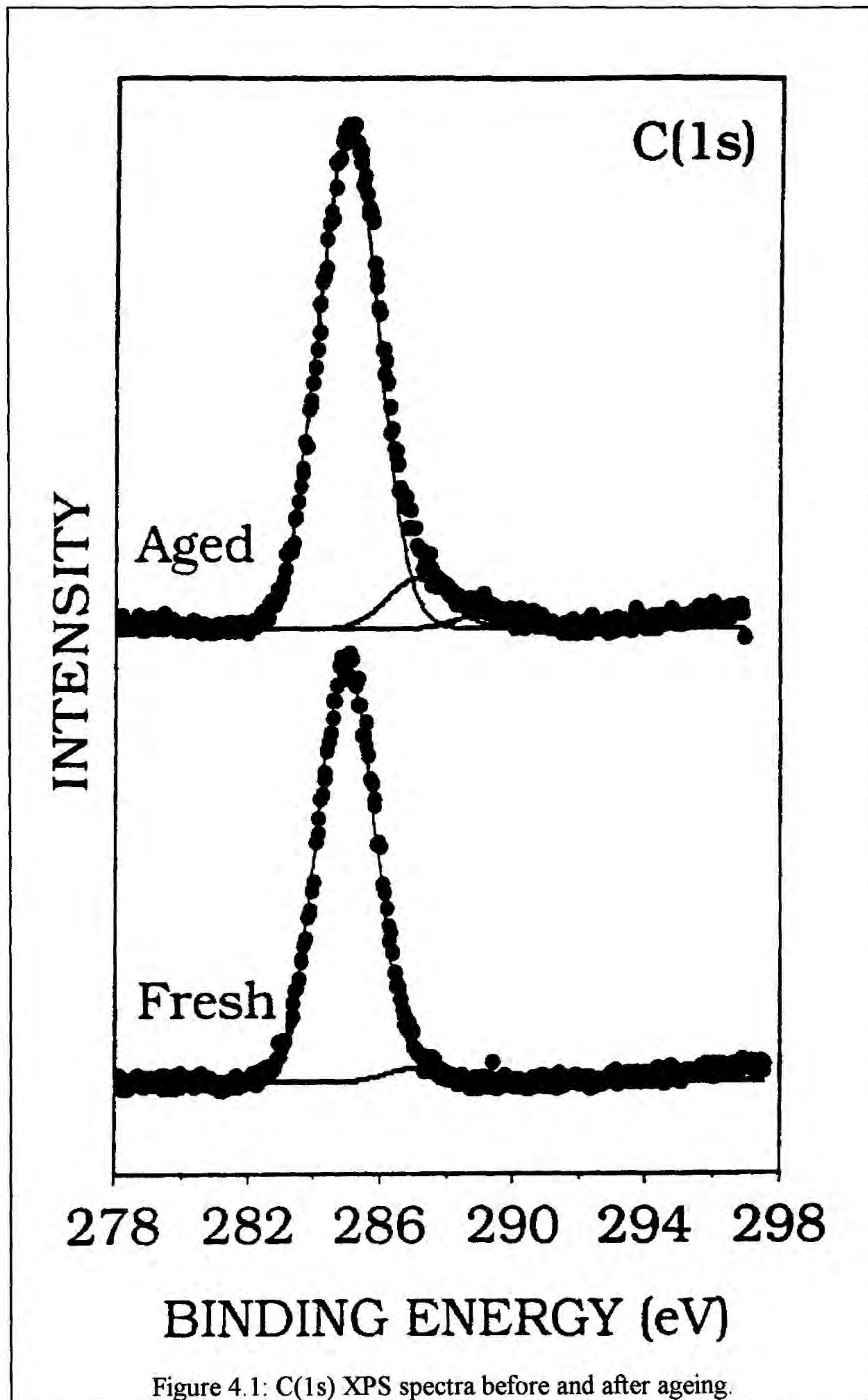

Figure 4.1: C(1s) XPS spectra before and after ageing.

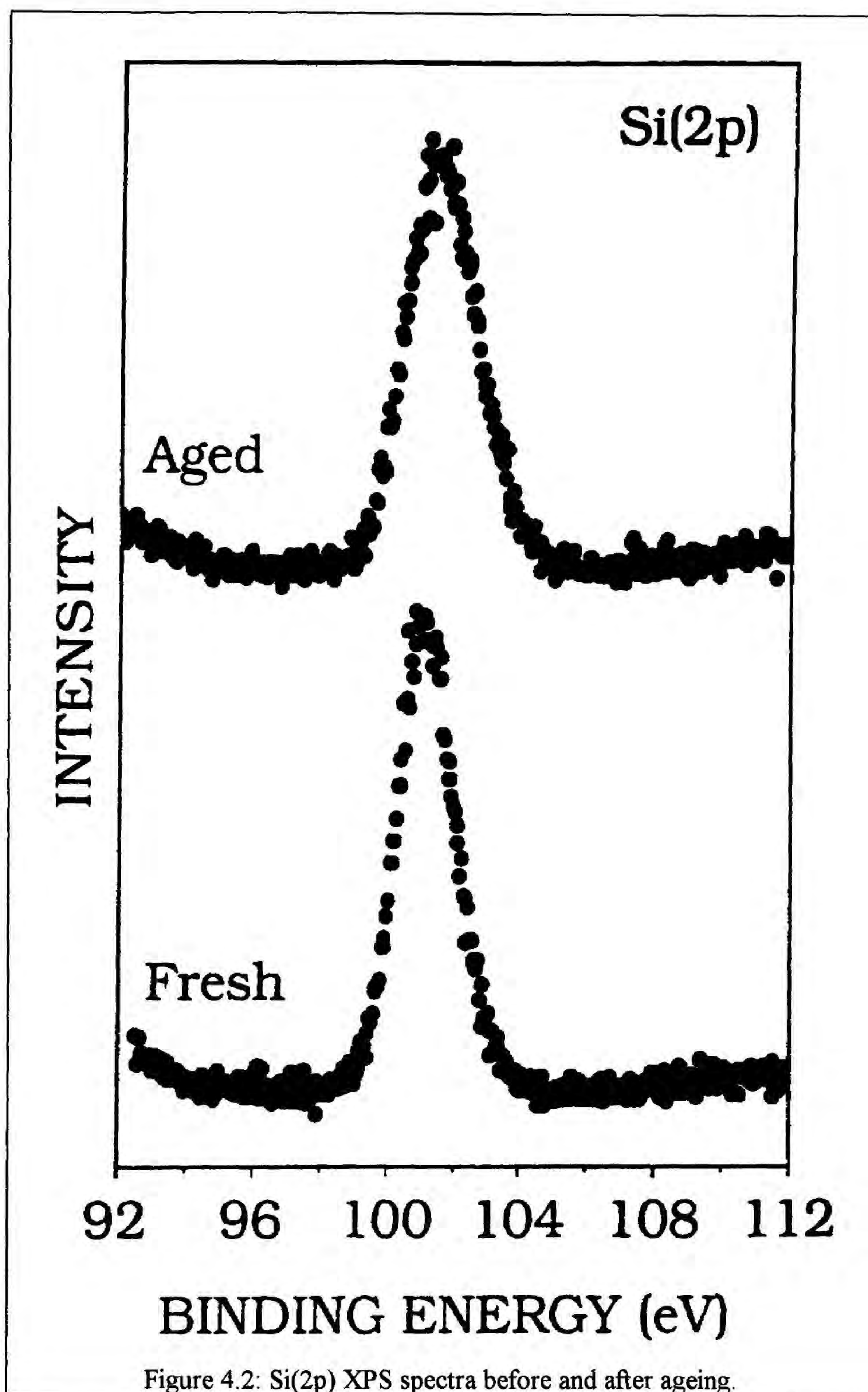

Figure 4.2: Si(2p) XPS spectra before and after ageing.

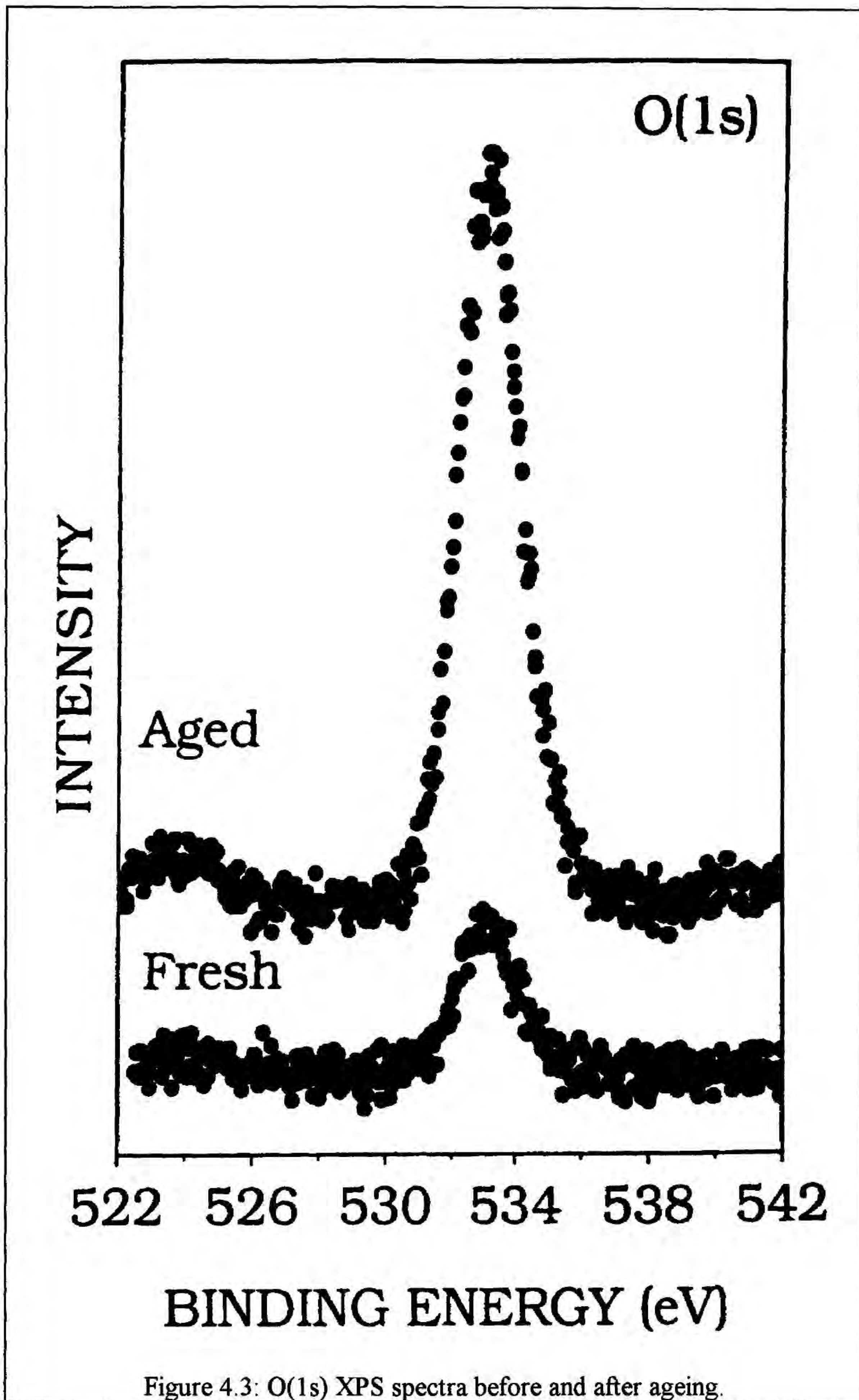

Figure 4.3: O(1s) XPS spectra before and after ageing.

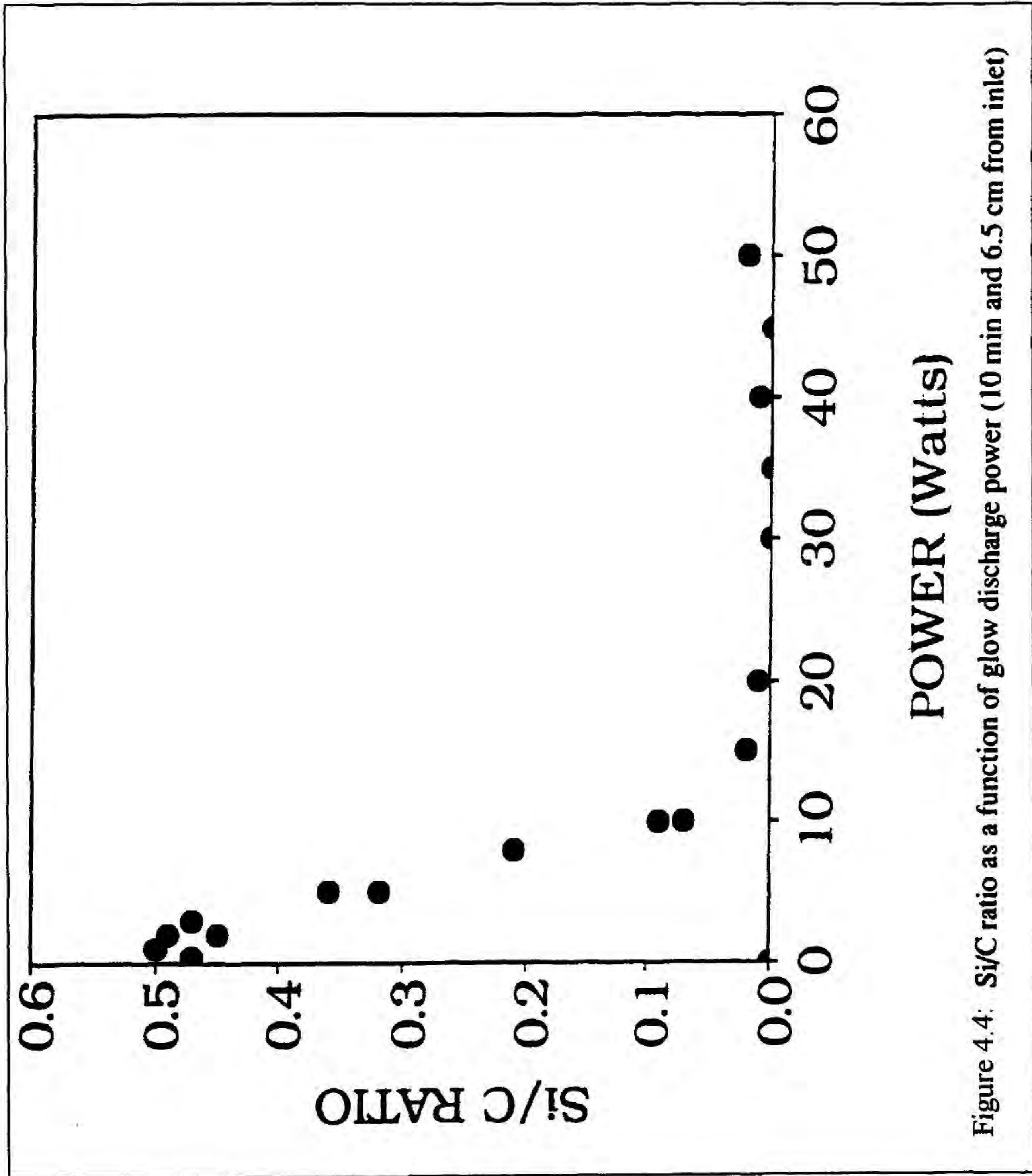

Figure 4.4: **Si/C ratio as a function of glow discharge power (10 min and 6.5 cm from inlet)**

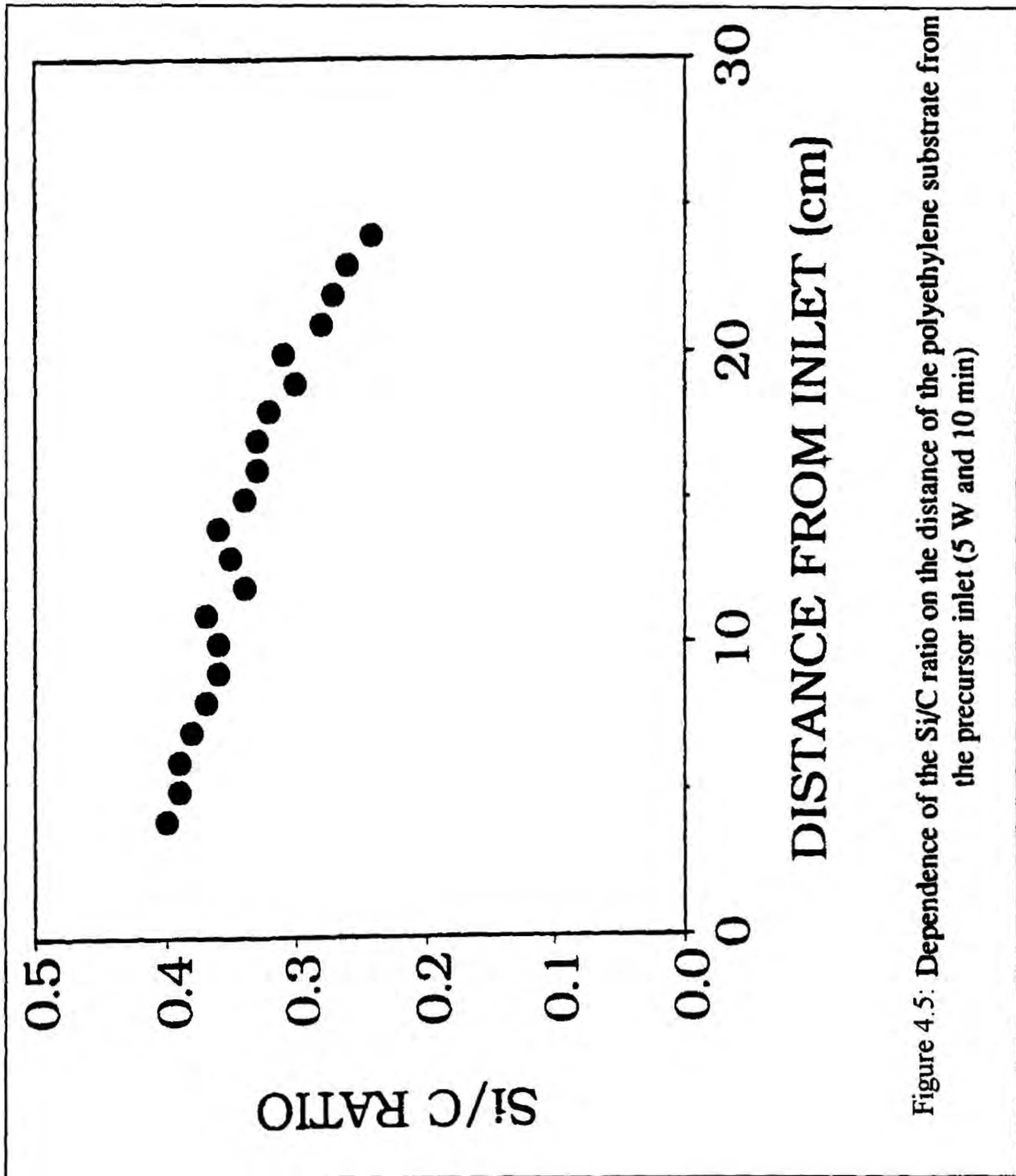

Figure 4.5: Dependence of the Si/C ratio on the distance of the polyethylene substrate from the precursor inlet (5 W and 10 min)

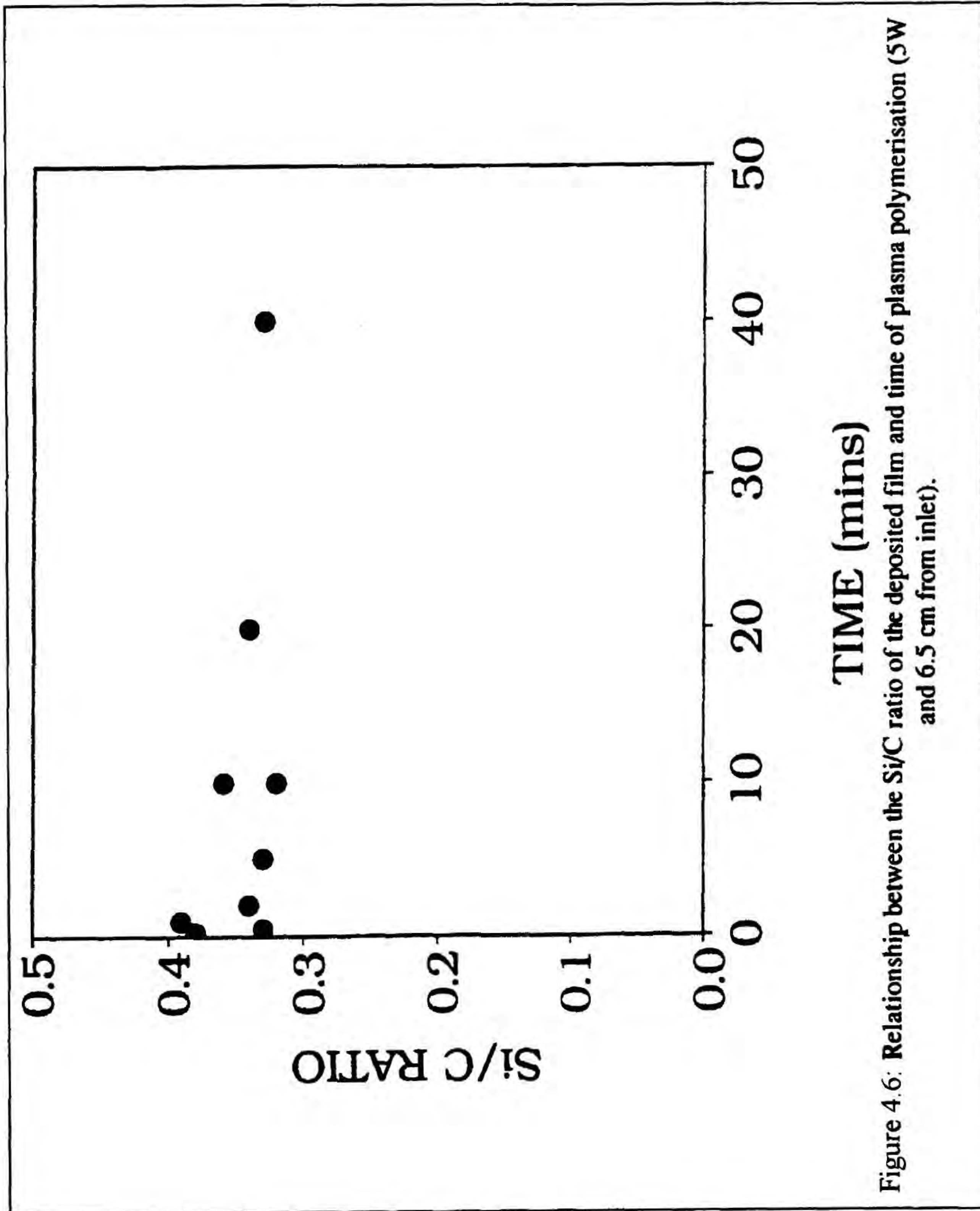

Figure 4.6: **Relationship between the Si/C ratio of the deposited film and time of plasma polymerisation (5W and 6.5 cm from inlet).**

between time and Si/C ratio at a plasma power of 5 Watts (W/F_M = 120 MJ/kg). It can be seen that the Si/C value does not vary significantly (this is within the experimental error of the data analysis). Therefore the deposition process must quickly reach a steady state.

4.3.2. Fourier transform infrared spectroscopy

Hexamethyldisilane possesses the following infrared absorption bands[5]: 2951 cm^{-1} (C-H asymmetrical stretching in CH_3), 2893 cm^{-1} (C-H symmetrical stretching in CH_3), 1246 cm^{-1} (CH_3 symmetric bending in $Si(CH_3)_n$), 835 cm^{-1} (CH_3 rocking in $Si(CH_3)_n$), and 721 cm^{-1}, 690 cm^{-1} and 607 cm^{-1} (Si-C stretching). Whereas the Si-Si stretch is infrared-inactive.

Typical FTIR spectra of the plasma deposit generated from HMDS are shown in Figure 4.7 for both fresh and aged powder. CH_3 stretching bands are known[6] to occur at 2962 cm^{-1} (C-H antisymmetrical stretching) and 2872 cm^{-1} (C-H symmetrical stretching). Whereas methylene groups (CH_2) in aliphatic and non-strained cyclic hydrocarbons exhibit C-H anti-symmetrical and symmetrical stretches at 2926 and 2853 cm^{-1} respectively[6] (the exact positions may vary across a range of ± 10 cm^{-1}). It should be noted that in strained rings, methylene stretching frequencies have been reported to increase. Therefore it can be concluded that the 2951 and 2895 cm^{-1} bands recorded in the FTIR spectra of the freshly deposited material arise as a result of the CH_3 stretching frequency.

The following silicon related bands were assigned for the freshly collected material[7-12]: 2104 cm^{-1} (Si-H stretching), 1408 cm^{-1} (Si-CH_3 anti-symmetrical stretching and/or CH_2 scissoring in $Si(CH_2)_n$), 1356 cm^{-1} (methylene twisting and wagging vibrations), 1254 cm^{-1} (CH_3 symmetrical bending in $Si(CH_3)_n$), (1044 cm^{-1} to Si-O-Si and/or Si-O-C and/or CH_2 wagging in Si-$(CH_2)_n$-Si), 835 cm^{-1} (CH_3 rocking in $Si(CH_3)_n$ (n = 2,3)), 785 cm^{-1} (CH_3 rocking in $Si(CH_3)_n$ (n=1,2)), and 685 cm^{-1} (Si-C stretching).

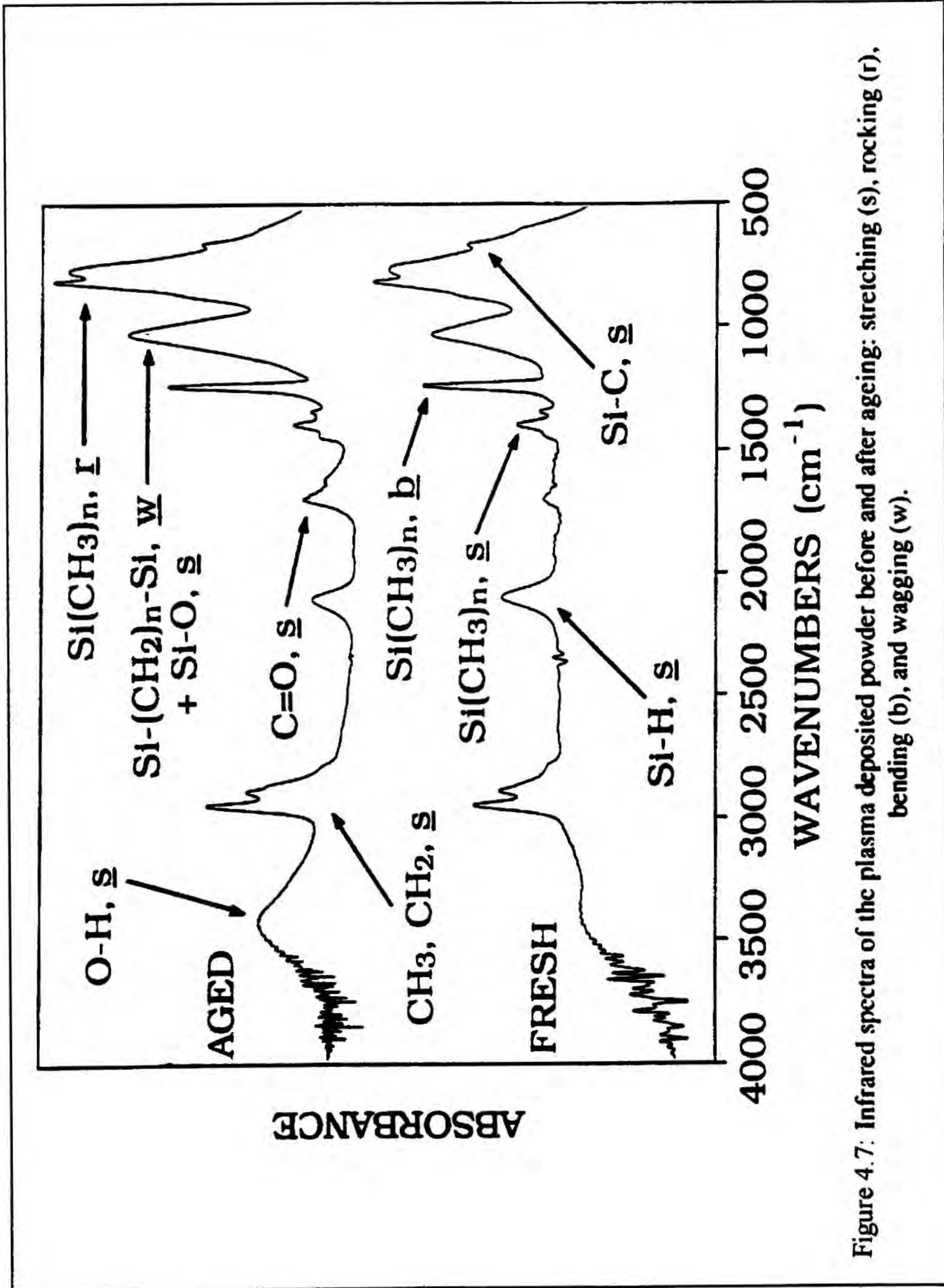

Figure 4.7: Infrared spectra of the plasma deposited powder before and after ageing: stretching (s), rocking (r), bending (b), and wagging (w).

It is interesting to note that all the cited infrared absorptions for the fresh powder shift to higher frequencies on ageing; this is consistent with the assumption that reactive centres in the solid product undergo crosslinking. There is also strong evidence for bulk oxidation, since the following additional bands emerge: 3426 cm^{-1} (OH stretching[6]), 1717 cm^{-1} (C=O stretching[6]), 1632 cm^{-1} (antisymmetrical stretching mode of C=O in carboxylates[6]), and the 1044 cm^{-1} band increases in intensity, which signifies the presence of Si-O-Si and/or Si-O-C bonding. Also it is highly likely that the 1632 cm^{-1} band may have an alkene component, since the C=C stretching mode of unconjugated olefins are known to possess a moderate to weak absorption[1] at 1667 - 1640 cm^{-1}, this would be consistent with trapped carbon centre free radicals undergoing recombination to form double bonds.

Infrared spectra of clean polyethylene and also polymer substrates which have been exposed to a range of hexamethyldisilane glow discharges are collated in Figure 4.8. The assignment of the bands related to clean polyethylene can be found in Table 3.3 (Chapter 3)..

Assignment of the infrared absorption bands observed for the plasma polymers deposited onto polyethylene film is presented in Figure 4.9. Most of these peaks are similar to those in the bulk plasma polymer. They include: 2118 cm^{-1} (stretching in Si-H), 1250 cm^{-1} (CH_3 symmetrical bending, in $Si(CH_3)_n$), 1036 cm^{-1} (Si-O-Si and/or Si-O-C, and/or CH_2 wagging in $Si-(CH_2)_n-Si$), 833 cm^{-1} (CH_3 rocking in $Si(CH_3)_n$, n = 2,3), 791 cm^{-1} (CH_3 rocking in $Si(CH_3)_n$, n = 1, 2), 689 cm^{-1} (Si-C stretching). An additional weak absorption band at 621 cm^{-1} was found for the coating obtained from the 2 Watts glow discharge, this can be attributed to the presence of vinyl groups[13].

At low plasma powers, there is a small occurrence of vinyl groups, which is accompanied by a considerable number of silicon related groups: $Si-(CH_2)_n-Si$, $Si(CH_3)_n$, and probably a minor fraction of Si-O-Si and/or Si-O-C originating from the reaction of trapped free radicals with oxygen and moisture in the air during sample transfer. With increasing power, the vinyl component gradually disappears, together with the groups associated with silicon, until the infrared spectrum corresponds to

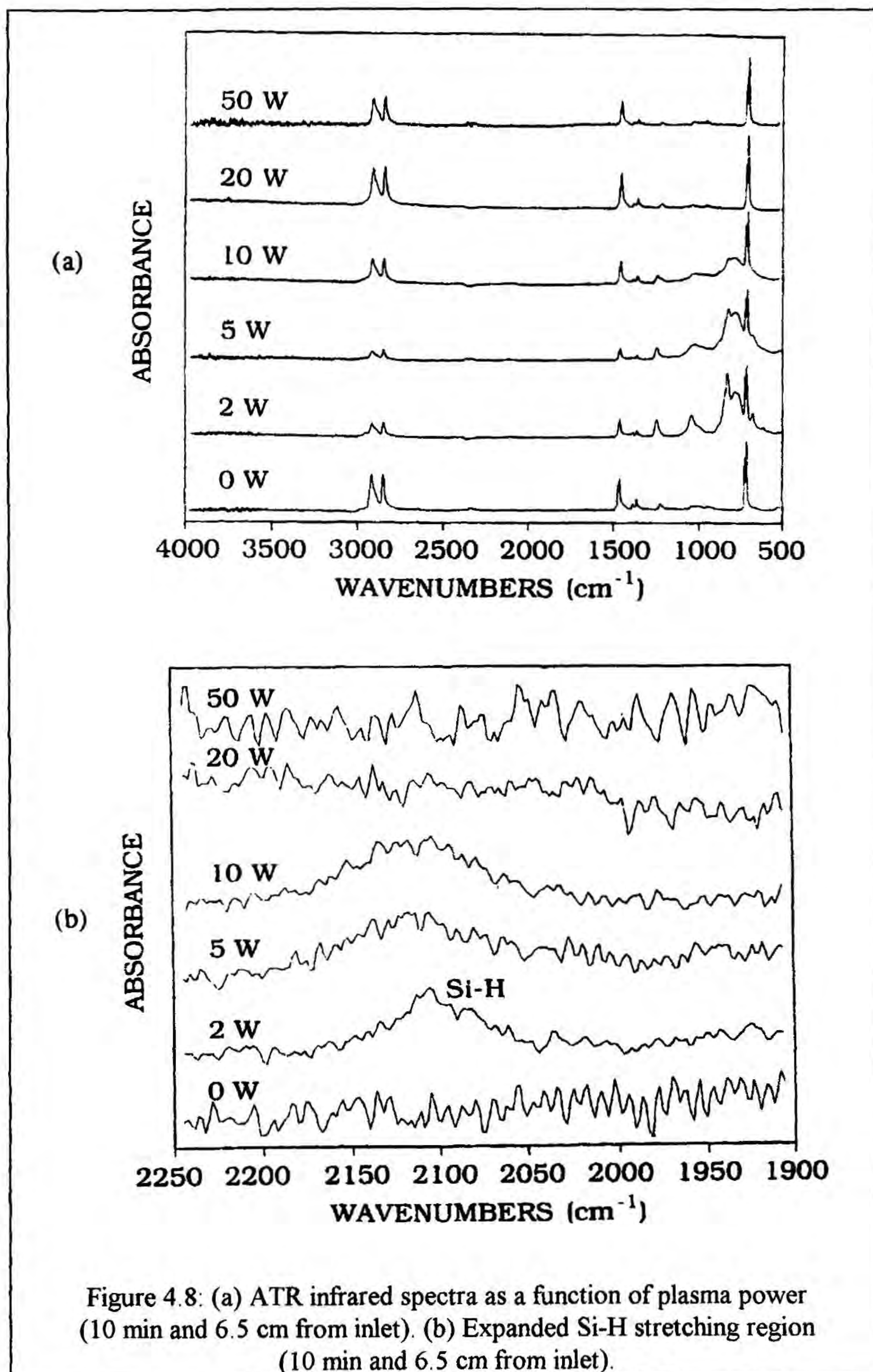

Figure 4.8: (a) ATR infrared spectra as a function of plasma power (10 min and 6.5 cm from inlet). (b) Expanded Si-H stretching region (10 min and 6.5 cm from inlet).

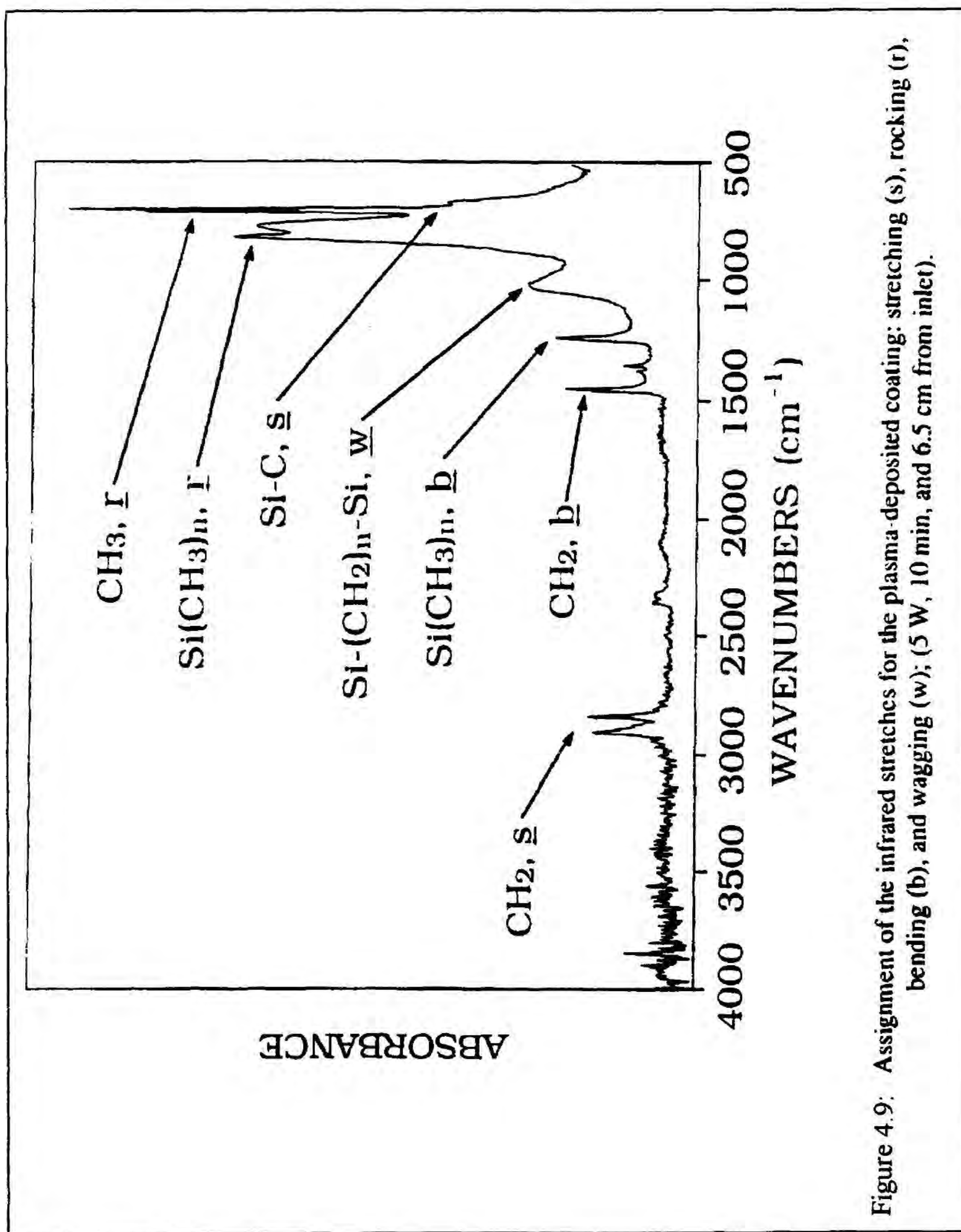

Figure 4.9: Assignment of the infrared stretches for the plasma-deposited coating: stretching (s), rocking (r), bending (b), and wagging (w); (5 W, 10 min, and 6.5 cm from inlet).

virtually that of clean polyethylene (20 and 50 Watts - W/F_M = 470 and 1200 MJ/kg), which implies that at these powers no deposition of plasma polymer occurs. It should be noted that as the power increases, the proportion of methyl groups linked to silicon decrease: at 2 Watts, the absorption at 833 cm^{-1} band (CH_3 rocking in $Si(CH_3)_n$, n = 2, 3) is much greater than that at 791 cm^{-1} (CH_3 rocking in $Si(CH_3)_n$, n = 1, 2), whereas these bands are of roughly the same intensity at 10 Watts (W/F_M = 230 MJ/kg).

The minimal absorbance intensity of the characteristic polyethylene features at 2915 cm^{-1} and 2847 cm^{-1} occurs at approximately 5 Watts (W/F_M = 120 MJ/kg). This correlates to the highest deposition rate of Si containing material observed in the XPS measurements. Since the sampling depth is inversely proportional to the infrared wavenumber, these bands are expected to be more surface sensitive than the other characteristic polyethylene features found at lower wavenumbers. Any incorporation of plasma polymer onto the polyethylene substrate could also contribute to this differential attenuation of polyethylene infrared features. This would be consistent with the observation that these infrared spectra are markedly different compared to those obtained for the bulk plasma polymer material (as in Chapter Three).

At high powers (50 Watts, W/F_M = 1200 MJ/kg), the methyl band at 1366 cm^{-1} band is of lower intensity than that seen for clean polyethylene, this implies a deficiency of methyl end groups at the substrate surface. The absorbance ratio of the strong 729 cm^{-1} and 720 cm^{-1} components of the methylene rocking doublet gives an indication of the relative changes in crystallinity and/or orientation at the polyethylene surface. On raising the plasma power, the polyethylene becomes more amorphous and/or disorientated in the vicinity of substrate-plasma polymer interface.

Figure 4.10 shows the infrared spectra of 5 Watts (W/F_M = 120 MJ/kg) treated polyethylene film which was located at different positions within the glow discharge (4 and 24 cm away from the monomer inlet). Deposition of Si-containing plasma polymer is greatest near the reactor inlet, since all the bands related to this material are more pronounced in this region.

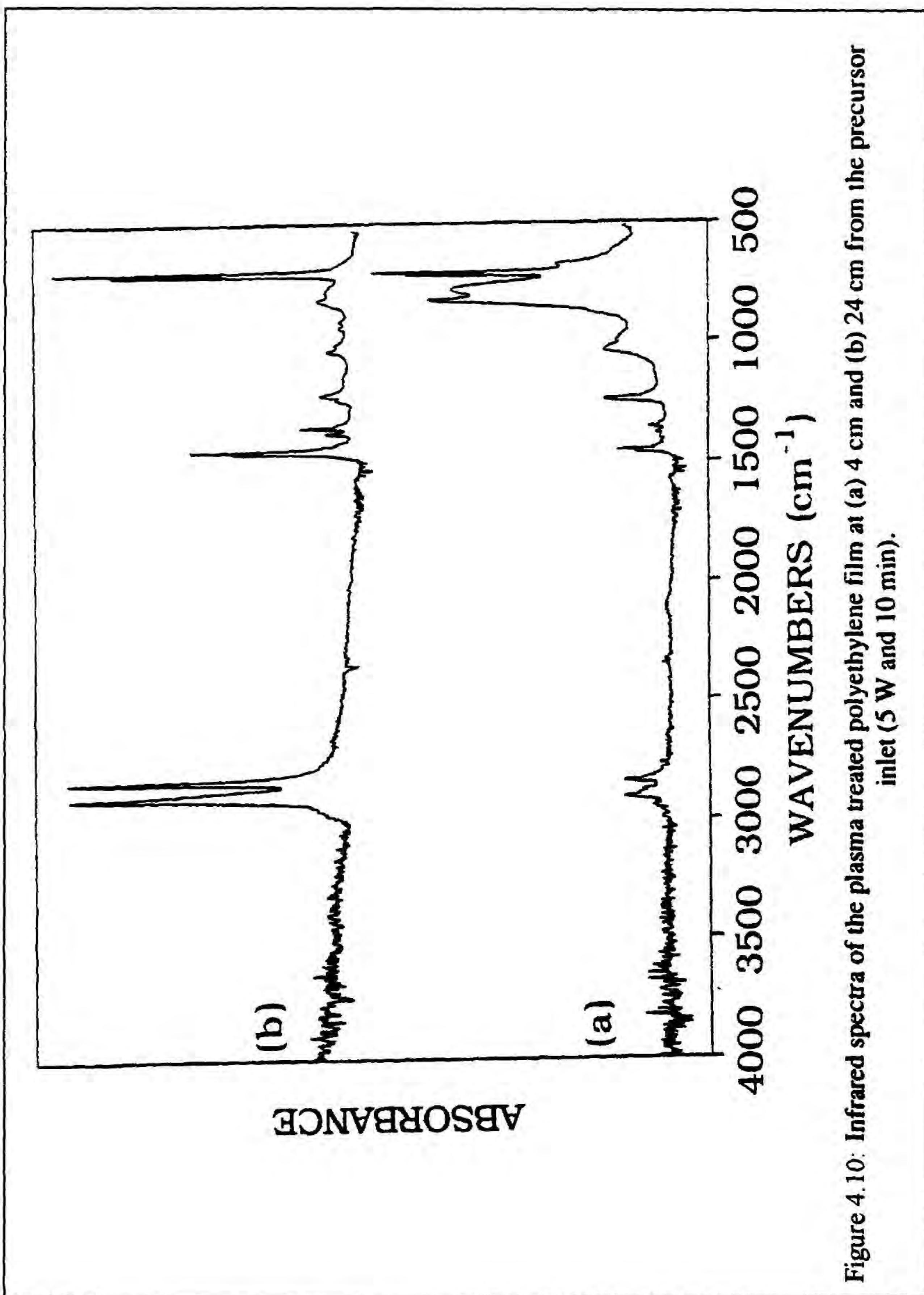

Figure 4.10: Infrared spectra of the plasma treated polyethylene film at (a) 4 cm and (b) 24 cm from the precursor inlet (5 W and 10 min).

4.3.3. Solid State NMR

All the NMR measurements are referenced with respect to tetramethylsilane, $(CH_3)_4Si$. The numerous ^{13}C and ^{29}Si NMR chemical shifts referred to in this section, have been assigned by using literature data for model compounds[14,15]. ^{13}C and ^{29}Si spectra are shown in Figures 4.11 and 4.12 respectively. The bandshapes are consistent with contributions from a wide variety of chemical species. In both the ^{13}C and ^{29}Si spectra, the most intense peak is around 0 ppm, arising from chemical environments similar to those found in tetramethylsilane. In other words, the major constituent of the deposited material is a silicon centre which is bound to a number of methyl groups.

In the ^{13}C spectrum there is a high frequency shoulder between +20 → +50 ppm range indicative of sp^3 carbon atoms within a hydrocarbon chain. Pure silicon carbide (depending on the polytype) also has characteristic peaks in this region[16]. The weak ^{13}C signal between +120 → +180 ppm suggests a small degree of unsaturation or oxygenation.

Following prolonged exposure of the material to air, there was a marked increase in intensity of ^{13}C environments between +190 → +210 ppm (ketones and aldehydes), and +150 → +185 ppm (carboxylic acids and esters). There is also a broadening of the main shoulder due to alcohols (+60 -> +70 ppm), and quaternary carbons (+30 -> +55 ppm).

The corresponding ^{29}Si NMR spectra for the freshly deposited plasma polymer consists of peaks at +6.6, +1.0, -9.2, -13.6 and -36.0 ppm. In general, organosilicon compounds of the type $R^1R^2R^3R^4Si$ yield ^{29}Si chemical shifts varying from -4.5 to +20.0 ppm. Extension of the alkyl chain results in a shift to high frequency, as illustrated by the following model compounds: $(CH_3)_4Si$ at 0.0 ppm, $(CH_3)_3Si(C_2H_5)$ at +1.6 ppm, $(CH_3)_2Si(C_2H_5)_2$ at +4.6 ppm, $(CH_3)Si(C_2H_5)_3$ at +6.5 ppm, and $(C_2H_5)_4Si$ at +7.1. Therefore likely candidates for the peak centred at +6.6 ppm are silicon centres bonded to hydrocarbon chains where not more than one R chain is a methyl group, as invoked by the following series of model compounds: $(C_2H_5)_3Si(CH_3)$ +6.5 ppm,

$(C_2H_5)_3Si(C_2H_5)$ +7.1 ppm, $(C_2H_5)_3Si(n\text{-}C_4H_9)$ +6.9 ppm. The signal at +1.0 ppm can be attributed to $(CH_3)_3Si$ functionality located at hydrocarbon chain ends, as suggested by the following set of model compounds: $(CH_3)_4Si$ at 0.00 ppm, $(CH_3)_3Si(C_2H_5)$ at +1.6 ppm, $(CH_3)_3Si(n\text{-}C_3H_7)$ at +0.7 ppm, $(CH_3)_3Si(n\text{-}C_4H_9)$ at +0.6 ppm, $(CH_3)_3Si(n\text{-}C_5H_{11})$ at +0.2 ppm, and $(CH_3)_3Si(CH_2CH_2CH(CH_3)_2)$ at +0.9 ppm. The shoulder at -9.2 ppm could either be from silicon centres with unsaturated carbon centres attached to the β position from the $(CH_3)_3Si$ group of the type $(CH_3)_3Si(CH{=}CHR)$ where R = H or CH_3, or $(CH_3)R_2SiH$ provided R has an alkyl chain containing at least two ($-CH_2-$) linkages, as seen from the following list of model compounds: $(CH_3)(n\text{-}C_3H_7)_2SiH$ at -10.9 ppm, $(CH_3)(n\text{-}C_4H_9)_2SiH$ at -9.8 ppm, $(CH_3)(n\text{-}C_5H_{11})_2SiH$ at -9.8 ppm, $(CH_3)(n\text{-}C_6H_{13})_2SiH$ at -9.9 ppm. Hexamethyldisilane, $(CH_3)_3SiSi(CH_3)_3$ gives a ^{29}Si NMR peak at -20.5 ppm, and therefore the feature at -13.6 ppm could have some contribution from Si-Si linkages. However silicon carbide type species are also known to occur in this region[16]. The weak feature at -36.0 ppm could be some form of $R^1R^2SiH_2$ linkage, as given by the following model compound: $(CH_3)_2SiH_2$ at -37.7 ppm.

On ageing, there is a marked increase in intensity of the shoulder at +6.9 ppm in the ^{29}Si spectrum. In general, $(CH_3)_3SiOR$ species have characteristic chemical shifts in this vicinity, eg. $(CH_3)_3SiO(C_2H_5)$ at +7.4 ppm. Other possibilities include $(CH_3)_3SiOSi(CH_3)_3$ at +6.0 ppm. The following series of compounds can be regarded as models for the varying degrees of crosslinking around a Si atom: $(CH_3)_3SiR^1$ at δ +1 ppm, $(CH_3)_2SiR^1R^2$ at δ +4 → +5 ppm, $(CH_3)SiR^1R^2R^3$ at δ +6 → +7 ppm, and $SiR^1R^2R^3R^4$ at δ +7 → +8 ppm; therefore any significant degree of crosslinking would also result in a contribution towards the shoulder at 6.9 ppm. Small components to the low frequency side of -40 ppm are assigned to silicon bound to increasing numbers (2, 3, or 4) of oxygen atoms, as seen from the following model compounds: $(n\text{-}C_4H_9)Si(OC_2H_5)_3$ at -47.4 ppm, $n\text{-}C_3H_7Si(OC_2H_5)_3$ at -47.0 ppm, $C_2H_5Si(OC_2H_5)_3$ at -45.9 ppm, $(CH_3)Si(OC_2H_5)_3$ at -45.5 ppm, $(CH_3)Si(OCH_3)_3$ at -41.5 ppm, and

(a) 13C FRESH

(x5)

($\underline{C}H_3)_3SiR$

$\underline{C}_xH_y(sp^3)$ / Si$\underline{C}$

$\underline{C}_xH_y(sp^2)$

200 150 100 50 0 ppm

200 150 100 50 0 ppm

(b) 13C AGED

(x5)

Crosslinking

R$\underline{C}H_2OH$

R$\underline{C}O_2H$, $R_2\underline{C}O_2$

$R_2\underline{C}$=O

200 150 100 50 0 ppm

200 150 100 50 0 ppm

Figure 4.11: ^{13}C solid-state NMR spectra: (a) before and (b) after ageing (extra features indicated).

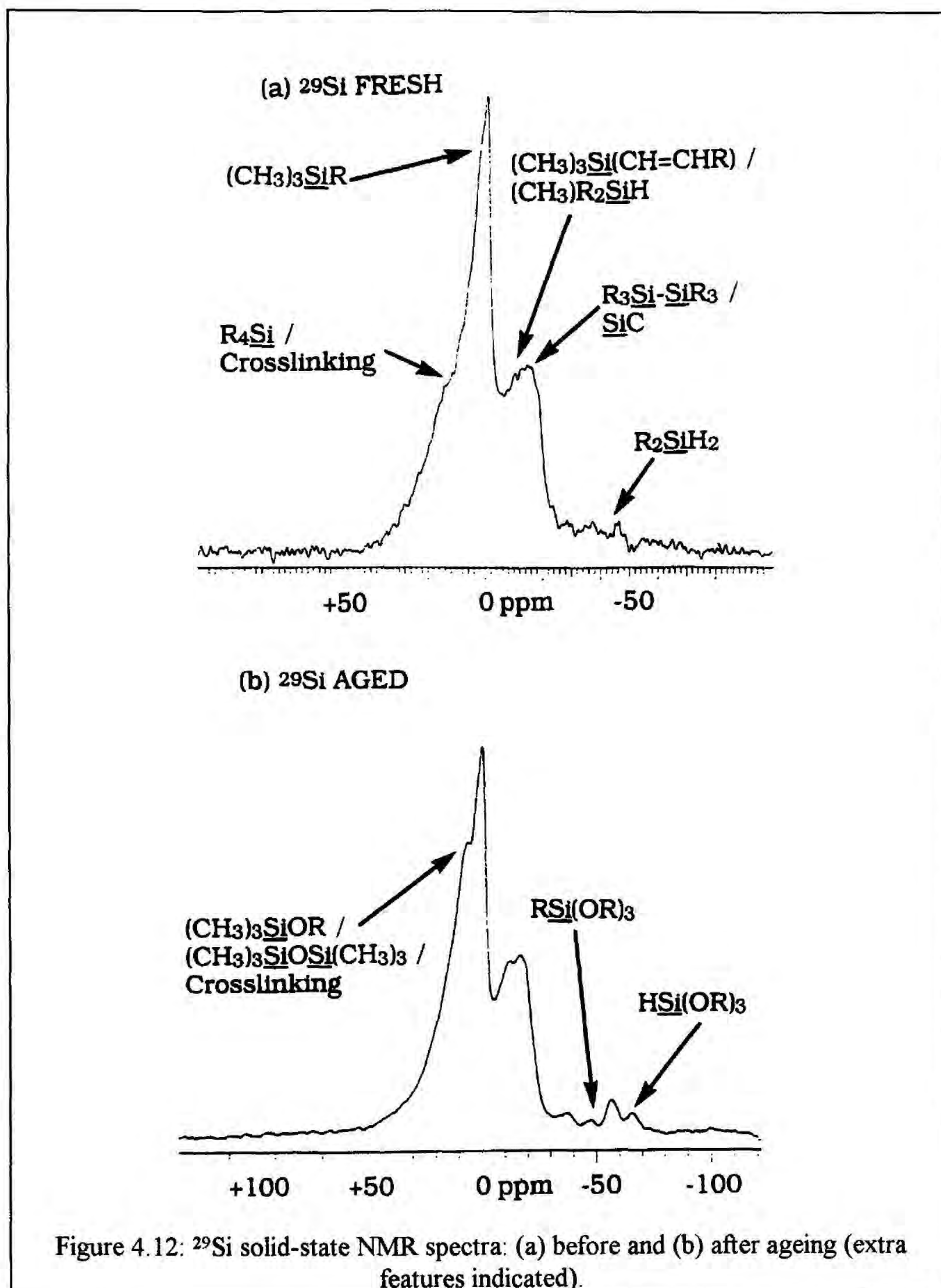

Figure 4.12: ^{29}Si solid-state NMR spectra: (a) before and (b) after ageing (extra features indicated).

$HSi(OC_2H_5)_3$ at -66.0 ppm. The -56.6 peak could be attributed to some form of crosslinking, eg. $(CH_3)_2Si[CH(n\text{-}C_3H_7)]_2$ at -59.8 ppm.

4.3.4. Emission Spectroscopy

As shown in the previous chapter, most of the lines in the carbosilane emission spectrum originate from electronic transitions within the hydrogen molecule[17-20], the $C^3\Pi_u \rightarrow B^3\Pi_g$ transition for a nitrogen molecule[21] [315.9 nm ($\upsilon' = 1$, $\upsilon'' = 0$), 337.1 nm (0, 0) and 357.7 nm (0, 1)], the $A^2\Pi \rightarrow X^2\Sigma$ transition for a CN radical[22-24], and the $A^2\Delta \rightarrow X^2\Pi$ transition for a CH radical was observed at 431.4 nm[25,26].

At high deposition rates (W/F_M = 120 MJ/kg), the HMDS glow discharge does not exhibit much emission from atomic or molecular hydrogen, Figure 4.13. On raising the RF power (W/F_M = 230 MJ/kg), the molecular hydrogen features undergo a greater increase in signal strength relative the atomic hydrogen lines. This observation can be explained by referring to the emission spectra from pure hydrogen plasmas at different inlet gas pressures, Figure 3.11 (Chapter 3): the atomic and molecular hydrogen intensities increase at higher hydrogen pressures. Therefore it can be concluded that more atomic and molecular hydrogen formation occurs in the case of the W/F_M = 230 MJ/kg HMDS glow discharge.

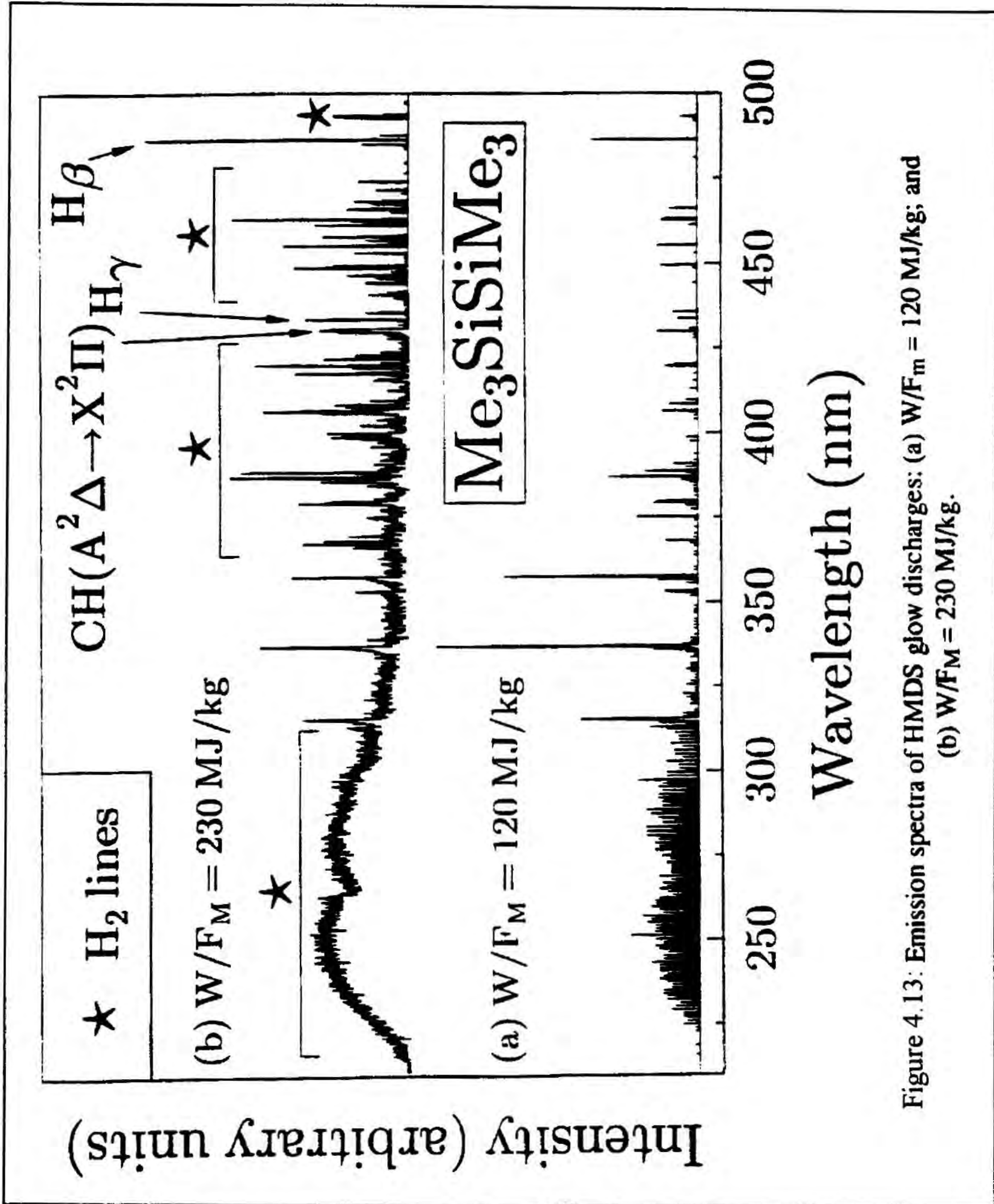

Figure 4.13: Emission spectra of HMDS glow discharges: (a) $W/F_m = 120$ MJ/kg; and (b) $W/F_M = 230$ MJ/kg.

4.4. Discussion

In most cases, plasma enhanced chemical vapour deposition yields fairly low amounts of product, however with hexamethyldisilane it was easy to obtain substantial quantities of solid material. This can be attributed to the high reactivity of this particular organosilicon monomer, which arises from the chromophoric character of the Si-Si bond. Electron-molecule and photon-molecule reactions are widely recognised as being two of the key processes responsible for ionisation and dissociation within a glow discharge. Free radicals can be generated from thermal[27], ultraviolet initiated[28], and electron induced decomposition[29] of HMDS:

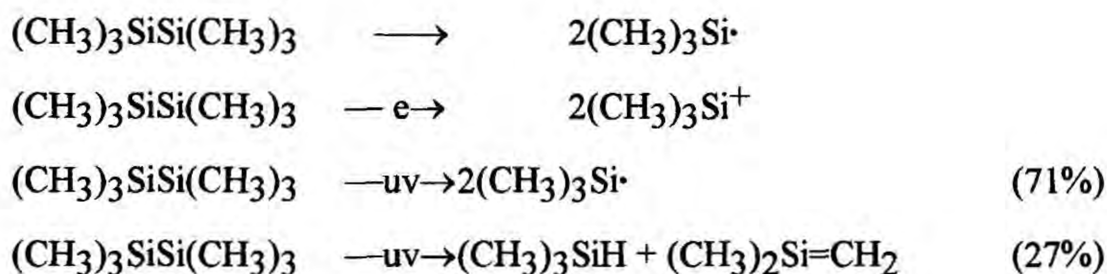

$(CH_3)_3SiSi(CH_3)_3 \longrightarrow 2(CH_3)_3Si\cdot$

$(CH_3)_3SiSi(CH_3)_3 \xrightarrow{e} 2(CH_3)_3Si^+$

$(CH_3)_3SiSi(CH_3)_3 \xrightarrow{uv} 2(CH_3)_3Si\cdot$ (71%)

$(CH_3)_3SiSi(CH_3)_3 \xrightarrow{uv} (CH_3)_3SiH + (CH_3)_2Si{=}CH_2$ (27%)

Also the following reaction is likely to be significant[30], since the HMDS precursor has a high hydrogen content:

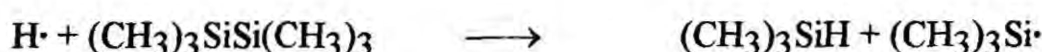

$H\cdot + (CH_3)_3SiSi(CH_3)_3 \longrightarrow (CH_3)_3SiH + (CH_3)_3Si\cdot$

All of these species can subsequently undergo polymerisation either in the gas phase or react with free radical centres at the substrate surface. It is energetically favourable[27,31,32] for the cleavage of Si-Si (196 $kJmol^{-1}$) bonds to form Si-C (291 $kJmol^{-1}$) or Si-H (322 $kJmol^{-1}$) linkages, and also for the rupture of the $Si\text{-}(CH_3)_3$ bond to produce C-C (356 $kJmol^{-1}$) and C-H (416 $kJmol^{-1}$) connections, thereby resulting in an extended network.

It is quite common for the occurrence of high internal stress within plasma deposited thin films[33], this can result in flaking, and therefore the production of a fine powder. However low coverages of organosilicon deposit do adhere well to a

polyethylene substrate. This can be attributed to the greater flexibility of polyethylene with respect to glass; and also since it is already organic in nature, it will be much more compatible with the plasma deposit, i.e. the plasma polymer / polyethylene interface will bond more easily than its plasma polymer / glass counterpart.

Also under comparable experimental conditions, the plasma polymerisation of hexamethyldisilane onto polyethylene film gave a weaker FTIR Si-H stretch at 2104 cm^{-1}, whereas the Si-H band of the freshly deposited powder was much stronger in intensity. Therefore one can deduce that the bulk material has a greater Si-H content than the thin layer deposited onto a polyethylene substrate. The differences observed in Si-H groups between the polyethylene and glass substrates can be explained on the basis of the effective surface area available for the plasma / solid interaction. Since a powder would be expected to have a far higher surface area than a thin coating, then there will be greater opportunity for attachment of $Me_3Si\cdot$ radicals to the surface and also for the incorporation of CH_3 groups into the plasma polymer, together with any Si-H bond formation.

The chemical nature of the as-collected bulk material and its subsequent ageing, are similar in some respects to plasma deposited thin films derived from tetramethylsilane[34] and vinyltrimethylsilane[35] precursors. For instance comparable infrared absorption bands are reported, and subsequent reactions with oxygen and moisture cause the same types of oxygenated functionality to be incorporated. However the hexamethyldisilane precursor is found to be much more susceptible towards plasma polymerisation, this is clearly evident from the high deposition rates obtained in our studies. Most plasma polymerisation reactions are restricted to coating applications due to their low yield, whereas the high efficiency offered by the hexamethyldisilane monomer means that bulk plasma polymers may become exploited in their own right in the future.

4.5. Conclusions

It has been demonstrated that by careful choice of precursor and glow discharge parameters, bulk organosilicon materials can be synthesised via plasma polymerisation. Hexamethyldisilane has proven to be a suitable monomer for this purpose due to the chromophoric character of its Si-Si bond. Reactive centres trapped within the plasma deposit are found to subsequently undergo crosslinking and oxidation during prolonged exposure to air. When treateing polyethylene surfaces, at high powers (50 W) ablation of the polymer surface occurred.

References

1. Inagaki, N; Katsuoka, H., *J. Memb. Sci.* **1987**, *34*, 297.
2. Clark, D.T.; Feast, W.J., *J. Macromol. Sci. Rev. Macromol. Chem.* **1975**, *12*, 191.
3. Clark, D.T.; Dilks, A., *J. Polym. Sci. Polym. Chem. Edn.* **1979**, *17*, 957.
4. Laoharojanaphand, P.; Lin, T.J.; Stoffer, J.O., J. Appl. Polym. Sci. **1990**, *40*, 369.
5. Hamada, K.; Morishita, H., *Spectros. Letts.* **1986**, *19*, 815.
6. Silverstein, R.M.; Bassler, G.C.; Morrill, T.C., *Spectrometric Indentification of Organic Compounds,* Wiley: Singapore, 1981.
7. Morinaka, A.; Asano, Y., *J. Appl. Polym. Sci.* **1982**, *27*, 2139.
8. Kobayashi, H.; Bell, A.T.; Shen, M., *Macromolecules* **1974**, *7*, 277.
9. Kobayashi, H.; Bell, A.T.; Shen, M., *J. Appl. Polym. Sci.* **1973**, *17*, 885.
10. Bieg, K.W.; Wischman, K.B., *Sol. Energ. Mater.* **1980**, *3*, 301.
11. Grebowicz, P.T.; Wróbel, A.M.; Kryszeski, M., *Thin Solid Films* **1980**, *65*, 351.
12. Akovali, G.; Boluk, M.Y., *Polym. Eng. Sci.* **1981**, *21*, 658.
13. Silverstein, R.M.; Bassler, G.C.; Morrill, T.C., *Spectrometric Indentification of Organic Compounds,* Wiley: Singapore, 1981.
14. Assink, R.A.; Hays, A.K.; Bild, R.W., J. Vac. Sci. Technol. **1985**, *A3*, 2629..
15. Marsmann, H., *NMR: Basic Principles and Progress* **1981**, *17*, 65.

16. Apperley, D.C.; Harris, R.K.; Marshall, G.L.; Thompson, D.P., *J. Am. Ceram. Soc.* **1991**, *74*, 777.

17. Kokai, F., Kubota, T., Ichijo, M. Wakai, K., *Abstr. Pap. Am. Chem. Soc.* **1987**, *193*, 117.

18. Pearse, R.W.B.; Gayon, A.G., *The Identification of Molecular Spectra*, Chapman and Hall: London, 1976.

19. Dike, G.H., *The Hydrogen Molecule Wavelength Tables of G.H. Dieke*, Crosswhite, H.M. (ed.), Wiley: New York, 1972.

20. Hollas, J.M., *Molecular Spectroscopy*, Wiley: New York, 1987.

21. *Spectroscopic Data Relative to Diatomic Molecules*, Rosen, B., (ed.), Pergamon: Oxford, 1970.

22. Herzberg, G.; Phillips, J.G., *Astrophys. J.* **1948**, *163*, 108.

23. LeBlanc, F.J., *J. Chem. Phys.* **1968**, *48*, 1980.

24. Herzberg, H., *The Spectra and Structure of Simple Free Radicals*, Cornell University Press: Ithaca, 1971.

25. Kiess, N. H.; Broida, H. P., *Astrophys. J.* **1956**, *123*, 166.

26. Moore, C.E.; Broida, H.P., *J. Res. Nat. Bur. Stand.* **1959**, *A-63*, 19.

27. Davidson, I.M.T; Howard, A.V., *J. Chem. Soc. Faraday Trans.* **1975**, *71*, 69.

28. Brix, T.; Bastian, E.; Potzinger, P., J. Photochem. Photobiol. A **1989**, *49*, 287.

29. Connor, B.; Finney, G.J.; Haszeldine, R.N.; Robinson, P.J.; Sedgwick, R.D.; Simmons, R.F., *J. Chem. Soc. Chem. Comm.* **1966**, 178.

30. Ellul, R.; Potzinger, P.; Reimann, B., *J. Phys. Chem.* **1984**, *88*, 2793.

31. Pilcher, G.; Leitao, M.L.P.; Meng-Yan, Y.; Walsh, R., *J. Chem. Soc. Faraday I*, **1991**, *841*, 249.

32. Cotton, F.A.; Wilkinson, G., *Advanced Inorganic Chemistry*; Wiley: New York, 1988.

33. Wolf, D., *Appl. Phys. Lett.* **1991**, *58*, 2081.

34. Szeto, R.; Hess, D.W., *J. Appl. Phys.*, **1981**, *52*, 903.

35. Vasile, M.J.; Smolinsky, G., *J. Electrochem. Soc.*, **1972**, *119*, 451.

Chapter Five

GLOW DISCHARGE OXIDATION OF PLASMA POLYMERISED ORGANOSILICON LAYERS

Contents

5.1. Introduction 110

5.2. Experimental 111

5.3. Results 111

- 5.3.1. X-ray Photoelectron Spectroscopy 111
- 5.3.2. ATR-FTIR Spectroscopy 119
- 5.3.3. Atomic Force Microscopy 122
- 5.3.4. Emission Spectroscopy 122
- 5.3.5. Gas Permeation 130

5.4. Discussion 130

5.5. Conclusions 131

5.1. Introduction

Conventional polysilane materials offer many attractive attributes for utilisation in microlithography[1,2]. These polymers are normally coated onto a substrate from solution. Their unique -Si-Si- backbone is σ-conjugated. The σ-σ* electronic transition is readily excited by UV laser irradiation, which in turn can lead to local photoablation of the polysilane polymer[3]. Subsequent exposure to a non-equilibrium oxygen glow discharge results in preferential etching of exposed underlayer material, whereas any remaining regions of polysilane polymer become etch-resistant via oxidation to SiO_xH_y together with a concomitant loss of volatile carbon and hydrogen oxides[4].

Plasma polymerised organosilicon[5,6] and organosiloxane[7,8] films are promising alternatives to polysilane polymers for use in dry resist applications. Organosilicon plasma polymers can be synthesised at room temperature with a large number of unsaturated centres, and a high silicon content[9-13]. These materials offer the additional benefit of enabling completely dry photolithographic processing: comprising of glow discharge carbosilicon polymerisation, followed by UV laser imaging, and finally oxygen reactive ion etching (RIE) for image transfer into the underlying substrate.

Plasma polymerisation of tetramethylsilane ($[CH_3]_4Si$) and hexamethyldisilane ($[CH_3]_3SiSi[CH_3]_3$) results in the formation of extended networks of -$[CH_3]_nSiH_n$- linkages (Chapters 3 and 4). The susceptibility of these carbosilicon coatings towards oxygen glow discharge modification has been investigated by X-ray photoelectron spectroscopy (XPS), attenuated total reflection Fourier transform infrared spectroscopy (ATR-FTIR), atomic force microscopy (AFM), and emission spectroscopy. Also the helium, oxygen, nitrogen, and argon gas permeabilities of these materials deposited onto polyethylene (prior to, and following oxygen glow discharge treatment) have been measured.

5.2. Experimental

TMS and HMDS plasma polymers were deposited using a power of 0.8 W on polyethylene, according the procedure described in Chapters 3 and 4. After the deposition, the system was pumped down to 0.001 Torr for 5 minutes. High purity oxygen (BOC, 99.6 %) was introduced into the reaction chamber at 0.1 Torr pressure. The deposited organosilicon was treated with an oxygen glow discharge. Finally the system was let up to atmosphere, and the appropriate analytical measurement undertaken.

5.3. Results

5.3.1. X-ray Photoelectron Spectroscopy

Plasma polymerisation of tetramethylsilane and hexamethyldisilane at 0.8 W yields organosilicon coatings with Si:C ratios of 0.35 ± 0.02 and 0.50 ± 0.02 respectively (as determined by XPS). Angle-resolved XPS studies reveal a small amount of oxygen at the surface (less than 4%), this was probably due to trapped free radicals in the plasma polymer layer reacting with the ambient atmosphere during sample transport from the deposition chamber to the XPS spectrometer. The main C(1s) peak centred at a binding energy of 285.0 eV can be assigned to C-H, C-C and C-Si environments[22,23]. The Si(2p) core level at 100.7 ± 0.1 eV for TMS and 101.2 ± 0.1 eV for HMDS is characteristic of Si-H and Si-C bonds[14,15].

Plasma oxidation of each organosilicon film was studied as a function of glow discharge power, Figures 5.1-5.2. This treatment was found to be very rapid down to the depths accessible by XPS (5 - 20 Å). A plateau is reached well below 5 W corresponding to 20% carbon, 43 % silicon, and 38% oxygen for the TMS plasma polymer, and 20% carbon, 35 % silicon, and 45% oxygen for the corresponding HMDS

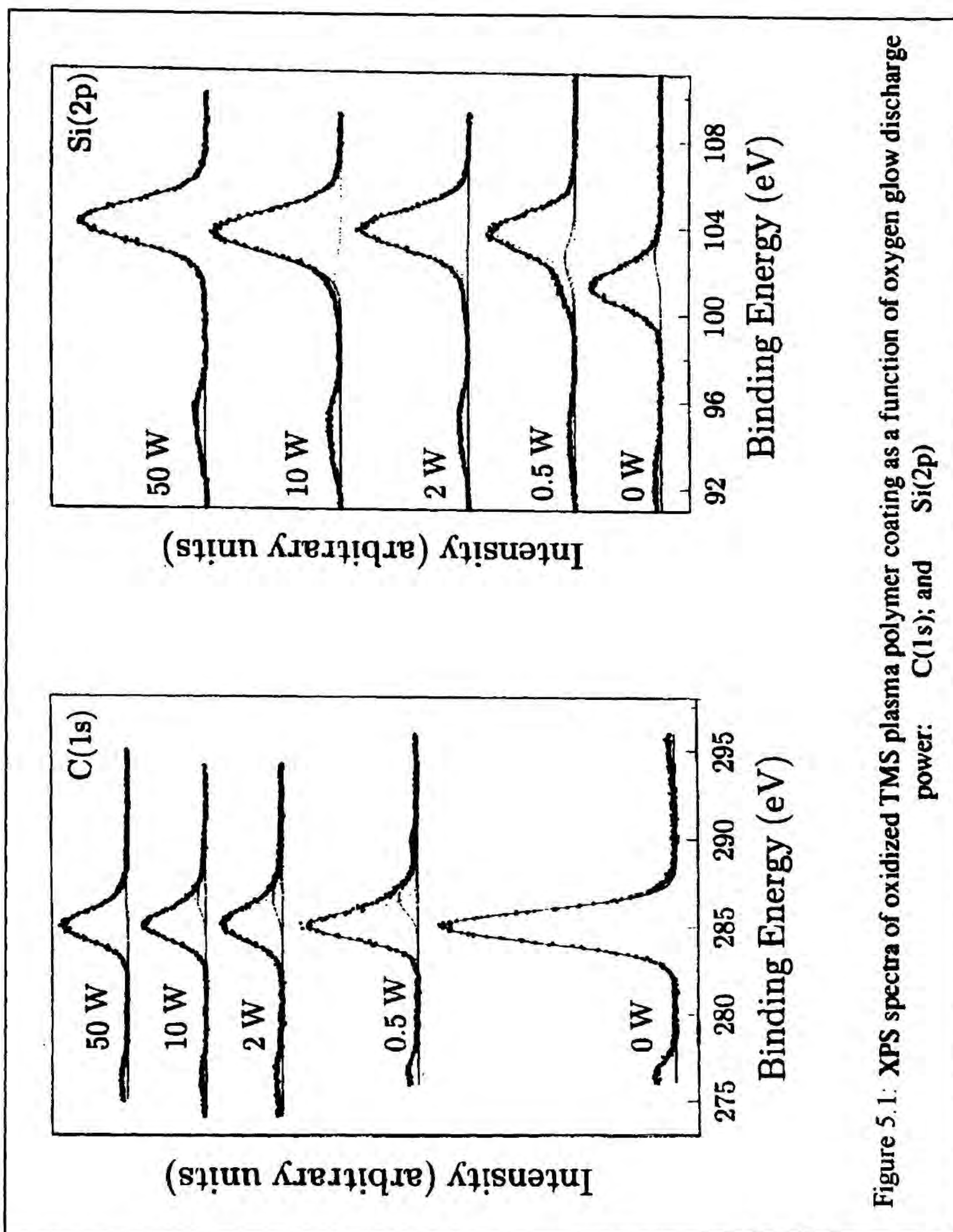

Figure 5.1: **XPS spectra of oxidized TMS plasma polymer coating as a function of oxygen glow discharge power: C(1s); and Si(2p)**

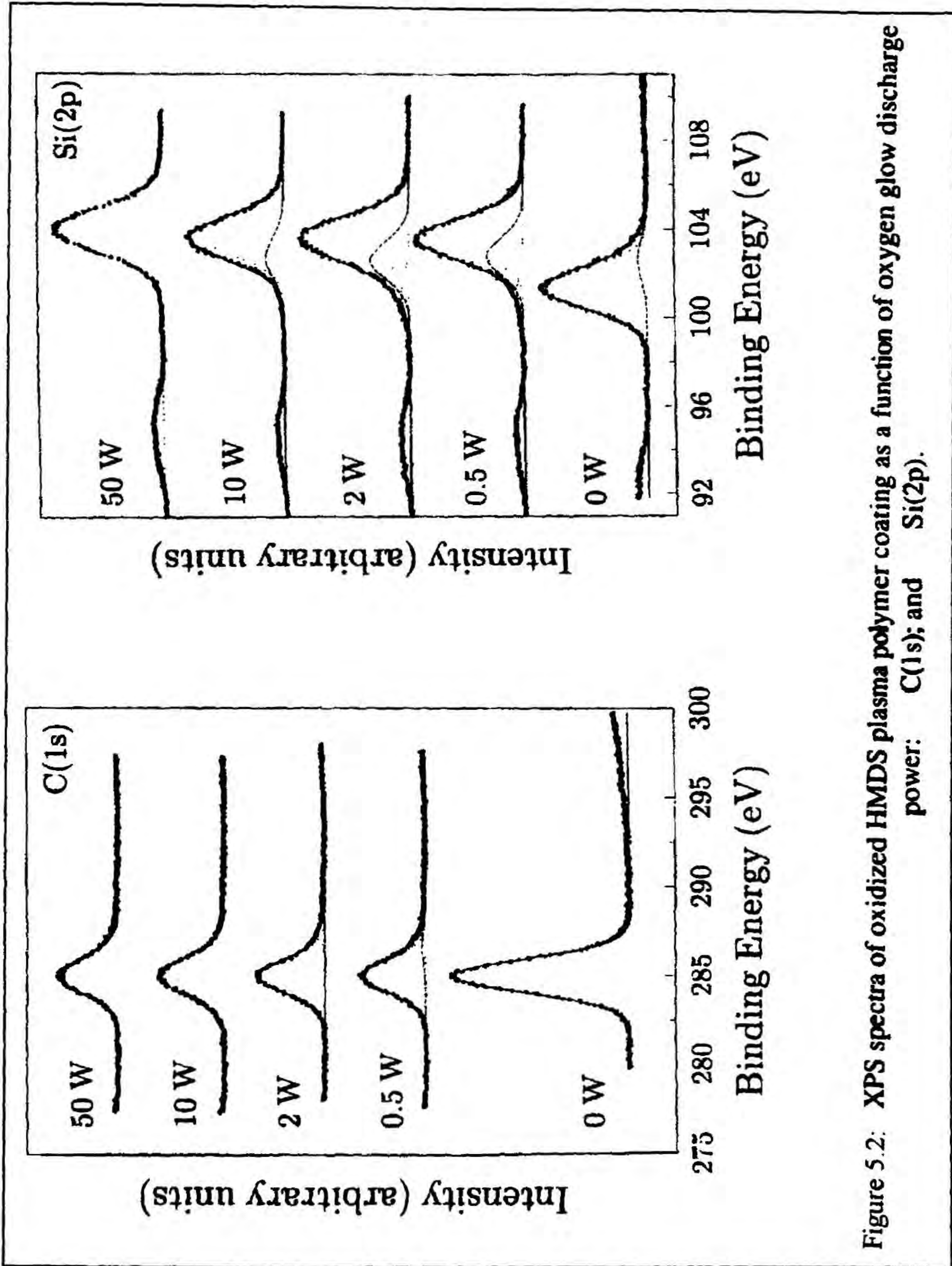

Figure 5.2: **XPS spectra of oxidized HMDS plasma polymer coating as a function of oxygen glow discharge power: C(1s); and Si(2p).**

material, Figures 5.3-5.4. Clearly this analysis excludes any hydrogen content, since it can not be detected by XPS. The Si(2p) core level binding energy shifts to higher binding energy during plasma oxidation, whereas the C(1s) peak was attenuated, together with the emergence of a weak oxidised component at high binding energy, which is a convolution of >C-O- (286.6 eV), >C=O / -O-C-O- (287.9 eV), -O-C=O (289.0 eV), and -O-CO-O- (290.4 eV) peaks[16]. The Si(2p) envelope can be fitted to Si-H / Si-C (101.2 eV), Si-[OC_xH_y]$_n$ (102.6 eV), and O-Si-O (104.0 eV) silicon environments[17], Figures 5.1-5.2.

XPS analysis in conjunction with Ar^+ ion depth profiling of the oxidised organosilicon layers confirmed the build-up of oxygenated silicon species in the near-surface region, Figures 5.5-5.6. It also indicated the presence of contamination (due to the condensation of hidrocarbons from the atmosphere/spectrometer chamber on the suraface): when the depth is increased, the C(1s) signal decreases, reaches a minimum, and then tends to its bulk value.

Passage of oxygen over the organosilicon layer in the absence of a glow discharge resulted in negligible surface oxidation.

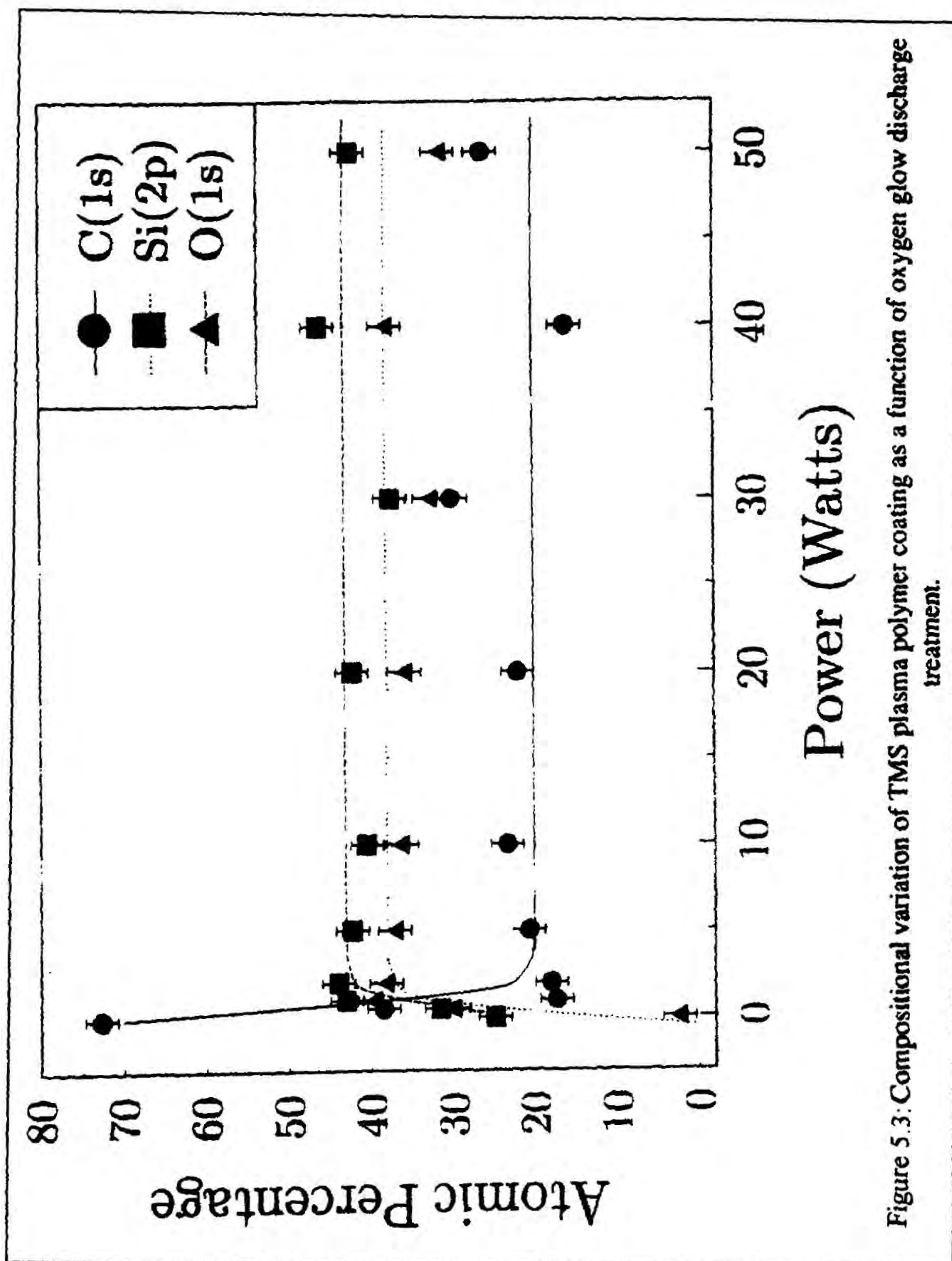

Figure 5.3: Compositional variation of TMS plasma polymer coating as a function of oxygen glow discharge treatment.

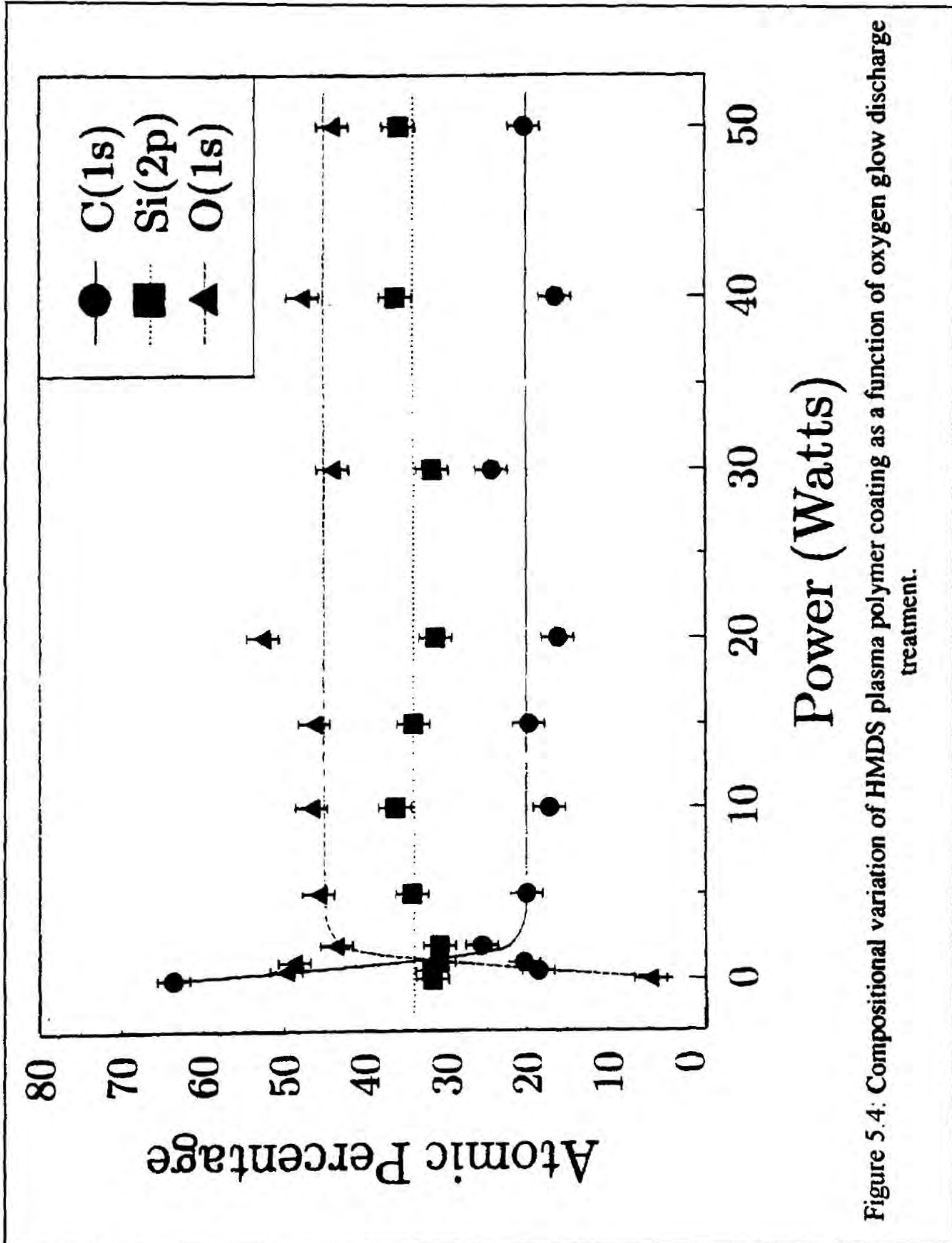

Figure 5.4: Compositional variation of HMDS plasma polymer coating as a function of oxygen glow discharge treatment.

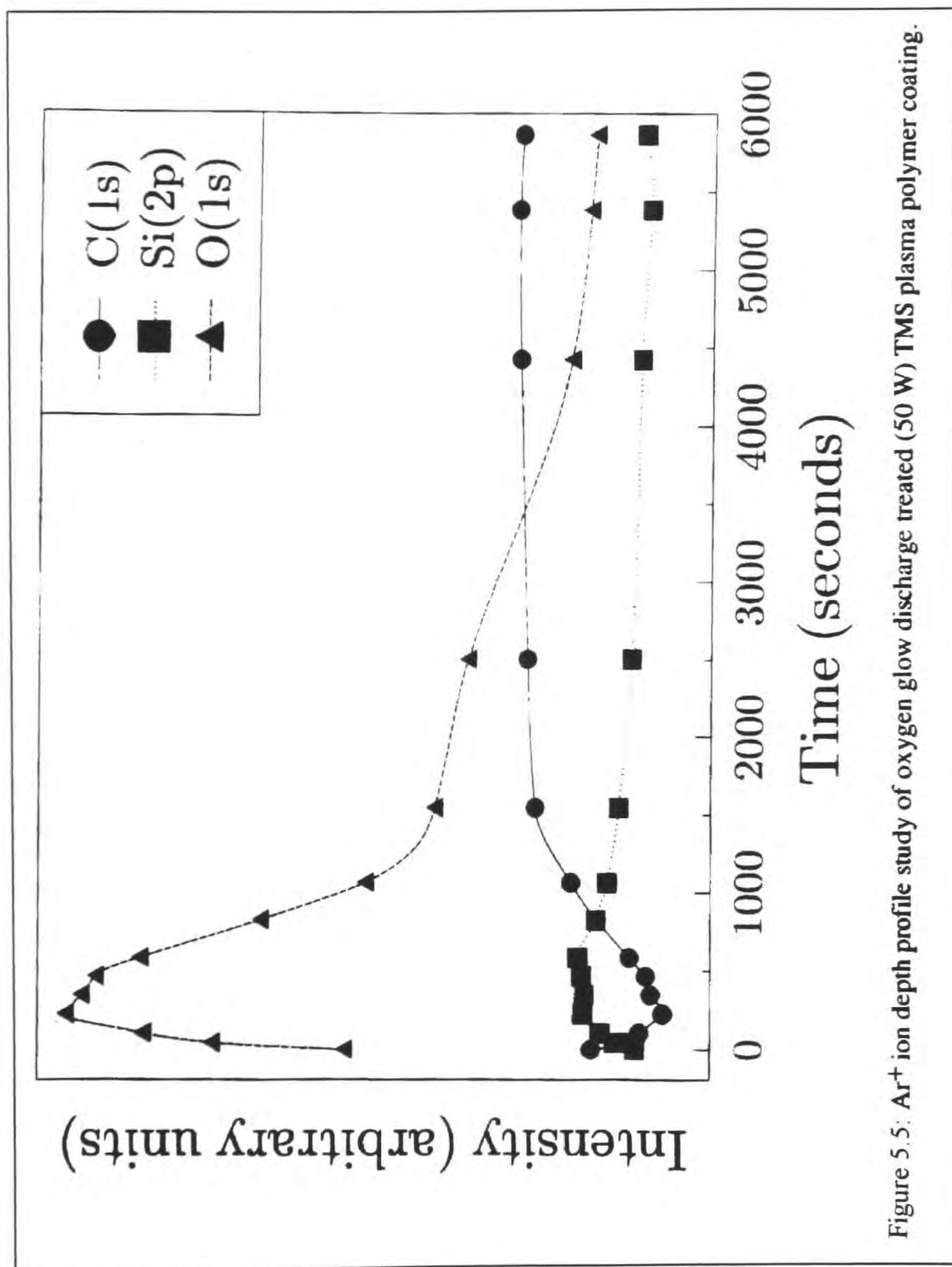

Figure 5.5: Ar^+ ion depth profile study of oxygen glow discharge treated (50 W) TMS plasma polymer coating.

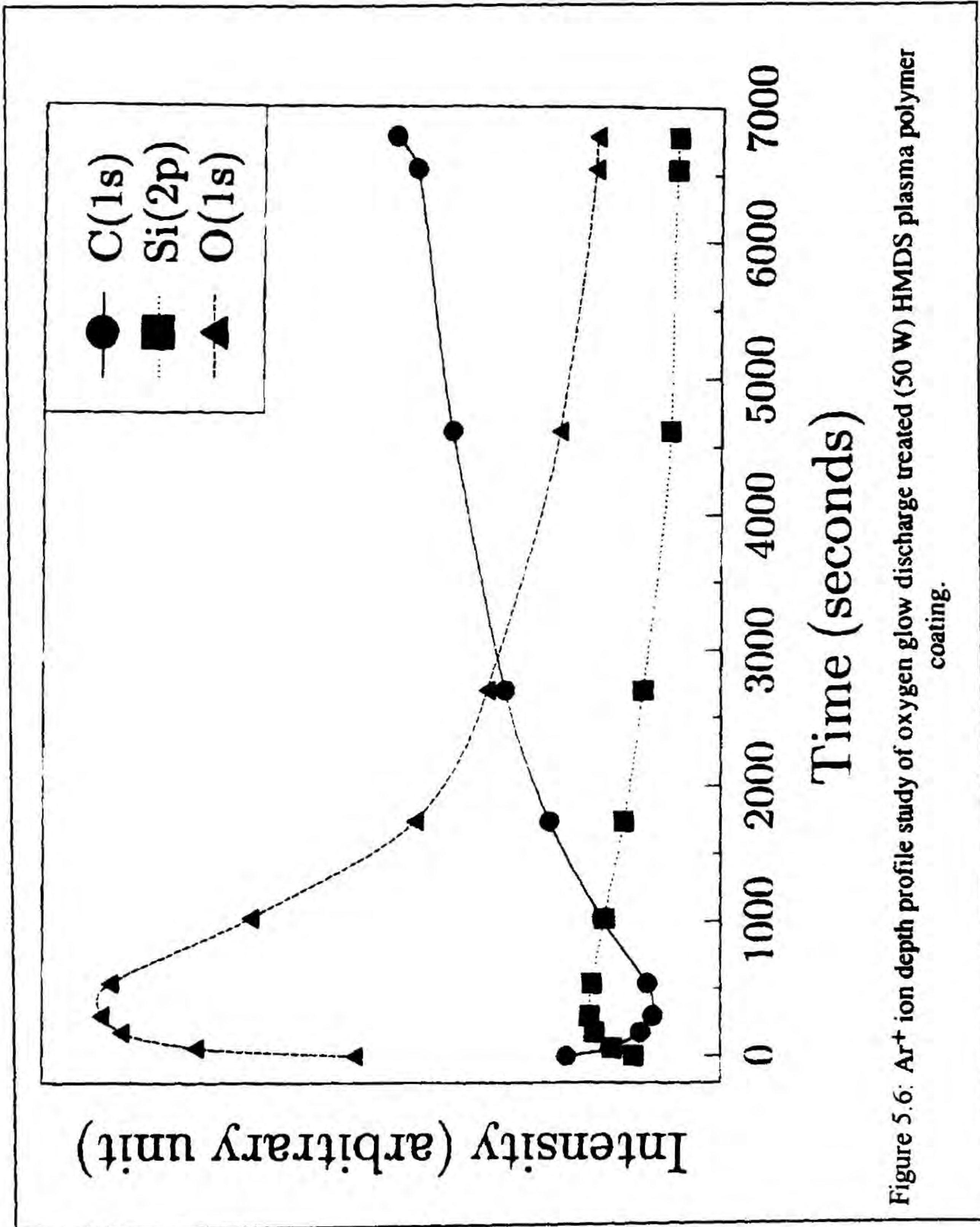

Figure 5.6: Ar^{+} ion depth profile study of oxygen glow discharge treated (50 W) HMDS plasma polymer coating.

5.3.2. ATR-FTIR Spectroscopy

The characteristic infrared absorption bands for clean polyethylene film are assigned in Chapter 3 (Table 3.3). Both the freshly deposited organosilicon coating and the underlying polyethylene substrate contribute to the CH_3 and CH_2 stretching bands occurring at 2951 cm^{-1} and 2895 cm^{-1}, Figures 5.7-5.8. CH_3-C linkages can also be identified by peaks at 1460 cm^{-1} (methyl asymmetric bending in CH_3-C), and 1375 cm^{-1} (methyl symmetric bending in CH_3-C). Silicon related infrared absorptions are assignable as follows[18]: 2110 cm^{-1} (Si-H stretching), 1408 cm^{-1} (CH_2 symmetrical scissoring in Si-CH_2), 1250 cm^{-1} (CH_3 symmetric bending in Si[CH_3]$_n$), 1026 cm^{-1} (CH_2 wagging in Si-[CH_2]$_n$-Si), 833 cm^{-1} (CH_3 rocking in Si[CH_3]$_n$, n = 2, 3), 791 cm^{-1} (CH_3 rocking in Si(CH_3)$_n$, n = 1, 2), and 685 cm^{-1} (Si-C stretching), Figures 5.7-5.8 (0 Watts O_2 plasma treatment).

ATR-FTIR analysis of glow discharge oxidised organosilicon plasma polymer layers all display a much stronger 1026 cm^{-1} (Si-O-Si and/or Si-O-C asymmetric stretching and/or CH_2 wagging in Si-[CH_2]$_n$-Si) absorbance. However it is clear that at the depths accessible to ATR-FTIR analysis (~ 0.1 - 10 μm), a significant amount of the virgin plasma polymer is still detectable. Therefore the high concentration of SiO_xH_y species located in the outer surface region must be acting as a reactive ion etch barrier. All of the silicon related absorbances are much stronger for the HMDS plasma polymer since it contains a higher silicon content.

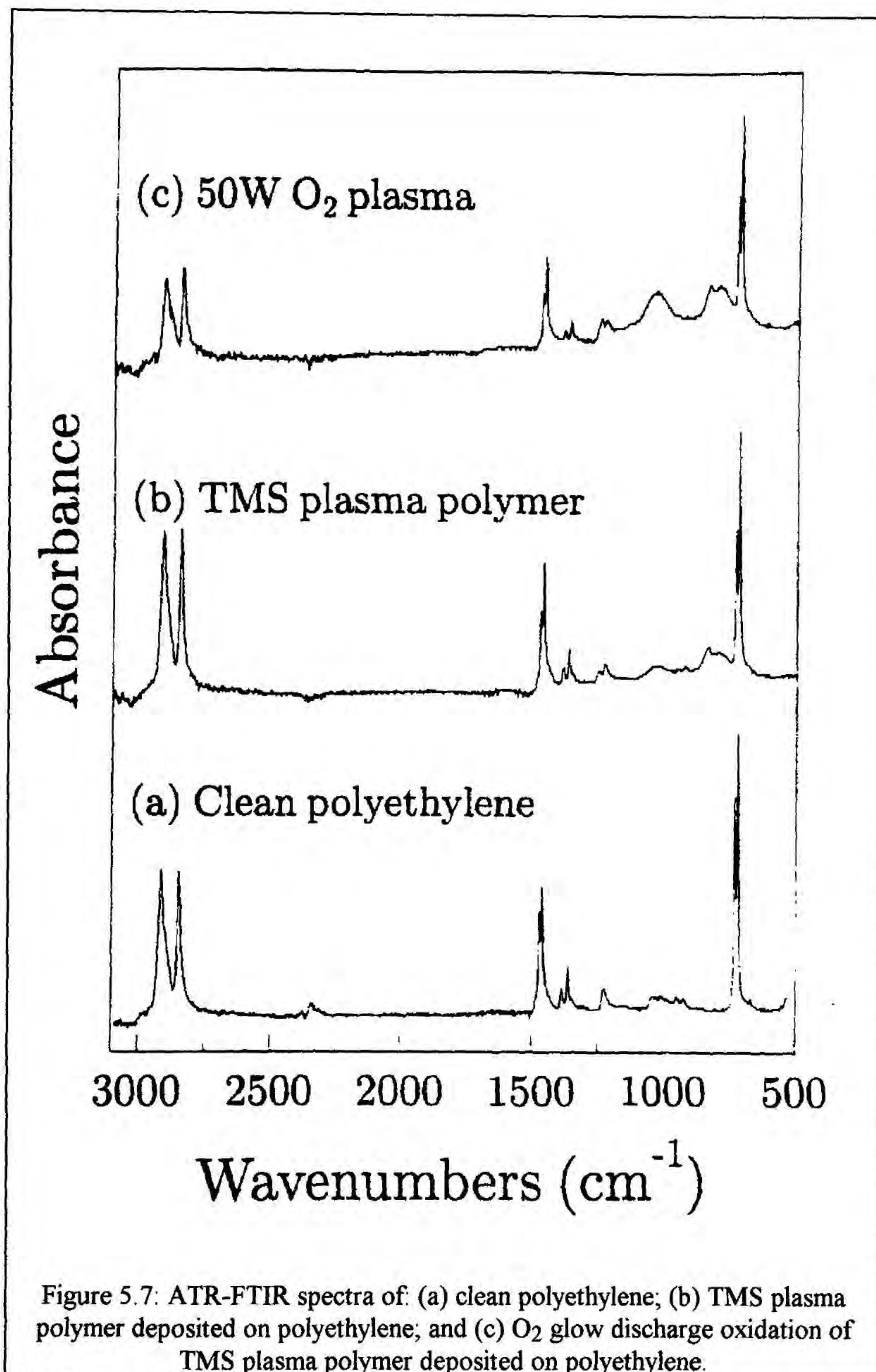

Figure 5.7: ATR-FTIR spectra of: (a) clean polyethylene; (b) TMS plasma polymer deposited on polyethylene; and (c) O_2 glow discharge oxidation of TMS plasma polymer deposited on polyethylene.

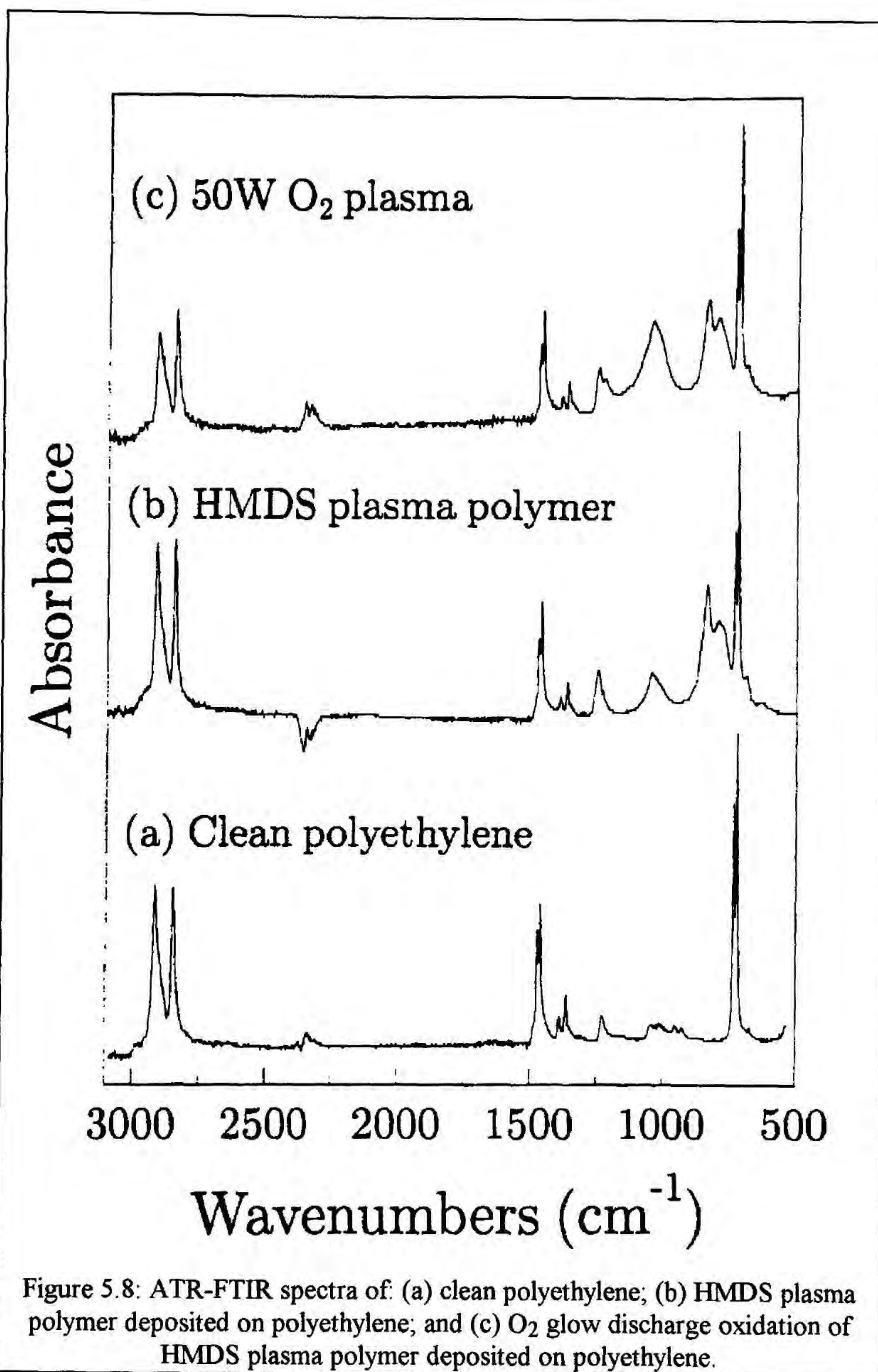

Figure 5.8: ATR-FTIR spectra of: (a) clean polyethylene; (b) HMDS plasma polymer deposited on polyethylene; and (c) O_2 glow discharge oxidation of HMDS plasma polymer deposited on polyethylene.

5.3.3. Atomic Force Microscopy

Examination of the plasma polymer layer morphologies by atomic force microscopy revealed the presence of agglomerated globular particles in the size range of 0.2 - 0.5 μm, Figures 5.9-5.12. Glow discharge oxidation did not lead to any significant alteration in the appearance of these globular features.

5.3.4. Emission Spectroscopy

The emission spectra taken during the oxygen glow discharge treatment of clean polyethylene film, TMS and HMDS plasma polymers are shown in Figure 5.13. Their assignments are summarised in Table 5.1, and were checked by running glow discharges of each of the constituent gases (i.e. H_2, H_2O, CO, CO_2, etc.), Figure 5.14. The main lines are due to transitions related to the presence of CO, OH and atomic hydrogen. For the carbosilicon plasma polymers, there is a strong attenuation in the CO line intensities with respect to clean polyethylene film, and also the appearance of an additional line (x) at 437.6 nm characteristic of the $H^3\Sigma_u^- \rightarrow X^3\Sigma_g^-$ transition in the Si-Si molecule. All of these observations are consistent with the formation of a $Si_xO_yH_z$ rich surface layer during the glow discharge oxidation of organosilicon plasma polymers. Other strong lines are due to the $C^3\Pi_u \rightarrow B^3\Pi_g$ transition for a nitrogen molecule: 315.9 nm ($\upsilon' = 1$, $\upsilon'' = 0$), 337.1 nm (0, 0) and 357.7 nm (0, 1). As in Chapters 3 and 4, these nitrogen lines are weaker by an approximate factor of 2000 compared to their normal intensity in a pure nitrogen plasma, and therefore the actual amount of molecular nitrogen in the reactor during plasma polymerisation must be less than 0.05%.

Chapter Five

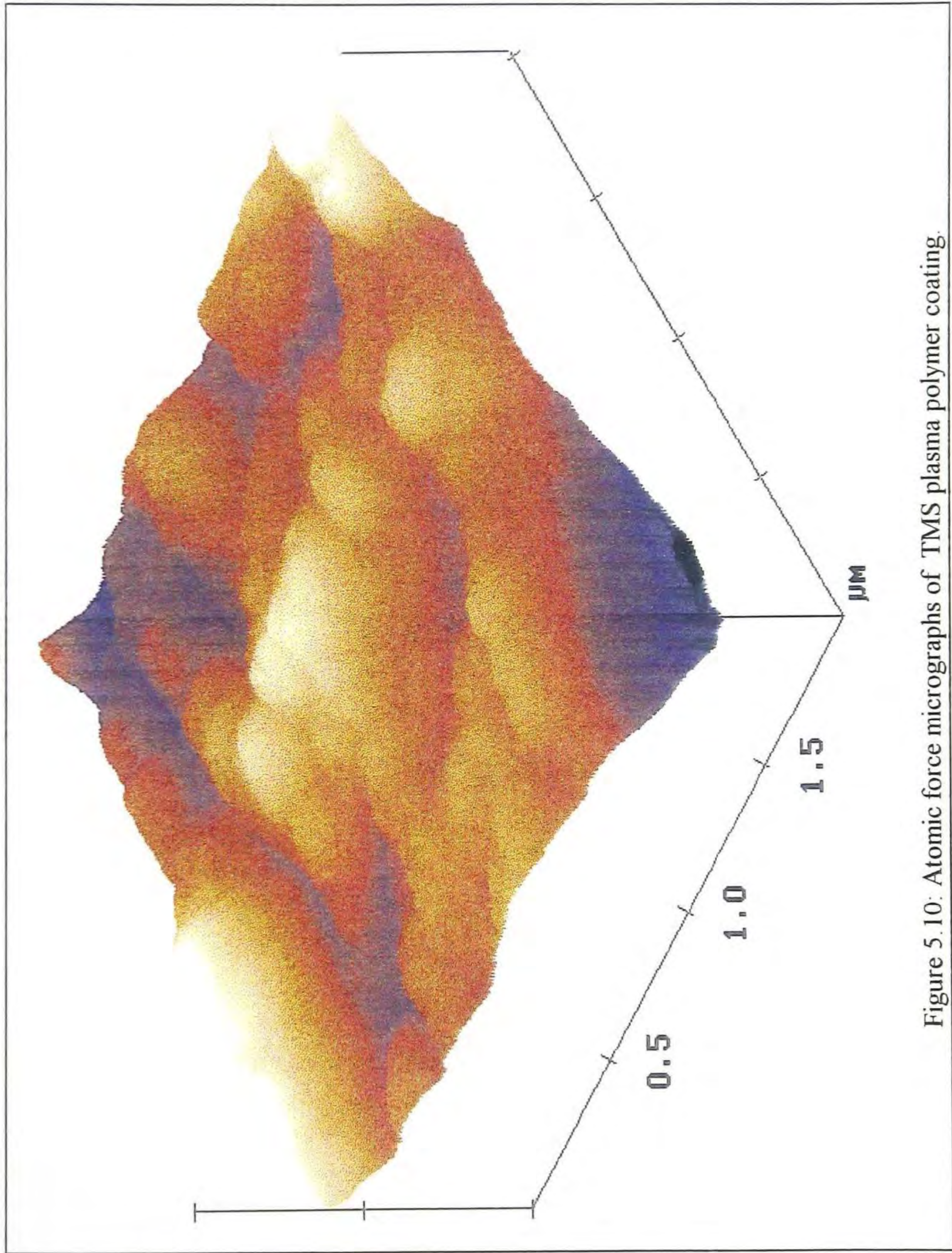

Figure 5.10: Atomic force micrographs of TMS plasma polymer coating.

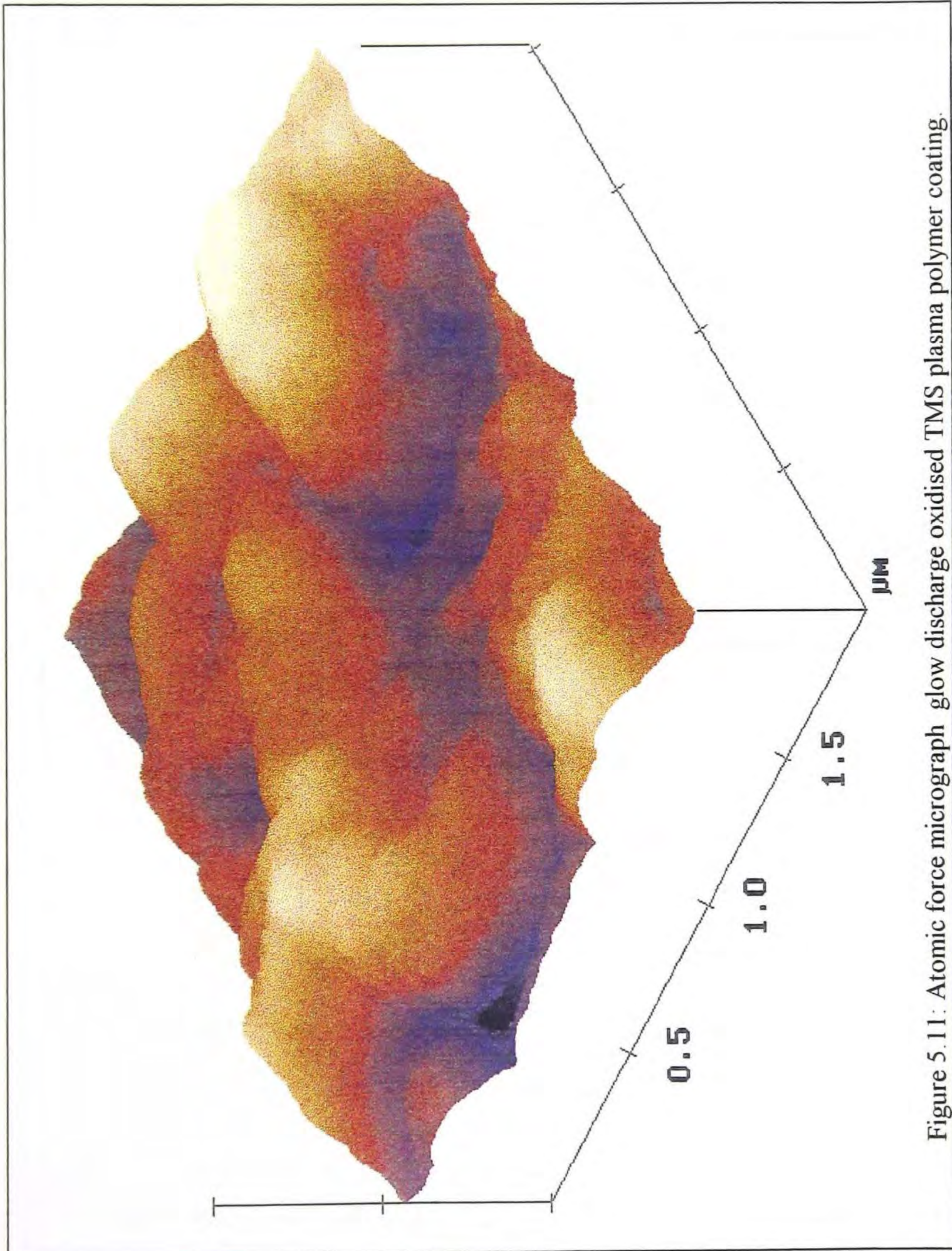

Figure 5.11: Atomic force micrograph glow discharge oxidised TMS plasma polymer coating.

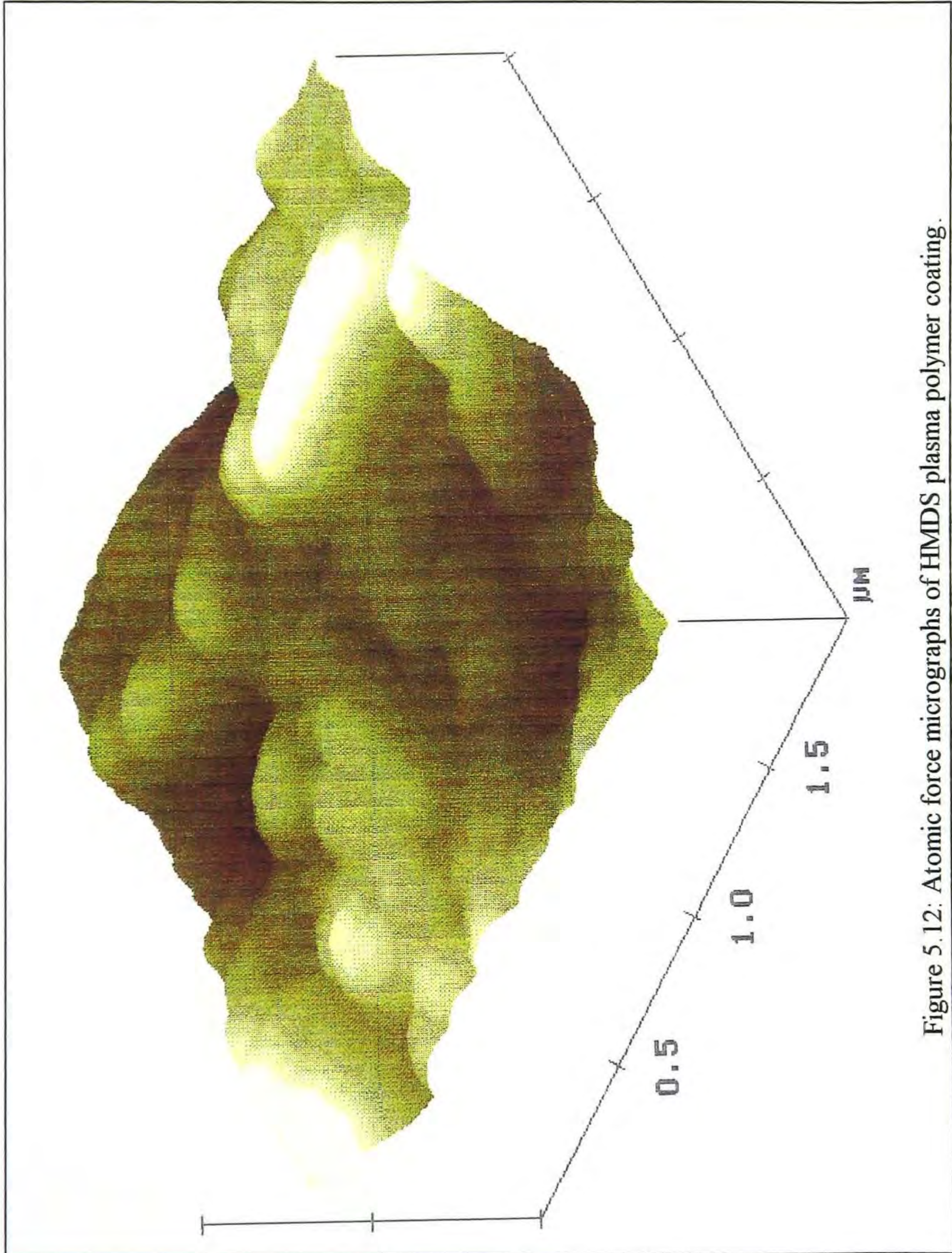

Figure 5.12: Atomic force micrographs of HMDS plasma polymer coating.

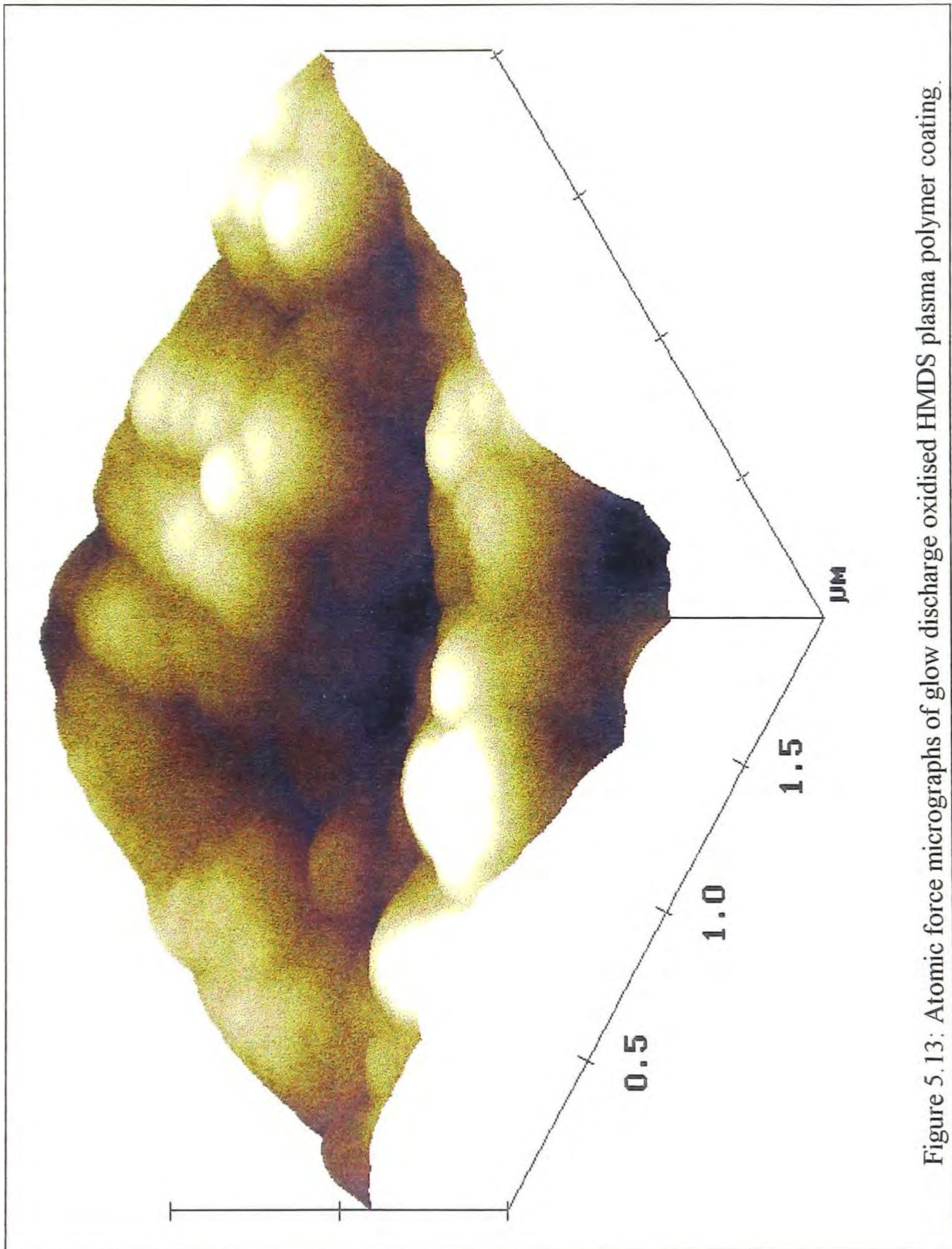

Figure 5.13: Atomic force micrographs of glow discharge oxidised HMDS plasma polymer coating.

Table 5.1 Assignment of glow discharge emission lines.

Transition	Line/Band	Vibrational Assignment
Balmer Lines[19] (H_β, H_γ, H_δ)	486.1 (a)	-
	434.0 (b)	-
	410.2 (c)	-
OH ($A^2\Sigma^+ \rightarrow X^2\Pi$)[20]	308.9 (d)	(0, 0)
	282.9 (e)	(1, 0)
CO ($C^1\Sigma \rightarrow A^1\Pi$)[20]	438.0 (h)	(0, 3)
	412.5 (j)	(0, 2)
	389.3 (k)	(0, 1)
	368.1 (m)	(0, 0)
CO ($b^3\Sigma \rightarrow a^3\Pi$)[21]	349.3 (n)	(0, 4)
	330.6 (o)	(0, 3)
	313.4 (p)	(0, 2)
	297.7 (q)	(0, 1)
	283.3 (e)	(0, 0)
	266.5 (s)	(1, 0)
CO ($B^1\Sigma \rightarrow A^1\Pi$)[22]	483.5 (f)	(0, 1)
	450.9 (g)	(0, 0)
	439.3 (h)	(1, 1)
	412.4 (j)	(1, 0)
CO^+ ($B^2\Sigma \rightarrow A^2\Pi$)[23]	420.9 (i)	(0, 1)
CO^+ ($A^2\Pi \rightarrow X^2\Sigma$)[24]	379.6 (l)	(4, 0)
N_2 ($C^3\Pi_u \rightarrow B^3\Pi_g$)[25]	315.9 (t)	(1, 0)
	337.4 (u)	(0, 0)
	357.7 (v)	(0, 1)
Si_2 ($H^3\Sigma_u^- \rightarrow X^3\Sigma_g^-$)[26]	437.6 (x)	(2, 4)

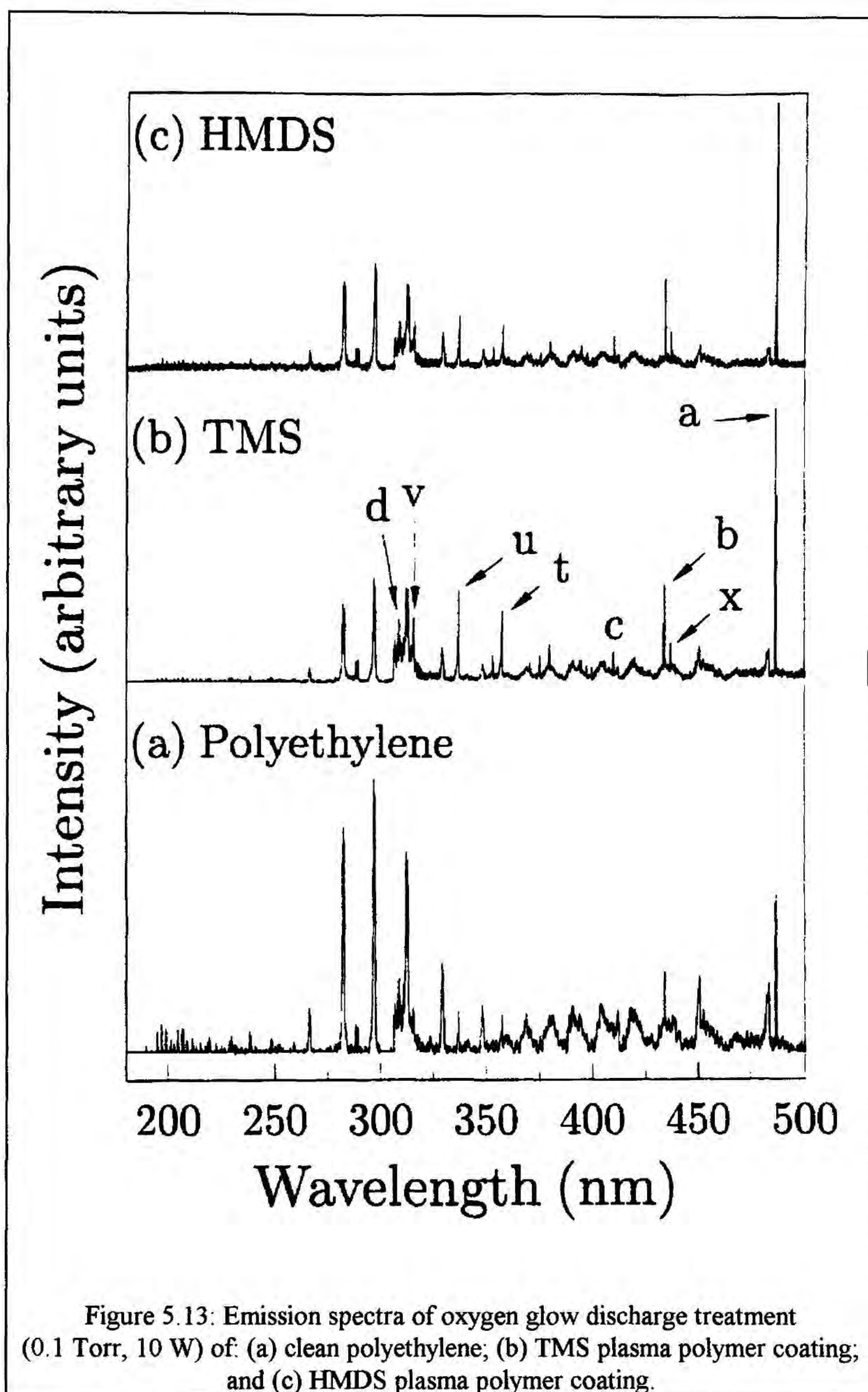

Figure 5.13: Emission spectra of oxygen glow discharge treatment (0.1 Torr, 10 W) of: (a) clean polyethylene; (b) TMS plasma polymer coating; and (c) HMDS plasma polymer coating.

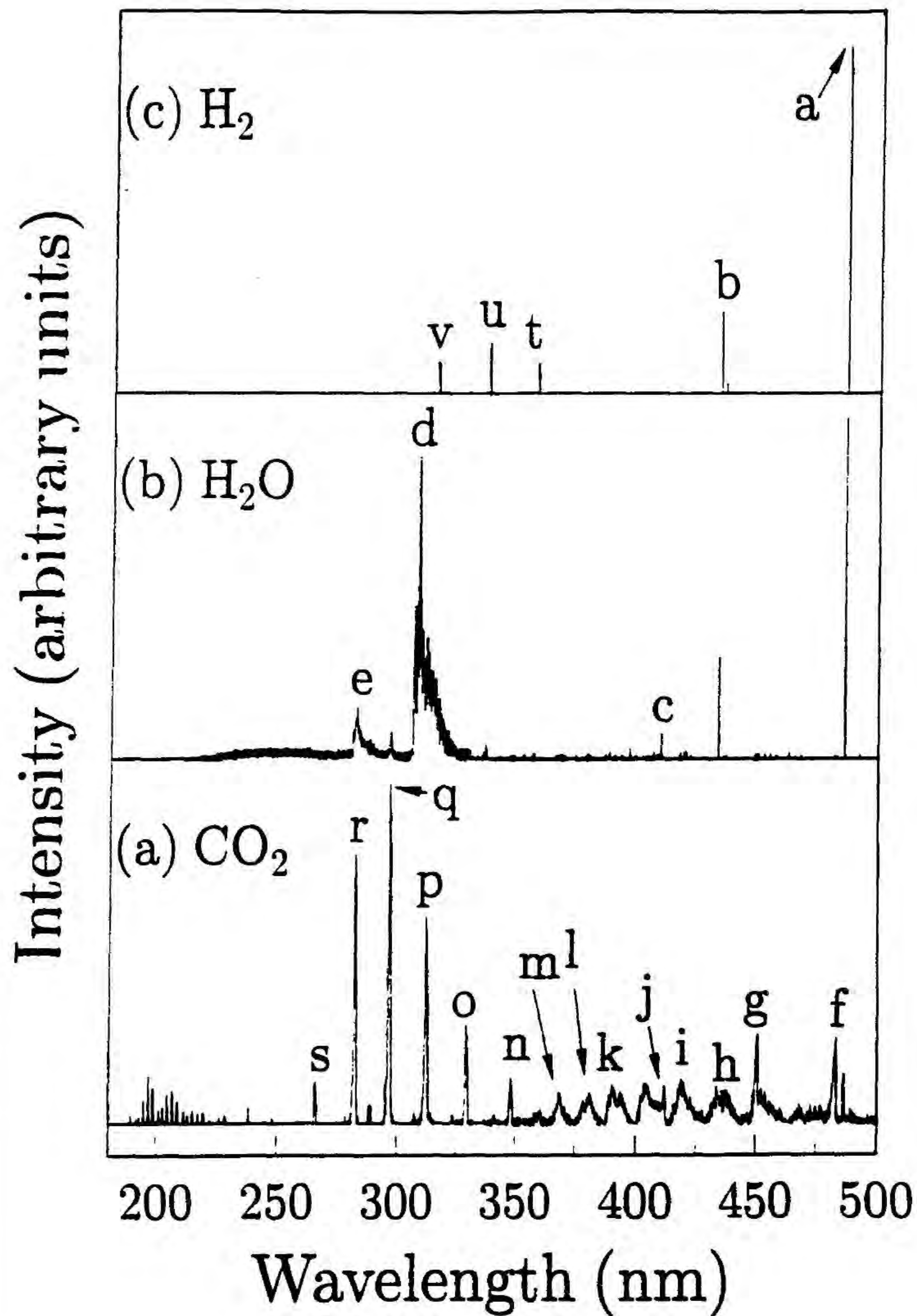

Figure 5.14: Emission spectra of glow discharges (0.1 Torr, 10 W): (a) CO_2; (b) H_2O; and (c) H_2.

5.3.5. Gas Permeation

Gas permeation measurements are summarised in Table 5.2. Deposition of organosilicon plasma polymer onto polyethylene does not strongly influence gas permeation. However, a subsequent oxygen glow discharge treatment clearly improves the gas barrier, and changes the permselectivity. Nitrogen, oxygen, and argon permeation are attenuated, whilst helium diffusion is slightly enhanced. These results are comparable to related studies on plasma polymerised organosiloxane coatings, where oxygen glow discharge post treatment is a prerequisite for improving the gas barrier[8].

Table 5.2 Gas Permeation Measurements (760 Torr back pressure).

Sample	Permeant Pressure / 10^{-9} Torr			
	He	O_2	N_2	Ar
Polyethylene (PE)	12.7 ± 4.4	4.6 ± 0.2	1.4 ± 0.1	9.1 ± 0.9
HMDS Plasma Polymer/PE	12.7 ± 0.3	4.2 ± 0.1	1.4 ± 0.1	8.3 ± 0.5
O_2 Plasma/HMDS Plasma Polymer/PE	14.9 ± 1.4	3.5 ± 0.2	1.0 ± 0.1	6.0 ± 0.3

5.4. Discussion

Plasma polymerisation of tetramethylsilane and hexamethyldisilane yield silicon-rich plasma polymers[11,18], comprising of mainly Si-CH_2, Si-$[CH_2]_n$-Si, and Si$[CH_3]_n$, moieties. The lower Si(2p) XPS binding energy value for the as-deposited TMS plasma polymer can be explained in terms of this material being effectively more electron-rich than its HMDS counterpart. In Chapter 3, solid state NMR and ATR-FTIR experiments have shown that the former contains a higher degree of unsaturation. In the case of HMDS plasma polymer, the Si(2p) peak shifts much more readily to higher binding energies with increasing oxygen glow discharge power, this can be attributed to the

higher silicon content in the as-deposited layer, giving rise to a greater number of chromophoric Si-Si linkages being present, akin to those found in conventional polysilane polymers. The TMS plasma polymer yields a lower SiO_xH_y because it is less Si-rich, and it shows a more pronounced C(1s) oxidation shoulder upon glow discharge oxidation. This can be explained in terms of the inherent unsaturation of the TMS plasma polymer; unsaturated hydrocarbon polymers are known to oxidise much more readily than their saturated counterparts[28]. The globular-like appearance of both organosilicon plasma polymers can be attributed to either the nucleation and growth of particles on the walls of the deposition zone, or the formation of organosilicon plasma dust which coagulate during condensation at the substrate surface[29].

5.5. Conclusions

Coatings derived from the plasma polymerisation of tetramethylsilane and hexamethyldisilane are excellent candidates for use as oxygen reactive ion etch barriers. A thin skin SiO_xH_y rich layer is formed at the surface of the organosilicon coating during oxygen glow discharge treatment, which restricts any further subsurface oxidation.

References

1. Miller, R.D., *Chem. Rev.* **1989,** *89*, 1359.
2. Miller, R.D. *Angew. Chem. Int. Ed. Engl. Adv. Mater.* **1989**, *28,*1733.
3. Kunz, R.R.; Horn, M.W.; Wallraff, G.M.; Bianconi, P.A.; Miller, R.D.; Goodman, R.W; Smith, D.A.; Eshelman, J.R.; Ginsberg, E.J. *Jpn. J. Appl. Phys.* **1992**, *31*, 4327.
4. Watanabe, F., Ohnishi, Y. *J. Vac. Sci. Technol.* **1986,** *B4*, 422.

5. Weidman, T.W.; Joshi, A.M. *Appl. Phys. Lett.* **1993**, *62*, 372.
6. Horn, M.W.; Pang, S.W.; Rothschild, M. *J. Vac. Sci. Technol.* **1990**, *B(8)*, 1493.
7. Hartney, M.A.; Chiang, J.N.; Hess, D.W.; Soane, D.S. *Appl. Phys. Lett.* **1989**, *54*, 1510.
8. Morra, M.; Occhiello, E.; Garbassi, F. *J. Appl. Polym. Sci.* **1993**, *48*, 1331.
9. Nguyen, V.S.; Underhill, J.; Fridman, S.; Pan P. *J. Electrochem. Soc.* **1985**, *132*, 1925.
10. Park, S.Y.; Kim, N.; Hong, S.I.; Sasabe, H. *Polym. J.* **1990**, *22*, 242.
11. Hays, A.K., *Thin Solid Films* **1981**, *84*, 401.
12. Inagaki, N.; Kishi, A., *J. Polym. Sci. Polym. Chem. Ed.* **1983**, *21*, 1847.
13. Shard, A.G.; Munro, H.S.; Badyal, J.P.S. *Polym. Comm.*, **1991**, *32*, 152.
14. Inagaki, N.; Katsuoka *J. Memb. Sci.* **1987**, *34*, 297.
15. Gray, R.C.; Carver, J.C.; Hercules, D.M. *J. Electron Spectrosc.* **1976**, *8*, 343.
16. Laoharojanaphand, P.; Lin, T.J.; Stoffer, J.O. *J. Appl. Polym. Sci.* **1990**, *40*, 369.
17. Clark, D.T.; Dilks, A. *J. Polym. Sci. Polym. Chem. Ed.*, **1979**, *17*, 957.
18. Wróbel, A.M., *J. Macromol. Sci.-Chem.* **1985**, *A22*, 1089.
19. Herzberg, G., *Atomic Spectra and Atomic Structure*, Dover Publications: New York, 1944.
20. Dieke, G.H.; Crosswhite, H.M. *J. Quant. Spectrosc. Rad. Transfer.* **1962**, *2*, 97. Stoebner, A.; Delbourgo, R. *J. Chim. Phys.* **1967**, *64*, 1115.
21. Duffendack, O.S.; Fos, G.W. *Astrophys. J.* **1927**, *65*, 214.
22. Johnson, R.C.; Asundi, R.K. *Proc. Royal Soc.* **1929**, *123*, 560.
23. Baldet, M.F., *C.R. Acad. Sci. (Paris)* **1924**, *178*, 1525.
24. Rao, K.N. *Astrophys. J.* **1950**, *111*, 306.
25. Pearse, R.W.B.; Gayon, A.G. *The Identification of Molecular Spectra*, Chapman and Hall: London, 1976.
26. Douglas, A.E. *Canad. J. Phys.* **1955**, *33*, 801.
27. Wells, R.K.; Drummond, I.W.; Robinson, K.S.; Street, F.J.; Badyal, J.P.S. *J. Adhes. Sci. Technol.* **1993**, *7*, 1129.

28. Bouchoule, A. *Physics World* **1993**, August, 47

Chapter Six

GLOW DISCHARGE OXIDATION OF POLYCYCLOHEXYLMETHYLSILANE AND POLYPHENYLMETHYLSILANE THIN FILMS

Contents

6.1. Introduction 135

6.2. Experimental 135

6.3. Results 136

6.3.1. X-ray Photoelectron Spectroscopy 136

6.3.2. Fourier Transform Infrared Spectroscopy 142

6.3.3. Emission Spectroscopy 142

6.4. Discussion 146

6.5. Conclusions 147

6.1. Introduction

In this fourth experimental chapter, the susceptibility of an aliphatic substituted (polycyclohexylmethylsilane) and an aromatic substituted (polyphenylmethylsilane) polysilane polymer towards oxygen glow discharge modification has been investigated by X-ray photoelectron spectroscopy (XPS), and Fourier transform infrared spectroscopy (FTIR). Structurally, both polysilane polymers are identical apart from the former containing a saturated 6-membered ring, whereas the latter has a phenyl substituent instead:

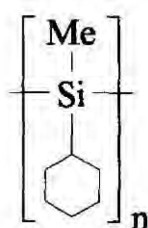

Polycyclohexylmethylsilane (PCHMS)

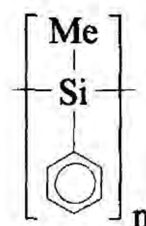

Polyphenylmethylsilane (PPMS)

6.2. Experimental

In this chapter, use was made of the same experimental set up used in Chapter 5, apart from the following point:

- The polysilane films (PCHMS and PPMS, from ABCR) to be treated by glow discharge oxidation were spin coated onto polyethylene (XPS analysis and AFM) and on KBR discs (FTIR - transmission method) using 2% weight/volume toluene solutions.

6.3. Results

6.3.1. X-ray Photoelectron Spectroscopy

The main C(1s) peak centred at a binding energy of 285.0 eV for both of the polysilanes can be assigned to C-H, C-C and C-Si environments[1,2], Figures 6.1-6.2. In the case of polyphenylmethylsilane, there was an additional C(1s) component around 291.6 eV having an area of 3% of the main C(1s) peak, this exhibited a Gaussian profile of different FWHM, and can be attributed to π-π^* shake-up transitions accompanying core level ionisation of the aromatic rings[3]. For both polysilanes there is one major type of Si(2p) core level environment at 100.0 eV, characteristic of the $-[(R_1)Si(R_2)]_n-$ structure[4]. A weak shoulder at 101.8 eV was discernible (less than 1%), and could be attributed to either the occurrence of silicon atoms adjacent to a carbon atom rather than a silicon centre along the polymeric backbone, or slight oxidation at the polymer surface.

Plasma oxidation of each polysilane spin coated onto a polyethylene substrate was studied as a function of glow discharge power, Figures 6.1-6.2. This treatment was found to be very rapid down to the depths accessible by XPS (5 - 20 Å), Table 6.1. A plateau in the elemental concentrations is reached well below 5 W corresponding to 30% carbon, 35% silicon, and 35% oxygen for the polycyclohexylmethylsilane polymer, and 41% carbon, 31% silicon, and 28% oxygen for the corresponding polyphenylmethylsilane material, Figures 6.3-6.4. The aliphatic polysilane yields a higher level of oxidation at the surface compared to its aromatic counterpart, whilst the latter reaches its limiting elemental percentages at lower glow discharge powers. One can clearly see that the amount of oxygen and silicon on the surface after oxidation is much greater in the case of the plasma polymers discussed in Chapter 5.

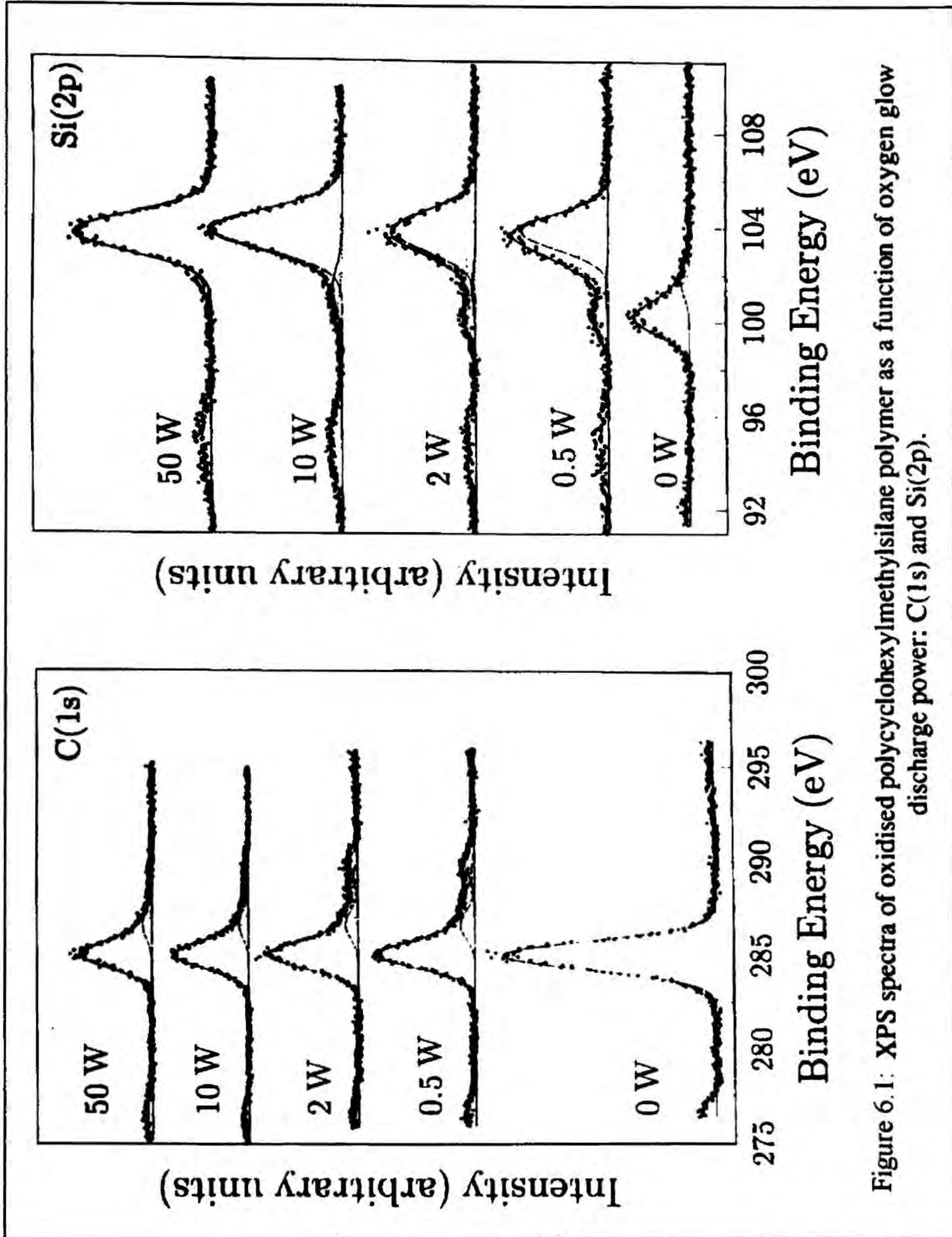

Figure 6.1: XPS spectra of oxidised polycyclohexylmethylsilane polymer as a function of oxygen glow discharge power: C(1s) and Si(2p).

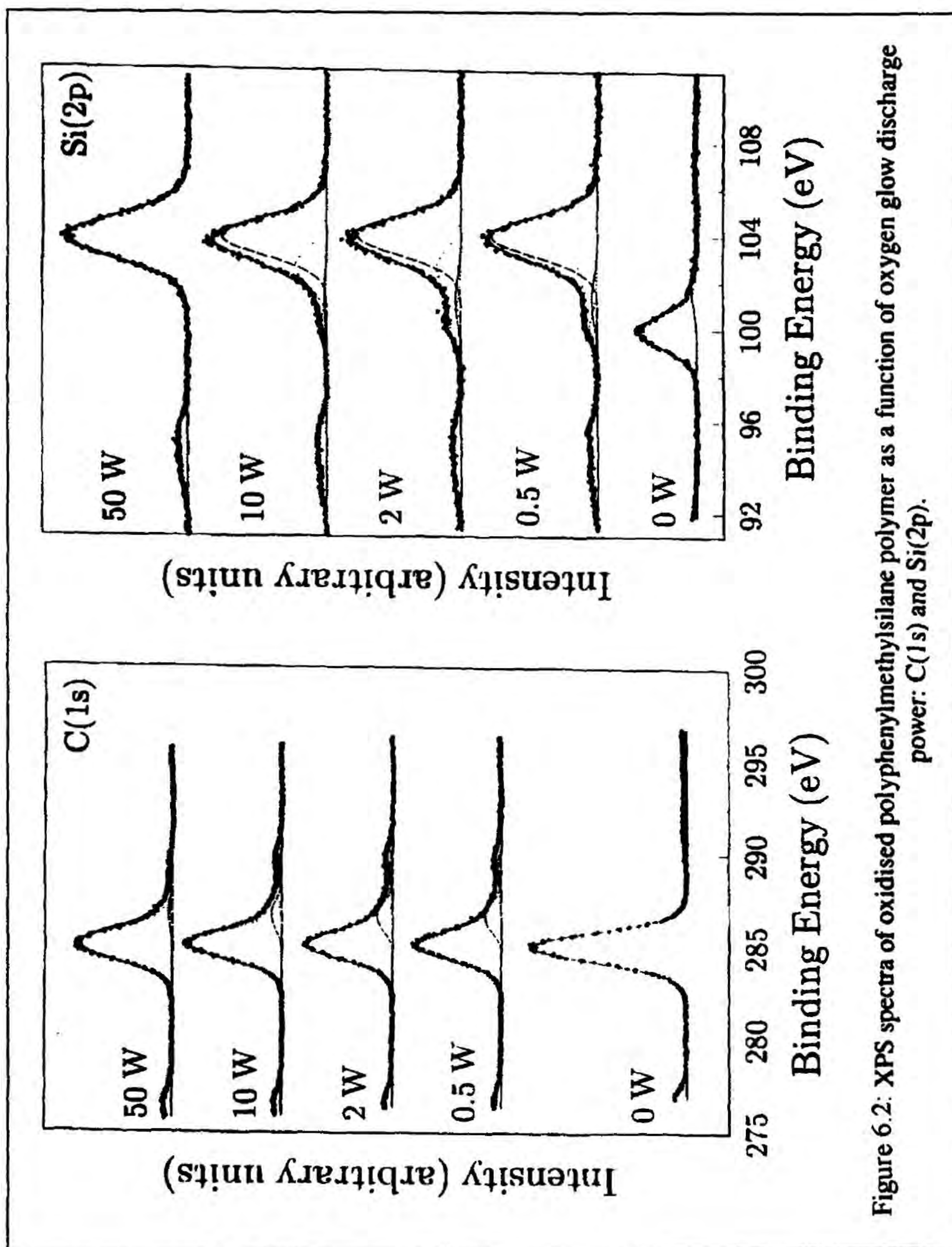

Figure 6.2: XPS spectra of oxidised polyphenylmethylsilane polymer as a function of oxygen glow discharge power: C(1s) and Si(2p).

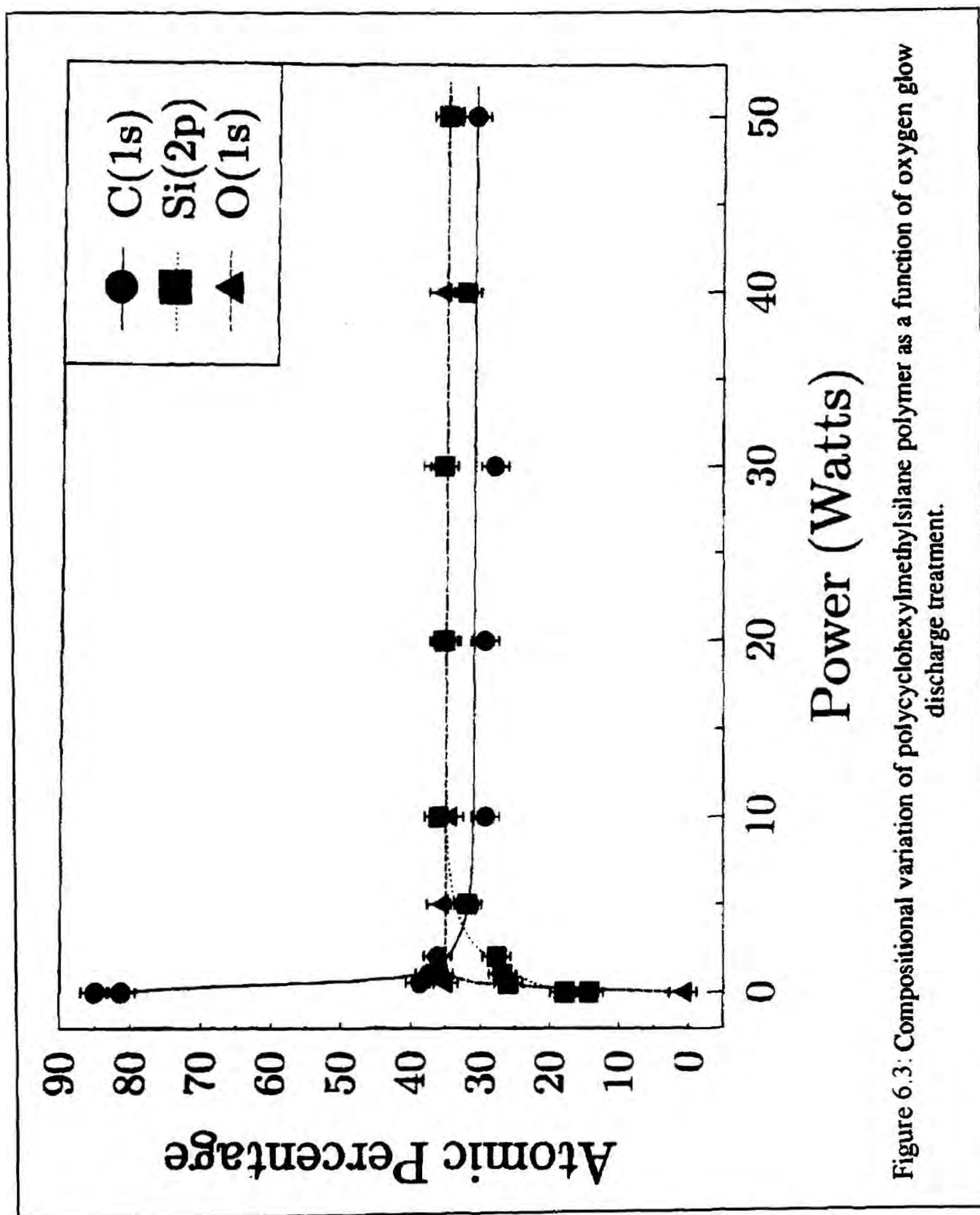

Figure 6.3: **Compositional variation of polycyclohexylmethylsilane polymer as a function of oxygen glow discharge treatment.**

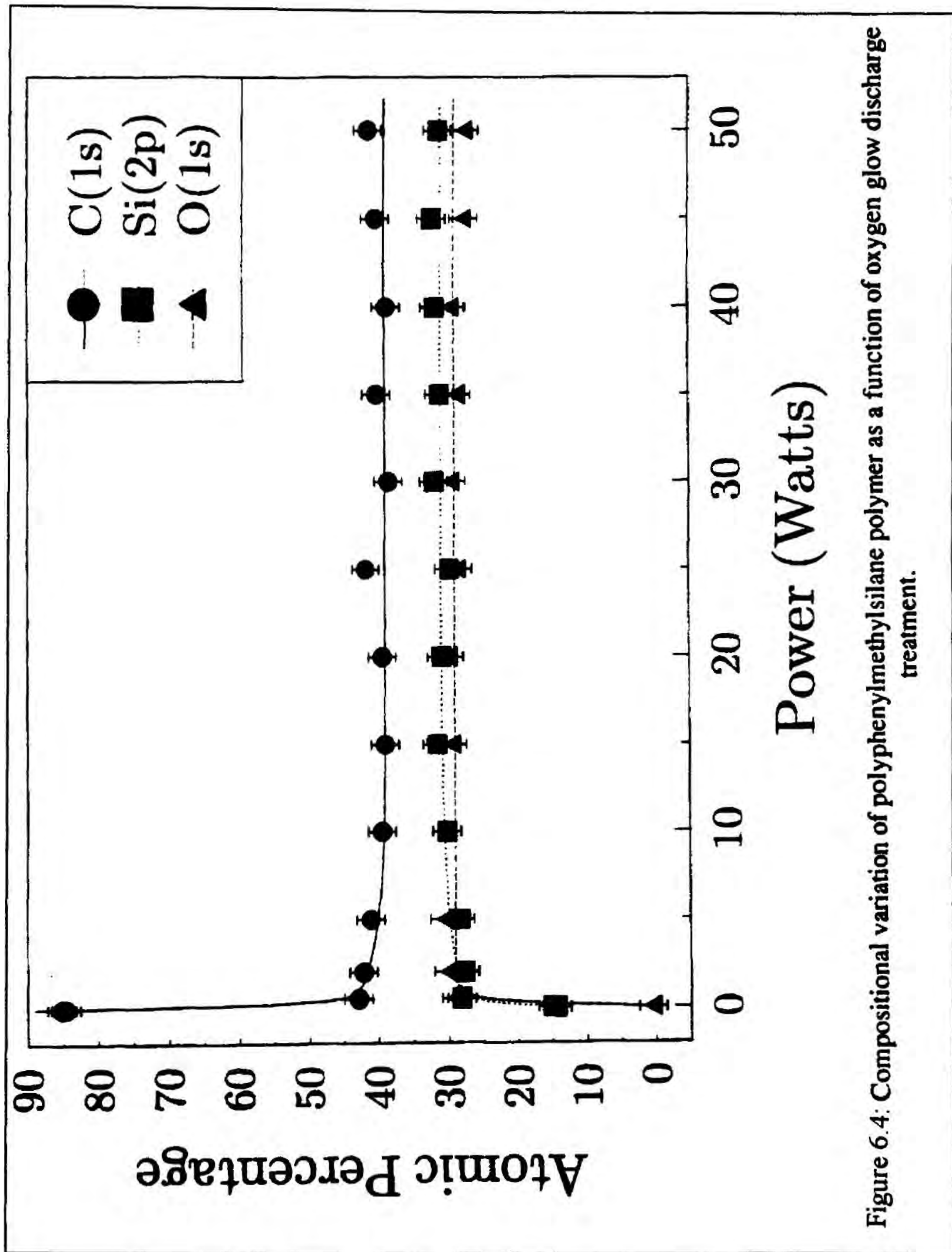

Figure 6.4: Compositional variation of polyphenylmethylsilane polymer as a function of oxygen glow discharge treatment.

Table 6.1 Elemental percentages as determined by XPS.

Sample	Elemental Composition		
	%C	%Si	%O
PCHMS (theoretical)	87.5	12.5	0
PCHMS (experimental)	85 ± 2	14 ± 2	≤1
O_2 Plasma / PCHMS / PE	30 ± 2	35 ± 2	35 ± 2
PPMS (theoretical)	87.5	12.5	0
PPMS (experimental)	85 ± 2	14 ± 2	≤1
O_2 Plasma / PPMS / PE	41 ± 2	31 ± 2	28 ± 2

During plasma oxidation, the Si(2p) peak gains intensity and shifts by approximately 3.7 eV towards higher binding energy. The Si(2p) envelope could be fitted to Si-Si (100.1 eV), Si-H / Si-C (101.2 eV), Si-$[OC_xH_y]_n$ (102.6 eV), and O-Si-O (104.0 eV) silicon centres[5]. Whilst an attenuation in the C(1s) peak is observed in conjunction with the emergence of a weak oxidised component at high binding energy, which can be taken as a convolution of >C-O- (286.6 eV), >C=O / -O-C-O- (287.9 eV), -O-C=O (289.0 eV), and -O-CO-O- (290.4 eV) functionalities[6].

Passage of oxygen over the polysilanes polymer in the absence of a glow discharge resulted in negligible surface oxidation.

XPS in conjunction with Ar^+ ion depth profiling of the oxidised polysilane layers confirmed the build-up of oxygenated silicon species in the near-surface region, Figures 6.5-6.6. A comparison of O(1s) profiles obtained from the Ar^+ ion sputtering experiments shows that the aromatic polysilane is oxidised to a greater depth.

6.3.2. Fourier Transform Infrared Spectroscopy

Thin layers of polysilane were spin coated onto a pressed KBr disc and then oxygen plasma treated.

Clean polycyclohexylmethylsilane[7] exhibits strong infrared absorbances related to (Figure 6.7): C-H stretching in CH_3 and CH_2 (**a**: 2920 and 2847 cm^{-1}), -CH_2- bending (**b**: 1447 cm^{-1}), CH_3 bending in $SiCH_3$ (**c**: 1244 cm^{-1}), C-C stretching (**d**: 995 cm^{-1}), CH_3 rocking in $SiCH_3$ (**e**: 774 cm^{-1}), -CH_2- rocking (**f**: 745 cm^{-1}), and Si-C stretching (**g**: 661 cm^{-1}). The vibrational modes of the -Si-Si- polymer backbone are infrared inactive[8].

The phenyl substituted polysilane[7] polymer displayed the following absorbances (Figure 6.8): aromatic C-H stretching (**h**: 3067, 3050, and 2993 cm^{-1}), methyl C-H stretching (**i**: 2957 and 2895 cm^{-1}), C-H bending (**j**: 1427 cm^{-1}), CH_3 bending in $SiCH_3$ (**k**: 1247 cm^{-1}), monosubstituted benzene (**l**: 1099 cm^{-1}), CH_3 rocking in $SiCH_3$ (**m**: 781 cm^{-1}), out of plane C-H bending (**n**: 754 and 729 cm^{-1}), ring C-C bending (**o**: 696 cm^{-1}), Si-C stretching (**p**: 667 cm^{-1}), out of plane C-C ring bending (**q**: 463 cm^{-1}).

Glow discharge oxidation of polyphenylmethylsilane resulted in the appearance of absorbances related to Si-O-Si and/or Si-O-C stretches[9] (**r**: 1130-990 cm^{-1}). However, plasma oxidation of the polycyclohexylmethylsilane surface was not detected by infrared spectroscopy.

6.3.3. Emission Spectroscopy

Emission spectra (Figure 6.9, lines and bands assigned in Table 5.1) of oxygen plasmas (10 W) were not sensitive enough to register any major difference between discharges on polyethylene and polyethylene spin-coated with both polysilanes, while the plasma polymers analysed in Chapter 5 showed a drastic reduction in the intensity of the CO related lines.

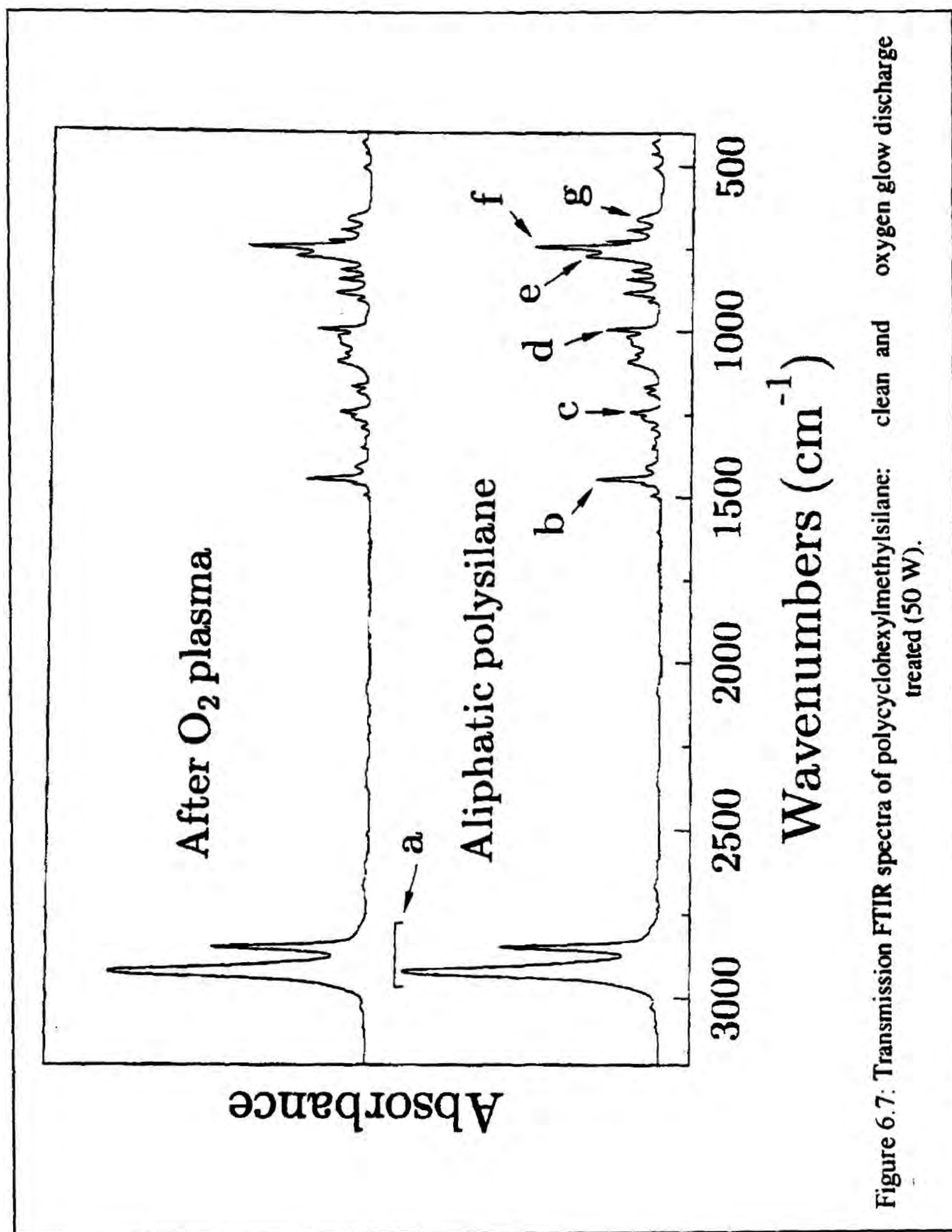

Figure 6.7: Transmission FTIR spectra of polycyclohexylmethylsilane: clean and oxygen glow discharge treated (50 W).

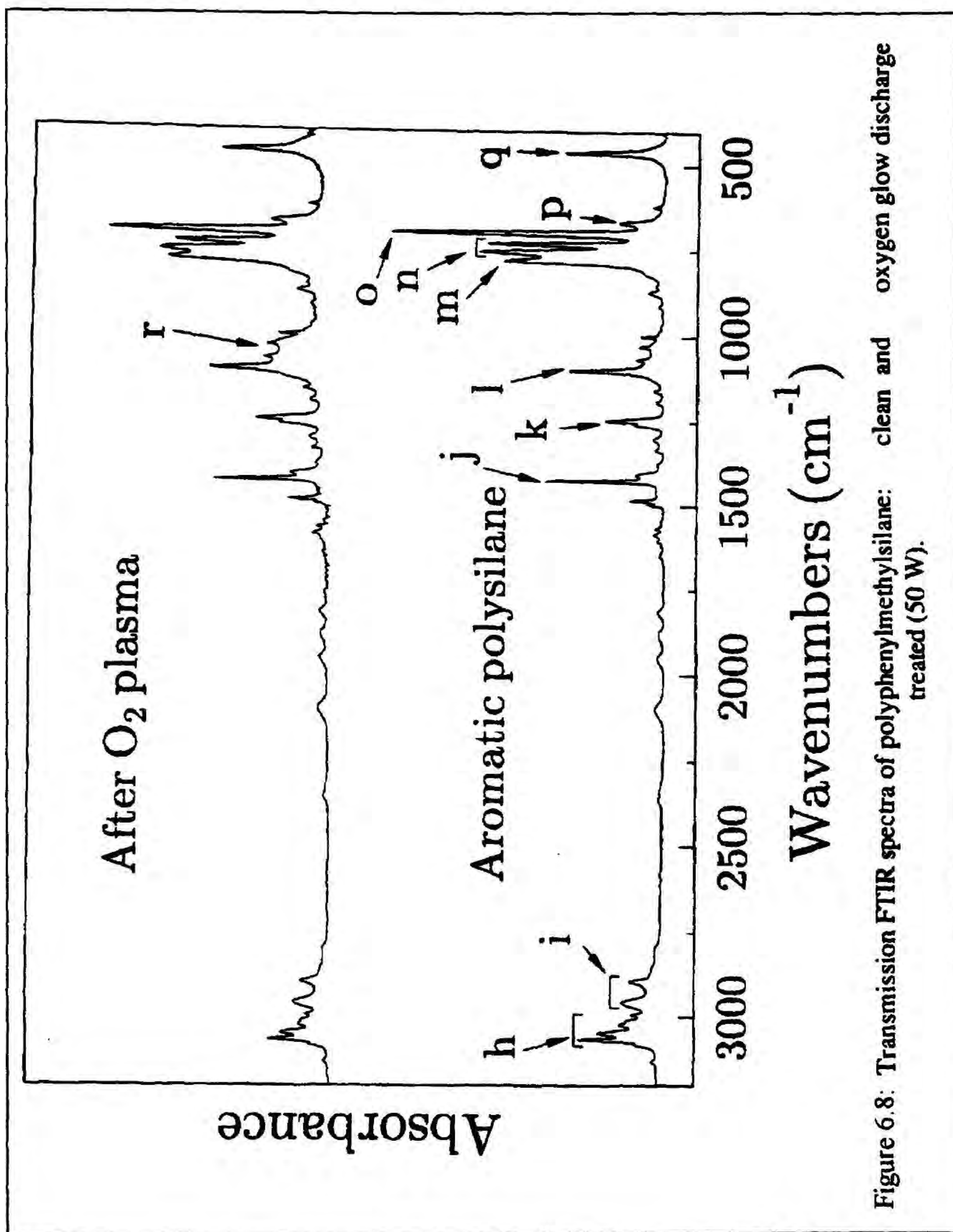

Figure 6.8: Transmission FTIR spectra of polyphenylmethylsilane: clean and oxygen glow discharge treated (50 W).

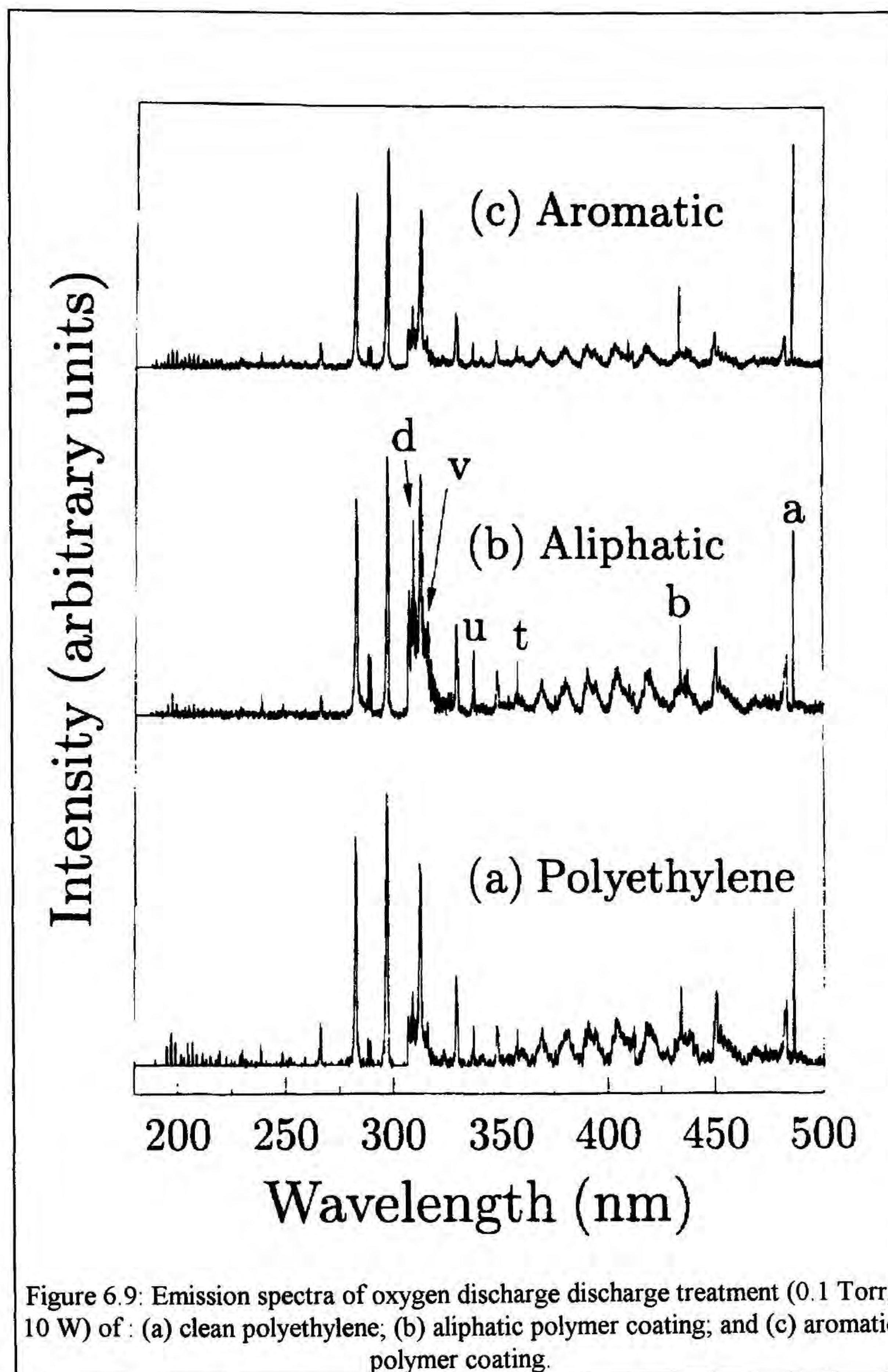

Figure 6.9: Emission spectra of oxygen discharge discharge treatment (0.1 Torr, 10 W) of : (a) clean polyethylene; (b) aliphatic polymer coating; and (c) aromatic polymer coating.

6.4. Discussion

A pure oxygen plasma contains ions, atoms, ozone, and metastables of atomic and molecular oxygen, as well as electrons and a broad electromagnetic spectrum[10]. This highly reactive medium readily leads to oxidation at a polysilane surface. Polycyclohexylmethylsilane (λ_{max} = 320 nm) and polyphenylmethylsilane (λ_{max} = 337 nm) will both absorb the vacuum ultraviolet irradiation generated by the oxygen plasma, and thereby undergo scissoring and crosslinking, this can then be followed by surface oxidation. In the case of conventional hydrocarbon polymers, phenyl containing polymers are more resistant to plasma etching than their aliphatic analogues[11].

For polymers that undergo scissoring and crosslinking simultaneously, the relative efficiencies of each process can be estimated by monitoring the changes in the number- and weight-average molecular weights ($\overline{M}_n$ and $\overline{M}_w$, respectively) as a function of the absorbed dose[12,13]. The relationships between the molecular weights and the respective quantum yields are described by equations 6.1 and 6.2:

$$\frac{1}{\overline{M}_n} = \frac{1}{\overline{M}_n^0} + \left(\Phi(s) - \Phi(x)\right)\frac{D}{N_A} \tag{6.1}$$

$$\frac{1}{\overline{M}_w} = \frac{1}{\overline{M}_w^0} + \left(\Phi(s) - 4\Phi(x)\right)\frac{D}{2N_A} \tag{6.2}$$

In these equations, $\overline{M}_n^0$ and $\overline{M}_w^0$ are the initial molecular weights, $\Phi(s)$ and $\Phi(x)$ are the quantum yields for the scissoring and crosslinking reactions, respectively; D is absorbed dose; and N_A is Advogrado's number.

Table 6.2 summarises some reported quantum yield data for the two polysilane polymers used in this investigation. It can be seen that the aliphatic polysilane has a greater tendency to undergo scissoring than the aromatic one; whilst the later polymer crosslinks more easily.

Table 6.2: Quantum yield data for polycyclohexylmethylsilane (PCHMS) and polyphenylmethylsilane (PPMS)[12,13]

Polysilane	Solvent	$\overline{M}_n^o(\times 1000)$	λ(nm)	Solution		Solid Film	
				$\Phi(s)$	$\Phi(x)$	$\Phi(s)$	$\Phi(x)$
PCHMS	Toluene	41.4	355	1.2	0.06	0.022	0
PPMS	THF	245	313	0.97	0.12	0.015	0.002

From this data, one would expect a greater build-up of SiO_xH_y species in the case of the polycyclohexylmethylsilane polymer, since its aliphatic side groups preferably undergo rupture or oxidation. Whereas an effectively thicker oxidised layer is generated in the case of polyphenylmethylsilane due to the phenyl rings in the parent polymer being able to participate in crosslinking as well as rupture and oxidation. The aforementioned description is consistent with the XPS, Ar^+ ion depth profiling, and FTIR results of plasma oxidised polysilane films used in this study, where the concentration of SiO_xH_y moieties at the surface is found to be greatest for polycyclohexylmethylsilane, whilst polyphenylmethylsilane is oxidised to a greater depth.

6.5. Conclusions

A thin SiO_xH_y-rich skin is formed during oxygen glow discharge treatment of polycyclohexylmethylsilane and polyphenylmethylsilane thin films. The type of substituents along the polysilane backbone can have a strong influence upon the surface oxidation chemistry: aliphatic side groups are more readily lost than aromatic substituents, and therefore yield a thinner, but more SiO_xH_y-rich layer. Both polysilanes undergo less oxidation, compared to the organosilicon plasma polymers.

References

1. Shard, A.G.; Munro, H.S.; Badyal, J.P.S. *Polym. Comm.* **1991**, *32*, 152.
2. Ehrlich, C.D.; Basford, J.A., *J. Vac. Sci. Technol.* **1992**, A10, 1.
3. Johansson, G.; Hedman, J.; Berndtsson, A.; Klasson, M.; Nilsson, R. *J. Electron Spectr.* **1973**, *2*, 295.
4. Johansson, G.; Hedman, J.; Berndtsson, A.; Klasson, M.; Nilsson, R., *J. Electron Spectr.* **1973**, *2*, 295.
5. Inagaki, N.; Katsuoka, J., *J. Memb. Sci.* **1987**, *34*, 297.
6. Gray R.C.; Carver, J.C.; Hercules, D.M. *J. Electron Spectrosc.* **1976**, *8*, 343.
7. Clark, D.T.; Dilks, A., *J. Polym. Sci., Polym. Chem. Ed.* **1976**, *14*, 533.
8. Hofer, D.C.; Miller, R.D.; Wilson, C.G., *Adv. Res. Technol.* **1984**, *469*, 16.
9. Laoharojanaphand, P.; Lin, T.J.; Stoffer, J.O., *J. Appl. Polym. Sci.* **1990**, *40*, 369.
10. Clark, D.T.; Dilks, A., *J. Polym. Sci. Polym. Chem. Ed.* **1979**, *17*, 957.
11. Silverstein, R.M.; Bassler, G.C.; Morrill, T.C., *Spectrometric Indentification of Organic Compounds,* Wiley: Singapore, 1981.
12. Cui, C.X.; Kertesz, M., *Macromolecules* **1992**, *25*, 1103.
13. Nguyen, L.T.; Sung, N.H.; Suh, N.P., *J. Polym. Sci. Polym. Lett. Ed.* **1980**, *18*, 541.
14. Hollahan, J. R.; Bell, A. T., Eds.; *Techniques and Applications of Plasma Chemistry*; Wiley: New York, 1974.
15. Egitto, F.D.; Vukanovic, V.; Taylor, G.N., *Plasma Etching of Organic Polymers,* in *Plasma Deposition, Treatment and Etching of Polymers*, d'Agostino, R. (ed.), Academic Press: New York, 1990.
16. Miller, R.D.; Guillet, J.E. and Moore, J., *Polym. Prepr.* **1988**, *29*, 552.
17. Hofer, D.C; Miller, R.D. and Wilson, C.G., *Adv. Resist Tech.* **1984**, *469*, 16.

Chapter Seven

FINAL DISCUSSION AND CONCLUSIONS

The first point to be approached is the maximum deposition rate for tetramethylsilane (TMS), and hexamethyldisilane (HMDS). They occurred at W/F_M = 280 MJ/kg, in the case of TMS (Chapter 3), and W/F_M = 120 MJ/kg, in the case of HMDS (Chapter 4). One can relate these results to the empirical expression developed by Park for the plasma polymerisation of organosilanes[1]:

$$D_p \propto F_M \exp[-E_a/(W/F_M)]$$

In this equation, the deposition rate D_p (in fact the average deposition rate along the whole reactor length) is described as being governed by an Arrhenius-type of activation energy E_a. Using this model, for a fixed flow rate, the overall plasma polymer deposition rate should increase at higher W/F_M ratios towards a maximum value. In this study, the rate of TMS plasma polymerisation at a local position in the reactor passes through a maximum with increasing W/F_M. This can be understood in terms of the mass flow rate (F_M) varying along the reactor length due to precipitation of plasma polymer (i.e. F_M drops on moving downstream), this will in turn influence the local deposition rate, Figure 7.1. For a given position in the reaction vessel, there will be no deposition in the absence of any electromagnetic field (W = 0), and also when there is a very low concentration of reactive species (F_M = 0). The latter situation will arise at high glow discharge powers, since virtually all of the polymerisable species will have been consumed upstream. The lower the value of E_a, the lower will be the value of W/F_M related to the maximum deposition rate. In other words, HMDS has a lower value of E_a than the TMS one, which implies that the first is the most reactive monomer.

If we extend this analysis to atoms, we can see that E_a would have its lowest value for the deposition of Si groups: one can see in Figure 3.3 (dependence of Si/C ratio upon W/F_M for TMS) that it is between 0 and 50 MJ/kg (the value for HMDS being of the same order of magnitude). The atomic nature of plasma polymerisation

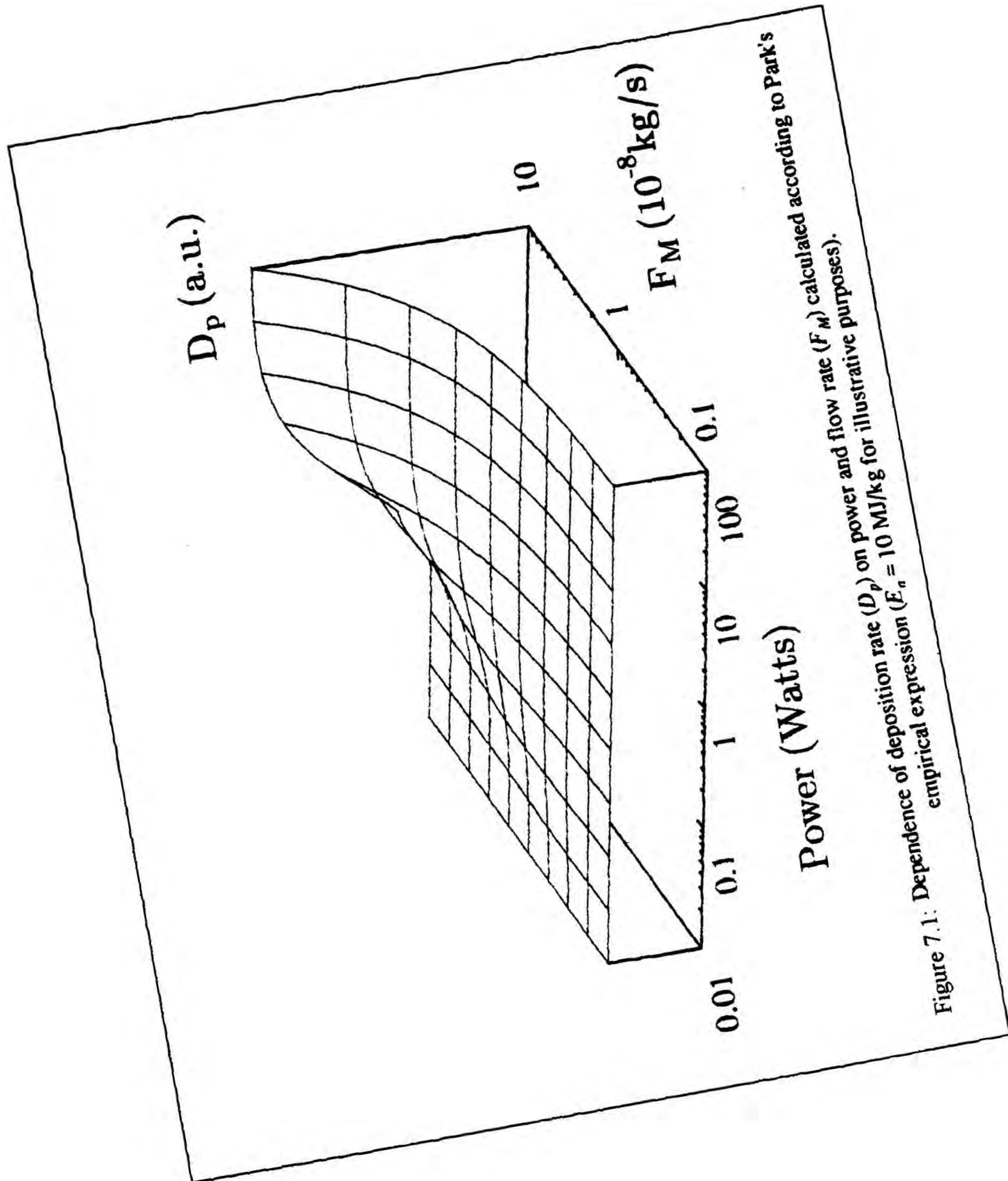

Figure 7.1: Dependence of deposition rate (D_p) on power and flow rate (F_M) calculated according to Park's empirical expression (E_a = 10 MJ/kg for illustrative purposes).

clearly emerges at this point: the total E_a is the result of the contribution of several E_as, which govern the excitation, breaking down and recombination of different bonds which are present in each monomer. Of course, the weaker the chemical bond, the lower the apparent energy of activation. In other words, the Si-Si bond present in the HMDS monomer would make this monomer more susceptible to decomposition. Apart from the presence of the weaker Si-Si bond in the HMDS precursor, it was also seen in Chapter 4 that HMDS provides the possibility of formation of silene groups >Si=CH2, which could be polymerised via conventional polymerisation:

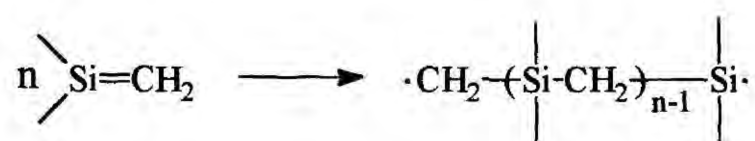

Short times of deposition yielded films. Long times resulted in the formation of amorphous powders. The formation of powders can be the result of precipitation of particles of dust from the plasma, as well as the result of internal stresses within plasma polymer films (the presence of internal stresses was characterised by the curling of the polyethylene films after being subjected to organosilane plasma treatment).

Since a higher value of W/F_M was used to synthesise TMS derived samples at their highest deposition rate, the resultant samples were product of conditions in which the breaking down of bonds was less selective: stronger C-H and C-C bonds would have a higher probability of being broken. In other words, one would expect the TMS derived plasma polymer to be richer in trapped free radicals, in organic character, as well as in double bonds.

XPS experiments revealed a lower value of binding energy for the Si(2p) core electron in the case of the TMS plasma polymer. This is consistent with an electron richer environment in this case (with more trapped free radicals). Infrared analysis characterised the TMS derived plasma polymer as the one with a more pronounced organic character. Infrared analysis also indicated that the main groups present in the plasma polymers were Si-CH_3, and this was characterised by NMR experiments, as well.

The results from elemental analysis indicated a lower H/C ratio for the TMS plasma polymer. The more pronounced presence of conjugation in this plasma polymer was also characterised via solid state NMR analysis and, in terms of plasma phase, emission spectroscopy (which also showed that, for both monomers, the main by-product of the decomposition was hydrogen). This information indicates that the plasma polymers synthesised in this thesis can be characterised as a network of Si-$(CH_3)_n$ groups (with the possibility of occurrence of silicon carbide-like moieties), sometimes linked to organic groups like methylene, being these organic groups more conjugated in the case of the TMS plasma polymer. The extremely crosslinked character of these hard powders manifested itself through their insolubility (even when using hot alkaline solutions).

Both plasma polymers suffered oxidation, when exposed to the atmosphere. This can be related to the fact that Si-O and C-O have bond dissociation energies of 531 $kJmol^{-1}$, 340 $kJmol^{-1}$ respectively[2], and therefore it is energetically favourable for trapped reactive centres to interact with oxygen and moisture from the air[3]:

$$\geq C\bullet + H_2O \longrightarrow \geq C\text{-}OH$$

$$\geq C\bullet + O_2 \longrightarrow \geq C\text{-}OO\bullet \longrightarrow \geq C\text{-}OOH \longrightarrow \geq C\text{-}OH,\ \geq C{=}O,\ \geq C(=O)\text{-}H$$

$$\geq Si\bullet + H_2O \longrightarrow \geq Si\text{-}OH$$

Following ageing, the shift in the Si(2p) XPS peak to a higher binding energy, the increase in oxygen atomic percentage, the appearance of shoulders in both the C(1s) and Si(2p) regions, and the presence of O-H[2] (bond energy = 492 $kJmol^{-1}$), CO_x and Si-O related NMR/FTIR bands supports this explanation. NMR/FTIR bands also

showed the occurrence of crosslinking in both samples, as a result of ageing.

The colour of the HMDS plasma polymer changed from brown to yellow, while the brown colour of the TMS plasma polymer was stable. That was another evidence of the higher occurrence of conjugation in this sample: conjugation makes the free radicals present in the sample more stable to oxidation due to stabilisation by resonance. This explanation was supported by NMR results.

The possibility of using both plasma polymers as barriers in reactive ion etching was analysed: ATR-FTIR spectroscopy, X-ray photoelectron spectroscopy, and emission spectroscopy showed the HMDS plasma polymer as the one with the best performance. FTIR spectroscopy and XPS showed the presence of SiO_X environments as a result of the oxygen plasma treatment of polyethylene surfaces previously treated with organosilane plasmas. These techniques also showed that further oxidation was avoided due to the presence of this hard skin, being the film previously treated with a HMDS plasma having an SiO_X-richer layer, after oxidation. The topography of the organosilane plasma-treated surfaces did not change after treatment with oxygen plasmas.

Ordinary polysilanes (polycyclohexylmethylsilane, PCHMS, and polyphenylmethylsilane, PPMS) were also used as etching barriers, for the sake of comparison with the cited plasma polymers. Among the polysilanes, the aliphatic one (PCHMS) had the best performance, but still bellow the performance of the plasma polymerised organosilanes. As a consequence, plasma polymerised organosilanes were considered to be exceptional options for application as reactive ion etch barriers (in particular the main object of study of this thesis: plasma polymerised HMDS).

References

1. Park, S.Y.; Kim, N. *J. Appl. Polym. Sci. Appl. Polym. Symp.* **1990**, *46*, 91.
2. Cotton, F.A.; Wilkinson, G., Advanced Organic Chemistry; Wiley: New York, 1988.
3. Yasuda, H., *Plasma Polymerisation*, Academic Press: Orlando, 1985.

Appendix

RESEARCH COLLOQUIA GIVEN AT DURHAM UNIVERSITY FROM MARCH 1991 TO MARCH 1994.

REVISED VERSION

UNIVERSITY OF DURHAM

Board of Studies in Chemistry

COLLOQUIA, LECTURES AND SEMINARS GIVEN BY INVITED SPEAKERS
1ST AUGUST 1990 TO 31ST JULY 1991

ALDER, Dr. B.J. (Lawrence Livermore Labs., California) — 15th January, 1991
Hydrogen in all its Glory

BELL†, Prof. T. (SUNY, Stoney Brook, U.S.A.) — 14th November, 1990
Functional Molecular Architecture and Molecular Recognition

BOCHMANN†, Dr. M. (University of East Anglia) — 24th October, 1990
Synthesis, Reactions and Catalytic Activity of Cationic Titanium Alkyls

BRIMBLE, Dr. M.A. (Massey University, New Zealand) — 29th July, 1991
Synthetic Studies Towards the Antibiotic Griseusin-A

BROOKHART, Prof. M.S. (University of N. Carolina) — 20th June, 1991
Olefin Polymerizations, Oligomerizations and Dimerizations Using Electrophilic Late Transition Metal Catalysts

BROWN, Dr. J. (Oxford University) — 28th February, 1991
Can Chemistry Provide Catalysts Superior to Enzymes?

BUSHBY†, Dr. R. (Leeds University) — 6th February, 1991
Biradicals and Organic Magnets

COWLEY, Prof. A.H. (University of Texas) — 13th December, 1990
New Organometallic Routes to Electronic Materials

CROUT, Prof. D. (Warwick University) — 29th November, 1990
Enzymes in Organic Synthesis

DOBSON†, Dr. C.M. (Oxford University) — 6th March, 1991
NMR Studies of Dynamics in Molecular Crystals

GERRARD†, Dr. D. (British Petroleum) — 7th November, 1990
Raman Spectroscopy for Industrial Analysis

HUDLICKY, Prof. T. (Virginia Polytechnic Institute) — 25th April, 1991
Biocatalysis and Symmetry Based Approaches to the Efficient Synthesis of Complex Natural Products

JACKSON†, Dr. R. (Newcastle University) — 31st October, 1990
New Synthetic Methods: α-Amino Acids and Small Rings

KOCOVSKY†, Dr. P. (Uppsala University) — 6th November, 1990
Stereo-Controlled Reactions Mediated by Transition and Non-Transition Metals

LACEY, Dr. D. (Hull University) — 31st January, 1991
Liquid Crystals

LOGAN, Dr. N. (Nottingham University) — 1st November, 1990
Rocket Propellants

MACDONALD, Dr. W.A. (ICI Wilton) — 11th October, 1990
Materials for the Space Age

MARKAM, Dr. J. (ICI Pharmaceuticals) — 7th March, 1991
DNA Fingerprinting

PETTY, Dr. M.C. (Durham University) — 14th February, 1991
Molecular Electronics

PRINGLE+, Dr. P.G. (Bristol University) — 5th December, 1990
Metal Complexes with Functionalised Phosphines

PRITCHARD, Prof. J. (Queen Mary & Westfield College, London University) — 21st November, 1990
Copper Surfaces and Catalysts

SADLER, Dr. P.J. (Birkbeck College London) — 24th January, 1991
Design of Inorganic Drugs: Precious Metals, Hypertension + HIV

SARRE, Dr. P. (Nottingham University) — 17th January, 1991
Comet Chemistry

SCHROCK, Prof. R.R. (Massachusetts Institute of Technology) — 24th April, 1991
Metal-ligand Multiple Bonds and Metathesis Initiators

SCOTT, Dr. S.K. (Leeds University) — 8th November, 1990
Clocks, Oscillations and Chaos

SHAW+, Prof. B.L. (Leeds University) — 20th February, 1991
Syntheses with Coordinated, Unsaturated Phosphine Ligands

SINN+, Prof. E. (Hull University) — 30th January, 1991
Coupling of Little Electrons in Big Molecules. Implications for the Active Sites of (Metalloproteins and other) Macromolecules

SOULEN+, Prof. R. (South Western University, Texas) — 26th October, 1990
Preparation and Reactions of Bicycloalkenes

WHITAKER+, Dr. B.J. (Leeds University) — 28th November, 1990
Two-Dimensional Velocity Imaging of State-Selected Reaction Products

+ Invited specifically for the postgraduate training programme.

UNIVERSITY OF DURHAM

Board of Studies in Chemistry

COLLOQUIA, LECTURES AND SEMINARS FROM INVITED SPEAKERS

1991 - 1992 (August 1 - July 31)

1991

	Month	Day	Speaker / Title
	October	17	Dr. J.A. Salthouse, University of Manchester Son et Lumiere - a demonstration lecture
	October	31	Dr. R. Keeley, Metropolitan Police Forensic Science Modern forensic science
*	November	6	Prof. B.F.G. Johnson†, Edinburgh University Cluster-surface analogies
	November	7	Dr. A.R. Butler, St. Andrews University Traditional Chinese herbal drugs: a different way of treating disease
	November	13	Prof. D. Gani†, St. Andrews University The chemistry of PLP-dependent enzymes
*	November	20	Dr. R. More O'Ferrall†, University College, Dublin Some acid-catalysed rearrangements in organic chemistry
	November	28	Prof. I.M. Ward, IRC in Polymer Science, University of Leeds The SCI lecture: the science and technology of orientated polymers
	December	4	Prof. R. Grigg†, Leeds University Palladium-catalysed cyclisation and ion-capture processes
	December	5	Prof. A.L. Smith, ex Unilever Soap, detergents and black puddings
	December	11	Dr. W.D. Cooper†, Shell Research Colloid science: theory and practice

1992

	Month	Day	Speaker / Title
*	January	22	Dr. K.D.M. Harris†, St. Andrews University Understanding the properties of solid inclusion compounds
	January	29	Dr. A. Holmes†, Cambridge University Cycloaddition reactions in the service of the synthesis of piperidine and indolizidine natural products

	Month	Day	Speaker and title
	January	30	Dr. M. Anderson, Sittingbourne Research Centre, Shell Research Recent Advances in the Safe and Selective Chemical Control of Insect Pests
*	February	12	Prof. D.E. Fenton†, Sheffield University Polynuclear complexes of molecular clefts as models for copper biosites
	February	13	Dr. J. Saunders, Glaxo Group Research Limited Molecular Modelling in Drug Discovery
*	February	19	Prof. E.J. Thomas†, Manchester University Applications of organostannanes to organic synthesis
	February	20	Prof. E.Vogel, University of Cologne *The Musgrave Lecture* Porphyrins: Molecules of Interdisciplinary Interest
	February	25	Prof. J.F. Nixon, University of Sussex *The Tilden Lecture* Phosphaalkynes: new building blocks in inorganic and organometallic chemistry
*	February	26	Prof. M.L. Hitchman†, Strathclyde University Chemical vapour deposition
	March	5	Dr. N.C. Billingham, University of Sussex Degradable Plastics - Myth or Magic?
*	March	11	Dr. S.E. Thomas†, Imperial College Recent advances in organoiron chemistry
	March	12	Dr. R.A. Hann, ICI Imagedata Electronic Photography - An Image of the Future
*	March	18	Dr. H. Maskill†, Newcastle University Concerted or stepwise fragmentation in a deamination-type reaction
	April	7	Prof. D.M. Knight, Philosophy Department, University of Durham Interpreting experiments: the beginning of electrochemistry
	May	13	Dr. J-C Gehret, Ciba Geigy, Basel Some aspects of industrial agrochemical research

† Invited specially for the postgraduate training programme.

UNIVERSITY OF DURHAM

Board of Studies in Chemistry

COLLOQUIA, LECTURES AND SEMINARS FROM INVITED SPEAKERS

1992 - 1993 (August 1 - July 31)

1992

October 15 — Dr M. Glazer & Dr. S. Tarling, Oxford University & Birbeck College, London
It Pays to be British! - The Chemist's Role as an Expert Witness in Patent Litigation

* October 20 — Dr. H. E. Bryndza, Du Pont Central Research
Synthesis, Reactions and Thermochemistry of Metal (Alkyl) Cyanide Complexes and Their Impact on Olefin Hydrocyanation Catalysis

* October 22 — Prof. A. Davies, University College London
The Ingold-Albert Lecture The Behaviour of Hydrogen as a Pseudometal

* October 28 — Dr. J. K. Cockcroft, University of Durham
Recent Developments in Powder Diffraction

October 29 — Dr. J. Emsley, Imperial College, London
The Shocking History of Phosphorus

November 4 — Dr. T. P. Kee, University of Leeds
Synthesis and Co-ordination Chemistry of Silylated Phosphites

November 5 — Dr. C. J. Ludman, University of Durham
Explosions, A Demonstration Lecture

November 11 — Prof. D. Robins, Glasgow University
Pyrrolizidine Alkaloids : Biological Activity, Biosynthesis and Benefits

November 12 — Prof. M. R. Truter, University College, London
Luck and Logic in Host - Guest Chemistry

* November 18 — Dr. R. Nix, Queen Mary College, London
Characterisation of Heterogeneous Catalysts

November 25 — Prof. Y. Vallee. University of Caen
Reactive Thiocarbonyl Compounds

November 25 — Prof. L. D. Quin, University of Massachusetts, Amherst
Fragmentation of Phosphorous Heterocycles as a Route to Phosphoryl Species with Uncommon Bonding

November 26 — Dr. D. Humber, Glaxo, Greenford
AIDS - The Development of a Novel Series of Inhibitors of HIV

December 2 — Prof. A. F. Hegarty, University College, Dublin
Highly Reactive Enols Stabilised by Steric Protection

December 2 — Dr. R. A. Aitken, University of St. Andrews
The Versatile Cycloaddition Chemistry of $Bu_3P.CS_2$

December 3 — Prof. P. Edwards, Birmingham University
The SCI Lecture - What is Metal?

December 9 — Dr. A. N. Burgess, ICI Runcorn
The Structure of Perfluorinated Ionomer Membranes

1993

* January 20	Dr. D. C. Clary, University of Cambridge Energy Flow in Chemical Reactions
January 21	Prof. L. Hall, Cambridge NMR - Window to the Human Body
January 27	Dr. W. Kerr, University of Strathclyde Development of the Pauson-Khand Annulation Reaction : Organocobalt Mediated Synthesis of Natural and Unnatural Products
January 28	Prof. J. Mann, University of Reading Murder, Magic and Medicine
February 3	Prof. S. M. Roberts, University of Exeter Enzymes in Organic Synthesis
* February 10	Dr. D. Gillies, University of Surrey NMR and Molecular Motion in Solution
February 11	Prof. S. Knox, Bristol University *The Tilden Lecture* Organic Chemistry at Polynuclear Metal Centres
February 17	Dr. R. W. Kemmitt, University of Leicester Oxatrimethylenemethane Metal Complexes
February 18	Dr. I. Fraser, ICI Wilton Reactive Processing of Composite Materials
February 22	Prof. D. M. Grant, University of Utah Single Crystals, Molecular Structure, and Chemical-Shift Anisotropy
February 24	Prof. C. J. M. Stirling, University of Sheffield Chemistry on the Flat-Reactivity of Ordered Systems
March 10	Dr. P. K. Baker, University College of North Wales, Bangor 'Chemistry of Highly Versatile 7-Coordinate Complexes'
March 11	Dr. R. A. Y. Jones, University of East Anglia The Chemistry of Wine Making
March 17	Dr. R. J. K. Taylor, University of East Anglia Adventures in Natural Product Synthesis
March 24	Prof. I. O. Sutherland, University of Liverpool Chromogenic Reagents for Cations
* May 13	Prof. J. A. Pople, Carnegie-Mellon University, Pittsburgh, USA *The Boys-Rahman Lecture* Applications of Molecular Orbital Theory
May 21	Prof. L. Weber, University of Bielefeld Metallo-phospha Alkenes as Synthons in Organometallic Chemistry
June 1	Prof. J. P. Konopelski, University of California, Santa Cruz Synthetic Adventures with Enantiomerically Pure Acetals
June 2	Prof. F. Ciardelli, University of Pisa Chiral Discrimination in the Stereospecific Polymerisation of Alpha Olefins
June 7	Prof. R. S. Stein, University of Massachusetts Scattering Studies of Crystalline and Liquid Crystalline Polymers

June 16	Prof. A. K. Covington, University of Newcastle Use of Ion Selective Electrodes as Detectors in Ion Chromatography
June 17	Prof. O. F. Nielsen, H. C. Ørsted Institute, University of Copenhagen Low-Frequency IR - and Raman Studies of Hydrogen Bonded Liquids

File Ref. CG137/E(CH)

UNIVERSITY OF DURHAM

1ST EDITION

Board of Studies in Chemistry

COLLOQUIA, LECTURES AND SEMINARS FROM INVITED SPEAKERS

1993 - 1994 (August 1 - July 31)

1993

	September 13	Prof. Dr. A.D. Schluter, Freie Universität Berlin Synthesis and Characterisation of Molecular Rods and Ribbons
	September 13	Dr. K.J. Wynne, Office of Naval Research, Washington Polymer Surface Design for Minimal Adhesion
	September 14	Prof. J.M. DeSimone, University of North Carolina, Chapel Hill Homogeneous and Heterogeneous Polymerisations in Environmentally Responsible Carbon Dioxide
	September 28	Prof. H. Ila, North Eastern Hill University, India Synthetic Strategies for Cyclopentanoids via Oxoketene Dithioacetals
*	October 4	Prof. F.J. Fehert, University of California, Irvine Bridging the Gap between Surfaces and Solution with Sessilquioxanes
	October 14	Dr. P. Hubberstey, Nottingham University Alkali Metals: Alchemist's Nightmare, Biochemist's Puzzle and Technologist's Dream
	October 20	Dr. P. Quaylet, University of Manchester Aspects of Aqueous ROMP Chemistry
	October 21	Prof. R. Adamst, University of South Carolina Chemistry of Metal Carbonyl Cluster Complexes : Development of Cluster Based Alkyne Hydrogenation Catalysts
*	October 27	Dr. R.A.L. Jonest, Cavendish Laboratory Perambulating Polymers
*	November 10	Prof. M.N.R. Ashfoldt, University of Bristol High Resolution Photofragment Translational Spectroscopy : A New Way to Watch Photodissociation
*	November 17	Dr. A. Parkert, Laser Support Facility, RAL Applications of Time Resolved Resonance Raman Spectroscopy to Chemical and Biochemical Problems
	November 24	Dr. P.G. Brucet, University of St. Andrews Structure and Properties of Inorganic Solids and Polymers
	November 25	Dr. R.P. Wayne, Oxford University The Origin and Evolution of the Atmosphere
	December 1	Prof. M.A. McKerveyt, Queen's University, Belfast Synthesis and Applications of Chemically Modified Calixerenes
	December 8	Prof. O. Meth-Cohent, University of Sunderland Friedel's Folly Revisited - A Super Way to Fused Pyridines
	December 16	Prof. R.F. Hudson, F.R.S., University of Kent Close Encounters of the Second Kind

1994

* January 26	Prof. J. Evans†, University of Southampton Shining Light on Catalysts
February 2	Dr. A. Masters†, University of Manchester Modelling Water Without Using Pair Potentials
February 9	Prof. D. Young†, University of Sussex Chemical and Biological Studies on the Coenzyme Tetrahydrofolic Acid
February 16	Prof. K.H. Theopold, University of Delaware, USA Paramagnetic Chromium Alkyls : Synthesis and Reactivity
February 23	Prof. P.M. Maitlis F.R.S.†, University of Sheffield Across the Border : From Homogeneous to Heterogeneous Catalysis
March 2	Dr. C. Hunter†, University of Sheffield Non Covalent Interactions between Aromatic Molecules
March 9	Prof. F. Wilkinson, Loughborough University of Technology Nanosecond and Picosecond Laser Flash Photolysis
March 10	Prof. S.V. Ley, University of Cambridge New Methods for Organic Synthesis
March 25	Dr. J. Dilworth, University of Essex Technetium and Rhenium Compounds with Applications as Imaging Agents

† Invited specially for the graduate training programme.